LUNG INJURY AND REPAIR

In Search of New Treatment Modalities

Jeroen Tibboel

The work presented in this thesis was conducted at the Department of Physiology and Experimental Medicine, the Hospital for Sick Children, Toronto, Canada and the Department of Pediatrics, Division of Pediatric Pulmonology, Erasmus University Medical Center – Sophia Children's Hospital, Rotterdam, the Netherlands.

The experiments described in this thesis were supported by:
- An operating grant (MOP-86472) from the Canadian Institute of Health Research.
- Infrastructure grants (CCURE, CSCCD) from the Canadian Foundation for Innovation.

Cover design: © 2013 by Lara Smink, 'A Canadian Touch to Lung Injury'.
Lay-out & Print: Optima Grafische Communicatie, Rotterdam, the Netherlands.
ISBN: 978-94-6169-43-55

LUNG INJURY AND REPAIR

In Search of New Treatment Modalities

LONGSCHADE EN HERSTEL

Naar Nieuwe Methodes van Behandeling

Proefschrift

ter verkrijging van de graad van doctor aan de
Erasmus Universiteit Rotterdam
op gezag van de rector magnificus

Prof.dr. H.A.P. Pols

en volgens besluit van het College voor Promoties.

De openbare verdediging zal plaatsvinden op
dinsdag 12 november 2013 om 13.30 uur

door

Jeroen Tibboel
geboren te Rotterdam

PROMOTIECOMMISSIE

Promotoren:	Prof. dr. J.C. de Jongste
	Prof. dr. M. Post (University of Toronto / Hospital for Sick Children)
Overige leden:	Prof. dr. L.J.I. Zimmermann
	Prof. dr. R.W. Hendriks
	Prof. dr. W.A. Helbing

Voor Emma en Kees

CONTENTS

Chapter 1

General Introduction

INTRODUCTION

The lung contains the largest surface of our body that is exposed to the environment. Day in, day out, our lungs are being exposed to many injurious components, ranging from noxious gasses and particles caused by traffic and chemical industries to a multitude of microorganisms. The lung has a host of defense mechanisms to combat this constant invasion, ranging from the simplest, the nasopharyngeal barrier, to the most intricate one, the immune system[1]. This natural defense mechanism of the lung is dependent on an intact pulmonary epithelium, abundance of pulmonary macrophages, neutrophils and dendritic cells. But even with all these barriers, exogenous factors can still lead to lung injury. This thesis will characterize lung injury, and most importantly, lung repair, using animal models of two lung diseases: Bronchopulmonary Dysplasia and Chronic Obstructive Pulmonary Disease.

Worldwide, 15 million babies are born prematurely each year, and this incidence is on the rise. In developed countries, 8.6% of babies are born premature[2]. Preterm birth is an important risk factor for the development of Bronchopulmonary Dysplasia (BPD). BPD is a disorder of the lungs that was first described in 1967 by Northway *et al.*[3]. It may develop in premature infants who underwent mechanical ventilation and oxygen supplementation in the setting of an immature, surfactant-deficient lung, with a relative shortage of antioxidant defenses[4]. BPD was originally characterized by lung parenchymal fibrosis, edema, vascular changes and persistent inflammation of the airways[5]. Over the past 40 years, with the introduction of exogenous surfactant treatment, the use of prenatal steroids, improved modes of ventilation and better nutritional support, the survival of infants with very low birthweight (VLBW) has improved. The downside to this is that VLBW infants, partly due to their low gestational age and immature lungs, are prone to develop lung problems. This is called 'new BPD' which, in contrast to the 'old BPD', is characterized by interrupted septation and abnormal vascularization, leading to fewer and enlarged alveoli[6]. BPD is believed to have a multifactorial pathogenesis, with many pre- and postnatal factors playing a role[7] (Figure 1). BPD is presently defined as the need for supplemental oxygen at 36 weeks post conception. The incidence is around 52% in infants with a birthweight between 501 and 750 gram, and decreases with increased birthweight to 7% in infants with a birthweight between 1251 and 1500 gram[8], making it the most common chronic lung disease in infancy[9]. Long-term follow-up indicates that preterm infants with BPD develop reduced lung function and abnormal lung structure through childhood[10,11] and into adolescence[12,13]. Structural lung abnormalities resembling emphysema have been reported in young adults with BPD[14].

Even though progress has been made in the management of infants with BPD, current treatment remains symptomatic and limited, and there is a need for more effective strategies for prevention and treatment of BPD. Researchers have successfully used hyperoxia exposure in newborn mice during the postnatal period to establish an animal model of BPD. Sphingolipids are structural components of the cell membrane and have recently

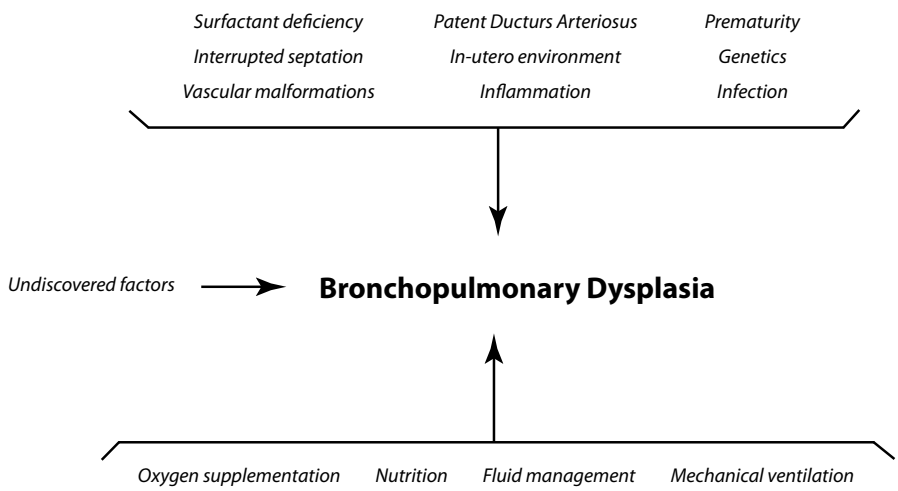

Figure 1. *Multifactorial pathogenesis of BPD.*

been discovered to exhibit important functions as messenger molecules in the regulation of proliferation and apoptosis. The function of sphingolipids, both in healthy and diseased state is described in detail in chapter 2. We aimed to examine the importance of a class of biologically active molecules, the sphingolipids, in the onset of BPD and set out to investigate the effect of a new therapeutic strategy, pharmacological sphingolipid inhibitor treatment, in the hyperoxia-induced animal model of BPD (Chapter 3). Furthermore we examined the effect of hypoxia-inducible-factor 1 alpha (HIF-1α) overexpression on alveolarization and investigated its potential therapeutic effect in our hyperoxia-induced animal model (Chapter 4).

Pulmonary emphysema and chronic bronchitis, together chronic obstructive pulmonary disease (COPD), are the most common chronic lung diseases in adults in the developed world, and are associated with a high mortality risk[15], the third leading cause of death in 2020[16]. Due to exacerbations leading to hospitalization and home oxygen use, COPD poses a large economic burden[17], estimated at 60-70 billion dollars annually in the US[18]. Pulmonary emphysema is characterized by progressive destruction of alveolar walls, leading to loss of elastic recoil, airflow obstruction and hyperinflation. Patients experience a decrease in lung function, shortness of breath and fatigue. The severity of the disease is determined by the amount of airflow limitation, measured by the Forced Expiratory Volume in 1 second (FEV1) as percentage of the predicted value based on control values from healthy controls. Pulmonary emphysema has a multifactorial pathogenesis. Oxidative stress, sustained inflammation and protease-antiprotease imbalance are believed to be major contributors to the pathogenesis of COPD. These factors also play a role in the development of BPD, and hence the pathogenesis of COPD and BPD have features in common[19]. Development of COPD is strongly related to air pollution and cigarette smoke exposure. Why only a minority of all smokers develops emphysema remains unclear. To date no

curative therapies are available. Smoking cessation and domiciliary oxygen supplementation only prolong survival in a small subset of patients with resting PaO_2 < 60 mmHg[20]. Apoptosis plays an important role in the pathofysiology of COPD. Since sphingolipids have been shown to modulate the balance between apoptosis and proliferation, we set out to examine the role of sphingolipid metabolism in the pathofysiology of pulmonary emphysema, and the effect of pharmacological inhibition on the sphingolipid pathway in an elastase-induced emphysema model (Chapter 5). The elastase-induced rodent emphysema model, which is based on the injection of porcine pancreatic elastase, mimics the histological findings seen in the lungs of emphysema patients and has been used for decades to investigate new treatment strategies in COPD. Another intriguing area of therapeutic research focuses on the use of stem cells to repair injured tissue. Therefore, as part of this thesis, we set out to investigate the effects of mesenchymal stem cell treatment in the elastase-induced pulmonary emphysema model (Chapter 6).

OUTLINE OF THIS THESIS

As an introduction to this thesis, **Chapter 1** describes BPD and COPD, the two lung diseases that will be addressed in this thesis. **Chapter 2** introduces the topic of sphingolipids and focuses on the role of sphingolipids in healthy and diseased state and the influence of sphingolipids on lung growth and development. **Chapter 3** focuses on the recovery period after hyperoxia-induced lung injury in a rodent model of BPD, and the positive effect of artificial sphingosine-1-phosphate supplementation on lung structure. **Chapter 4** focuses on the role of HIF-1α during lung development and the effects of activation of HIF-1α on hyperoxia-induced lung injury. **Chapter 5** describes the role of ceramides in the development of elastase-induced emphysema, and the effect of multiple ceramide-based pharmacological treatments on lung structure and function. **Chapter 6** reports a study on the effect of mesenchymal stem cell treatment on lung structure and function in elastase-induced emphysema. **Chapter 7** discusses the findings of the above mentioned chapters, puts them into perspective, and discusses future directions. **Chapter 8** summarizes this thesis.

REFERENCES

1. Nicod LP. Pulmonary defence mechanisms. *Respiration; international review of thoracic diseases*. 1999;66(1):2–11.
2. World Health Organization. Born too soon. *http://www.who.int/pmnch/media/news/2012/201204_borntoosoon-report.pdf*. 2012.
3. Northway WH, Rosan RC, Porter DY. Pulmonary disease following respirator therapy of hyaline-membrane disease. Bronchopulmonary dysplasia. *The New England journal of medicine*. 1967;276(7):357–68.
4. Abman SH, Mourani PM, Sontag M. Bronchopulmonary dysplasia: a genetic disease. *Pediatrics*. 2008;122(3):658–9.
5. Coalson JJ. Pathology of bronchopulmonary dysplasia. *Seminars in perinatology*. 2006;30(4):179–84.
6. Jobe AJ. The new BPD: an arrest of lung development. *Pediatric research*. 1999;46(6):641.
7. Gien J, Kinsella JP. Pathogenesis and treatment of bronchopulmonary dysplasia. *Current opinion in pediatrics*. 2011;23(3):305–13.
8. Ehrenkranz R a, Walsh MC, Vohr BR, et al. Validation of the National Institutes of Health consensus definition of bronchopulmonary dysplasia. *Pediatrics*. 2005;116(6):1353–60.
9. Bland RD. Neonatal chronic lung disease in the post-surfactant era. *Biology of the neonate*. 2005;88(3):181–91.
10. Fakhoury KF, Sellers C, Smith EO, Rama J a, Fan LL. Serial measurements of lung function in a cohort of young children with bronchopulmonary dysplasia. *Pediatrics*. 2010;125(6):e1441–7.
11. Filbrun AG, Popova AP, Linn MJ, McIntosh N a, Hershenson MB. Longitudinal measures of lung function in infants with bronchopulmonary dysplasia. *Pediatric pulmonology*. 2011;46(4):369–75.
12. Trachsel D, Brutsche MH, Hug-Batschelet H, Hammer J. Progressive static pulmonary hyperinflation in survivors of severe bronchopulmonary dysplasia by mid-adulthood. *Thorax*. 2011:2–3.
13. Doyle LW, Anderson PJ. Long-term outcomes of bronchopulmonary dysplasia. *Seminars in Fetal and Neonatal Medicine*. 2009;14(6):391–395.
14. Wong PM, Lees AN, Louw J, et al. Emphysema in young adult survivors of moderate-to-severe bronchopulmonary dysplasia. *European Respiratory Journal*. 2008;32(2):321.
15. Mannino DM, Braman S. The epidemiology and economics of chronic obstructive pulmonary disease. *Proceedings of the American Thoracic Society*. 2007;4(7):502–6.
16. Jemal A, Ward E, Hao Y, Thun M. Trends in the leading causes of death in the United States, 1970-2002. *JAMA* 2005;294(10):1255–9.
17. Faulkner M a, Hilleman DE. The economic impact of chronic obstructive pulmonary disease. *Expert opinion on pharmacotherapy*. 2002;3(3):219–28.
18. Wouters EFM. Economic analysis of the Confronting COPD survey: an overview of results. *Respiratory medicine*. 2003;97 Suppl C:S3–14.
19. Bourbon JR, Boucherat O, Boczkowski J, Crestani B, Delacourt C. Bronchopulmonary dysplasia and emphysema: in search of common therapeutic targets. *Trends in molecular medicine*. 2009;15(4):169–79.
20. Sin DDD, McAlister FFA, Man SFP, Anthonisen NR. Contemporary management of chronic obstructive pulmonary disease: scientific review. *JAMA* 2003;290(17):2301–2312.

Chapter 2

Sphingolipids in Lung Growth and Repair

Jeroen Tibboel[1,2]
Irwin Reiss[2]
Johan C. de Jongste[2]
Martin Post[1]

[1] Dept. of Physiology and Experimental Medicine, Hospital for Sick Children, Toronto, Canada.
[2] Dept. of Pediatrics, Erasmus University Medical Center – Sophia Children's Hospital, Rotterdam, the Netherlands.

CHEST in press

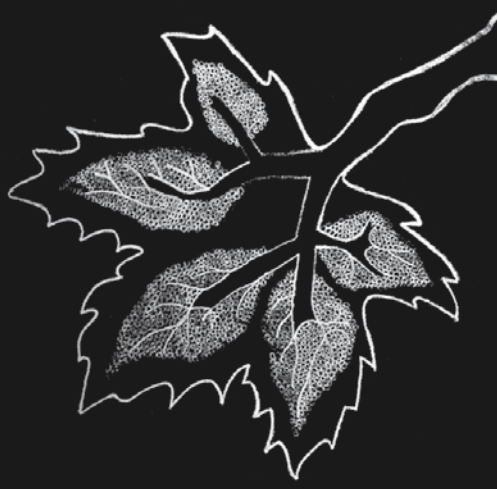

ABSTRACT

Sphingolipids comprise a class of bioactive lipids that are involved in a variety of pathophysiological processes, including cell death and survival. Ceramide and sphingosine-1-phosphate (S1P) form the centre of sphingolipid metabolism and determine the pro-and anti-apoptotic balance. Findings in animal models have suggested a possible pathophysiological role of ceramide and S1P in diseases such as COPD, cystic fibrosis and asthma. Sphingolipid research is now focusing on the role of ceramides during lung inflammation and its regulation by sphingomylinases. Recently, sphingolipids have been shown to play a role in the pathogenesis of bronchopulmonary dysplasia (BPD). Ceramide upregulation has been linked with VEGF suppression and decreased surfactant protein B levels, pathways important for the development of BPD. In a murine model of BPD, intervention with an S1P-analog had a favourable effect on the histological abnormalities and ceramide levels. Ceramides and S1P also regulate endothelial permeability via cortical actin cytoskeletal rearrangement, which is relevant for the pathogenesis of the acute respiratory distress syndrome (ARDS). Based on these observations, the feasibility of pharmacological intervention in the sphingolipid pathway to influence disease development and progression is presently explored, with promising early results. The prospect of new strategies to prevent and repair lung disease by interfering with sphingolipid metabolism is exciting and could potentially reduce morbidity and mortality in patients with severe lung disorders.

INTRODUCTION

Sphingolipids are structure-bearing components of the cell membrane which have been shown to function as messenger molecules, exhibiting effects on cell proliferation, apoptosis, cell contact and adhesion, endothelial barrier function and playing a role during the immune response[1–9]. They have recently been identified as an important class of molecules involved in a variety of diseases, such as atherosclerosis, chronic heart failure[5], asthma[10], diabetes, sepsis, cystic fibrosis, COPD[11], Alzheimer's disease[12] and cancer[13]. Emerging evidence also suggests an important role for sphingolipids in lung development and in damage and repair processes after early lung injury. An important process in the development of the human lung is alveolarization, which occurs between 36 weeks of pregnancy and 2 years postnatally, when secondary septa subdivide the immature saccules into smaller alveolar units[14–16] to increase the surface area for gas exchange. Between birth and 3 years of age, the capillary monolayer is formed in these septa, thereby reducing the septal thickness to improve gas exchange properties[17]. A host of growth factors, morphogens, receptors, transcription factors, hormones, cellular processes and physical determinants are crucial during the various stages of lung development[15,18]. Disruption of any of the above mentioned processes during this critical developmental period results in structural and/or functional abnormal lungs, such as can be seen, for instance, in bronchopulmonary dysplasia. This review will focus on the role of sphingolipids during lung development, damage and repair.

BIOLOGICAL IMPORTANCE OF SPHINGOLIPIDS IN THE LUNG

Sphingolipids consist of a hydrophobic sphingoid long chain base (sphingosine, sphinganine or phytosphingosine) and a hydrophilic fatty acid that varies in chain length, degree of hydroxylation and saturation, creating a large variety in possible sphingolipid composition[19,20]. Two important sphingolipids are ceramide and sphingosine-1-phosphate (S1P). Ceramide is the centre of sphingolipid metabolism[21], acts as precursor for the creation of all other sphingolipids and also functions as a stress signal for multiple stimuli, such as radiation, ischemia and reperfusion, chemotherapeutics and cytokines[22,23]. S1P functions as a pro-survival signal and promotes cell proliferation and differentiation. Since S1P is generated from ceramide via sphingosine, it has been proposed that these two sphingolipids determine the apoptotic balance[7]. The regulation of sphingolipid metabolism is complicated and involves many enzymes (Figure 1). There are 3 main pathways to create ceramide: *de-novo* synthesis from serine and palmitoyl CoA by serine palmitoyltranferase; breakdown of sphingomyelin by acid or neutral sphingomyelinases and production from sphingosine by ceramide synthase. Spingosine can also be converted into S1P by sphingosine kinase. Various sphingolipids play an important role in cellular homeostasis. Ceramide leads to cell-cycle arrest and apoptosis, whereas S1P has an opposite role, facilitating proliferation and differentiation of cells. Therefore, ceramide and S1P are considered as a pro- and anti-apoptotic 'rheostat'[24,25]. The interplay between these two processes

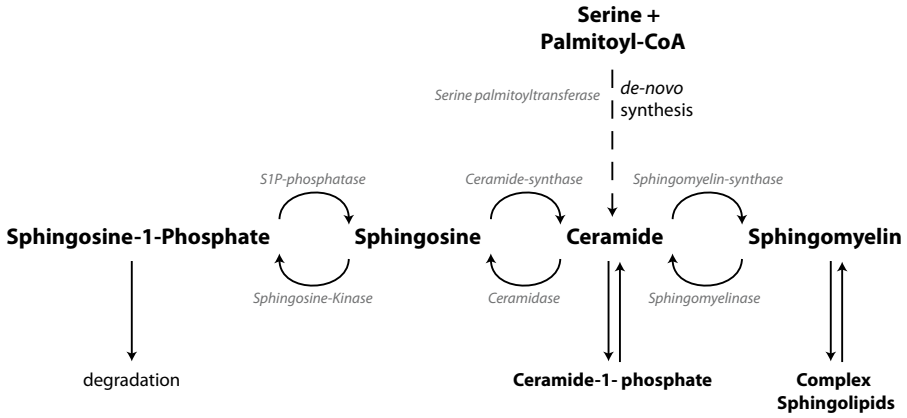

Figure 1. *Pathway of sphingolipid metabolism. Enzymes are marked with italics.*

determines the formation of lung structure, both macroscopically and on a cellular level, during all stages of lung development. Based on these findings, sphingolipid research has intensified. Animal models showed altered sphingolipid levels in LPS-induced macrophage dysfunction[26], colitis[27], melanoma[28], ischemia-reperfusion injury[29] and spinal cord injury[30]. In the lung, sphingolipids have been shown to be involved in vascular permeability, allergic response and apoptosis[31]. Altered sphingolipid levels have been shown to play a role in hyperoxia-induced lung injury or bronchopulmonary dysplasia[32], radiation-induced lung injury[33], cigarette-smoke induced lung injury[34–36], cystic fibrosis[37], asthma[38,39] and pulmonary infection, stressing the biological importance of sphingolipid metabolism in lung disease (Table 1 shows an overview of sphingolipids in lung disease).

SPHINGOMYELIN AS BIOMARKER FOR FETAL LUNG DEVELOPMENT

Alveolar sphingomyelin levels are thought to remain constant for the entire gestational period[40]. Dipalmitoylphosphatidylcholine (DPPC) is the main surface-active component in the alveolar lining during fetal development and its level remains constant for most of the gestation, and increases from week 32-33 towards term[41]. Since the alveolar compartment and the amniotic fluid are connected[42], phosphatidylcholine (lecithin) levels also increase in the amniotic fluid towards term. The lecithin/sphingomyelin ratio in amniotic fluid is traditionally considered as a marker of lung maturation[43]. In 1997, Longo *et al.* had an in-depth look at sphingomyelin levels during lung development in rats and actually found that sphingomyelin and sphingosine levels in lung homogenates and microsomes increased 2-fold and 6-fold, respectively, during fetal lung development, with highest levels at birth[44]. This increase was caused by an increase in serine palmitoyltransferase activity, the rate-limiting enzyme of *de-novo* synthesis of ceramide, the intermediate precursor of sphingomyelin. Acid and neutral sphingomyelinase activity increased during fetal lung development, peaking at day 19, but decreased towards low levels at birth. Ceramidases

Table 1. *Sphingolipids in lung disease.*

Disease / Model Used	Ceramides	S-1-P	Sphingolipids	Effect	Enzyme / Mechanism	Ref.
CFTR-deficiency CF-mouse model	↑	nm	nm	Inflammation ↑ / Apoptosis ↑	Acid sphingomyelinase	9,37,50
LPS-induced lung inflammation mouse model	↑	nm	nm	Inflammation ↑	Serine palmitoyltransferase	51
Hyperoxia-induced BPD mouse model	↑	nm	nm	Inflammation ↑ / Apoptosis ↑	na	32
Fenretinide-induced emphysema rat model	↑	=	Dihydroceramide ↑	Apoptosis ↑	na	75
S1P-recepter antagonist mouse model		↓	nm	Pulmonary vascular endothelial barrier integrity ↓	na	83
Hyperoxia-induced ARDS mouse model	↑	nm	nm	Pulmonary vascular endothelial barrier integrity ↓	Acid sphingomyelinase	84
LPS-induced chorioamnionitis in sheep	↑	nm	nm	Inflammation ↑	Acid sphingomyelinase	88
LPS, lavage and ventilation-induced triple hit model in piglets	↑	nm	nm	Inflammation ↑ / Apoptosis ↑ Pulmonary vascular endothelial barrier integrity ↓	Acid sphingomyelinase	89,90
Radiation-induced lung injury mouse model	↑	=	nm	Inflammation ↑ / Apoptosis ↑ Pulmonary vascular endothelial barrier integrity ↓	na	33
Cigarette-smoke cell culture model (rat microvascular cells)	↑	=	nm	Apoptosis ↑ / Pulmonary vascular endothelial barrier integrity ↓	Neutral sphingomyelinase	35,36
VEGFR inhibition emphysema in mice	↑	nm	nm	Apoptosis ↑	RTP801	34
Cell culture model	nm	↑	Sphingosine ↓	Mast cell activation ↑	Sphingosine + MAP kinase	100
Cell culture model (human airway smooth muscle (ASM) cells)	nm	↑	nm	Inflammation ↑ / ASM proliferation + contraction / IL-6 secretion ↑	MAP-kinase / cAMP / calcium transport/ mobilization	10,91

nm = not measured, na=not analyzed

showed a similar pattern. These findings are similar to those found in the rabbit[45,46]. In contrast, sphingomyelin levels decreased during fetal lung development in monkey and lamb[47,48]. The above described variations in sphingolipid levels during gestation suggests that the paradigm of constant sphingolipid levels throughout pregnancy needs to be studied in humans in more detail, and perhaps reconsidered[40].

SPHINGOLIPIDS AND LUNG INFLAMMATION

Research on sphingolipids in lung disease has focused on their role in inflammation. An important finding was the accumulation of ceramide in the lungs of cystic fibrosis (CF) patients, as measured by histological staining on resected lungs when these patients received a bilateral lung transplantation due to severe CF[49]. Donor lungs that were not transplanted were used as controls. The number of neutrophils, detected using neutrophil elastase and myeloperoxidase staining, correlated with the amount of ceramide staining and so did *Pseudomonas aeruginosa* colonization. This was followed by publications in animal models of CF, showing that ceramide accumulation caused inflammation and increased the susceptibility to lung infection in CF mice[50]. Becker *et al.* showed that the levels of inflammation correlated to the amount of acid sphingomyelinase (ASMase) activity[37], and that inhibition of ASMase reduced inflammation[9]. Dechecchi *et al.* showed that an inhibitor of *de-novo* ceramide synthesis decreased lipopolysaccharide-induced pulmonary inflammation in CF mice[51]. Inflammation is an important process in chorioamnionitis, a common cause of preterm birth[52,53]. Most premature deliveries before 30 weeks of gestation exhibit histological chorioamnionitis[54]. Severe histological chorioamnionitis is associated with an increased risk for developing bronchopulmonary dysplasia (BPD)[55,56]. Animal models of chorioamnionitis show impaired alveolarization[57–59] and disrupted microvasculature[60] in the fetal lungs, most likely caused by the increased production of pro-inflammatory cytokines, together with the massive influx of inflammatory cells in the amniotic fluid and chorioamnion[61]. The role of sphingolipids in the pathogenesis of BPD is therefore of great interest, as it may represent a target for prevention and treatment of this severe condition.

SPHINGOLIPIDS AND BPD

BPD is a chronic lung disease that develops in a subset of preterm infants who were subjected to mechanical ventilation and/or supplemental oxygen[62]. The disease was originally described by Northway *et al.* in 1967[63] and was characterized by a heterogeneous pattern of persistent airway inflammation, parenchymal fibrosis, edema and abnormal pulmonary vascular development. The nature of BPD has changed in the last 40 years due to advancements in neonatal care, such as less invasive ventilation, the use of steroids and exogenous surfactant and better nutrition. This has made it possible that extreme prematures now survive, and these often suffer from an arrest in lung development with interrupted septa-

tion, vascular abnormalities, and reduced alveolar numbers and increased alveolar size, also called 'new' BPD[64,65]. BPD is a clinical diagnosis, and the incidence of 'new' BPD is estimated between 7 and 52% in infants born with a birthweight between 1500 and 500g, respectively[66]. BPD has a multifactorial origin with prematurity, often complicated by chorioamnionitis, oxygen toxicity, barotrauma from mechanical ventilation, lung infection and malnutrition being the most important risk factors[67]. BPD patients show lower lung volumes and decreased forced expiratory flows, during the first 2 years of life[68], and lung function abnormalities often persist into adolescence and adulthood[69,70]. BPD survivors often have nonspecific and asthma-like respiratory symptoms and may develop chest deformities including flaring of the ribs and a funnel chest. Abnormal radiological findings are present in infants with BPD and persist into adulthood. A high prevalence of airtrapping[71], parenchymal abnormalities[72] and emphysema-like structural defects have been reported in over 80% of adult survivors of 'old' BPD[73,74], and it seems likely that long-term consequences of 'new' BPD will be similar if not worse, due to the lower gestational age that these 'new' BPD patients present themselves, as shown in CT-images of a 12 year old BPD patient (Figure 2). Is it possible that sphingolipids are involved in the pathogenesis of BPD? As we have recently demonstrated, altered sphingolipid levels do play a role

Figure 2. *Spirometer controlled inspiratory (A,C) and expiratory (B,D) chest CT scan of a 12 year old male patient with severe BPD in the axial and coronal plane. Note the emphysematous aspect of the left lung. Most functional lung tissue is present in the right lung as indicated by the density changes from inspiration to expiration. The lung architecture is severely distorted. The mosaic pattern of the right lung is caused by redistribution of blood flow through the healthier regions of the lung.*

in hyperoxia-induced lung injury or bronchopulmonary dysplasia[32]. We reported a rise in ceramide levels during hyperoxia exposure in newborn mice, correlating with decreased lung function, which returned to control levels during recovery in normoxia. By adding an artificial S1P analog, D-sphingosine, during the recovery period, ceramide levels decreased more rapidly and histological abnormalities were ameliorated. Recently, ceramide upregulation has been shown to decrease Vascular Endothelial Growth Factor (VEGF) via suppression of Hypoxia-Inducible Factor(HIF)-1α, suggesting a role for sphingolipids in VEGF regulation[75]. VEGF has an important role in pulmonary vascular development. Deletion of a single VEGF allele during embryogenesis is lethal[76] and decreased postnatal VEGF expression leads to reduced alveolarization[77,78]. Decreased levels of VEGF have been measured in a rodent animal model of BPD[79] and inhibition of VEGF-receptor 1 leads to a disorganized alveolar capillary network[80]. Together these findings suggest that sphingolipids may regulate lung vascular development via VEGF. Ceramides also decreased surfactant protein B (SP-B) formation by reducing DNA binding and transcriptional activity of Nkx2-1, an important transcription factor for SP-B gene expression[81], thereby contributing to decreased SP-B production in a lung already deficient in surfactant. The possible involvement of the sphingolipid pathway in several aspects of the development of BPD is highly relevant, as to date there is no treatment available for BPD, and intervening via the sphingolipid pathway could provide a new approach to prevent or reduce neonatal lung damage in prematures.

SPHINGOLIPIDS AND ACUTE RESPIRATORY DISTRESS SYNDROME

Acute Respiratory Distress Syndrome (ARDS) is an important cause of death in preterm infants and is characterized by decreased surfactant levels and a disrupted endothelial barrier, resulting in pulmonary edema. Endothelial barrier function is regulated by sphingolipids via two distinct pathways. The first pathway is through S1P that binds to $S1P_1$ receptors on endothelial cells which stabilizes barrier function via α-actinin-1 and 4 expression in caveolin-rich domains which results in cortical actin cytoskeletal rearragement[82]. Blocking of this pathway leads to pulmonary edema[83]. The second pathway is ASMase upregulation, leading to increased ceramide formation. Increased ceramide formation has been shown to induce inflammasome activation resulting in IL-1β production that damages the epithelium, leading to TNF-α and IL-6 production and combined with a decreased trans-epithelial resistance, leads to increased pulmonary vascular endothelial leakage[84]. One pathway to influence ASMase levels is via Caveolin-1, a resident protein of lipid rafts and caveolae of airway epithelium, smooth muscle cells, fibroblasts and pulmonary vasculature[85] that plays a role in protein trafficking and signal transduction[86]. Caveolins are downregulated in many lung diseases[87] and have been shown to increase ASMase levels and thereby ceramide production in LPS-induced chorioamnionitis[88]. Blocking the ASMase pathway decreased pulmonary edema formation[84,89,90]. These findings suggest that sphingolipids should be studied further as a therapeutic target in ARDS.

SPHINGOLIPIDS IN OTHER LUNG DISORDERS

Exposure of adult mice to radiation increased expression of sphingosine kinase and ceramide levels in broncho-alveolar lavage, plasma and lung tissue. These sphingolipid changes were correlated with increased vascular endothelial leakage and more severe histological abnormalities and were abrogated with the use of S1P analogs[33].

Sphingolipid metabolism also plays a role during cigarette-smoke induced lung injury[34–36]. Cigarette smoke has been shown to upregulate neutral sphingomyelinase (nSMase), leading to increased ceramide production and alveolar cell apoptosis. This increase in nSMase is blocked by the addition of glutathione, suggesting a role for H_2O_2-production as a trigger for nSMase expression. Cigarette smoke also induces the expression of RTP801, a stress response protein that triggers NF-κB mediated inflammation. RTP801 and ceramide function as mutual up-regulators, thereby further increasing inflammation and alveolar cell apoptosis[34]. Apart from increased apoptosis, cigarette smoke, via ceramide upregulation, leads to p38 mitogen-activated protein(MAP) kinase, JNK and Rho kinase activation, which causes actin cytoskeletal rearrangement, loss of junctional protein zonula occludens-1 and intercellular gap formation. All these effects were abolished by the addition of glutathione and nSMase inhibition using GW4869[36].

Although increased S1P is beneficial to most diseases in which sphingolipid levels are altered, findings in asthma also showed its potentially negative effects. Segmental airway challenge and BAL from asthma patients showed increased levels of S1P when compared to controls, and correlated with the amount of airway inflammation as measured by inflammatory cell number and differentiation count in the BAL. Human airway smooth muscle cells express S1P receptors, and S1P increases phosphoinositide turnover and intracellular calcium mobilization, two processes which play an important role in airway smooth muscle contraction. S1P has also been shown to modulate adenylate cyclase acitivity and cAMP accumulation and although inhibiting TNF-α, it induced IL-6 secretion. Another possible role for increased S1P levels in asthmatics is its mitogenic effect, playing a role in the remodelling that takes place in asthma[10]. The role of S1P in asthma has been extensively reviewed by Jolly *et al.*[91] Figure 3 provides an overview of the proposed role of the Ceramide-S1P rheostat during lung injury and repair.

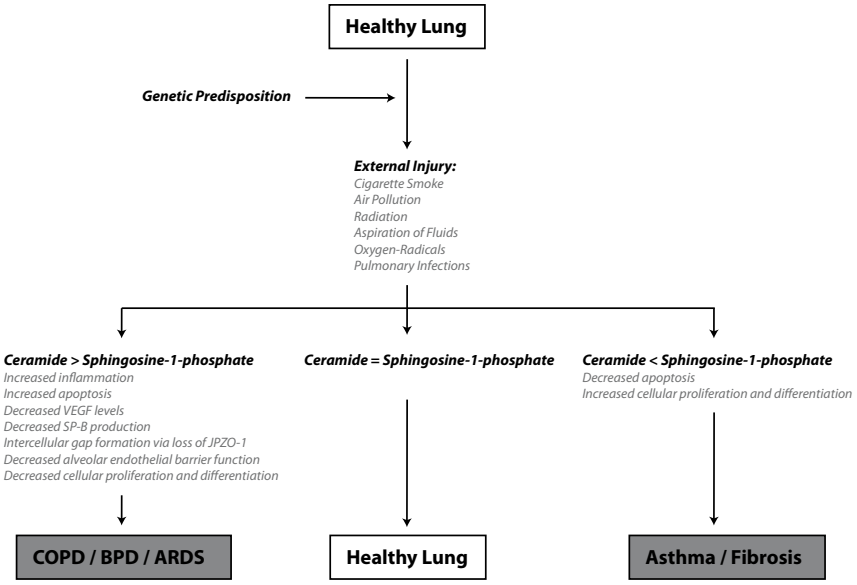

Figure 3. *An overview of the possible roles for ceramides and sphingosine-1-phosphate in lung homeostasis. JPZO-1: junctional protein zonula occludens-1. VEGF: vascular endothelial growth factor. SP-B: surfactant protein B. COPD: chronic obstructive pulmonary disease. BPD: bronchopulmonary dysplasia. ARDS: acute respiratory distress syndrome.*

INTERVENTIONS IN THE SPHINGOLIPID PATHWAY

Since altered sphingolipid levels seem to be involved in many diseases in multiple organ systems, pharmacological interventions have been developed to target sphingolipid metabolism[92–96]. At present, there is some evidence that such interventions are effective. Inhibition of acid sphingomyelinase by amitripyline, trimipramine and desipramine has shown significant improvement in lung function, histology and the incidence of *Pseudomonas aeruginosa* infections in an animal model of cystic fibrosis by decreasing ceramide levels[9]. Lin *et al.* have recently shown that neutrophils from patients with ARDS show elevated intracellular levels of ceramide, and that neutral sphingomyelin inhibition, using sphingolactone, sphingosine kinase inhibitor and p38 MAP-kinase inhibitor, decreased lung inflammation and increased survival in an LPS model of ARDS[97]. We found that S1P analog D-sphingosine promoted recovery of ceramide levels and histology, but not lung function, after hyperoxia-induced alveolar arrest in a mouse model of BPD[32]. As described earlier, S1P analogs also protect mice from radiation induced lung injury[33] and has been shown to improve alveolar cell survival and decrease alveolar airspace enlargement in a vascular endothelial growth factor receptor (VEGFR)-inhibitor induced model of pulmonary emphysema[98]. Inhibiting serine palmitoyltransferase by using Myriocin (Cayman Chemicals, Ann Arbor, MI) decreased lung inflammation and fibrosis, measured by

collagen and α-smooth muscle actin expression, after thoracic radiation with 20 Gy and delayed the onset of radiation-induced death from 15 to 18 weeks[99].

CONCLUSION

Sphingolipids play an important role in many biological processes, including apoptosis and proliferation, inflammation, vascular barrier integrity and smooth muscle cell contraction. The actions of S1P promote proliferation and increased vascular barrier integrity, whereas ceramide enhances apoptosis and decreases vascular barrier integrity. These effects have been shown in a number of human and animal disease models, in relation to severe and prevalent diseases such as COPD, BPD, asthma and ARDS. Interventions in the sphingolipid pathway aimed at restoring the balance between ceramide and S1P levels have produced promising results in animal models and pharmacological strategies to restore the balance of S1P and ceramide should now be tested in humans. Studies in newborns are specifically required to establish effects in BPD, and this will be a challenge. There is good reason to pursue the clinical use of sphingolipid inhibitors, as they may offer protection and benefit for patients with a variety of diseases that are associated with lung damage and repair, for which limited alternative treatments are available.

ACKNOWLEDGEMENTS

The authors thank Prof. H.A.W.M. Tiddens, Erasmus University Medical Center-Sophia Children's Hospital for providing us with the chest CT images.

REFERENCES

1. Olivera A, Rivera J. Sphingolipids and the Balancing of Immune Cell Function : Lessons from the Mast Cell. *The journal of immunology*. 2005:1153–1158.
2. Spiegel S, Milstien S. Sphingosine-1-phosphate: an enigmatic signalling lipid. *Nature reviews. Molecular cell biology*. 2003;4(5):397–407.
3. Waeber C, Blondeau N, Salomone S. Vascular sphingosine-1-phosphate S1P1 and S1P3 receptors. *Drug news & perspectives*. 2004;17(6):365–82.
4. Rosen H, Goetzl EJ. Sphingosine 1-phosphate and its receptors: an autocrine and paracrine network. *Nature reviews. Immunology*. 2005;5(7):560–70.
5. Gulbins E, Li PL. Physiological and pathophysiological aspects of ceramide. *American journal of physiology. Regulatory, integrative and comparative physiology*. 2006;290(1):R11–26.
6. Thon L, Möhlig H, Mathieu S, et al. Ceramide mediates caspase-independent programmed cell death. *The FASEB journal*. 2005;19(14):1945–56.
7. Taha TA, Mullen TD, Obeid LM. A house divided: ceramide, sphingosine, and sphingosine-1-phosphate in programmed cell death. *Biochimica et biophysica acta*. 2006;1758(12):2027–36.
8. McVerry BJ, Garcia JGN. Endothelial cell barrier regulation by sphingosine 1-phosphate. *Journal of cellular biochemistry*. 2004;92(6):1075–85.
9. Becker KA, Riethmuller J, Luth A, Doring G, Kleuser B, Gulbins E. Acid sphingomyelinase inhibitors normalize pulmonary ceramide and inflammation in cystic fibrosis. *American journal of respiratory cell and molecular biology*. 2010;42(6):716–724.
10. Ammit AJ, Hastie AT, Edsall LC, et al. Sphingosine 1-phosphate modulates human airway smooth muscle cell functions that promote inflammation and airway remodeling in asthma. *The FASEB journal*. 2001;15(7):1212–4.
11. Lahiri S, Futerman a H. The metabolism and function of sphingolipids and glycosphingolipids. *Cellular and molecular life sciences : CMLS*. 2007;64(17):2270–84.
12. He X, Huang Y, Li B, Gong C-X, Schuchman EH. Deregulation of sphingolipid metabolism in Alzheimer's disease. *Neurobiology of aging*. 2010;31(3):398–408.
13. Ponnusamy S, Meyers-Needham M, Senkal CE, et al. Sphingolipids and cancer: ceramide and sphingosine-1-phosphate in the regulation of cell death and drug resistance. *Future oncology*. 2010;6(10):1603–24.
14. Roth-Kleiner M, Post M. Genetic Control of Lung Development. *Biology of the Neonate*. 2003;84(1):83–88.
15. Rutter M, Post M. *Molecular basis for normal and abnormal lung development*. (Bancalari E, ed.). Philadelphia, PA: Saunders Elsevier; 2008:3–42.
16. Warburton D. Lung organogenesis. *Curr. Top. Dev. Biol.* 2010;90:73–158.
17. Burri PH. *Lung development and pulmonary angiogenesis*. (Gaultier C, Post M, eds.). New York: Oxford University Press; 1999:122–151.
18. Joza S, Post M. *Development of the respiratory system (including the preterm infant)*.; 2012.
19. Futerman AH, Hannun Y a. The complex life of simple sphingolipids. *EMBO reports*. 2004;5(8):777–82.
20. Dickson RC, Lester RL. Sphingolipid functions in Saccharomyces cerevisiae. *Biochimica et biophysica acta*. 2002;1583(1):13–25.
21. Hannun Y a, Obeid LM. The Ceramide-centric universe of lipid-mediated cell regulation: stress encounters of the lipid kind. *The Journal of biological chemistry*. 2002;277(29):25847–50.
22. Nikolova-Karakashian MN, Rozenova KA. Ceramide in stress response. *Advances in experimental medicine and biology*. 2010;688:86–108.

23. Hannun YA. Functions of ceramide in coordinating cellular responses to stress. *Science*. 1996;274(5294):1855–9.
24. Payne SG, Milstien S, Spiegel S. Sphingosine-1-phosphate: dual messenger functions. *FEBS letters*. 2002;531(1):54–7.
25. Morita Y, Tilly JL. Sphingolipid regulation of female gonadal cell apoptosis. *Annals of the New York Academy of Sciences*. 2000;905:209–20.
26. Schilling JD, Machkovech HM, He L, et al. Palmitate and LPS trigger synergistic ceramide production in primary macrophages. *The Journal of biological chemistry*. 2012.
27. Bauer J, Liebisch G, Hofmann C, et al. Lipid alterations in experimental murine colitis: role of ceramide and imipramine for matrix metalloproteinase-1 expression. *PloS one*. 2009;4(9):e7197.
28. Lee Y-S, Choi K-M, Lee S, et al. Myriocin, a serine palmitoyltransferase inhibitor, suppresses tumor growth in a murine melanoma model by inhibiting de novo sphingolipid synthesis. *Cancer biology & therapy*. 2012;13(2):92–100.
29. Llacuna L, Mari M, Garcia-Ruiz C, Fernandez-Checa JC, Morales A. Critical role of acidic sphingomyelinase in murine hepatic ischemia-reperfusion injury. *Hepatology*. 2006;44(3):561–572.
30. Cuzzocrea S, Deigner HP, Genovese T, et al. Inhibition of ceramide biosynthesis ameliorates pathological consequences of spinal cord injury. *Shock*. 2009;31(6):635.
31. Yang Y, Uhlig S. The role of sphingolipids in respiratory disease. *Therapeutic advances in respiratory disease*. 2011;5(5):325–44.
32. Tibboel J, Joza S, Reiss I, Jongste JC De, Post M. Amelioration of hyperoxia-induced lung injury using a sphingolipid-based intervention. European Respiratory Journal. 2012; (416).. 2012;(416).
33. Mathew B, Jacobson JR, Berdyshev E, et al. Role of sphingolipids in murine radiation-induced lung injury: protection by sphingosine 1-phosphate analogs. *The FASEB journal*. 2011:1–13.
34. Kamocki K, Van Demark M, Fisher A, et al. RTP801 Is Required for Ceramide-Induced Cell-Specific Death in the Murine Lung. *American journal of respiratory cell and molecular biology*. 2013;48(1):87–93.
35. Levy M, Khan E. Neutral sphingomyelinase 2 is activated by cigarette smoke to augment ceramide-induced apoptosis in lung cell death. *American Journal of Physiology-Lung Cellular and Molecular Physiology*. 2009;(29):125–133.
36. Schweitzer KS, Hatoum H, Brown MB, et al. Mechanisms of lung endothelial barrier disruption induced by cigarette smoke: role of oxidative stress and ceramides. *American Journal of Physiology-Lung Cellular and Molecular Physiology*. 2011;301(6):L836–46.
37. Becker KA, Tummler B, Gulbins E, Grassmé H. Accumulation of ceramide in the trachea and intestine of cystic fibrosis mice causes inflammation and cell death. *Biochemical and biophysical research communications*. 2010;403(3-4):368–374.
38. Idzko M, Hammad H. Local application of FTY720 to the lung abrogates experimental asthma by altering dendritic cell function. *Journal of Clinical Investigation*. 2006;116(11):2935–2944.
39. Sawicka E, Zuany-Amorim C, Manlius C, et al. Inhibition of Th1- and Th2-mediated airway inflammation by the sphingosine 1-phosphate receptor agonist FTY720. *Journal of immunology*. 2003;171(11):6206–14.
40. Gluck L, Kulovich M V, Borer RC, Brenner PH, Anderson GG, Spellacy WN. Diagnosis of the respiratory distress syndrome by amniocentesis. *American journal of obstetrics and gynecology*. 1971;109(3):440–5.
41. Gluck L, Motoyama E, Smits H, Kulovich M. The Biochemical Development of Surface Activity in Mammalian Lung. *Pediatric research*. 1970:352–364.
42. Scarpelli EM. The lung, tracheal fluid, and lipid metabolism of the fetus. *Pediatrics*. 1967;40(6):951–61.

43. Whitfield C, Chan W. Amniotic fluid lecithin: sphingomyelin ratio and fetal lung development. *British medical Journal*. 1972;(April):85–86.
44. Longo C a, Tyler D, Mallampalli RK. Sphingomyelin metabolism is developmentally regulated in rat lung. *American journal of respiratory cell and molecular biology*. 1997;16(5):605–12.
45. Rooney SA, Wai-Lee TS, Gobran L, Motoyama EK. Phospholipid content, composition and biosynthesis during fetal lung development in the rabbit. *Biochimica et biophysica acta*. 1976;431(3):447–58.
46. Hallman M, Gluck L. Formation of acidic phospholipids in rabbit lung during perinatal development. *Pediatric research*. 1980;14(11):1250–9.
47. Fujiwara T, Adams FH, el-Salawy A, Sipos S. "Alveolar" and whole lung phospholipids of newborn lambs. *Proceedings of the Society for Experimental Biology and Medicine*. 1968;127(3):962–9.
48. Perelman RH, Engle MJ, Kemnitz JW, Kotas R V, Farrell PM. Biochemical and physiological development of fetal rhesus lung. *Journal of applied physiology: respiratory, environmental and exercise physiology*. 1982;53(1):230–5.
49. Brodlie M, McKean MC, Johnson GE, et al. Ceramide is increased in the lower airway epithelium of people with advanced cystic fibrosis lung disease. *American journal of respiratory and critical care medicine*. 2010;182(3):369–75.
50. Teichgräber V, Ulrich M, Endlich N, et al. Ceramide accumulation mediates inflammation, cell death and infection susceptibility in cystic fibrosis. *Nature Medicine*. 2008;14(4):382–391.
51. Dechecchi MC, Nicolis E, Mazzi P, et al. Modulators of sphingolipid metabolism reduce lung inflammation. *American journal of respiratory cell and molecular biology*. 2011;45(4):825–33.
52. Romero R, Espinoza J. The role of inflammation and infection in preterm birth. *Seminars in reproduction medicine*. 2007.
53. Bastek J a, Gómez LM, Elovitz M a. The role of inflammation and infection in preterm birth. *Clinics in perinatology*. 2011;38(3):385–406.
54. Goldenberg R, Hauth J, Andrews W. Intrauterine infection and preterm delivery. *New England Journal of Medicine*. 2000;342(20):1500–1507.
55. Kasper DC, Mechtler TP, Böhm J, et al. In utero exposure to Ureaplasma spp. is associated with increased rate of bronchopulmonary dysplasia and intraventricular hemorrhage in preterm infants. *Journal of perinatal medicine*. 2011;39(3):331–6.
56. Viscardi RM, Muhumuza CK, Rodriguez A, et al. Inflammatory markers in intrauterine and fetal blood and cerebrospinal fluid compartments are associated with adverse pulmonary and neurologic outcomes in preterm infants. *Pediatric research*. 2004;55(6):1009–17.
57. Willet KE, Kramer BW, Kallapur SG, et al. Intra-amniotic injection of IL-1 induces inflammation and maturation in fetal sheep lung. *American Journal of Physiology-Lung Cellular and Molecular Physiology*. 2002;282(3):L411–20.
58. Ueda K, Cho K, Matsuda T, et al. A rat model for arrest of alveolarization induced by antenatal endotoxin administration. *Pediatric research*. 2006;59(3):396–400.
59. Kallapur SG, Bachurski CJ, Le Cras TD, Joshi SN, Ikegami M, Jobe AH. Vascular changes after intra-amniotic endotoxin in preterm lamb lungs. *American Journal of Physiology-Lung Cellular and Molecular Physiology*. 2004;287(6):L1178–85.
60. Jobe a H, Ikegami M. Mechanisms initiating lung injury in the preterm. *Early human development*. 1998;53(1):81–94.
61. Kallapur S, Willet K. Intra-amniotic endotoxin: chorioamnionitis precedes lung maturation in preterm lambs. *American journal of physiology - Lung cellular and molecular physiology*. 2001.
62. Abman SH, Mourani PM, Sontag M. Bronchopulmonary dysplasia: a genetic disease. *Pediatrics*. 2008;122(3):658–9.
63. Northway WH, Rosan RC, Porter DY. Pulmonary disease following respirator therapy of hyaline-membrane disease. Bronchopulmonary dysplasia. *The New England journal of medicine*. 1967;276(7):357–68.

64. Jobe AJ. The new BPD: an arrest of lung development. *Pediatric research*. 1999;46(6):641.
65. Jobe A. The new bronchopulmonary dysplasia. *Current opinion in pediatrics*. 2011;23(2):167–172.
66. Ehrenkranz R a, Walsh MC, Vohr BR, et al. Validation of the National Institutes of Health consensus definition of bronchopulmonary dysplasia. *Pediatrics*. 2005;116(6):1353–60.
67. Chess PR, D'Angio CT, Pryhuber GS, Maniscalco WM. Pathogenesis of bronchopulmonary dysplasia. *Seminars in perinatology*. 2006;30(4):171–8.
68. Fakhoury KF, Sellers C, Smith EO, Rama J a, Fan LL. Serial measurements of lung function in a cohort of young children with bronchopulmonary dysplasia. *Pediatrics*. 2010;125(6):e1441–7.
69. Filippone M, Bonetto G. Childhood course of lung function in survivors of bronchopulmonary dysplasia. *JAMA: the journal of the american medical association*. 2009:1–3.
70. Fawke J, Lum S, Kirkby J, et al. Lung function and respiratory symptoms at 11 years in children born extremely preterm: the EPICure study. *American journal of respiratory and critical care medicine*. 2010;182(2):237–45.
71. Aquino S, Schechter M, Chiles C, Ablin D, Chipps B, Webb W. High-resolution inspiratory and expiratory CT in older children and adults with bronchopulmonary dysplasia. *American Journal of Roentgenology*. 1999;173(4):963.
72. Aukland SM, Rosendahl K, Owens CM, Fosse KR, Eide GE, Halvorsen T. Neonatal bronchopulmonary dysplasia predicts abnormal pulmonary HRCT scans in long-term survivors of extreme preterm birth. *Thorax*. 2009;64(5):405–10.
73. Wong PM, Lees AN, Louw J, et al. Emphysema in young adult survivors of moderate-to-severe bronchopulmonary dysplasia. *European Respiratory Journal*. 2008;32(2):321.
74. Wong P, Murray C, Louw J, French N, Chambers D. Adult bronchopulmonary dysplasia: Computed tomography pulmonary findings. *Journal of medical imaging and radiation oncology*. 2011;55(4):373–8.
75. Yasuo M, Mizuno S, Allegood J, et al. Fenretinide causes emphysema, which is prevented by sphingosine 1-phoshate. *PloS one*. 2013;8(1):e53927.
76. Ferrara N, Carver-Moore K, Chen H, et al. Heterozygous embryonic lethality induced by targeted inactivation of the VEGF gene. *Nature*. 1996;380(6573):439–42.
77. Jakkula M, Le Cras TD, Gebb S, et al. Inhibition of angiogenesis decreases alveolarization in the developing rat lung. *American Journal of Physiology-Lung Cellular and Molecular Physiology*. 2000;279(3):L600–7.
78. Le Cras TD, Markham NE, Tuder RM, Voelkel NF, Abman SH. Treatment of newborn rats with a VEGF receptor inhibitor causes pulmonary hypertension and abnormal lung structure. *American Journal of Physiology-Lung Cellular and Molecular Physiology*. 2002;283(3):L555–62.
79. Hosford GE, Olson DM. Effects of hyperoxia on VEGF, its receptors, and HIF-2alpha in the newborn rat lung. *American Journal of Physiology-Lung Cellular and Molecular Physiology*. 2003;285(1):L161–8.
80. Yamamoto Y, Shiraishi I, Dai P, Hamaoka K, Takamatsu T. Regulation of embryonic lung vascular development by vascular endothelial growth factor receptors, Flk-1 and Flt-1. *Anatomical record*. 2007;290(8):958–73.
81. Sparkman L, Chandru H, Boggaram V. Ceramide decreases surfactant protein B gene expression via down-regulation of TTF-1 DNA binding activity. *American Journal of Physiology-Lung Cellular and Molecular Physiology*. 2006;290(2):L351–8.
82. Singleton P a, Dudek SM, Chiang ET, Garcia JGN. Regulation of sphingosine 1-phosphate-induced endothelial cytoskeletal rearrangement and barrier enhancement by S1P1 receptor, PI3 kinase, Tiam1/Rac1, and alpha-actinin. *FASEB journal*. 2005;19(12):1646–56.
83. Sanna MG, Wang S-K, Gonzalez-Cabrera PJ, et al. Enhancement of capillary leakage and restoration of lymphocyte egress by a chiral S1P1 antagonist in vivo. *Nature chemical biology*. 2006;2(8):434–41.

84. Kolliputi N, Galam L, Parthasarathy PT, Tipparaju SM, Lockey R. NALP-3 inflammasome silencing attenuates ceramide induced transepithelial permeability. *Journal of cellular physiology*. 2011;(November):1–26.
85. Jin Y, Lee S-J, Minshall RD, Choi AMK. Caveolin-1: a critical regulator of lung injury. *American Journal of Physiology-Lung Cellular and Molecular Physiology*. 2011;300(2):L151–60.
86. Williams TM, Lisanti MP. The Caveolin genes: from cell biology to medicine. *Annals of medicine*. 2004;36(8):584–95.
87. Gosens R, Mutawe M, Martin S, et al. Caveolae and caveolins in the respiratory system. *Current molecular medicine*. 2008;8(8):741–53.
88. Kunzmann S, Collins JJP, Yang Y, et al. Antenatal inflammation reduces expression of caveolin-1 and influences multiple signaling pathways in preterm fetal lungs. *American journal of respiratory cell and molecular biology*. 2011;45(5):969–76.
89. Preuss S, Stadelmann S, Omam FD, et al. Inositol-trisphosphate reduces alveolar apoptosis and pulmonary edema in neonatal lung injury. *American journal of respiratory cell and molecular biology*. 2012;47(2):158–69.
90. Von Bismarck P, Wistädt C-FG, Klemm K, et al. Improved pulmonary function by acid sphingomyelinase inhibition in a newborn piglet lavage model. *American journal of respiratory and critical care medicine*. 2008;177(11):1233–41.
91. Jolly PS, Rosenfeldt HM, Milstien S, Spiegel S. The roles of sphingosine-1-phosphate in asthma. *Molecular immunology*. 2002;38(16-18):1239–45.
92. Canals D, Perry DM, Jenkins RW, Hannun Y a. Drug targeting of sphingolipid metabolism: sphingomyelinases and ceramidases. *British journal of pharmacology*. 2011;163(4):694–712.
93. Kornhuber J, Tripal P, Reichel M, et al. Identification of new functional inhibitors of acid sphingomyelinase using a structure-property-activity relation model. *Journal of medicinal chemistry*. 2008;51(2):219–37.
94. Kornhuber J, Tripal P, Reichel M, et al. Functional Inhibitors of Acid Sphingomyelinase (FIASMAs): a novel pharmacological group of drugs with broad clinical applications. *Cellular Physiology and Biochemistry*. 2010;26(1):9–20.
95. Proksch D, Klein JJ, Arenz C. Potent inhibition of Acid ceramidase by novel B-13 analogues. *Journal of lipids*. 2011;2011(type 1):971618.
96. Wascholowski V, Giannis A. Sphingolactones: selective and irreversible inhibitors of neutral sphingomyelinase. *Angewandte Chemie (International ed. in English)*. 2006;45(5):827–30.
97. Lin W-C, Lin C-F, Chen C-L, Chen C-W, Lin Y-S. Inhibition of Neutrophil Apoptosis via Sphingolipid Signaling in Acute Lung Injury. *The Journal of pharmacology and experimental therapeutics*. 2011.
98. Diab KJ, Adamowicz JJ, Kamocki K, et al. Stimulation of sphingosine 1-phospate signaling as an alveolar cell survival strategy in emphysema: Online supplement. *American journal of respiratory and critical care medicine*. 2010.
99. Gorshkova I, Zhou T, Mathew B, et al. Inhibition of serine palmitoyltransferase delays the onset of radiation-induced pulmonary fibrosis through the negative regulation of sphingosine kinase-1 expression. *Journal of lipid research*. 2012;53(8):1553–68.
100. Prieschl EE, Csonga R, Novotny V, Kikuchi GE, Baumruker T. The balance between sphingosine and sphingosine-1-phosphate is decisive for mast cell activation after Fc epsilon receptor I triggering. *The Journal of experimental medicine*. 1999;190(1):1–8.

Chapter 3

Amelioration of Hyperoxia-induced Lung Injury using a Sphingolipid-based Intervention

Jeroen Tibboel[1,3]
Stephen Joza[1,2]
Irwin Reiss[3]
Johan C. de Jongste[3]
Martin Post[1,2]

[1] Dept. of Physiology and Experimental Medicine, Hospital for Sick Children, Toronto, Canada.
[2] Dept. of Laboratory Medicine and Pathobiology, University of Toronto, Toronto, Canada.
[3] Dept. of Pediatrics, Erasmus University Medical Center – Sophia Children's Hospital, Rotterdam, the Netherlands.

Eur Resp J. 2013 Sep;42(3):776-84

ABSTRACT

Aim: To characterize lung function and broncho-alveolar lavage sphingolipid profile of newborn mice during hyperoxia exposure and recovery in room air, and to examine the effect of D-sphingosine supplementation during recovery.
Methods: Newborn mice were exposed to 80% O_2 for 4 weeks and allowed to recover in room air for another 4 weeks. Lung function measurements and morphometrical analysis of lung tissue were performed and BAL fluid was collected during hyperoxia and recovery with and without D-sphingosine supplementation.
Results: Hyperoxia exposure altered lung function, which partially recovered in room air. Lungs had fewer and enlarged alveoli which persisted during recovery. Multiple sphingolipids were significantly increased after hyperoxia. Ceramides were increased after 2 weeks of recovery, but normalized to control values after 4 weeks. Addition of D-sphingosine during the first 5 days of recovery accelerated the normalization of ceramide levels at 2 weeks and partially reversed the hyperoxia-induced increase in alveolar size and arrest in alveolarization at 4 weeks.
Conclusion: Exposure of newborn mice to hyperoxia caused restrictive and obstructive lung function changes that partially recovered in room air, while alveolar morphology remained abnormal. Hyperoxia increased ceramide levels, with normalization after recovery. D-sphingosine addition during recovery reduced ceramide levels and ameliorated hyperoxia-induced alveolar arrest.

INTRODUCTION

Respiratory Distress Syndrome (RDS) in preterm infants is often managed by mechanical ventilation and supplemental oxygen. This occurs in the setting of an immature, surfactant-deficient lung, devoid of anti-oxidant defenses. A subset of survivors develop Bronchopulmonary Dysplasia (BPD)[1], originally characterized by parenchymal fibrosis, edema, vascular changes and persistent inflammation. Advances in neonatal care, including exogenous surfactant, prenatal steroids, better nutritional management and new modes of ventilation have improved survival of infants with very low birthweight (VLBW). However, these VLBW infants are prone to develop 'new BPD' with fewer and larger alveoli as a result of interrupted septation and abnormal vascular organization[2]. Even though progress has been made in the management of infants with BPD, current treatment remains symptomatic.

Studies looking at the hyperoxia-induced model of BPD are numerous, but to this date no studies have examined the influence of sphingolipids in this model. Sphingolipids are important structure-bearing constituents of the cell membrane which also function as regulatory molecules of cell proliferation and cell death, endothelial barrier function, angiogenesis, and immune response[3]. Altered sphingolipid levels have been found in a variety of diseases, such as atherosclerosis, chronic heart failure[4],asthma[5], diabetes, sepsis, cystic fibrosis and COPD[6]. Two sphingolipids, ceramide and sphingosine-1-phosphate determine the pro- and anti-apoptotic balance[7]. In this 'rheostat', ceramide stimulates apoptosis and cell cycle arrest, and sphingosine-1-phosphate stimulates cell survival and proliferation. Increased apoptosis has been found in epithelial cells of BPD patients[8] and in animal models of BPD[9] and total lung ceramide levels are upregulated in hyperoxia-exposed neonatal rats[10]. To date, no detailed analysis of the sphingolipid metabolome has been reported in the hyperoxia-induced BPD model[11]. Furthermore, little is known about the evolution of lung injury in murine models of BPD. Mice exposed to >60% oxygen during the first days of life showed lung function abnormalities that persisted until 67 weeks of age[12], but the precise evolution of lung function during the acute phase of hyperoxic injury, followed by recovery in room air, has not been examined.

The objective of our study was to determine the evolution of lung function and sphingolipids in hyperoxia-exposed newborn mice during both the acute hyperoxic phase and during recovery in room air. In addition, we studied the effect of pharmacological intervention on hyperoxia-induced lung damage by D-sphingosine supplementation during the recovery phase.

MATERIALS AND METHODS

Animals

C57BL/6 mice were obtained from Charles River (St. Constant, Quebec, Canada) and animal studies were conducted according to criteria established by the Canadian Council for Animal Care and approved by the Animal Care and Use Committee of the Hospital for Sick Children, Toronto, ON, Canada.

Hyperoxia-induced BPD

We used a modified hyperoxia model as described by Warner *et al.*[13]. Two pathogen-free timed pregnant C57BL/6 mice gave birth in room air. At postnatal day 1, the mothers and their pups were placed in paired Oxycycler exposure chambers (Biospherix Ltd, Lacona, NY). Litters were exposed to hyperoxia (80% O_2) or room air for 28 days. Litter sizes were kept at 6 pups in both the hyperoxia and room air groups. Dams were switched daily. Oxygen exposure was maintained for 28 days, after which the mice had gained enough weight to perform lung function measurements. Hyperoxia-treated litters were then exposed to room air for 7, 14 or 28 days. Room air control litters were treated in the same manner. D-sphingosine (Sigma-Aldrich) was administered daily (1.25 µg per g bodyweight, *ip*) to a subset of hyperoxia-treated litters during the first 5 days of recovery in room air. Control animals were treated with D-sphingosine in the same manner. At various times during these conditions, lung function was assessed, broncho-alveolar lavage (BAL) was performed, and tissues was processed for histology (Supplementary figure S1).

Lung function measurements

Twenty-eight days after the start of hyperoxia, the Flexivent rodent ventilator (Scireq, Montreal, Canada) was used to assess lung function as described in detail in the supplementary methods section. For the long-term follow-up experiments of hyperoxic mice in room air, mice were subjected to lung function measurements at postnatal day 35, 42 and 56.

Bronchoalveolar lavage

Lungs were infused through the endotracheal tube with 600 µl sterile saline, followed by withdrawal and re-infusion two more times[14,15]. The collected fluid was centrifuged at 1400 *g* for 8 minutes. The supernatant was collected in a siliconized eppendorf tube and stored at -80°C for mass spectrometry analysis.

Measurement of sphingolipids

Sphingolipid levels in BAL were measured as described in the supplementary methods section.

Histology and morphometry

Following lung function measurements, the lungs were pressure inflated and processed for histology and morphometry as described in the supplementary methods section.

Statistics

All values are expressed as mean ± standard error of the mean, assuming a normal distribution (Sigmaplot version 11 for Windows). Differences were assessed by Student's t-test or, for comparison of three or more groups, by one-way analysis of variance followed by Tukey HSD comparison. Significance was inferred as $p<0.05$.

RESULTS

Lung function measurements

In newborn mice exposed to 28 days of hyperoxia, Flexivent measurements revealed a significant increase in resistance and reduced compliance, total lung capacity, and forced vital capacity compared to controls (Figure 1A, Table 1). Long term follow-up of hyperoxia-exposed mice showed recovery of lung function parameters to control levels after 1 week of recovery in room air. Total lung capacity, static and dynamic compliance took 2 weeks to normalize (Figure 1B). However, forced expirations remained abnormal during the 4 weeks of recovery in room air. Flow-volume curves at 0 and 4 weeks of recovery showed persistent obstructive abnormalities with improvement of volume (Supplementary figure S2, Table 1). Addition of D-sphingosine during recovery in room air did not significantly improve lung function.

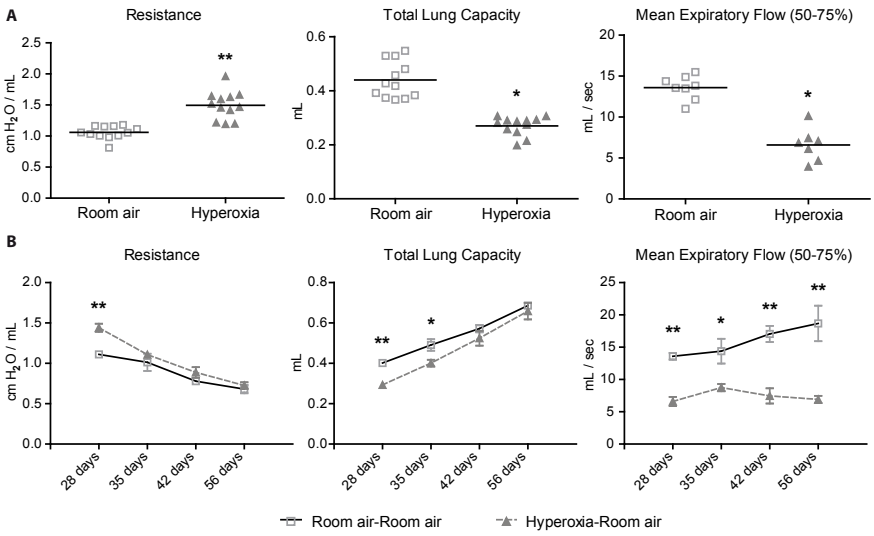

Figure 1. *Lung function measurements after 4 weeks of hyperoxia-exposure (A) and during recovery in room air (B) of hyperoxia-exposed mice and room air controls (n=12 per group for the 28 days' timepoint except for MEF and PEF where n=8. n=6 for the 35, 42 and 56 days' timepoints). Data are expressed as mean ± SEM. * = p<0.05, ** = p<0.001.*

Table 1. *Lung function measurements during hyperoxia exposure and recovery in room air.*

Parameter	Unit	28 days		35 days		42 days		56 days	
		Room air (n=8)	Hyperoxia (n=7)	Room air (n=6)	Hyperoxia (n=6)	Room air (n=5)	Hyperoxia (n=5)	Room air (n=6)	Hyperoxia (n=6)
Resistance	cmH_2O/mL	1.13 (1.04-1.16)	1.46 (1.265-1.62) **	0.96 (0.88-1.02)	1.12 (1.05-1.17)	0.71 (0.66-0.84)	0.95 (0.77-1.02)	0.64 (0.61-0.66)	0.72 (0.66-0.77)
Elastance	cmH_2O/mL	54.6 ± 8.2	70.7 ± 8.7 **	45.2 ± 5.1	45.2 ± 3.1	34.2 ± 5.7	35.1 ± 8.9	29.0 ± 2.6	29.8 ± 7.9
Compliance	mL/cmH_2O	0.018 (0.017-0.019)	0.014 (0.014-0.016) *	0.022 (0.020-0.024)	0.022 (0.021-0.024)	0.030 (0.025-0.034)	0.025 (0.024-0.039)	0.034 (0.032-0.038)	0.036 (0.032-0.041)
Airway Resistance	cmH_2O/mL	0.32 (0.14-0.39)	0.40 (0.04-0.47) *	0.40 (0.38-0.41)	0.47 (0.44-0.49)	0.34 (0.32-0.35)	0.42 (0.26-0.51)	0.30 (0.29-0.34)	0.34 (0.29-0.39)
Tissue Elasticity	cmH_2O/mL	52.0 ± 7.2	57.7 ± 9.0	42.2 ± 5.5	40.4 ± 2.8	33.7 ± 5.3	30.9 ± 7.5	29.4 ± 3.2	27.0 ± 8.7
Total lung capacity	mL	0.39 (0.37-0.42)	0.29 (0.29-0.30) **	0.49 (0.44-0.56)	0.39 (0.37-0.42) *	0.56 (0.51-0.63)	0.50 (0.47-0.66)	0.69 (0.65-0.71)	0.66 (0.58-0.74)
Inspiratory Capacity from zero pressure	mL	0.60 (0.56-0.73)	0.32 (0.29-0.33) **	0.80 (0.65-0.84)	0.58 (0.53-0.63) *	0.89 (0.81-1.02)	0.65 (0.62-1.18)	1.14 (1.12-1.20)	1.01 (0.85-1.24)
Static Compliance	mL/cmH_2O	0.04 (0.04-0.05)	0.02 (0.02-0.02) **	0.06 (0.04-0.06)	0.04 (0.04-0.04) *	0.06 (0.06-0.07)	0.04 (0.04-0.08)	0.08 (0.08-0.09)	0.07 (0.06-0.09)
Static Elastance	cmH_2O/mL	25.1 (22.5-26.4)	49.3 (46.4-53.3) **	18.0 (17.4-23.0)	25.0 (23.3-27.0) *	16.0 (13.9-17.8)	23.6 (11.8-24.1)	12.5 (11.6-12.7)	14.8 (11.0-17.2)
Forced Vital Capacity	mL	0.44 (0.41-0.47)	0.34 (0.33-0.37) **	0.60 (0.53-0.65)	0.53 (0.52-0.55)	0.69 (0.63-0.84)	0.64 (0.61-1.00)	0.80 (0.75-0.88)	0.85 (0.74-0.97)
Mean Forced Expiratory Flow	mL/sec	13.7 (12.8-14.6)	6.8 (5.0-7.3) **	14.7 (11.6-17.9)	9.4 (7.1-9.7) *	19.7 (18.0-20.4)	5.3 (4.1-7.8) **	21.4 (20.8-21.8)	6.6 (6.3-8.0) **
Peak Expiratory Flow	mL/sec	16.1 (15.2-16.5)	14.9 (14.7-15.2)	24.9 (20.8-27.6)	18.4 (16.0-21.7)	26.7 (23.3-28.9)	21.5 (18.9-22.7) *	32.5 (30.6-33.0)	22.3 (21.4-23.5) **
Forced Expiratory Flow 0.05 sec / FVC	%	95.4 (92.0-96.4)	69.8 (63.0-87.7) *	93.0 (90.5-94.5) *	74.9 (63.8-87.6)*	93.5 (91.4-94.5)	60.5 (52.2-70.5) *	92.0 (71.4-92.8)	65.9 (54.4-68.7) *
Forced Expiratory Flow 0.1 sec / FVC	%	99.4 (98.9-99.7)	73.5 (67.6-97.9) *	98.8 (97.8-99.4)	84.2 (71.4-96.4) *	99.5 (98.9-99.7)	79.6 (71.6-83.5) *	98.3 (84.2-98.9)	86.2 (84.8-88.1)
Forced Expiratory Flow 0.2 sec / FVC	%	98.6 (98.3-99.1)	95.0 (72.8-99.0)	99.5 (99.5-99.6)	98.6 (98.0-99.7)	99.5 (99.2-99.6)	96.9 (89.3-98.1) *	99.4 (95.2-99.8)	98.4 (97.4-99.5)

*During Flexivent measurements, an average for each individual mouse was calculated from 4 accepted (coefficient of determination: COD>0.95) measurements for each parameter. * = p<0.05, ** = p<0.001 when compared to control animals at the same time-point.*

Sphingolipid measurements

Sphingolipid levels in BAL by LC-MS/MS are shown in Tables 2-4. A significant increase in multiple sphingomyelin and ceramide species was found after 2 and 4 weeks of hyperoxia exposure (Figure 2, Table 2). In particular, long chain ceramides (Cer16:0 and Cer18:0) and very long chain ceramides (Cer24:0 and Cer24:1) were greatly elevated (Figure 2, Table 2). Small, but significant increases were also found in sphinganine and a few dihydroceramides, both precursors of ceramides formed by the *de novo* pathway. All four major sphingomyelins (SM16:0, SM18:0, SM24:0, SM24:1) showed 2-4 fold increases after hyperoxia exposure. Following 2 weeks of recovery in room air, all sphingomyelin species in the BAL of the hyperoxia-treated group returned to control levels, but many ceramide species were still significantly elevated compared to controls (Figure 2, Tables 3 and 4). Treatment with D-sphingosine accelerated the normalization of ceramides in room-air (Figure 3, Tables 3 and 4).

Histological analysis

Compared to room air controls (Figure 4A), histological sections of hyperoxia-exposed lungs (Figure 4B) showed a homogeneous pattern of decreased alveolar septation,

Table 2. *Sphingolipids in bronchoalveolar lavage at 14 and 28 days of hyperoxia exposure.*

Sphingolipid	Exposure time 14 days		Exposure time 28 days	
	Room air	Hyperoxia	Room air	Hyperoxia
Sphinganine	0.31 (0.27-0.37)	0.15 (0.13-0.22) *	0.32 ± 0.07	0.34 ± 0.10
Sphingosine	1.24 ± 0.27	0.66 ± 0.18 **	0.79 ± 0.17	1.64 ± 0.30 **
Ceramide 16:0	4.35 ± 1.08	2.43 ± 0.83 **	3.75 (3.61-4.17)	37.28 (24.52-44.05) *
Ceramide 18:0	0.99 (0.92-1.17)	1.12 (0.95-1.21)	1.06 (0.93-1.17)	3.07 (2.38-3.49) **
DihydroCeramide 18:0	0.12 (0.09-0.18)	0.10 (0.08-0.14)	0.18 (0.12-0.23)	0.29 (0.26-0.42) *
Ceramide 20:0	0.47 (0.41-0.56)	0.54 (0.51-0.64) *	0.60 (0.55-0.70)	1.91 (1.68-2.32) **
Ceramide 22:0	2.91 (2.56-3.26)	2.34 (2.22-2.94)	4.08 (3.50-4.93)	7.47 (7.03-9.50) *
Ceramide 24:0	7.74 (7.31-8.81)	7.48 (6.72-9.03)	18.66 (15.59-20.99)	32.49 (26.7-39.29) **
Ceramide 24:1	9.65 (8.93-10.80)	10.72 (9.55-13.42)	14.75 ± 7.11	38.81 ± 8.96 **
DihydroCeramide 24:0	0.37 (0.33-0.43)	0.40 (0.28-0.53)	0.79 (0.73-1.12)	1.72 (1.42-1.90) *
Sphingomyelin 16:0	156.5 (152.6-168.3)	237.6 (207.5-281.5) **	219.3 (196.9-248.3)	708.0 (511.6-757.7) **
Sphingomyelin 18:0	10.29 (9.51-11.13)	20.05 (15.8-25.0) **	13.50 (12.17-15.96)	47.75 (33.73-53.61) **
Sphingomyelin 24:0	38.93 (36.91-41.58)	78.64 (62.19-110.09) **	82.00 (66.70-92.07)	273.00 (244.20-351.00) **
Sphingomyelin 24:1	105.1 (100.5-114.1)	245.0 (187.4-322.0) **	137.2 (112.7-167.6)	806.4 (501.7-903.3) **

*BAL fluid from 12 mice per group was collected and sphingolipids were quantified by LC-MS/MS. Results are expressed in ng / 200µl of BAL fluid. * = p<0.05, ** = p<0.001 when compared to control animals at the same time-point.*

Table 3. *Sphingolipid measurements after D-sphingosine supplementation at 1 week of recovery.*

Sphingolipid	Room air for 35 days	Room air+ 7 days room air + D-sphingosine	Hyperoxia+ 7 days room air	Hyperoxia+ 7 days room air +D-sphingosine
Sphinganine	0.38 ± 0.04	0.39 ± 0.05	0.54 ± 0.14	0.65 ± 0.15 *
Ceramide 16:0	11.65 (11.51-13.19)	15.43 (13.43-16.46)	23.04 (19.91-25.99) *	23.46 (17.45-28.41) *
Ceramide 18:0	1.26 ± 0.24	1.30 ± 0.13	2.26 ± 0.34 *	1.95 ± 0.54
DihydroCeramide 18:0	0.11 ± 0.01	0.15 ± 0.07	0.23 ± 0.10	0.34 ± 0.29
Ceramide 20:0	0.63 ± 0.14	0.66 ± 0.11	1.26 ± 0.19 *	1.03 ± 0.29
Ceramide 22:0	3.57 ± 0.64	3.94 ± 0.58	5.81 ± 0.10 *	5.02 ± 1.33
Ceramide 24:0	10.97 ± 2.08	12.44 ± 0.91	21.89 ± 1.32 *	20.43 ± 6.25 *
Ceramide 24:1	10.83 ± 1.26	12.72 ± 1.79	19.67 ± 1.36 *	20.20 ± 5.81 *
DihydroCeramide 24:0	0.39 ± 0.11	0.48 ± 0.03	0.75 ± 0.02 *	0.80 ± 0.09 *
Sphingomyelin 16:0	208.25 ± 17.24	263.87 ± 27.13	458.93 ± 67.89 *	408.40 ± 113.22 *
Sphingomyelin 18:0	8.07 ± 0.99	9.93 ± 1.91	30.15 ± 4.88 *	20.35 ± 7.89 *
Sphingomyelin 24:0	40.83 ± 3.60	51.28 ± 15.89	169.73 ± 30.46 *	119.80 ± 45.65 *
Sphingomyelin 24:1	82.66 ± 9.98	101.71 ± 25.85	270.85 ± 25.53 *	232.93 ± 63.17 *

*BAL fluid from 3 mice per group was collected and sphingolipids were quantified by LC-MS/MS. Results are expressed in ng / total amount of BAL fluid per mouse. * = p<0.05, ** = p<0.001 when compared to the room air controls at the same time-point.*

Table 4. *Sphingolipid measurements after D-sphingosine supplementation at 2 weeks of recovery.*

Sphingolipid	Room air for 42 days	Room air+ 14 days room air + D-sphingosine	Hyperoxia+ 14 days room air	Hyperoxia+ 14 days room air +D-sphingosine
Sphinganine	0.50 ± 0.10	0.47 ± 0.09	0.46 ± 0.08	0.47 ± 0.09
Ceramide 16:0	12.85 ± 1.51	13.27 ± 1.04	18.70 ± 5.20	15.71 ± 0.48
Ceramide 18:0	1.11 ± 0.11	1.32 ± 0.11	1.87 ± 0.42 *	1.59 ± 0.09
DihydroCeramide 18:0	0.22 ± 0.17	0.14 ± 0.01	0.19 ± 0.08	0.14 ± 0.02
Ceramide 20:0	0.56 ± 0.07	0.63 ± 0.07	0.92 ± 0.21 *	0.84 ± 0.13
Ceramide 22:0	3.23 ± 0.39	3.92 ± 0.50	4.72 ± 0.99 *	4.71 ± 0.26 *
Ceramide 24:0	11.28 ± 1.05	11.28 ± 1.13	19.69 ± 5.04 *	17.03 ± 0.97
Ceramide 24:1	10.52 ± 1.29	11.52 ± 0.96	17.78 ± 4.40 *	15.45 ± 1.06
DihydroCeramide 24:0	0.33 ± 0.04	0.41 ± 0.05	0.84 ± 0.20 *	0.71 ± 0.34
Sphingomyelin 16:0	283.7 ± 38.1	254.2 ± 24.08	319.3 ± 90.74	278.3 ± 38.9
Sphingomyelin 18:0	10.24 (9.69-11.6)	9.18 (8.52-9.52)	11.50 (8.24-15.80)	9.37 (8.54-9.98)
Sphingomyelin 24:0	48.60 (3.29-49.72)	39.69 (37.14-42.49)	55.60 (37.60-71.05)	49.02 (44.34-54.46)
Sphingomyelin 24:1	110.5 (107.7-111.3)	105.6 (93.0-106.1)	176.2 (123.2-218.0)	115.5 (110.3-118.5)

*BAL fluid from 3 mice per group was collected and sphingolipids were quantified by LC-MS/MS. Results are expressed in ng / total amount of BAL fluid per mouse. * = p<0.05, ** = p<0.001 when compared to room air controls at the same time-point.*

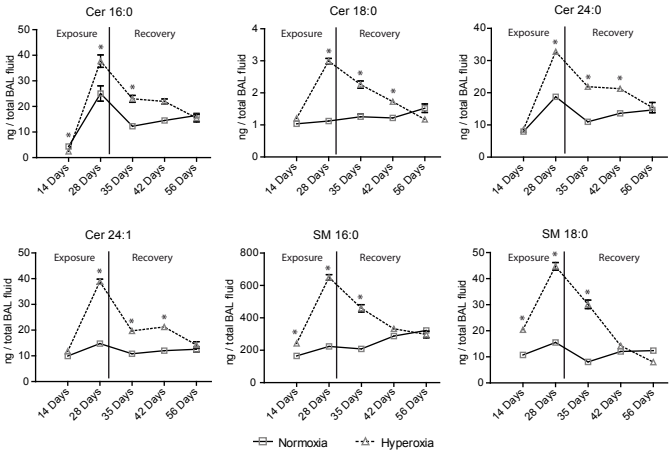

Figure 2. *Representative sphingolipid measurements performed during hyperoxia treatment and recovery in room air. Results represent a total of 12 mice per group for the 14 and 28 days' time-points in hyperoxia and 3 mice per group for the 35,42 and 56 days' time-points of recovery in room-air Cer: ceramide, SM: sphingomyelin. * = p<0.05, ** = p<0.001, when compared to room air treated mice at the same time-point.*

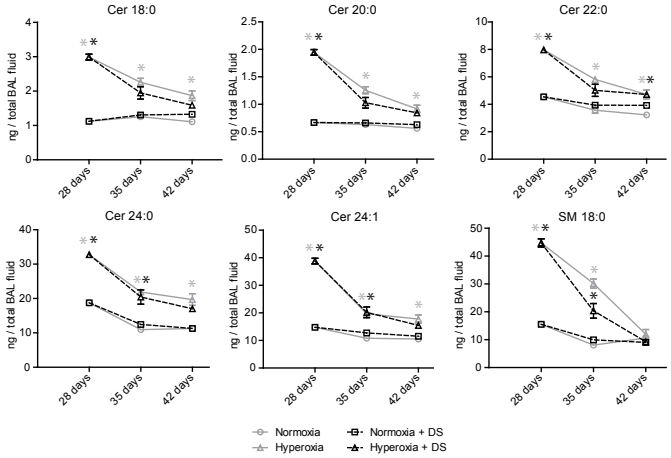

Figure 3. *Representative sphingolipid measurements after 1 and 2 weeks recovery in room-air with and without D-sphingosine (DS) treatment. Results represent a total of 12 mice per group for 28 days' time-point in hyperoxia and 3 mice per group for the 35, 42 and 56 days' time-points of recovery in room-air and the D-sphingosine supplementation experiments. Cer: ceramide, SM: sphingomyelin. Grey * represents a significant change in hyperoxia treated mice when compared to normoxia treated mice at the same time-point. Black * represents a significant change in hyperoxia + DS treated mice when compared to normoxia + DS treated mice at the same time-point. * = p<0.05, ** = p<0.001.*

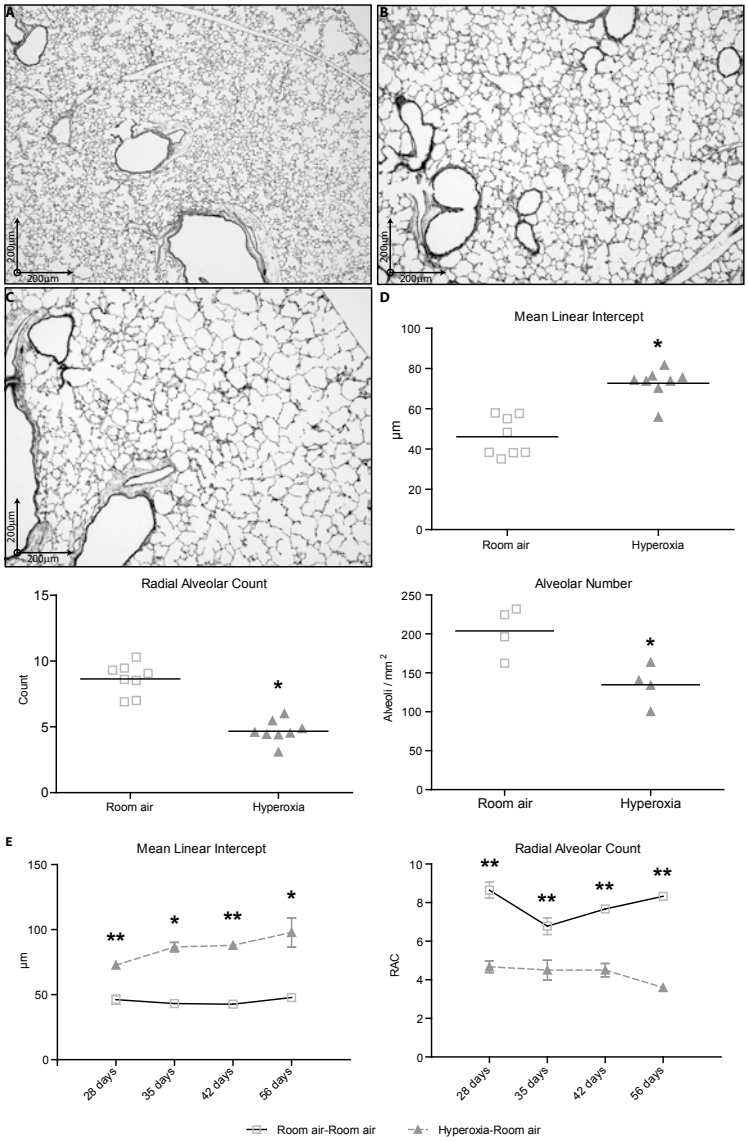

Figure 4. *Effect of hyperoxia and subsequent room air recovery on lung histology. Representative histological sections of room air-exposed newborn mice (A), hyperoxia-treated newborn mice after 4 weeks of exposure (B) and hyperoxia-treated newborn mice that were allowed to recover for another 4 weeks in room-air (C) are shown. Sections were stained with hematoxylin and eosin. Morphometry results (D) are expressed as mean ± SEM for both room air and hyperoxia groups for mean linear intercept (n=8), radial alveolar counts (n=8), and alveolar number (n=4). Morphometry results for 4 weeks of recovery in room-air (E) are expressed as mean ± SEM for mean linear intercept (n=4) and radial alveolar count (n=3). * = p<0.05 ** = p<0.001. (See colour section, page 185).*

compared to room air-exposed newborn mice. Morphometry demonstrated a significant increase in mean linear intercept, a reduction in radial alveolar count and in the number of alveoli. Lung sections of mice exposed to 4 weeks of hyperoxia and allowed to recover in room air (Figure 4C) showed fewer and enlarged alveoli when compared to room air controls. No significant difference in mean linear intercept and radial alveolar count was noted at 1, 2 and 4 (Figure 4E) weeks of recovery in room air. Interestingly, when compared to hyperoxia-exposed non-treated mice (Figure 5A), mice treated with D-sphingosine for 5 days immediately after hyperoxia exposure (Figure 5B) had a significantly lower mean linear intercept and higher radial alveolar count (Figure 5C) at 2 weeks of recovery in room air. Mean linear intercept and radial alveolar counts of hyperoxia-exposed and D-sphingosine-treated mice did not return to control levels.

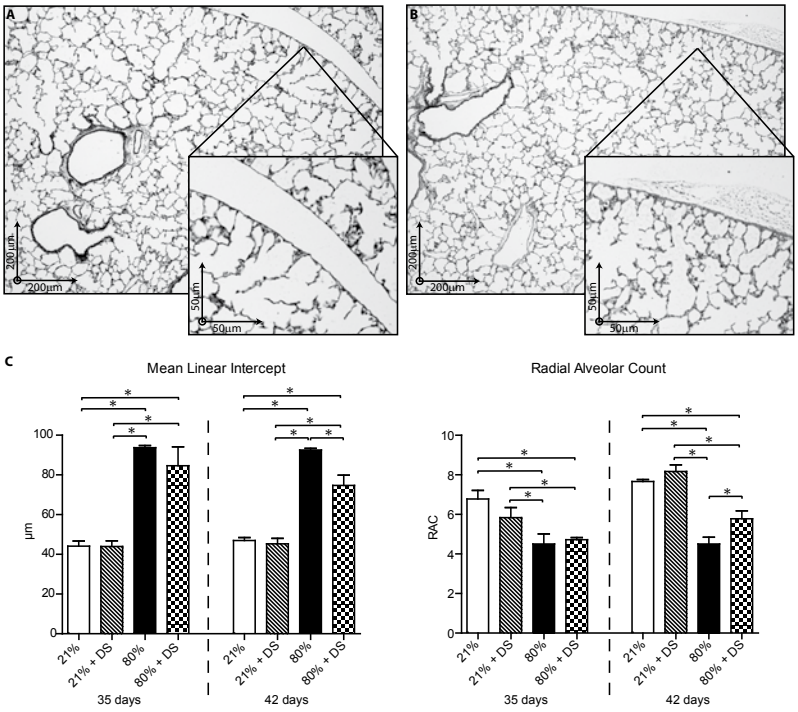

Figure 5. *Effect of D-sphingosine supplementation on lung histology. Representative histological lung sections are shown after 4 weeks of hyperoxia exposure followed by 2 weeks of room air recovery (A), and 4 weeks of hyperoxia exposure followed by 2 weeks of room air recovery with D-sphingosine supplementation (B). Sections were stained with hematoxylin and eosin. High power inserts were taken at 200x magnification. Morphometry results (C) represent a total of 3 mice per group and are expressed as mean ± SEM for all groups. * = p<0.05. (See colour section, page 186).*

DISCUSSION

In this study we examined BAL sphingolipid levels, lung function and histology in newborn mice during hyperoxia exposure and after recovery in normoxia. Our findings showed that 4 weeks of hyperoxia exposure causes alveolar damage and obstructive lung function abnormalities, together with increased sphingolipid levels, including ceramides. We demonstrated normalization of ceramides and partial improvement of lung function, but found no improvement in histological abnormalities within 4 weeks of recovery in room air. D-sphingosine supplementation during normoxic recovery accelerated ceramide normalization and improved hyperoxia-induced alveolar arrest, but did not affect lung function.

In our hyperoxia model, the increased airway resistance, decreased mean forced expiratory flow and forced expiratory volume could be caused by airway remodelling as a consequence of ongoing inflammation[13]. The observed changes in lung function are similar to those reported for newborn mice after 14 days of 85% oxygen exposure[16]. Another possible explanation for the lung function changes is a reduced number of alveolar attachments leading to decreased radial traction, which would result in airway narrowing and earlier airway collapse during expiration[17]. Prolonged exposure to hyperoxia in newborn mice caused an arrest in alveolarization, thereby delaying the formation of secondary septa, reducing alveolar number and increasing alveolar wall thickness. In the present study, this decrease in alveolarization was reflected in the radial alveolar counts.

At the end of 4 weeks hyperoxia exposure, we observed a combined obstructive and restrictive pattern that shifted to an obstructive pattern at the end of 4 weeks recovery in room air. The persistent abnormal forced expiration measurements, as well as the abnormal morphology after 4 weeks in room air indicate incomplete recovery and a permanently altered lung structure. Velten *et al.* studied newborn mice exposed to 85% O_2 for 14 days, which recovered for 14 days in room air, and these newborns developed an increased resistance at 14 days, followed by an increased compliance of the lungs at 28 days[16]. Yee *et al.* noted a reduced compliance after 4 days of 100% O_2 exposure in newborn mice, and an increased compliance at 67 weeks of age[12]. They speculated that the transient decrease in compliance during the acute phase of hyperoxic injury was due to pulmonary edema, impaired surfactant protein-C production and pro-inflammatory free oxygen radicals. Both studies seemed to indicate that the response of the newborn lung to hyperoxia can be divided into two stages: acute lung injury characterized by a less compliant lung, and chronic lung injury, characterized by a more compliant lung. Our measurements after 4 weeks of recovery could reflect an intermediary phase, between acute and long term hyperoxia-induced lung injury, in which edema and inflammation decreases, and the lung becomes more compliant. We observed partial recovery of lung function, but no apparent recovery in morphology after 4 weeks of recovery in room air. This emphasizes the importance of obtaining both structural and physiological data when tracking changes in disease state or monitoring the effects of an intervention. The persistence of morpho-

logical abnormalities in our mouse model is in line with the abnormalities seen in adult survivors of BPD[18,19], and the persistent abnormal lung function parameters are consistent with results of lung function measurements performed in human survivors of BPD[20,21], making this model a good choice for intervention studies aimed at repairing hyperoxia-induced lung damage.

Ceramides play an important role in apoptosis and lung inflammation[22,23]. Kolliputti *et al.* recently showed that ceramides regulate endothelial permeability and the inflammatory process caused by hyperoxia in adult mice[24]. Ceramides have long been known to mediate acute lung injury by increasing alveolar permeability and proinflammatory cytokine production[25], but no studies have reported detailed ceramide profiles in neonatal hyperoxia-induced lung damage and during recovery in room air. Our study shows that multiple ceramide and sphingomyelin species are increased during exposure of neonatal pups to hyperoxia. Long chain ceramides (Cer16:0, Cer18:0, Cer20:0) have anti-proliferative and pro-apoptotic effects[26], whereas very long-chain ceramides (Cer22:0, Cer24:0, Cer24:1) promote cell proliferation[27]. We observed an 8-fold increase in long chain Cer16:0 during hyperoxia, suggesting a role for increased apoptosis via ceramide signaling in this hyperoxia model. Indeed, increased apoptosis has been observed in the lungs of mice and rats exposed to hyperoxia[28–30], similar to the findings in autopsy lungs of BPD patients[31]. Very long chain(24:0, 24:1) ceramides demonstrated a 2-3 fold increase in our model, suggesting a role for proliferation, possibly of smooth muscle cells, which have been shown to proliferate in rat and mouse models of hyperoxia-induced BPD[12,29,32]. Both ceramides and sphingomyelin levels were increased, suggesting that the increase in ceramides is not caused by breakdown of sphingomyelin via sphingomyelinase. The increased sphingosine levels (Table 2) may indicate increased ceramide formation via the salvage pathway, although the general increase in most sphingolipids argued against activation of that pathway. Based on the observation that both sphinganine and dihydroceramides were increased (Table 2), we hypothesize that hyperoxia activates the pulmonary *de novo* pathway of ceramide synthesis in the newborn. Further studies focusing on the activity of the rate-limiting enzyme serine palmitoyltransferase would be needed to confirm the increase in the *de novo* synthesis.

Long chain ceramides have been shown to increase the permeability of endothelium[33], which causes endothelial leakage[34] and might contribute to the reduced compliance of the lungs seen in our hyperoxia model. We postulate that reduced forced expiratory flows might be related to structural changes, such as a reduced number of alveolar attachments, and remained low during air recovery. In contrast, resistance and compliance may be determined by reversible factors in the lung, such as inflammation and endothelial leakage. Our study shows that sphingolipid levels, including ceramides, returned to normal within 4 weeks of recovery in room air, corresponding to the time course of lung function changes. It may well be that when the primary stress factor (hyperoxia) disappears during recovery in room air, leading to a decrease in sphingolipids, lung inflammation and edema, resulting in partial recovery of lung function. However, no additional effect of

D-sphingosine supplementation on partial lung function recovery was observed. Note that sphingolipid levels were measured in BAL, providing a good estimate of the sphingolipid metabolism in the broncho-alveolar compartment, but they may not represent sphingolipid metabolism in the interstitial and vascular compartment. Further research into the complexity of the interaction between these different compartments is warranted.

Treatment with D-sphingosine significantly decreased ceramide levels after 1 and 2 weeks of recovery in room air. Lung morphometry showed an improvement of mean linear intercept and radial alveolar count after 4 weeks of recovery in the D-sphingosine-treated animals compared to untreated control mice. These findings suggest that D-sphingosine supplementation had a beneficial effect on the alveolar injury caused by hyperoxia exposure, and that lower ceramide levels might be responsible for this improvement in alveolar histology. A reduction in the amount of apoptosis is the most likely mechanism by which D-sphingosine acts, but further experiments are needed to confirm this hypothesis.

No obvious beneficial effects on lung function were found, which could well be due to imperfect agreement between measures of lung structure and function. The incomplete recovery of histology, sphingolipid levels and lung function after D-sphingosine treatment and the absence of a significant difference in these parameters between hyperoxic mice with and without D-sphingosine might be due to dose and/or timing of the supplementation, or might have been missed due to a relatively small number of observations. Our D-sphingosine dose was based on a study by Diab *et al.* who showed that adult mice injected with D-sphingosine at 20µg per mouse for 5 consecutive days had significantly increased sphingosine-1-phosphate (a pro-survival sphingolipid) levels in homogenized lung tissue at day 5 after the start of administration[35]. The administration of D-sphingosine in our model started after hyperoxia exposure and lasted for 5 days. It is possible that earlier or longer supplementation might yield better results.

One could argue that prevention of damage by adding D-sphingosine at an earlier time point would be preferable. We decided for another approach, as currently there are no reliable predictors to indicate which infant will develop BPD, making it difficult to target preventative treatment to those who might benefit. Therefore, we supplemented D-sphingosine only during the recovery phase to see if this might stimulate repair of hyperoxia-induced damage.

In summary, we demonstrated that hyperoxia in the newborn mouse lung caused a transient increase of sphingolipids, including ceramides, which returned to normal during recovery in room air, while histology remained abnormal. The time course of sphingolipid reduction during recovery matched the normalization of airway resistance and compliance. Importantly, D-sphingosine supplementation during recovery accelerated the normalization of ceramides, and significantly improved hyperoxia-induced lung damage. We propose that D-sphingosine and other inhibitors of bioactive sphingolipids should be studied further for their potential to reduce lung damage in human preterm infants who

require neonatal oxygen treatment. The ultimate goal would be to develop a new strategy to prevent or correct bronchopulmonary dysplasia.

ACKNOWLEDGEMENTS

This work was supported by an operating grant (MOP-86472) from the Canadian Institute of Health Research and infrastructure grants (CCURE, CSCCD) from the Canadian Foundation for Innovation. Martin Post is the holder of a Canadian Research Chair in Fetal, Neonatal and Maternal Health.

SUPPLEMENTARY METHODS

Lung function measurements

Animals were anesthetized with an *ip* injection of Ketamine (150 mg/kg) and Xylazine (10 mg/kg) before tracheostomy. A 25G endotracheal tube was inserted and sutured in place to prevent leakage. After intraperitoneal injection of Pancuronium (5 mg/kg) the animal was ventilated at 150 breaths/min with a tidal volume of 10 mL/kg and lung function was measured using the Flexivent ventilator (SCIREQ, Montreal, QC, Canada). The flexivent measures flow-volume relations of the respiratory system and uses forced oscillations to discriminate between the airways and the alveolar compartment. The "Total Lung Capacity" (TLC), "Snapshot" (based on single-compartment model), and "Primewave-8" (based on constant phase model) perturbations were used to measure lung function. For the "TLC" maneuver, the lung is inflated to +30 cmH_2O and deflated afterwards. For the "Snapshot" maneuver, three sinusoidal waves of in- and expiration provide the resistance, elastance and compliance parameters. For the "prime-wave 8", multiple frequency forced oscillations were applied which result in the tissue elasticity and airway resistance parameters. Volume-driven pressure-volume loops were also obtained and provided the total lung capacity, inspiratory capacity from zero pressure and static and dynamic compliance. All measurements were repeated until 4 successful recordings with a coefficient of determination of >0.95 were obtained. Animals also underwent forced expirations by inflating to TLC and then rapidly applying a negative pressure of -55 cmH_2O to the expiratory valve. In the current state of small animal ventilator technology, this technique is the closest to mimicking forced expiratory spirometry in humans. Parameters obtained from this maneuver were the forced vital capacity, mean forced expiratory flow, peak forced expiratory flow and forced expiratory flow at 0.05, 0.1 and 0.2 seconds divided by forced vital capacity.

Measurement of sphingolipids

BAL samples (200 µL), transferred to siliconized glass tubes containing 800 µL ultra-pure water, were spiked with a mixture of internal standards (C17 (d18:1/17:0) ceramide, (d17:1) sphingosine, (d17:1) sphingosine-1-phosphate and 17:0 (d18:1/17:0) sphingomyelin; 10 ng of each). After addition of 2 mL of methanol/chloroform (1:1) samples were vortexed, centrifuged and the chloroform layer collected. After drying, samples were reconstituted in 100 µL ethanol that was acidified with 0.2 mL of formic acid and transferred to siliconized minivials for analysis. Liquid chromatography tandem mass spectrometry was performed on an Agilent 1200 Series binary pump (Agilent Technologies Inc., Santa Clara, CA, USA) coupled to an API4000 triple-quadruple mass spectrometer (SCIEX, Concord, ON, Canada). Prior to analysis, Multiple Reaction Monitoring (MRM) mass transition parameters were optimized by infusion of pure standards (5 µl/min of 1 µg/mL). Reverse phase high performance liquid chromatography (HPLC) was performed using a Kinetex C18 column (Phenomenex, Torrance, CA, USA). Sample injection volume was 1-5 µL. The mobile phase consisted of (A) water/acetonitrile/methanol (2/1/1, v/v/v) and (B) tetrahydrofuran/acetonitrile/methanol (2/1/1, v/v/v) with both components containing 0.05%

formic acid. At a flow of 400 µL/min the HPLC gradient was as follows: initial conditions of 60:40 (A:B) were held for 4.5 min prior to injection, then held for another 2 min post injection and ramped to 15:85 (A:B) over 13 min. Conditions were held for 15 min and then returned to initial conditions. MS analysis was performed in positive electrospray Ionization mode. The source temperature was maintained at 400°C with the ion spray voltage set at 5,000 V and nitrogen used as the Collision Induced Dissociation gas (Table 5 shows the MRM mass transitions and chromatographic retention times). For quantitative analysis a separate standard curve was generated for each analyte measured using MRM area ratios (Analyte Peak Area/IS Peak Area). Results were then calculated by plotting the sample area ratios against their respective analyte standard curve[36,37].

Table 5. *Sphingolipid LC-MS/MS MRM mass transitions and chromatic retention times.*

Name	MRM mass transition (Da)	Collision Energy (eV)	Retention Time (min)
(IS) So (d17:1)	286.400/268.100	23	0.95
(IS) Sphingosine-d7		19	1.14
So (d18:1)	307.400/289.500 300.400/282.100	23	1.16
Sa (d18:1)	302.400/284.100	23	1.32
(IS) So1P (d17:1)	366.400/250.100 380.400/264.200	30	1.74
So1P (d18:1)	426.600/264.400	30	2.34
Cer 8:0	647.700/184.100	40	5.59
SM 12:0	649.700/184.100	40	5.72
SM (DiHy) 12:0	482.600/264.400	40	5.99
Cer 12:0	734.900/184.200	40	7.19
(IS) SM 16:0-D31	703.700/184.100	80	7.21
SM 16:0	729.700/184.100	40	7.31
SM 18:1	717.700/184.100	40	7.47
(IS) SM 17:0	510.600/264.400	40	7.78
Cer 14:0	731.700/184.100	40	8.26
SM 18:0	569.800/265.500	40	8.38
(IS) Cer 16:0-D31	538.600/264.400	36	9.37
Cer 16:0	564.600/264.400	40	9.54
Cer 18:1	566.600/284.500	30	9.78
Cer(DiHy) 18:1	552.500/264.400	30	10.27
(IS)Cer C 17	566.600/264.400	60	10.18
Cer 18:0	813.700/184.500 568.600/284.500	40	10.69
SM 24:1	815.600/184.100	40	10.63
Cer(DiHy) 18:0	594.600/264.400	30	10.94
SM 24:0	648.600/264.400	40	11.27
Cer 20:0		40	11.31
Cer 24:1		40	11.75

IS: internal standards, Cer: ceramide, Cer (diHy): dehydroceramide, SM: sphingomyelin, So: sphingosine, Sa: sphinganine.

Histology and morphometry

Following lung function measurements, animals were exsanguinated by cutting the abdominal aorta while still under anesthesia. After opening the thoracic cavity, heparin dissolved in phosphate buffered saline (PBS) was injected into the right ventricle of the heart and the lungs were flushed free of blood. A catheter was inserted into the trachea to allow 4% (w/v) paraformaldehyde (PFA) to inflate the tissue at a constant pressure of 20 cm H_2O. After 5 minutes, the catheter was removed and the trachea tied off. The lungs were removed from the thorax as a single block and fixed in 4% PFA overnight. Fixed lungs were embedded in paraffin at 60°C. Randomly orientated tissue blocks were cut into 7 µm sections, stained with hematoxylin-eosin and Hart's elastin stain, and morphometry was performed on digital images taken at x200 magnification. Images were captured from 5 non-overlapping fields from each slide, with 4 slides per animal. Mean linear intercepts (Lm) and radial alveolar count (RAC) was measured and calculated[38,39]. For alveolar number determination, 20 randomly selected non-overlapping fields from sections obtained from 4 animals per group were examined. Each field was viewed at x200 magnification and alveolar number was counted and expressed per mm^2 [40].

SUPPLEMENTARY FIGURES.

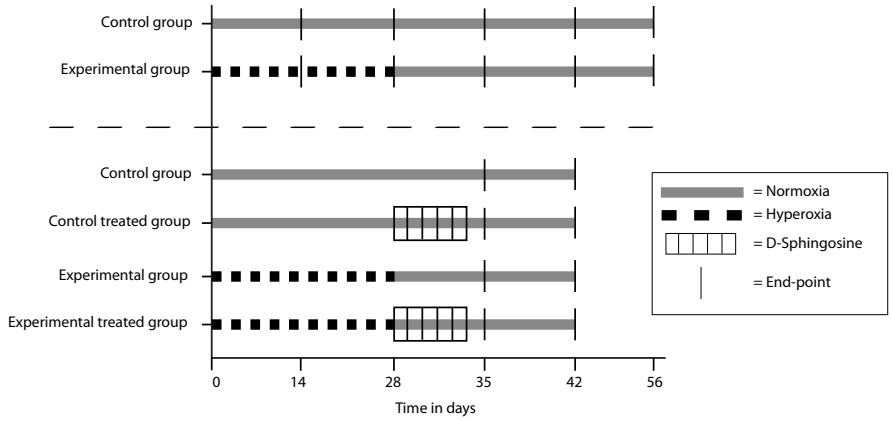

Supplementary figure S1. *Time-line of experiments performed to measure lung function, collect BAL, and assess histology during hyperoxia exposure and recovery.*

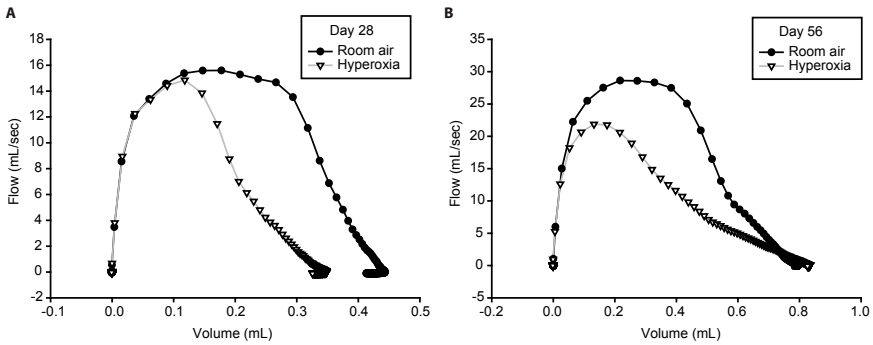

Supplementary figure S2. *Example of flow-volume curves after 4 weeks of hyperoxia exposure (A) and 4 weeks of hyperoxia exposure followed by 4 weeks of room air recovery (B).*

REFERENCES

1. Abman SH, Mourani PM, Sontag M. Bronchopulmonary dysplasia: a genetic disease. *Pediatrics*. 2008;122(3):658–9.
2. Jobe AJ. The new BPD: an arrest of lung development. *Pediatric research*. 1999;46(6):641.
3. Hannun Y a, Obeid LM. Many Ceramides. *The Journal of biological chemistry*. 2011;(36).
4. Gulbins E, Li PL. Physiological and pathophysiological aspects of ceramide. *American Journal of Physiology-Regulatory, Integrative and Comparative Physiology*. 2006;290(1):R11–26.
5. Ammit AJ, Hastie AT, Edsall LC, et al. Sphingosine 1-phosphate modulates human airway smooth muscle cell functions that promote inflammation and airway remodeling in asthma. *The FASEB journal*. 2001;15(7):1212–4.
6. Lahiri S, Futerman a H. The metabolism and function of sphingolipids and glycosphingolipids. *Cellular and molecular life sciences*. 2007;64(17):2270–84.
7. Payne SG, Milstien S, Spiegel S. Sphingosine-1-phosphate: dual messenger functions. *FEBS letters*. 2002;531(1):54–7.
8. May M, Strobel P, Preisshofen T, Seidenspinner S, Marx a., Speer CP. Apoptosis and proliferation in lungs of ventilated and oxygen-treated preterm infants. *European Respiratory Journal*. 2004;23(1):113–121.
9. Dieperink H, Blackwell T. Hyperoxia and apoptosis in developing mouse lung mesenchyme. *Pediatric research*. 2006;59(2):185–190.
10. Husari AW, Dbaibo GS, Bitar H, et al. Apoptosis and the activity of ceramide, Bax and Bcl-2 in the lungs of neonatal rats exposed to limited and prolonged hyperoxia. *Respiratory research*. 2006;7:100.
11. Pappas CT, Obara H, Bensch KG, Northway WH. Effect of prolonged exposure to 80% oxygen on the lung of the newborn mouse. *Laboratory investigation*. 1983;48(6):735–48.
12. Yee M, White RJ, Awad H a, Bates W a, McGrath-Morrow S a, O'Reilly M a. Neonatal hyperoxia causes pulmonary vascular disease and shortens life span in aging mice. *The American journal of pathology*. 2011;178(6):2601–10.
13. Warner BB, Stuart LA, Papes RA, Wispé JR. Functional and pathological effects of prolonged hyperoxia in neonatal mice. *American Journal of Physiology-Lung Cellular and Molecular Physiology*. 1998;275(1):L110.
14. Tsuchida S, Engelberts D, Roth M, McKerlie C, Post M, Kavanagh BP. Continuous positive airway pressure causes lung injury in a model of sepsis. *American Journal of Physiology-Lung Cellular and Molecular Physiology*. 2005;289(4):L554–64.
15. Ridsdale R, Roth-Kleiner M, D'Ovidio F, et al. Surfactant palmitoylmyristoylphosphatidylcholine is a marker for alveolar size during disease. *American journal of respiratory and critical care medicine*. 2005;172(2):225–32.
16. Velten M, Heyob KM, Rogers LK, Welty SE. Deficits in lung alveolarization and function after systemic maternal inflammation and neonatal hyperoxia exposure. *Journal of applied physiology*. 2010;108(5):1347–56.
17. Baraldi E, Filippone M. Chronic lung disease after premature birth. *The New England journal of medicine*. 2007;357(19):1946–55.
18. Aquino S, Schechter M, Chiles C, Ablin D, Chipps B, Webb W. High-resolution inspiratory and expiratory CT in older children and adults with bronchopulmonary dysplasia. *American Journal of Roentgenology*. 1999;173(4):963.
19. Wong PM, Lees AN, Louw J, et al. Emphysema in young adult survivors of moderate-to-severe bronchopulmonary dysplasia. *European Respiratory Journal*. 2008;32(2):321.
20. May C, Kennedy C, Milner AD, Rafferty GF, Peacock JL, Greenough A. Lung function abnormalities in infants developing bronchopulmonary dysplasia. *Archives of disease in childhood*. 2011.
21. Robin B, Kim Y-J, Huth J, et al. Pulmonary function in bronchopulmonary dysplasia. *Pediatric pulmonology*. 2004;37(3):236–42.

22. Park JYJY, Kim MJMJ, Kim YKYK, Woo JSJS. Ceramide induces apoptosis via caspase-dependent and caspase-independent pathways in mesenchymal stem cells derived from human adipose tissue. *Archives of Toxicology*. 2011;85(9):1–9.
23. Dechecchi MC, Nicolis E, Mazzi P, et al. Modulators of sphingolipid metabolism reduce lung inflammation. *American journal of respiratory cell and molecular biology*. 2011;45(4):825–33.
24. Kolliputi N, Galam L, Parthasarathy PT, Tipparaju SM, Lockey R. NALP-3 inflammasome silencing attenuates ceramide induced transepithelial permeability. *Journal of cellular physiology*. 2011;(November):1–26.
25. Mathias S, Peña L a, Kolesnick RN. Signal transduction of stress via ceramide. *The Biochemical journal*. 1998;335 (Pt 3:465–80.
26. Hartmann D, Lucks J, Fuchs S, et al. Long chain ceramides and very long chain ceramides have opposite effects on human breast and colon cancer cell growth. *The international journal of biochemistry & cell biology*. 2012;44(4):620–8.
27. Mesicek J, Lee H, Feldman T, et al. Ceramide synthases 2, 5, and 6 confer distinct roles in radiation-induced apoptosis in HeLa cells. *Cellular signalling*. 2010;22(9):1300–7.
28. Xu D, Perez RE, Ekekezie II, Navarro A, Truog WE. Epidermal growth factor-like domain 7 protects endothelial cells from hyperoxia-induced cell death. *American Journal of Physiology-Lung Cellular and Molecular Physiology*. 2008;294(1):L17–23.
29. Franco-Montoya M-L, Bourbon JR, Durrmeyer X, Lorotte S, Jarreau P-H, Delacourt C. Pulmonary effects of keratinocyte growth factor in newborn rats exposed to hyperoxia. *American Journal of Physiology-Lung Cellular and Molecular Physiology*. 2009;297(5):L965–76.
30. Alejandre-Alcázar M a, Kwapiszewska G, Reiss I, et al. Hyperoxia modulates TGF-beta/BMP signaling in a mouse model of bronchopulmonary dysplasia. *American Journal of Physiology-Lung Cellular and Molecular Physiology*. 2007;292(2):L537–49.
31. Hargital B, Szabó V, Hajdu J, et al. Apoptosis in Various Organs of Preterm Infants: Histopathologic Study of Lung, Kidney, Liver, and Brain of Ventilated Infants.pdf. *Pediatric Research*. 2001;50(1):110–114.
32. De Visser YP, Walther FJ, Laghmani EH, et al. Phosphodiesterase 4 inhibition attenuates persistent heart and lung injury by neonatal hyperoxia in rats. *American Journal of Physiology-Lung Cellular and Molecular Physiology*. 2012;302(1):L56–67.
33. Schweitzer KS, Hatoum H, Brown MB, et al. Mechanisms of lung endothelial barrier disruption induced by cigarette smoke: role of oxidative stress and ceramides. *American Journal of Physiology-Lung Cellular and Molecular Physiology*. 2011;301(6):L836–46.
34. Göggel R, Winoto-Morbach S, Vielhaber G, et al. PAF-mediated pulmonary edema: a new role for acid sphingomyelinase and ceramide. *Nature medicine*. 2004;10(2):155–60.
35. Diab KJ, Adamowicz JJ, Kamocki K, et al. Stimulation of sphingosine 1-phosphate signaling as an alveolar cell survival strategy in emphysema. *American journal of respiratory and critical care medicine*. 2010;181(4):344.
36. Bielawski J, Szulc ZM, Hannun YA, Bielawska A. Simultaneous quantitative analysis of bioactive sphingolipids by high-performance liquid chromatography-tandem mass spectrometry. *Methods*. 2006;39(2):82–91.
37. Yoo HH, Son J, Kim D-H. Liquid chromatography-tandem mass spectrometric determination of ceramides and related lipid species in cellular extracts. *Journal of chromatography*. 2006;843(2):327–33.
38. Dunnill MS. Quantitative Methods in the Study of Pulmonary Pathology. *Thorax*. 1962;17(4):320–328.
39. Cooney TP, Thurlbeck WM. The radial alveolar count method of Emery and Mithal: a reappraisal 1–postnatal lung growth. *Thorax*. 1982;37(8):572.
40. Karadag A, Sakurai R, Wang Y, et al. Effect of maternal food restriction on fetal rat lung lipid differentiation program. *Pediatric pulmonology*. 2009;44(7):635–44.

Chapter 4

HIF-1α Overexpression Stimulates Alveolar Development but does not Prevent O_2-induced Lung Injury

Jeroen Tibboel[1,4*]
Freek A. Groenman[1,3*]
Johanna Selvaratnam[1]
Jinxia Wang[1]
Irene Tseu[1]
Zhen Huang[1]
Isabella Caniggia[2]
Daochun Luo[1]
Minke van Tuyl[1,3]
Cameron Ackerley[1]
Johan C. de Jongste[4]
Dick Tibboel[3]
Martin Post[1,2]

[1] Dept. of Physiology and Experimental Medicine, Hospital for Sick Children, Toronto, Canada.
[2] Dept. of Physiology, University of Toronto, Toronto, Canada.
[3] Dept. of Pediatric Surgery, Erasmus University Medical Center – Sophia Children's Hospital, Rotterdam, the Netherlands.
[4] Dept. of Pediatrics, Erasmus University Medical Center – Sophia Children's Hospital, Rotterdam, the Netherlands.

[*] *These two authors contributed equally to this work.*

Submitted

ABSTRACT

Aim: The formation of alveoli is a largely postnatal process that involves the development of an extensive vascular network. The hypoxia-inducible factor (HIF) family of transcriptional regulators has been implicated in early pulmonary vasculature development. Our aim was to investigate whether HIF influences postnatal vascularization and alveologenesis in mice, and whether stable (constitutive-active) HIF could prevent hyperoxia-induced lung injury.
Methods: We assessed postnatal vessel and alveolar formation in transgenic mice, expressing a stable, constitutive-active, HIF-1α-subunit (HIF-1αΔODD) in the distal lung epithelium. In addition, we compared lung function, histology and morphometry of neonatal transgenic and wild type mice subjected to hyperoxia.
Results: Postnatal lungs of HIF-1αΔODD mice had a greater peripheral vessel density and displayed advanced alveolarization compared to control lungs. Stable HIF-1α expression was associated with an increased postnatal expression of angiogenic factors including vascular endothelial growth factor, angiopoietins 1 and 2, Tie2, and EphrinB2 and EphB4. Hyperoxia-exposed neonatal HIF-1αΔODD mice exhibited worse lung function and abnormal surfactant composition but had similar histological abnormalities compared to hyperoxia-exposed wild-type controls.
Conclusion: Expression of constitutive-active HIF-1α in the lung epithelium stimulated postnatal vessel growth via upregulation of angiogenic factors. The increase in postnatal vasculature was accompanied by enhanced alveolar formation. However, stable HIF-1α expression did not prevent hyperoxia-induced lung injury in neonates but instead worsened lung function due to alterations in surfactant composition.

INTRODUCTION

Interaction between airways and blood vessels is critical for lung development[1,2]. Early lung development occurs in a relatively hypoxic environment *in utero*[3]. This low oxygen environment is beneficial for pulmonary vascular development and is mediated via the hypoxia-inducible factor (HIF) family of transcriptional regulators[1,2]. Growth and maturation of the capillary network is vital for creating a proper blood-air barrier and to make gas exchange possible. Alveoli are formed through the process of septation, whereby secondary septa emerge from existing primary septa[4]. The capillary layer from the primary septum is pulled into the newly formed secondary septum and therefore the new septum contains a double capillary layer, which is later reduced to a single capillary layer[5]. Although birth is often considered the end of organogenesis and the start of growth and maturation, the development and maturation of alveoli in humans and most other mammals is largely a postnatal process. Impaired septation has been observed as one of the consequences of neonatal pulmonary damage in preterm newborns, called Bronchopulmonary Dysplasia (BPD)[6]. Important features of BPD are decreased alveolarization and abnormal vessel growth[7,8]. Furthermore, patients suffering from BPD have low levels of pulmonary vascular endothelial growth factor (VEGF)[9]. Indeed, pharmacological blockade of VEGF signaling impairs postnatal lung development in newborn rats[10]. Hyperoxia exposure in newborn mice has been used to replicate the characteristic alveolar arrest seen in BPD[11], and is used to study the pathogenesis and pathophysiology of BPD[12,13] and develop potential treatments[14–16]. For instance, VEGF gene therapy improved vascular development and prevented hyperoxia-induced BPD in newborn rats[14]. VEGF is a target gene for HIF and pharmacological HIF stabilization has been shown to increase the expression of VEGF and to stimulate angiogenesis[17–20]. Thus, strategies aimed at increasing HIF are of major interest as a way to potentially improve the outcome of early lung injury in prematures.

The HIF family consists of heterodimers comprised of one of three alpha subunits and a beta subunit. The most extensively studied isoform of the three α-subunits is HIF-1α. HIF-1α is a highly conserved transcription factor present in almost all human organs and cell types[21]. HIF-1α controls up to 500 genes, many of these being involved in endothelial cell proliferation and survival[20]. Under normoxic conditions the α-subunit is rapidly hydroxylated and targeted for proteosomal degradation[22]. Since oxygen regulates the interaction between airways and vessels during development via HIF[1,2], we investigated whether expression of a stable (constitutive-active) HIF-1α in the developing lung epithelium during postnatal lung development would result in accelerated vascularization and alveolarization[23]. Furthermore, since decreased levels of HIF-1α have been found in BPD[17,24] we investigated whether stable expression of HIF-1α during postnatal hyperoxia exposure could promote alveolarization and prevent or ameliorate the lung damage in a hyperoxia-induced BPD model[12,13].

MATERIALS AND METHODS

Transgenic Mice

The human full-length HIF-1α cDNA construct (generous gift of Dr. Semenza, Johns Hopkins University) was used as template to generate the HIF-1αΔODD mutant. The deletion mutant (HIF-1α$\Delta_{401\text{-}603}$) was constructed by overlap extension using PCR as previously described[25]. The biological activity of the HIF-1αΔODD mutant was confirmed in JEG3 and 293T cells using a HIF-responsive reporter construct (Supplementary figure S1). Transgenic SFPTC-HIF-1αΔODD (C57BL/6 X SJL) F2 embryos were generated according to Hogan et al[26]. Mice were bred according to a protocol approved by the Animal Care and Use Committee of the Hospital for Sick Children.

Hyperoxia-induced BPD model

We used a modified hyperoxia model as described previously[27]. Briefly, two pathogen-free timed pregnant C57BL/6 and two HIF-1αΔODD mutant mice gave birth in room air. At postnatal day 1, the mothers and their pups were placed in paired Oxycycler exposure chambers (Biospherix Ltd, Lacona, NY). Litters were exposed to hyperoxia (80% O_2) or room air. Litter sizes were kept at 6 pups in both the hyperoxia and room air groups. Dams were switched daily. Oxygen exposure was maintained for 28 days, after which the mice had gained enough weight to perform lung function measurements and histology.

Lung function measurements

Twenty-eight days after the start of hyperoxia, the Flexivent rodent ventilator (Scireq, Montreal, Canada) was used to assess lung function as described previously[27].

Immunostaining, immunoblotting and quantitative RT-PCR (qPCR)

Lungs were fixed under constant inflation at 10 cm H_2O. Immunostaining was performed using the avidin-biotin (ABC) immunoperoxidase method[28]. Immunoblotting was performed as previously described[29] on lysates of nuclei (Nuclear enrichment kit, Pierce). qPCR was carried out as described in the supplementary methods section.

Morphometric analysis of paraffin-embedded lung

All morphometric assessments were performed on the right middle lobe. The lungs were embedded in paraffin wax, cut in 5 μm sections and stained with haematoxylin and eosin. Morphometric assessments were performed on coded images to mask control and transgenic lungs. Digital images were captured using a Leica digital imaging system (Leitz, Wetzlar, Germany) at 20X magnification with random sampling of all tissue in an unbiased fashion. Images of 10 non-overlapping fields from each slide, with 3 slides/animal, and 5 animals per group were captured. Tissue fractions and secondary crests densities were measured as previously described[30]. Mean linear intercepts (Lm) were measured and calculated as described by Dunnill[31]. Radial alveolar counts (RAC) were performed as described by Cooney[32]. Alveolar surface area per unit lung volume were calculated as described by Kawakami and coworkers[33]. Slides were stained for elastin to enhance recog-

nition of vessels after wich the number of small vessels (diameter range 20 to 65 μm) per field was assessed. Average values were calculated for 10 images per slide, and the average value for the 3 slides was used to calculate an average value for each animal.

Light- and electron microscopy of resin-embedded lung

Postnatal lung tissues were fixed under constant inflation at 10 cm H_2O and processed for electron microscopy as previously described[34]. Alveolar vessel and lipid-laden interstitial cell density was determined as described in the supplementary methods section.

Statistical Analysis

All values are presented as mean ± SEM. Statistical significance was determined by one way ANOVA, followed by post hoc analysis using Duncan's multiple range test where significant differences were found between groups (JMP software); a value of $p<0.05$ was inferred as statistically significant. A more detailed description of all methods can be found in the supplementary methods section.

RESULTS

HIF-1α expression

In control mice, pulmonary expression of mouse HIF-1α mRNA remained stable between embryonic day 18.5 and postnatal day 21 (Figure 1A). In contrast, pulmonary levels of total (mouse plus human) HIF-1α mRNA were significantly increased (>15-fold) in E18.5 HIF-1αΔODD mice. The total amount of HIF-1α mRNA decreased postnatally in the transgenic mice, but it remained significantly greater (>3-fold) than that of C57BL/6 control lungs as a result of *Sftpc*-driven expression of human HIF-1αΔODD in the transgenes (Figure 1B). Immunohistochemical analysis revealed that HIF-1α protein was upregulated in the distal epithelial type II cells of transgenic lungs when compared to control lungs during all postnatal ages (Supplementary figure S2). Western blot analysis corroborated these findings and further showed that the immunoreactive product was the 80 kDa HIF-1αΔODD recombinant protein (Figure 2A-top panel).

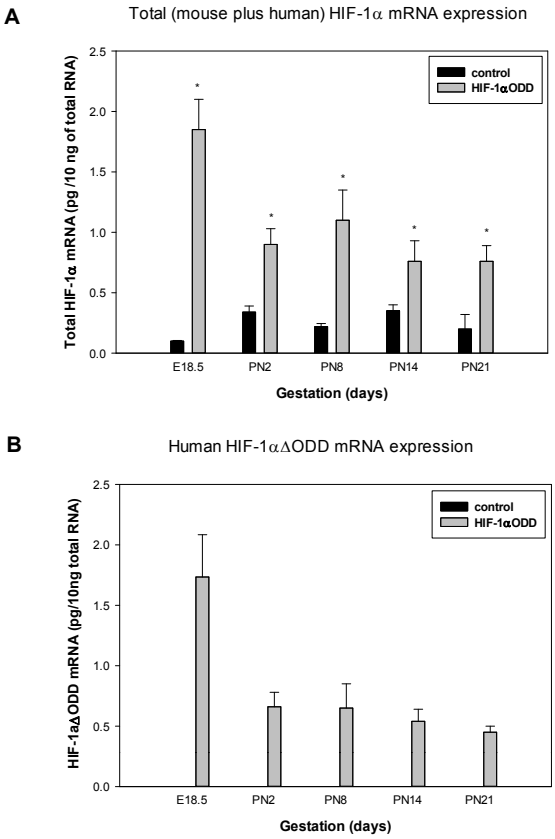

Figure 1. *Measurements of total HIF-1α and human HIF-1αΔODD gene expression in C57 control lungs and HIF-1αΔODD lungs during postnatal development. Levels of (A) total (mouse and human) HIF-1α mRNA and (B) human HIF-1αΔODD in murine postnatal lung, as assessed by real-time qPCR. The number of HIF-1α transcripts was significantly greater in HIF-1αΔODD mice, which was due to increased human HIF-1αΔODD mRNA expression. Data are expressed as mean ± SEM for 4 lungs in each group. * = p<0.05.*

VEGF expression

Total VEGF expression in C57BL/6 control lungs was constant between E18.5 and postnatal day 21 (Figure 2B-top panel). The amount of total VEGF mRNA was significantly greater in HIF-1αΔODD lungs at all gestational days compared to control lungs. We tested the possibility that VEGF isoform expression could be different among the control and HIF-1αΔODD lungs. We found that the mRNA expression of the $VEGF_{188}$ isoform was specifically increased in the HIF-1αΔODD lungs at all gestational days (Figure 2B-bottom panel). Transcript levels for the $VEGF_{120}$ isoform were slightly, but significantly, increased at postnatal day 2 and 8, while $VEGF_{164}$ mRNA expression was not altered in the HIF-1αΔODD lungs. Western blot analysis confirmed an increase in VEGF, migrating as a 23 kDa protein in SDS-PAGE under reducing conditions, in HIF-1αΔODD lungs at E18.5 and

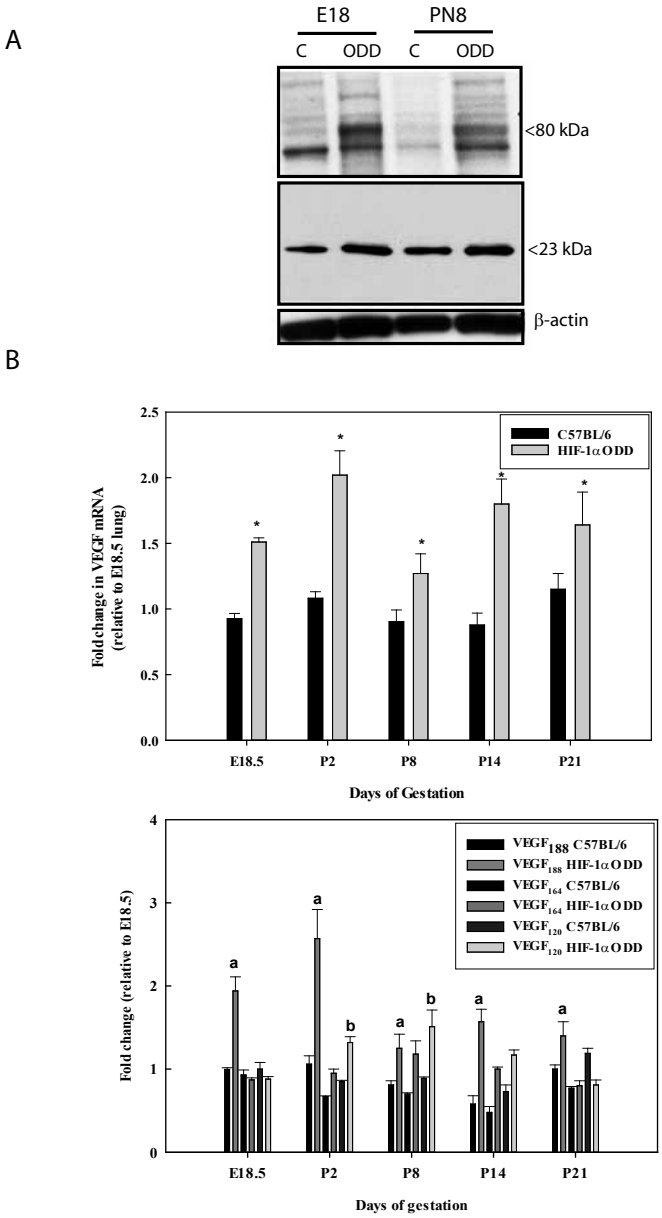

Figure 2. *Immunoblot analysis of HIF-1α and VEGF gene expression in C57 control lungs and HIF-1αΔODD lungs. (A) Western blot of HIF-1α and VEGF on E18.5 and PN8 lungs. Equal loading and transfer was probed with β-actin. (B) Expression of total VEGF mRNA and expression of $VEGF_{188}$, $VEGF_{164}$ and $VEGF_{120}$ mRNA in murine lung, as assessed by real-time qPCR. Data are expressed as relative fold changes in expression when compared to E18.5 lungs. Data are expressed as mean ± SEM for 4 lungs in each group. * = p<0.05. (See colour section, page 187).*

postnatal day 8 (Figure 2A-middle panel). VEGFR2 mRNA expression was not affected by HIF-1αΔODD overexpression when compared to controls (not shown). Pulmonary Angiopoietin(Ang)1, Ang2 and Tie2 mRNA levels were increased at postnatal days 8 and 14 while transcript levels for EphrinB2 and EphB4 were increased in the transgenic lungs at postnatal days 2, 8 and 14 (Supplementary figure S3).

Vessel formation

To assess if vascularization was increased in HIF-1αΔODD lungs we counted the number of small peripheral vessels (diameter ranging from 20 to 65 μm) and found a significant increase in postnatal vessel density in the HIF-1αΔODD lungs compared to the C57BL/6 control lungs (Figure 3A). In addition, we determined the alveolar vessel density by electron microscopy. We observed a greater alveolar vessel density in HIF-1αΔODD transgenes compared to control C57BL/6 mice at postnatal days 14 and 21 (Figure 3B). Increased expression of the endothelial marker CD31 (Pecam-1) at postnatal days 8 and 14 further corroborated these findings (not shown).

Alveolarization

HIF-1αΔODD lungs exhibited increased structural complexity in comparison to C57BL/6 pups during days 2, 8, and 14 of the post gestational period (Figure 4a, b, c vs. e, f, g). Tissue fraction analysis confirmed a significant increase in the tissue-to-air ratio in HIF-1αΔODD pups *vs.* C57BL/6 control pups on postnatal days 2, 8, and 14 (Figure 4). The number of alveoli per unit area was higher in HIF-1αΔODD pups *vs.* C57BL/6 control pups in general, but significantly higher in HIF-1αΔODD pups on postnatal days 8 and 14 (Figure 4). To quantify alveolar development, we calculated the secondary crest number per field and the secondary crest/tissue ratio. Secondary crest counts per unit area were significantly increased in HIF-1αΔODD pups *vs.* C57BL/6 control pups on postnatal days 2, 8, and 14, but when corrected per tissue fraction secondary crest formation was only increased during the early postnatal period (Figure 4). The number of Ki67-positive (proliferative) crests was significantly increased in the HIF-1 mutant mice at postnatal days 2, 8 and 14 (not shown), suggestive of increased secondary crest formation. To further evaluate alveolar development, we measured mean linear intercept (Lm) and alveolar surface area per unit lung volume. The Lm decreased in the HIF-1αΔODD and C57BL/6 control pups with advancing postnatal age (Figure 5A). HIF-1αΔODD pups had significantly lower Lm on postnatal days 8 and 14 when compared to C57BL/6 control pups, consistent with a reduction in airspace diameter and enhanced alveolar formation. In line with these findings, alveolar surface density increased in both HIF-1αΔODD and C57BL/6 control pups throughout postnatal gestation (Figure 5A). We observed a significantly increased alveolar surface density in HIF-1αΔODD pups on postnatal days 8 and 14 when compared to C57BL/6 control pups, consistent with enhanced alveolar formation.

Surfactant protein C (SFPTC) is a marker for alveolar type II cells[35] while aquaporin 5 and T1α are alveolar type I cell markers[36]. *Sftpc* mRNA expression peaked around birth and decreased with advancing postnatal gestation as previously described[37]. Constitutive-active HIF-1α had no effect on *Sftpc* gene expression (Figure 5B), although the percent-

A

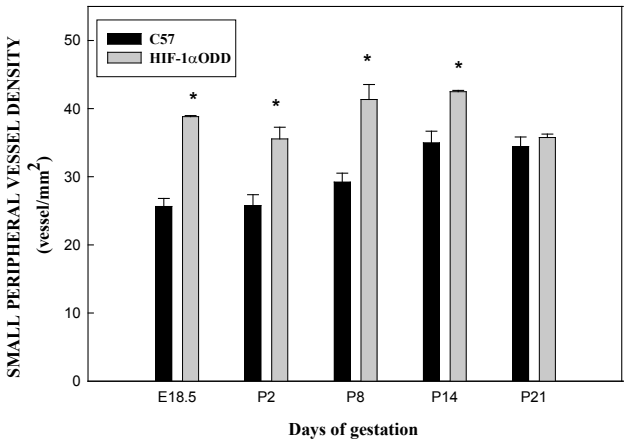

B

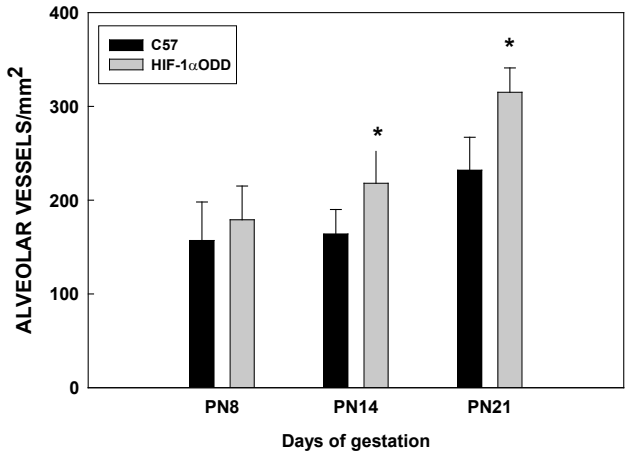

Figure 3. *Effect of stable HIF-1α-expression on vascular formation during postnatal development. (A) Small vessel (diameter range 20 to 65 μm) density was increased in HIF-1αΔODD lungs compared to C57 control lungs at all gestational ages except at PN21. (B) Alveolar vessel density was also increased in HIF-1αΔODD lungs, specifically at PN14 and 21.*

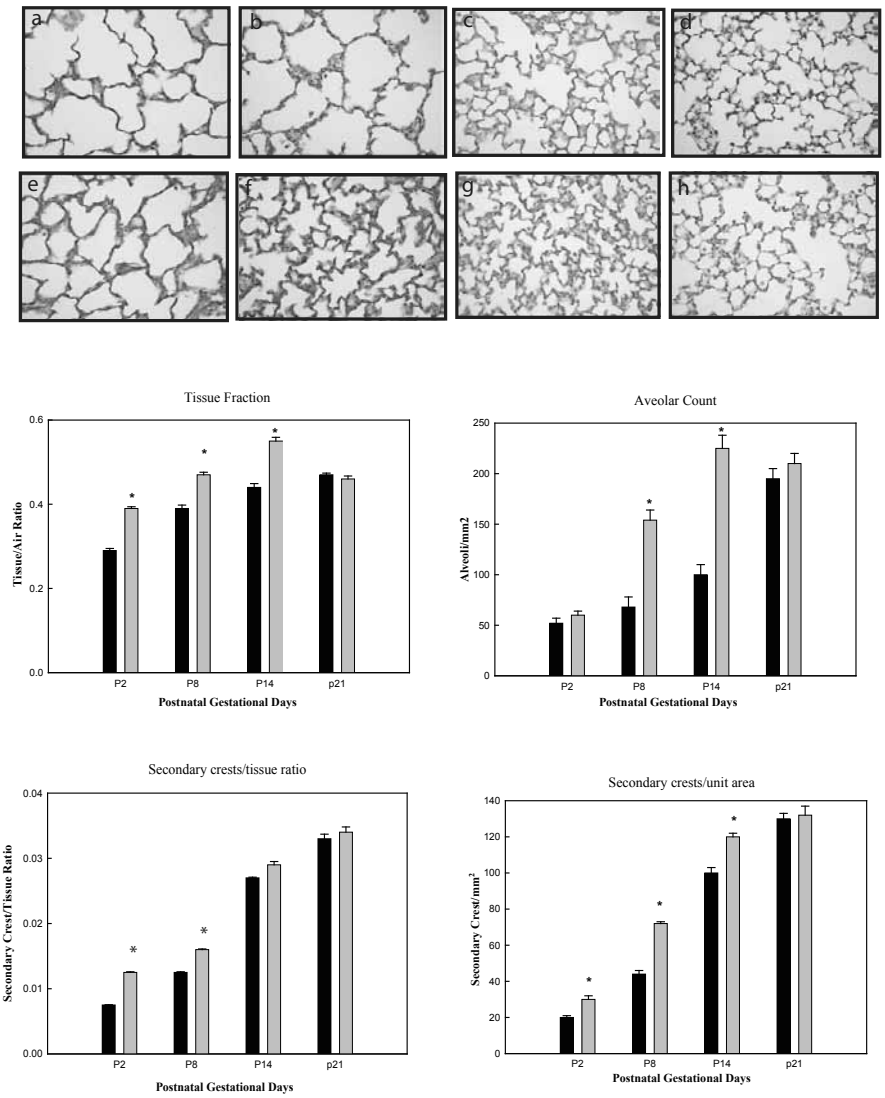

Figure 4. *Histology and morphometry of neonatal C57BL/6 control lungs and HIF-1αΔODD lungs. Hematoxylin and eosin staining of HIF-1αΔODD lungs (e-h) showed increased parenchymal tissue per unit area of lung and smaller distal airspaces compared to C57BL/6 lungs (a-d) consistent with enhanced alveologenesis (Bar = 200 μm). Tissue fraction and number of alveoli per unit area were significantly increased in HIF-1αΔODD lungs at postnatal day 2, 8 and 14. The secondary crest/tissue ratio was increased in HIF-1αΔODD pups at postnatal days 2 and 8. Secondary crest number per unit area was significantly increased in HIF-1αΔODD lungs at postnatal days 2, 8 and 14. Data are expressed as mean ± SEM for five pups in each group. * = p<0.05. (See colour section, page 188).*

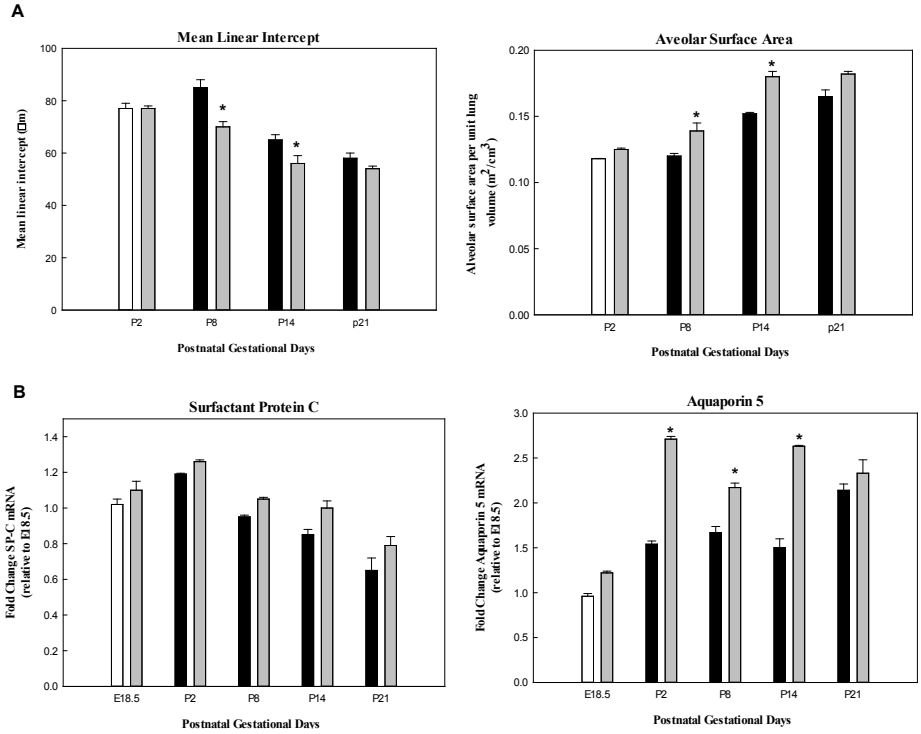

Figure 5. *Morphometric alveolar measurements and expression of surfactant protein C and aquaporin 5. (A) A significant decrease in mean linear intercept and alveolar surface area per unit lung volume was observed in HIF-1αΔODD pups at postnatal days 8 and 14, consistent with enhanced alveolar formation. Values are presented as mean ± SEM for five pups in each group. (B) Expression of surfactant protein C and aquaporin 5 mRNA expression in murine lung, as assessed by qPCR. Data are expressed as relative fold changes in expression when compared to E18.5 lungs. Data are expressed as mean ± SEM for 4 lungs in each group. * = p<0.05.*

age of SFTPC-positive cells was increased at postnatal day 14 in the HIF-1αΔODD lungs (25.35±2.62 *vs* 17.97±2.18 % of total cells, HIF-1αΔODD *vs* control C57BL/6 lungs, P<0.05, n=4-6 animals per group; 6 fields per animal; minimum of 1500 cells counted). Aquaporin 5 gene expression increased with advancing gestation and was significantly upregulated in the HIF-1αΔODD lungs at postnatal days 2, 8 and 14 (Figure 5B). T1α transcript levels were also increased in the HIF-1αΔODD lungs compared to controls (not shown). The latter findings are consistent with enhanced alveolar type I cell formation. Gene expression of tropoelastin and lysyloxidase remained unchanged in HIF-1αΔODD mice compared to wild-type controls at all postnatal days (not shown).

Lipid droplet-laden interstitial cells

Electron microscopic analysis of the HIF-1αΔODD lungs revealed an increase in number of lipid droplet-laden interstitial cells. These cells resided in the interstitium (Figure 6A-C)

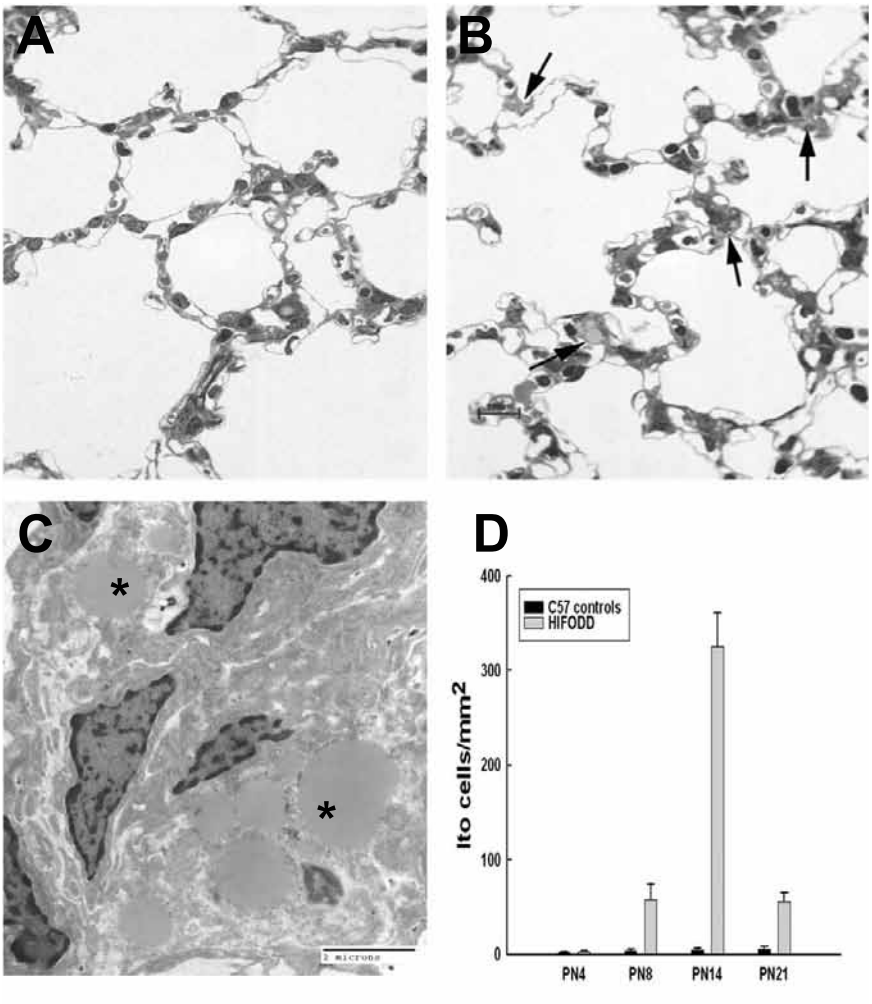

Figure 6. *Stable HIF-1α-expression increases number of lipid-laden interstitial (Ito) cells during postnatal development. Toluidine blue staining of ultrathin section shows an increase in lipid-laden cells (arrows) in HIF-1αΔODD lungs (A) vs. C57 control lungs (B) at PN14. (C) Electron micrograph of lipid droplet-laden interstitial (Ito) cells (* denotes lipid droplets). (D) Number of lipid droplet-laden interstitial cells was significantly increased at PN 8, 14 and 21. * = p<0.05. (See colour section, page 189).*

and their numbers were significantly increased in lungs of HIF-1αΔODD mice at postnatal days 8, 14 and 21 when compared to their C57 age-matched controls (Figure 6D).

Effects of hyperoxia

Prolonged (28 days) exposure of newborn C57BL/6 mice to hyperoxia increased lung resistance and reduced compliance and total lung capacity (Figure 7). While newborn HIF-1αΔODD mice showed similar lung function changes after prolonged hyperoxia

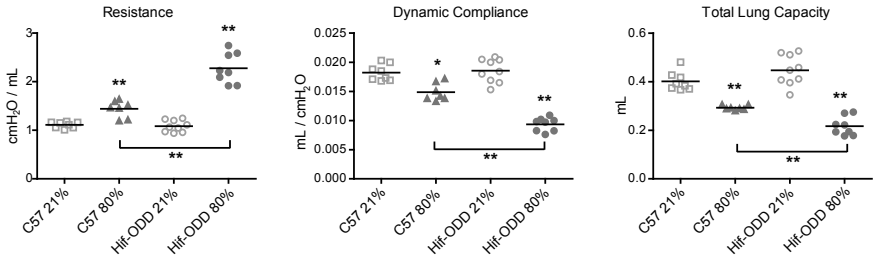

Figure 7. *Flexivent measurements of C57BL/6 mice exposed to hyperoxia show an increase in resistance, compliance and total lung capacity. Stable HIF-1α expression in the HIF-1αΔODD mice showed a further increase in resistance, compliance and total lung capacity, when compared to hyperoxia-treated C57BL/6 mice. Each dot represents the average of 4 accepted (coefficient of determination: COD>0.95) measurements for one individual mouse; the bar indicates the group mean. * = p<0.05, ** = p<0.001.*

exposure (Figure 8), these changes were significantly more pronounced than in C57BL/6 mice (Table 1). In contrast to lung function, histological and morphometric analyses revealed no difference between C57BL/6 and HIF-1αΔODD mice exposed to 80% oxygen (Figure 8). Both groups exhibited a similar reduction in alveolar septation when exposed to hyperoxia (Figure 8A *vs.* B, Figure 8D *vs.* C) which was corroborated by comparable morphometric changes in Lm and RAC when comparing hyperoxia- *vs.* normoxia-exposed mice (Figure 8E). Immunohistochemical analysis revealed an increase in the relative number of transgene HIF-1α expressing cells in hyperoxia-exposed neonatal HIF-1αΔODD mice compared to room air littermate controls while the percentage of SFTPC- and Ki67-positive cells remained constant (Table 2). Prolonged neonatal hyperoxia of C56BL/6 mice caused no change in the percentage of SFTPC-positive cells or HIF-1α mRNA expression. Since stable HIF-1α upregulated VEGF expression in normoxia we determined VEGF and VEGFR2 mRNA expression in HIF-1αΔODD mice exposed to hyperoxia. Surprisingly, pulmonary expression of both genes was significantly downregulated in hyperoxia (VEGF: 1.0±0.17 *vs.* 0.64±0.12 fold change relative to normoxia. VEGFR2: 1.0±0.07 *vs.* 0.49±0.23 fold change relative to normoxia. Normoxia *vs.* hyperoxia, mean± SD, p<0.05, n=6 pups per group). Since HIF has been shown to affect surfactant production[38,39], we examined whether changes in surfactant phosphatidylcholine (PC) content and composition could account for the worsening of lung function in the hyperoxia-exposed HIF-1αΔODD mice. Prolonged neonatal hyperoxia markedly increased total PC content in the bronchoalveolar lavage (BAL) of the HIF-1αΔODD mice and significantly altered its composition (increasing 16:0/14:0PC, decreasing 16:0/18:1PC and maintaining 16:0/16:0PC levels) when compared to normoxia-exposed littermates (Table 3).

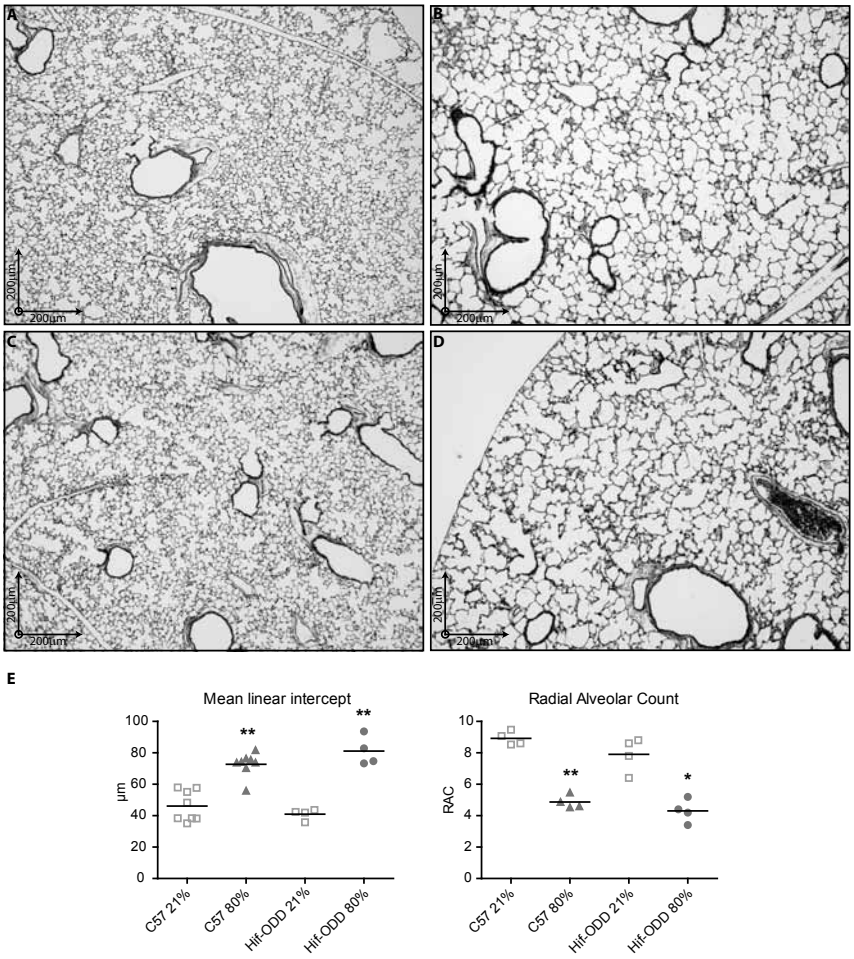

Figure 8. *Representative histological sections of normoxia-exposed C57BL/6 mice (A), hyperoxia-exposed C57BL/6 mice (B), normoxia-exposed HIF-1αΔODD mice (C) and hyperoxia-exposed HIF-1αΔODD mice (D) are shown. Sections were stained with hematoxylin and eosin. Morphometry results (E) are expressed as mean ± SEM for mean linear intercept and radial alveolar counts. * = p<0.05, ** = p<0.001. (See colour section, page 190).*

DISCUSSION

In the present study we found that pulmonary expression of constitutive-active HIF-1α accelerated postnatal alveolar formation via an increase in postnatal vascularization, probably as a result of up-regulated expression of VEGF and other angiogenic molecules. Nonetheless, constitutive-active HIF-1α did not protect newborn mice against hyperoxia-

Table 1. *Invasive (Flexivent) lung function measurements.*

Parameter	Unit	C57BL/6		HIF-1αΔODD	
		Normoxia (n=5)	Hyperoxia (n=6)	Normoxia (n=9)	Hyperoxia (n=8)
Resistance	cmH_2O/mL	1.13 (1.05-1.16)	1.46 (1.27-1.57) **	1.08 ± 0.04	2.28 ± 0.11 **/ ##
Dynamic Compliance	mL/cmH_2O	0.018 (0.017-0.019)	0.014 (0.014-0.016) *	0.018 ± 0.001	0.009 ± 0.001 **/ ##
Static Compliance	mL/cmH_2O	0.041 ± 0.001	0.020 ± 0.001 **	0.044 (0.037-0.049)	0.012 (0.011-0.016) **/ ##
Airway Resistance	cmH_2O/mL	0.39 (0.37-0.40)	0.45 (0.42-0.50) *	0.53 (0.46-0.58)	0.71 (0.64-0.72) **/ ##
Tissue Specific Elasticity	cmH_2O/mL	50.26 ± 1.27	53.38 ± 1.92	50.53 ± 1.85	87.41 ± 3.53 **/ ##
Total lung capacity	mL	0.39 (0.37-0.42)	0.29 (0.29-0.30) **	0.45 ± 0.02	0.22 ± 0.01 **/ ##
Inspiratory Capacity from zero pressure	mL	0.60 ± 0.02	0.33 ± 0.01 **	0.66 (0.56-0.73)	0.21 (0.20-0.27) **/ ##

*During invasive lung function measurements, an average for each individual mouse was calculated from 4 accepted (coefficient of determination: COD>0.95) measurements for each parameter. Values are expressed as mean ± SEM when normally distributed and median + (range) when not normally distributed. * = p<0.05, ** = p<0.001 when compared to control animals (C57BL/6 hyperoxia vs C57BL/6 normoxia and HIF-1αΔODD hyperoxia vs HIF-1αΔODD normoxia), ## = p<0.001 when compared C57BL/6 hyperoxia.*

Table 2. *Immunohistochemical analysis of hyperoxia-exposed HIF-1αΔODD.*

Marker	Normoxia (n=6)	Hyperoxia (n=6)	T-test
HIF-1α	3.42 ± 1.24	10.96 ± 4.00 *	0.003
SFTPC	25.35 ± 2.62	24.61 ± 2.71	NS
Ki67	14.42 ± 2.50	16.39 ± 4.89	NS

*Immunohistochemical analysis in hyperoxia-exposed neonatal HIF-1αΔODD mice compared to room air littermate controls. Values are % of totals cells with at least 1500 cells counted and expressed as mean ± SEM. * = p<0.05, when compared to control animals.*

Table 3. *Surfactant phosphatidylcholine (PC) content and composition in hyperoxia-exposed HIF-1αΔODD mice.*

Total PC	Normoxia (n=5)	Hyperoxia (n=5)	T-test
	23.58 ± 1.43	109.96 ± 19.04 *	0.002
PC Species	**Normoxia (n=5)**	**Hyperoxia (n=5)**	**T-test**
16:0/16:0	59.80 ± 2.82	58.35 ± 3.89	NS
16:0/14:0	3.93 ± 0.48	15.08 ± 1.87 *	0.000005
16:0/18:0	1.75 ± 0.30	2.03 ± 0.23	NS
16:0/18:1	21.87 ± 1.78	10.71 ± 1.99 *	0.000007
16:0/18:2	5.50 ± 0.60	5.24 ± 1.17	NS
16:0/20:4	3.25 ± 0.45	4.78 ± 0.92 *	0.005
18:0/18:1	0.50 ± 0.20	0.51 ± 0.09	NS
18:0/18:2	1.18 ± 0.28	1.97 ± 0.18	NS
18:0/20:4	2.10 ± 1.09	2.46 ± 0.65	NS

*Surfactant phosphatidylcholine (PC) content and composition in hyperoxia-exposed HIF-1αΔODD mice. Total PC is expressed in μg/150μl of BAL. PC species are expressed in % of total BAL PC. Data are expressed as mean ± SEM. * = p<0.05, when compared to control animals.*

induced alveolar arrest but instead worsened hyperoxia-induced lung function abnormalities and altered the surfactant composition.
HIF plays an important role in early pulmonary organogenesis and postnatal alveolarization. Blocking HIF-1α expression in the early embryonic lung led to a decrease in vascularization[1] while removal of HIF-1α in pulmonary epithelial cells caused pups to die with RDS-like symptoms within hours of parturition[39]. Removal of HIF-2α in mice resulted in impaired lung maturation[38], whereas overexpression of HIF-2α was found to be lethal and lungs from these mice revealed dilated alveoli, diminished alveolar type I cells and aberrant type II cells[40]. Loss of HIF was associated with diminished epithelial VEGF expression[38,39]. Conversely, stabilization of HIF enhanced early lung vascularization[2], enhanced lung growth, and improved oxygenation and lung compliance[19]. Enhancing HIF stability has been shown to increase the expression of VEGF and to stimulate angiogenesis[17,18]. VEGF gene therapy has been shown to prevent hyperoxia-induced BPD in newborn rats by stimulating vascular development[14]. Hence, strategies aimed at increasing HIF are of major interest as a way to potentially improve the outcome of early lung injury in prematures. Our studies were confined to the classical alveolarization period in mice (pnd 1-21) and suggested that stable (constitutive-active) expression of HIF mainly affects the early onset of septation (pnd 4-21). Prior to secondary crest eruption from the saccular walls, myofibroblasts proliferate and migrate to discrete areas of the saccular walls, where they deposit tropoelastin at the sites of future secondary crest formation, thus forming the elastic fibers. Although we found an increase in lipid droplet-laden interstitial cells (also termed lipofibroblasts), which have myofibroblasts properties and produce elastin and other extracellular matrix proteins[41], we did not notice any alteration in gene expression of tropoelastin or lysyloxidase (a cross-linking protein) in the HIF-1αΔODD mice compared to wild-type controls at all postnatal days. The catch-up in alveolarization at later gestation (pnd 21) was surprising since alveolar vessel density was still enhanced in the HIF-1αΔODD mice.

The exact mechanisms that regulate alveolar formation and development remain poorly understood, although experimental data have given some insight in molecular regulation of alveolarization[4,14,24,42]. Many studies showed loss of alveoli and pulmonary vasculature in neonatal pulmonary disease both in animal models and in humans[7,43,44]. We found that expression of stable HIF-1α enhances postnatal alveolarization as well as peripheral small vessel formation. We speculate that the continuous activation of the HIF-1 pathway and subsequent upregulation of the VEGF pathway accounted for this enhanced alveolar development. A specific isoform, $VEGF_{188}$, was upregulated in the HIF-1αΔODD mice at all gestational days. $VEGF_{188}$ is a cell surface- and extracellular matrix-associated isoform[45]. Galambos[46] and Ng[47] showed that a balance of VEGF isoforms is necessary for proper blood vessel branching morphogenesis in the lung. Moreover, absence of $VEGF_{164}$ and $VEGF_{188}$ isoforms impaired lung microvascular development and delays airspace maturation[46]. Hence, it is likely that the stimulation of alveolarization seen in HIF-1αΔODD mice is caused by the rise in $VEGF_{188}$ expression. This is further supported by observations showing that VEGF-induced angiogenesis was essential to alveolarization

in the developing rat lung, that VEGF and its receptors are decreased in lungs of infants dying with bronchopulmonary dysplasia[43] and that in experimental BPD pulmonary VEGF or VEGF gene therapy[14] stimulated vessel- and alveolar formation. These findings and our observations are compatible with the idea that distal lung vascularization is a driving force of alveolarization.

Based on previous pharmacological studies[17,18] we speculated that constitutively active HIF-1α would protect newborn mice against hyperoxia-induced alveolar injury since it upregulates VEGF and stimulates alveolar vascularization in normoxia. Surprisingly, we found that newborn HIF-1αΔODD mice, when exposed to hyperoxia, had even worse lung function than hyperoxia-exposed C57BL/6 control mice. Yet, hyperoxia-induced changes in alveolar morphology were similar in both mice, leading us to postulate that biochemical changes at the alveolar level were responsible for this effect. VEGF has been shown to prevent hyperoxia-induced alveolar simplification in mice[14] as well as enhance alveolarization in newborn mice after hyperoxia lung injury[48,49]. In contrast to normoxia, we found that stable HIF-1α expression during hyperoxia did actually decrease VEGF and VEGFR2 expression. Also, Hosford *et al.* showed that newborn rat lungs had decreased VEGF and VEGFR2 levels at day 9 and 12 of hyperoxia exposure[50]. Similar decreases in VEGF and VEGFR2 have been reported for the brain of mice exposed to hyperoxia[53]. Interestingly, the decreased levels of VEGF and VEGFR2 in the cerebral cortex was associated with transiently increased levels of HIF-1α and HIF-2α[51]. Thus, while HIF-1a transgene levels and VEGF mRNA correlate in room air they do not in the hyperoxia-treated group. Factor inhibiting HIF-1 (FIH-1) is an asparagyl hydroxylase, whose activity strictly depends on the presence of oxygen, which hydroxylates the HIF-1α carboxyl-terminal transactivation domain on Asn 803. This modification prevents its association with co-activators such as CBP/p300 that are needed for full transcriptional activity. Since the HIF-1αΔODD transgene contains the original Asn 803 site, it is possible that its hydroxylation by FIH-1 in hyperoxia reduces the transcriptional activity of the HIF-1α transgene and thereby VEGF.

In our experiments, BAL phosphatidylcholine content in HIF-1αΔODD mice exposed to hyperoxia was increased, in contrast to previous studies[39,52], and its composition altered. Altered BAL phosphatidylcholine composition has previously been shown to influence lung function both in animal disease models and in humans[53–56]. Previous studies in asthma, CF, idiopathic pulmonary fibrosis and acute respiratory distress patients showed that decreased lung function often correlates with decreased dipalmitoyl-PC (16:0/16:0PC) levels[53,55,56]. In our study, surface-active 16:0/16:0PC levels did not significantly change during hyperoxia exposure in the HIF-1αΔODD mice. A correlation between decreased palmitoyloleic-PC (16:0/18:1PC) levels and decreased lung function has been shown in a mouse model of bleomycin-induced pulmonary fibrosis[54], and our hyperoxia-exposed HIF-1αΔODD mice also showed decreased 16:0/18:1PC levels in BAL. Together with the increased palmitoylmyristoyl-PC (16:0/14:0PC) levels during hyperoxia-exposure this may affect the surface packing and adsorption of 16:0/16:0PC into the alveolar air/liquid inter-

face[57], thereby negatively affecting surfactant and lung compliance in hyperoxia-exposed HIF-1αΔODD mice.

In conclusion, our data show that overexpression of constitutive-active HIF-1α in room air was associated with increased postnatal vascularization and alveolarization through up-regulation of angiogenic factors. Stable HIF-1α overexpression did not prevent hyperoxia-induced injury in neonates, but led to worsening of lung function, due to an altered surfactant composition, specifically decreased palmitoyloleic phosphatidylcholine and increased palmitoylmyristoyl phosphatidylcholine levels.

ACKNOWLEDGEMENTS

The authors thank Angie Griffin for animal handling and care. Martin Post is the holder of a Canadian Research Chair in Fetal, Neonatal and Maternal Health.

SUPPLEMENTARY METHODS

Animal use

Animal protocols were in accordance with the Canadian Council for Animal Care guidelines and were approved by the Animal Care and Use Committee of the Hospital for Sick Children, Toronto, ON, Canada.

Transgene construction

The human full-length HIF-1α cDNA construct (generous gift of Dr. Semenza, Johns Hopkins University, Baltimore, MD, USA) was used as template to generate the HIF-1αΔODD mutant. The deletion mutant (HIF-1α$\Delta_{401\text{-}603}$) was constructed by overlap extension using PCR as previously described[25]. The deletion was confirmed by DNA sequencing. The biological activity of the HIF-1αΔODD mutant was confirmed using a HIF-responsive SEAP reporter construct. Two copies of EPO-HRE in tandem were subcloned into the Kpn I/Xho I restriction site of the pSEAP2-Promoter containing the SV40 promoter (Clontech, Mountain View, CA). JEG-3 and 293T cells were co-transfected with EPO-HRE-SEAP2 and either pcDNA3.1 vector, pcDNA3.1-HIF-1α, or pcDNA3.1 HIF-1αΔODD plasmid. SEAP2 activities were measured using the Phospho-Light TM reagent as outlined by the manufacturer (Tropix Inc. (Applied Biosystem) Bedford, MA). After confirmation of activity, the 1.95 kb HIF-1αΔODD cDNA was subcloned 3' of the 3.7 kb human SP-C promoter[38] and 5'of the SV40 small T intron and polyadenylation sequences. The expression cassette was excised with NdeI and NotI, purified using Glass Milk (Gene Clean Kit Bio 101, BioCan, Canada) and Elutip-D columns (Schleier and Schuell, NY), and ethanol precipitated.

Production of transgenic mice

Transgenic SFPTC-HIF-1αΔODD embryos were generated according to Hogan *et al.*[26]. DNA injections into pronuclei of (C57BL/6 X SJL) F2 embryos were carried out at a concentration of 3 ng/μl. The genotype was established by PCR analysis of genomic DNA extracted from the embryonic tail and confirmed by Southern blot analysis. The primers used were 5'-TCACCTCTGTCCCCTCTCCCTACG-3' and 5'-CATTTCTCTCATTT CCTCATGGTCA CATGG-3'.

Lung function measurements

Animals were anesthetized with an *ip* injection of Ketamine (150 mg/kg) and Xylazine (10 mg/kg) before tracheostomy. A 25G endotracheal tube was inserted and sutured into place to prevent leakage. After intraperitoneal injection of Pancuronium (5 mg/kg) the animal was ventilated at 150 breaths/min with a tidal volume of 10 mL/kg and lung function was measured using the Flexivent ventilator (SCIREQ, Montreal, QC, Canada). The flexivent measures flow-volume relations of the respiratory system and uses forced oscillations to discriminate between the airways and the alveolar compartment. The "Total Lung Capacity" (TLC), "Snapshot" (based on single-compartment model), and "Primewave-8" (based on constant phase model) perturbations were used to measure lung function. For the "TLC" maneuver, the lung is inflated to +30 cmH_2O and deflated afterwards. For the

"Snapshot" maneuver, three sinusoidal waves of in- and expiration provide the resistance, elastance and compliance parameters. For the "prime-wave 8", multiple frequency forced oscillations were applied which results in the tissue elasticity and airway resistance parameters. Volume-driven pressure-volume loops were also obtained and provided the total lung capacity, inspiratory capacity from zero pressure and static and dynamic compliance. All measurements were repeated until 4 successful recordings with a coefficient of determination of >0.95 were obtained.

Immunohistochemistry

Immunohistochemical analyses were performed as previously described[28]. Rabbit polyclonal antibodies against HIF-1α (Cell Signaling Technologies, Danvers, MA) and Ki67 (Dako Canada, Mississauga, ON) were used at 1:50 and 1:200 dilutions, respectively. Biotinylated goat anti-rabbit IgG (1:300) was used as secondary antibody. Color detection was performed according to instructions in the Vectastain ABC and DAB kit (Vector Laboratories, Burlingname, CA, USA) and counterstaining was performed with Carazzi's haematoxylin. Control experiments were carried out by replacing the primary antibody with normal goat serum.

Immunofluorescence microscopy

Postnatal lungs were fixed under constant inflation of 10 cmH_2O. Sections were incubated overnight with rabbit anti-VEGF (dilution of 1:800, Santa Cruz Biotechnology, Santa Cruz, CA), washed and incubated with biotinylated anti-rabbit IgG (dilution of 1:200, Vector Laboratories) and FITC-labelled strepavidin (dilution of 1:200, InVitrogen, Burlington, ON, Canada). Sections were thoroughly washed, incubated overnight with 1:50 diluted rabbit anti-HIF-1α, washed and incubated with biotinylated anti-rabbit IgG and $Fluo^R$594-labelled strepavidin (dilution of 1:200, InVitrogen). Sections were mounted with DAPI and digital images were recorded with a Zeiss LSM500e confocal microscope.

Electron microscopy

Postnatal lungs were fixed in 4% (v/v) paraformaldehyde (Sigma, St. Louis, MO, USA), 0.5% (w/v) glutaraldehyde (Sigma, St. Louis, MO, USA) in phosphate buffered saline (PBS). Tissues were then rinsed three times with PBS, exposed to 1% (w/v) osmium tetroxide (Marivac, PQ, Canada) followed by another three washes with PBS. The tissues were dehydrated through an ascending alcohol series and incubated three consecutive times in propylene oxide (Merivac, PQ, Canada). The propylene oxide was replaced with a 1:1 mixture of propylene oxide and Epon (Marivac, PQ, Canada) and finally 3 times with 100% Epon. The Epon infiltrated tissues were placed in molds and the Epon was polymerized at 70°C overnight. Ultrathin sections of the resulting blocks were cut using a diamond knife on a Reichert Ultracut microtome, placed onto 400-mesh copper grids and stained in 3% (w/v) uranyl acetate in double distilled water and then in 1% (w/v) lead citrate followed by several washes with double distilled water to remove excess stain. Samples were examined on a Philips 430 transmission electron microscope.

RNA isolation and real-time quantitative RT-PCR (qPCR)

Lung RNA was extracted with RNA easy kit (Qiagen, Mississauga, ON, Canada) and reverse transcribed using random hexamers (Invitrogen, Burlington, ON, Canada). The resulting templates were quantified by real-time PCR (ABI Prism 7900) using SYBR green I (Eurogentec North America, SanDiego, CA). Primers for total HIF-1α mRNA (measuring both mouse HIF-1α mRNA and human HIF-1αΔODD mRNA) were (F) 5'ATCCATGTGACCATGAGGAAATGAGAG3' and (R) 5'CCACACTGAGGTTGGTTACTGTTGGTA3' while primers for measuring specifically human HIF-1α ΔODD mRNA were (F) 5'GTTGTGAGTGGTATTATTCAGC ACGACTTG3' and (R) 5'AGTAGGTTCTTGTATTTGAGTCTGCAGCAAAG3'. Primers and TaqMan probes for total Vegf, $Vegf_{120}$, $Vegf_{164}$, and $Vegf_{188}$ were similar to previously published sequences[58], while primers and TaqMan probes for Ang1, Ang2, Tie2, EphrinB2, EphB4, Pecam-1, lysyl oxidase, tropoelastin, surfactant protein-C (Sftpc), aquaporin (Aqp) 5 and T1α were purchased from ABI as Assays-on-Demand™ for murine genes. Reactions were carried out in 96 well plates in triplicate. For each probe, a dilution series determined the efficiency of amplification of each primer-probe set. For the relative quantitation, PCR signals were compared between groups after normalization using 18S as an internal reference. Fold change was calculated according to Livak *et al.*[59].

Western blotting

Nuclei were isolated using a nuclear enrichment kit for tissue (Pierce, Rockford, IL). Western blot analyses of nuclear lysates were performed as previously described[(34)]. Primary antibodies were rabbit polyclonal anti-human HIF-1α (dilution of 1:1000, Cell Signaling Technology, Danvers, MA) and anti-VEGF (dilution of 1:350, Santa Cruz Biotechnology, Santa Cruz, CA) while goat anti-rabbit horseradish peroxidase–conjugated IgG was used as secondary antibody (dilution of 1:10,000, Jackson ImmunoResearch, Cedarlane Laboratories Limited, Canada).

Morphometric analysis of paraffin-embedded lung

As rates of lung maturation vary between regions of the lung, all morphometric assessments were performed on the right middle lobe. Lungs were embedded in paraffin wax, cut in 5 μm sections, and stained with haematoxylin and eosin. Morphometric assessments were performed on coded images to mask the control and transgenic lungs. Digital images were captured using a Leica digital imaging system at 20X magnification with random sampling of all tissue in an unbiased fashion. Images of 10 non-overlapping fields from each slide, with 3 slides per animal, and 5 animals per group were captured. Tissue fractions and secondary crests densities were measured as previously described[30]. Mean linear intercepts were measured and calculated as described by Dunnil[31]. Alveolar surface areas per unit lung volume were calculated as described by Kawakami *et al.*[33] Radial alveolar counts were counted according to the Emery and Mithal method[32]. Slides were stained for elastin to enhance recognition of vessels and the number of small vessels (diameter range 20 to 65 μm) per field was assessed. Average values were calculated for 10 images per slide, and the average value for the three slides was used to calculate an average value for each animal. All morphometric values are mean ± SEM of 5 animals per time point.

Morphometric analysis of resin-embedded lung

Overlapping images of toluidine blue stained 1μm sections were obtained using a Nikon digital camera and a 100X oil immersion lens. The images were analyzed using Image J (NIH, Bethesda, Md) and the total area in mm^2 of alveolar space was calculated. Both Ito cells and vessels profiles were counted within these areas and the density of either profile is expressed as Ito cells or alveolar vessels/mm^2. A minimum of 35 slides from each animal and 3 animals from each group were analyzed. Data are expressed as mean ± SD.

Data presentation

Statistical significance was determined by one way ANOVA, followed by post hoc analysis using Duncan's multiple range test where significant differences were found between groups (JMP software). A value of $p<0.05$ was inferred as statistically significant.

SUPPLEMENTARY FIGURES.

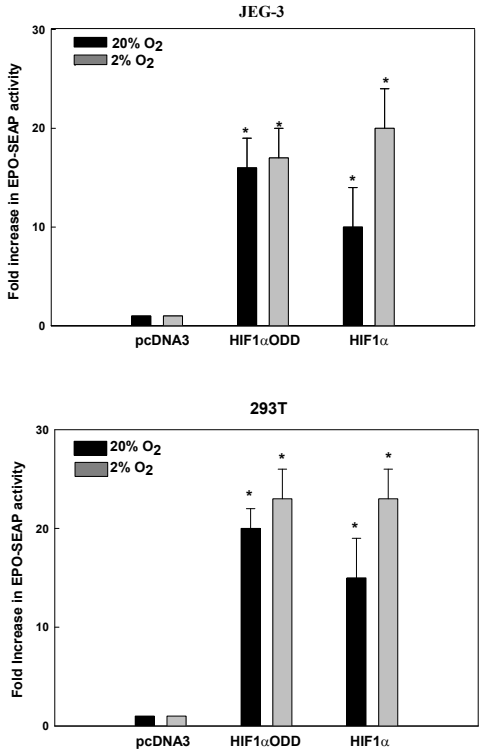

Supplementary figure S1. *Biological activity of the HIF-1αΔODD construct. JEG-3 and 293T cells maintained at either 2 or 20% oxygen were co-transfected with EPO-HRE-SEAP2 (reporter construct containing 2 EPO-HRE) and either pcDNA3.1 vector, pcDNA3.1-HIF-1α, or pcDNA3.1 HIF-1αΔODD plasmid. Both full length HIF-1α and HIF-1αΔODD significantly increased EPO-HRE-SEAP2 activities. Full length HIF-1α induction of EPO-HRE-SEAP2 decreased in cells cultured at 20% O_2 while HIF-1αΔODD induced EPO-HRE-SEAP2 activity remained constant.*

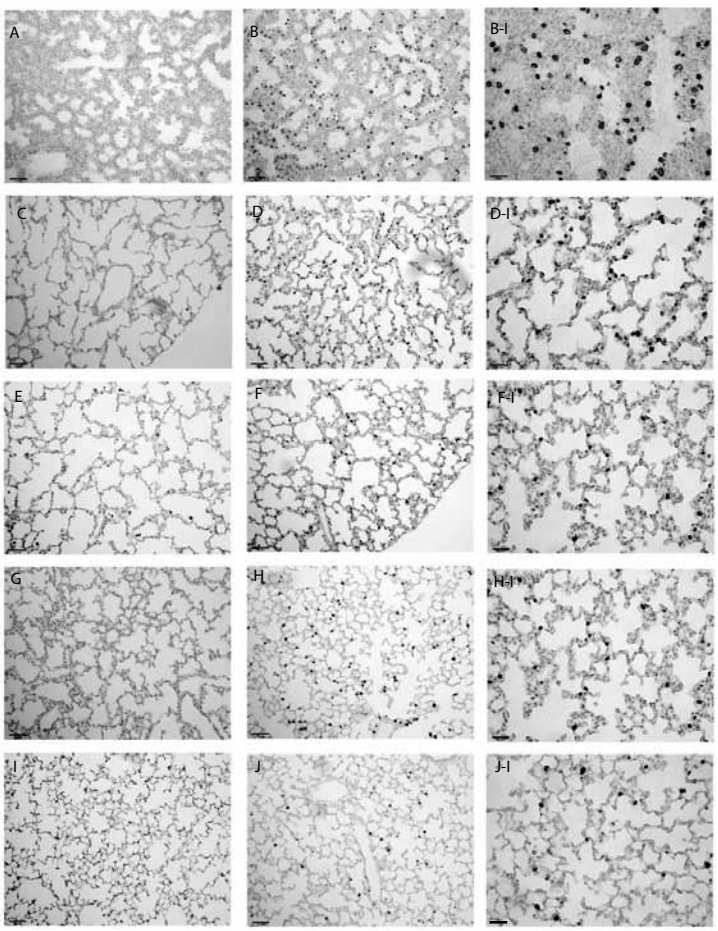

Supplementary figure S2. *Immunohistochemical analysis of HIF-1α in C57BL/6 control lungs and HIF-1αΔODD lungs. Strong positive brownish staining for HIF-1α is noted in the nuclei of distal airway epithelial type II cells of HIF-1αΔODD mice (B, B-I, D, D-I, F, F-I, H, H-I, J, J-I), but not C57BL/6 control mice (A,C,E,G,I) during all postnatal ages (E18.5: A,B,B-I; P2: C, D, D-I; P8: E, F, F-I; P14: G, H, H-I; P21: I, J, J-I. Bar = 200 μm (A-J); 50 μm (B-I, D-I, F-I, H-I, J-I). (See colour section, page 191).*

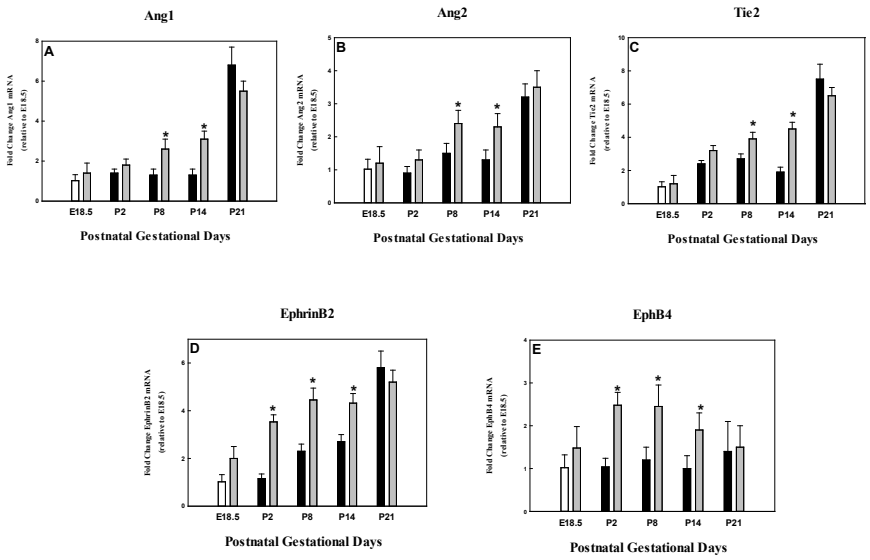

Supplementary figure S3. *Angiopoietin and ephrin expression in C57 control lungs and HIF-1αΔODD lungs during postnatal development. Expression of Ang1 (A), Ang2 (B), Tie2 (C), EphrinB2 (D) and EphB4 (E) expression mRNA in murine lung, as assessed by real-time qPCR. Data are expressed as relative fold changes in expression when compared to E18.5 lungs. Data are expressed as mean ± SEM for 4 lungs in each group. * = p<0.05.*

REFERENCES

1. Van Tuyl M, Liu J, Wang J, Kuliszewski M, Tibboel D, Post M. Role of oxygen and vascular development in epithelial branching morphogenesis of the developing mouse lung. *American Journal of Physiology-Lung Cellular and Molecular Physiology*. 2005;288(1):L167–78.
2. Groenman FA, Rutter M, Wang J, Caniggia I, Tibboel D, Post M. Effect of chemical stabilizers of hypoxia-inducible factors on early lung development. *American Journal of Physiology-Lung Cellular and Molecular Physiology*. 2007;293(3):L557–67.
3. Lee YM, Jeong CH, Koo SY, et al. Determination of hypoxic region by hypoxia marker in developing mouse embryos in vivo: a possible signal for vessel development. *Developmental dynamics*. 2001;220(2):175–86.
4. Roth-kleiner M, Post M. Similarities and Dissimilarities of Branching and Septation During Lung Development. *Pediatric pulmonology*. 2005;40(February):113–34.
5. Burri PH. Lung development and pulmonary angiogenesis. *Lung Development, New York: Oxford University Press*. 1999:122–151.
6. Jobe A. The new bronchopulmonary dysplasia. *Current opinion in pediatrics*. 2011;23(2):167–172.
7. Abman SH. Bronchopulmonary dysplasia: "a vascular hypothesis". *American journal of respiratory and critical care medicine*. 2001;164(10 Pt 1):1755–6.
8. Coalson JJ. Pathology of bronchopulmonary dysplasia. *Seminars in perinatology*. 2006;30(4):179–84.
9. Lassus P, Turanlahti M, Heikkilä P, et al. Pulmonary vascular endothelial growth factor and Flt-1 in fetuses, in acute and chronic lung disease, and in persistent pulmonary hypertension of the newborn. *American journal of respiratory and critical care medicine*. 2001;164(10 Pt 1):1981–7.
10. Le Cras TD, Markham NE, Tuder RM, Voelkel NF, Abman SH. Treatment of newborn rats with a VEGF receptor inhibitor causes pulmonary hypertension and abnormal lung structure. *American Journal of Physiology-Lung Cellular and Molecular Physiology*. 2002;283(3):L555–62.
11. Pappas CT, Obara H, Bensch KG, Northway WH. Effect of prolonged exposure to 80% oxygen on the lung of the newborn mouse. *Laboratory investigation*. 1983;48(6):735–48.
12. Alejandre-Alcázar M a, Kwapiszewska G, Reiss I, et al. Hyperoxia modulates TGF-beta/BMP signaling in a mouse model of bronchopulmonary dysplasia. *American Journal of Physiology-Lung Cellular and Molecular Physiology*. 2007;292(2):L537–49.
13. Balasubramaniam V, Mervis CF, Maxey AM, Markham NE, Abman SH. Hyperoxia reduces bone marrow, circulating, and lung endothelial progenitor cells in the developing lung: implications for the pathogenesis of bronchopulmonary dysplasia. *American Journal of Physiology-Lung Cellular and Molecular Physiology*. 2007;292(5):L1073–84.
14. Thébaud B, Ladha F, Michelakis ED, et al. Vascular endothelial growth factor gene therapy increases survival, promotes lung angiogenesis, and prevents alveolar damage in hyperoxia-induced lung injury: evidence that angiogenesis participates in alveolarization. *Circulation*. 2005;112(16):2477–86.
15. Chang YS, Choi SJ, Sung DK, et al. Intratracheal transplantation of human umbilical cord blood derived mesenchymal stem cells dose-dependently attenuates hyperoxia-induced lung injury in neonatal rats. *Cell transplantation*. 2011:1–32.
16. Balasubramaniam V, Ryan SSL, Seedorf GJ, et al. Bone marrow-derived angiogenic cells restore lung alveolar and vascular structure after neonatal hyperoxia in infant mice. *of Physiology-Lung*. 2010;298:L315–23.

17. Asikainen TM, Waleh NS, Schneider BK, Clyman RI, White CW. Enhancement of angiogenic effectors through hypoxia-inducible factor in preterm primate lung in vivo. *American Journal of Physiology-Lung Cellular and Molecular Physiology*. 2006;291(4):L588–95.
18. Asikainen TM, Schneider BK, Waleh NS, et al. Activation of hypoxia-inducible factors in hyperoxia through prolyl 4-hydroxylase blockade in cells and explants of primate lung. *Proceedings of the National Academy of Sciences of the United States of America*. 2005;102(29):10212–7.
19. Asikainen TM, Chang L-Y, Coalson JJ, et al. Improved lung growth and function through hypoxia-inducible factor in primate chronic lung disease of prematurity. *FASEB journal*. 2006;20(10):1698–700.
20. Manalo DJ, Rowan A, Lavoie T, et al. Transcriptional regulation of vascular endothelial cell responses to hypoxia by HIF-1. *Blood*. 2005;105(2):659–69.
21. Wiener C, Booth G, Semenza G. In Vivo Expression of mRNAs Encoding Hypoxia-Inducible Factor 1. *Biochemical and biophysical research communications*. 1996;488:485–488.
22. Kaelin WG, Ratcliffe PJ. Oxygen sensing by metazoans: the central role of the HIF hydroxylase pathway. *Molecular cell*. 2008;30(4):393–402.
23. Groenman F, Rutter M, Caniggia I, Tibboel D, Post M. Hypoxia-inducible factors in the first trimester human lung. *The journal of histochemistry and cytochemistry*. 2007;55(4):355–63.
24. Asikainen TM, Ahmad A, Schneider BK, White CW. Effect of preterm birth on hypoxia-inducible factors and vascular endothelial growth factor in primate lungs. *Pediatric pulmonology*. 2005;40(6):538–46.
25. Yang J, Wang J, Tseu I, Kuliszewski M, Lee W, Post M. Identification of an 11-residue portion of CTP-phosphocholine cytidylyltransferase that is required for enzyme-membrane interactions. *The Biochemical journal*. 1997;325 (Pt 1:29–38.
26. Hogan BL, Bedington RC., Lacy E. Manipulating the mouse embryo: a laboratory manual. *New York: Cold Spring Harbour Laboratory Press*. 1994.
27. Tibboel J, Joza S, Reiss I, Jongste JC De, Post M. Amelioration of hyperoxia-induced lung injury using a sphingolipid-based intervention. *European Respiratory Journal*. 2013;42(3):776-84.
28. Hsu SM, Raine L, Fanger H. Use of avidin-biotin-peroxidase complex (ABC) in immunoperoxidase techniques: a comparison between ABC and unlabeled antibody (PAP) procedures. *The journal of histochemistry and cytochemistry*. 1981;29(4):577–80.
29. MacPhee DJ, Mostachfi H, Han R, Lye SJ, Post M, Caniggia I. Focal adhesion kinase is a key mediator of human trophoblast development. *Laboratory investigation*. 2001;81(11):1469–83.
30. Yi M, Jankov RP, Belcastro R, et al. Opposing effects of 60% oxygen and neutrophil influx on alveologenesis in the neonatal rat. *American journal of respiratory and critical care medicine*. 2004;170(11):1188–96.
31. Dunnill MS. Quantitative Methods in the Study of Pulmonary Pathology. *Thorax*. 1962;17(4):320–328.
32. Cooney TP, Thurlbeck WM. The radial alveolar count method of Emery and Mithal: a reappraisal 1–postnatal lung growth. *Thorax*. 1982;37(8):572.
33. Kawakami M, Paul JL, Thurlbeck WM. The effect of age on lung structure in male BALB/cNNia inbred mice. *The American journal of anatomy*. 1984;170(1):1–21.
34. Ridsdale R, Post M. Surfactant lipid synthesis and lamellar body formation in glycogen-laden type II cells. *American Journal of Physiology-Lung Cellular and Molecular Physiology*. 2004;287(4):L743–51.
35. Kalina M, Mason RJ, Shannon JM. Surfactant protein C is expressed in alveolar type II cells but not in Clara cells of rat lung. *American journal of respiratory cell and molecular biology*. 1992;6(6):594–600.
36. Dahlin K, Mager EM, Allen L, et al. Identification of genes differentially expressed in rat alveolar type I cells. *American journal of respiratory cell and molecular biology*. 2004;31(3):309–16.

37. Glasser SW, Korfhagen TR, Bruno MD, Dey C, Whitsett JA. Structure and expression of the pulmonary surfactant protein SP-C gene in the mouse. *The Journal of biological chemistry*. 1990;265(35):21986–91.
38. Compernolle V, Brusselmans K, Acker T, et al. Loss of HIF-2alpha and inhibition of VEGF impair fetal lung maturation, whereas treatment with VEGF prevents fatal respiratory distress in premature mice. *Nature medicine*. 2002;8(7):702–10.
39. Saini Y, Harkema JR, LaPres JJ. HIF1alpha is essential for normal intrauterine differentiation of alveolar epithelium and surfactant production in the newborn lung of mice. *The Journal of biological chemistry*. 2008;283(48):33650–7.
40. Huang Y, Kempen MB, Munck AB, et al. Hypoxia-inducible factor 2α plays a critical role in the formation of alveoli and surfactant. *American journal of respiratory cell and molecular biology*. 2012;46(2):224–32.
41. McGowan SE, Torday JS. The pulmonary lipofibroblast (lipid interstitial cell) and its contributions to alveolar development. *Annual review of physiology*. 1997;59:43–62.
42. Thébaud B. Angiogenesis in lung development, injury and repair: implications for chronic lung disease of prematurity. *Neonatology*. 2007;91(4):291–7.
43. Bhatt AJ, Pryhuber GS, Huyck H, Watkins RH, Metlay LA, Maniscalco WM. Disrupted pulmonary vasculature and decreased vascular endothelial growth factor, Flt-1, and TIE-2 in human infants dying with bronchopulmonary dysplasia. *American journal of respiratory and critical care medicine*. 2001;164(10 Pt 1):1971–80.
44. Kinsella JP, Greenough A, Abman SH. Bronchopulmonary dysplasia. *Lancet*. 2006;367(9520):1421–31.
45. Ng Y-S, Krilleke D, Shima DT. VEGF function in vascular pathogenesis. *Experimental cell research*. 2006;312(5):527–37.
46. Galambos C, Ng Y-S, Ali A, et al. Defective pulmonary development in the absence of heparin-binding vascular endothelial growth factor isoforms. *American journal of respiratory cell and molecular biology*. 2002;27(2):194–203.
47. Ng YS, Rohan R, Sunday ME, Demello DE, D'Amore PA. Differential expression of VEGF isoforms in mouse during development and in the adult. *Developmental dynamics*. 2001;220(2):112–21.
48. Kunig AM, Balasubramaniam V, Markham NE, et al. Recombinant human VEGF treatment enhances alveolarization after hyperoxic lung injury in neonatal rats. *American Journal of Physiology-Lung Cellular and Molecular Physiology*. 2005;289(4):L529–35.
49. Kunig AM, Balasubramaniam V, Markham NE, Seedorf G, Gien J, Abman SH. Recombinant human VEGF treatment transiently increases lung edema but enhances lung structure after neonatal hyperoxia. *American Journal of Physiology-Lung Cellular and Molecular Physiology*. 2006;291(5):L1068–78.
50. Hosford GE, Olson DM. Effects of hyperoxia on VEGF, its receptors, and HIF-2alpha in the newborn rat lung. *American Journal of Physiology-Lung Cellular and Molecular Physiology*. 2003;285(1):L161–8.
51. Benderro GF, Sun X, Kuang Y, Lamanna JC. Decreased VEGF expression and microvascular density, but increased HIF-1 and 2α accumulation and EPO expression in chronic moderate hyperoxia in the mouse brain. *Brain research*. 2012;1471:46–55.
52. Ito Y, Ahmad A, Kewley E, Mason RJ. Hypoxia-inducible factor regulates expression of surfactant protein in alveolar type II cells in vitro. *American journal of respiratory cell and molecular biology*. 2011;45(5):938–45.
53. Mander A, Langton-Hewer S, Bernhard W, Warner JO, Postle AD. Altered phospholipid composition and aggregate structure of lung surfactant is associated with impaired lung function in young children with respiratory infections. *American journal of respiratory cell and molecular biology*. 2002;27(6):714–21.
54. Schmidt R, Ruppert C, Markart P, et al. Changes in pulmonary surfactant function and composition in bleomycin-induced pneumonitis and fibrosis. *Toxicology and applied pharmacology*. 2004;195(2):218–31.
55. Schmidt R, Markart P, Ruppert C, et al. Time-dependent changes in pulmonary surfactant function and composition in acute respiratory distress syndrome due to pneumonia or aspiration. *Respiratory research*. 2007;8:55.

56. Schmidt R, Meier U, Markart P, et al. Altered fatty acid composition of lung surfactant phospholipids in interstitial lung disease. *American Journal of Physiology-Lung Cellular and Molecular Physiology*. 2002;283(5):L1079–85.
57. Ridsdale R, Roth-Kleiner M, D'Ovidio F, et al. Surfactant palmitoylmyristoylphosphatidylcholine is a marker for alveolar size during disease. *American journal of respiratory and critical care medicine*. 2005;172(2):225–32.
58. Elson DA, Thurston G, Huang LE, et al. Induction of hypervascularity without leakage or inflammation in transgenic mice overexpressing hypoxia-inducible factor-1alpha. *Genes & development*. 2001;15(19):2520–32.
59. Livak KJ, Schmittgen TD. Analysis of relative gene expression data using real-time quantitative PCR and the 2(-Delta Delta C(T)) Method. *Methods*. 2001;25(4):402–8.

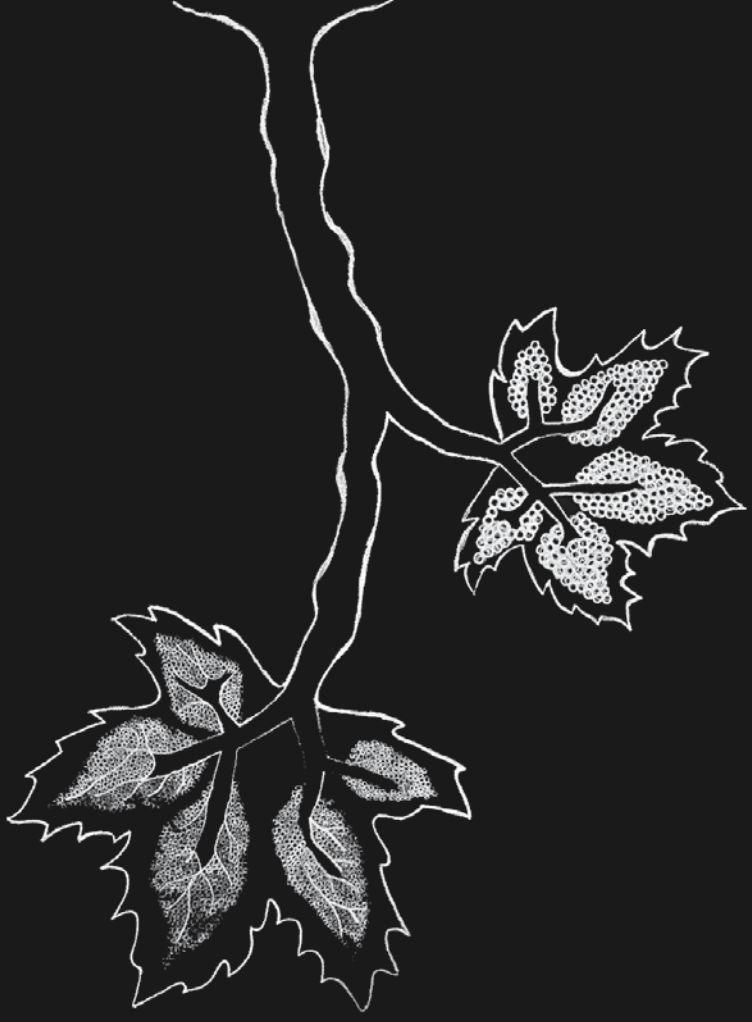

Chapter 5

Ceramides: a Potential Therapeutic Target in Pulmonary Emphysema

Jeroen Tibboel[1,3]
Irwin Reiss[3]
Johan C. de Jongste[3]
Martin Post[1,2]

[1] Physiology and Experimental Medicine Program, Hospital for Sick Children, Toronto, Canada.
[2] Dept. of Laboratory Medicine and Pathobiology, University Of Toronto, Toronto, Canada.
[3] Dept. of Pediatrics, Erasmus University Medical Center – Sophia Children's Hospital, Rotterdam, the Netherlands.

Respiratory Research in press

ABSTRACT

Aim: To characterize airway ceramide profiles in a rodent model of elastase-induced emphysema and to examine the effect of pharmacological intervention directed towards ceramide metabolism.
Methods: Adult mice were anesthetized and treated with an intratracheal instillation of elastase. Lung function was measured, broncho-alveolar lavage fluid collected and histological and morphometrical analysis of lung tissue performed within 3 weeks after elastase injection, with and without sphingomyelinase inhibitors or serine palmitoyl-transferase inhibitor. Ceramides in broncho-alveolar lavage (BAL) fluid were quantified by tandem mass spectrometry.
Results: BAL fluid showed a transient increase in total protein and IgM, and activated macrophages and neutrophils. Ceramides were transiently upregulated at day 2 after elastase treatment. Histology showed persistent patchy alveolar destruction at day 2 after elastase installation. Acid and neutral sphingomyelinase inhibitors had no effect on BAL ceramide levels, lung function or histology. Addition of a serine palmitoyltransferase inhibitor ameliorated lung function changes and reduced ceramides in BAL.
Conclusion: Ceramides were increased during the acute inflammatory phase of elastase-induced lung injury. Since addition of a serine palmitoyltransferase inhibitor diminished the rise in ceramides and ameliorated lung function, ceramides likely contributed to the early phase of alveolar destruction and are a potential therapeutic target in the elastase model of lung emphysema.

INTRODUCTION

Chronic Obstructive Pulmonary Disease (COPD) is a common and increasing source of morbidity and mortality in the developed world[1] and is associated with a large financial burden[2]. Pulmonary emphysema, an important component of COPD, is caused by permanent destruction of alveoli, airflow obstruction and lung hyperinflation, leading to a decreased lung function and breathlessness. The pathogenesis is related to smoke exposure, but why only a minority of all smokers develops emphysema remains unclear. Reports suggest that inflammation is partly responsible. The inflammatory infiltrate seen in emphysema is similar to that found in infection and correlates to the extent of emphysema[3], while the degree of cell death correlates to the amount of inflammation[4]. In humans, airway inflammation persists for many years after smoking cessation[5]. Sphingolipids are important structural components of biological membranes and have recently been shown to serve as messenger molecules in cell proliferation, apoptosis, cell contact and adhesion, endothelial barrier function and during inflammation[6–14]. Ceramide is the central molecule in the sphingolipid pathway[15] and is formed either *de novo* from the condensation of palmitate with serine via the activity of a serine palmitoyltransferase (SPT), by the salvage pathway via sphingosine or via degradation of sphingomyelin by sphingomyelinase (SMase)[16]. Ceramide is degraded by ceramidase to sphingosine which can be phosphorylated to sphingosine-1-phosphate (S1P)[17]. Ceramide and S1P form a rheostat[17,18] whereby ceramide stimulates apoptosis and cell cycle arrest while S1P stimulates cell survival and proliferation. Sphingolipid metabolism has been shown to be altered in a variety of diseases, including cystic fibrosis[19,20] and asthma[21]. Ceramide has been shown to trigger apoptosis in an experimental mouse model of emphysema[22], and increased levels of apoptosis have been found in the lungs of patients with severe cigarette-induced emphysema[23]. Increased ceramide levels have also been shown to influence surfactant production[24] and activity[25]. Since ceramide levels are increased in the lungs of patients with smoke-induced emphysema[22], ceramide upregulation might be an important pathogenetic element in emphysema development. We investigated ceramide profiles in the lungs and examined the effect of pharmacological interventions targeting SMases and SPT in an animal model of elastase-induced emphysema.

METHODS

Animals

Animals were obtained from Charles River (St. Constant, Quebec, Canada) and animal studies were conducted according to criteria established by the Canadian Council for Animal Care and approved by the Animal Care and Use Committee of the Hospital for Sick Children, Toronto, ON, Canada. Female adult C57BL/6 mice, weighing between 22 and 25 grams, were used for all experiments.

Elastase-induced lung injury
Porcine pancreatic elastase (Type I, aqueous suspension, ≥4.0 units/mg protein, Calbiochem, EMD biosciences, USA) was dissolved in sterile saline to create a volume for tracheal instillation of 100 µl per mouse with a concentration of 4.8 Units/100 g bodyweight. Animals were anesthetized with 3% isoflurane and intraperitoneal (*ip*) administration of Ketamine (75 mg/kg) and Xylazine (5 mg/kg). Following induction of anesthesia, a 25G intubation tube was inserted past the vocal cords and 100 µl of elastase instilled into the trachea. Control animals were treated similarly, but received sterile saline instead of elastase. BAL was collected from mice at t = 1, 2, 3, 4, 5, 8, 14 and 21 days after elastase instillation to measure sphingolipids and inflammatory markers.

Lung function measurements
At day 21 following instillation of elastase, the Flexivent rodent ventilator (Scireq, Montreal, Canada) was used to assess lung function as previously published[26].

Broncho-alveolar lavage
Lungs were infused through the endotracheal tube with 3x 600 µl sterile saline, followed by withdrawal[27,28]. The collected fluid was centrifuged at 1400 *g* for 8 min. The supernatant and remaining lung tissue was collected in siliconized eppendorf tubes and stored at -80°C for mass spectrometry analysis.

Histology of the lungs
Following lung function measurements, histology and morphometry of the lungs was performed as previously described[26].

Measurement of ceramides
Ceramide levels in BAL and remaining lung tissue were measured by tandem mass spectrometry as previously described[26]. The analysis was performed by the Analytical facility for Bioactive Molecules, The Hospital for Sick Children, Toronto, Canada.

Ceramide inhibitor experiments
Desipramine (acid SMase inhibitor, 20 mg/kg bodyweight), zoledronic acid (acid SMase inhibitor, 0.1 mg/kg bodyweight), sphingolactone (neutral SMase inhibitor, 1 mg/kg bodyweight) (Sigma–Aldrich, St. Louis, MO), and myriocin (SPT inhibitor, 1 mg/kg bodyweight) (Cayman Chemicals, Ann Arbor, MI) were administered via *ip* injection 2 hours before elastase instillation and 6, 24, 48 and 72 hours after elastase instillation. Each sphingolipid inhibitor experiment consisted of 4 groups: 1) control mice, 2) control mice treated with an *ip* injection of vehicle, 3) elastase-treated mice with an *ip* injection of vehicle and 4) elastase-treated mice with an *ip* injection of sphingolipid inhibitor dissolved in the appropriate vehicle. Half of the number of the mice in each group was sacrificed at day 2 after elastase instillation to measure sphingolipid levels and inflammatory markers in BAL. The other mice underwent lung function measurements at day 14 after elastase instillation before histology and morphometry.

Immunofluorescent staining

Immunofluorescencent staining was performed according to a previously published protocol with slight modification[29]. Tissue sections were de-waxed in xylene, rehydrated using decreasing ethanol series (100% to 70%), before being washed in 1xPBS/0.03% (vol/vol) Triton-100-X. Tissue permeabilization was achieved by boiling in 10 mM sodium citrate (pH 6) for 15 minutes at 95^{O}C, and cooled for 30 minutes in room temperature. Nonspecific antibody binding was blocked by incubation with a solution containing 10% (vol/ vol) normal donkey serum (Jackson ImmunoResearch, Cedarlane Laboratories, Burlington, Ontario) and 1% (vol/vol) bovine serum albumin in PBS at room temperature for 1 hour. The sections were washed and incubated for 1 hour with 1:100 diluted anti-ceramide monoclonal IgM antibodies (Glycobiotech, Borstel, Germany). The slides were washed again and stained for 30 min with a 1:200 diluted Cy3-labeled donkey anti-mouse IgM (Jackson ImmunoResearch,). After rinsing, the samples were mounted with 4,6-diamidino-2-phenylindole (DAPI) mounting medium (Vector, Burlington (ON)) and analyzed on a Leica fluorescence microscope.

Western Blotting

Lung tissues were lysed, protein content measured and aliquots (50 ug protein) were separated on 4-12% Bis-Tris precast polyacrylamide gels (Invitrogen, Cat. NP0322BOX) and transferred to PVDF membranes. After blocking with 5% (w/v) skim milk in TBST (20 mM Tris, 137 mM NaCl, 0.1% Tween 20) membranes were incubated with either goat anti-acid ceramidase antibody (1:500 dilution, T-20, Santa Cruz Biotechnology, CA), rabbit anti-acid sphingomyelinase (1:2000 dilution, H-181, Santa Cruz Biotechnology, CA) or goat anti-neutral ceramidase (1:500 dilution, S-20, Santa Cruz Biotechnology) overnight at 4°C. The next day the membranes were washed with TBST and incubated with either horseradish peroxidase–conjugated donkey anti-goat (1:20.000 dilution) or goat anti-rabbit (1:20.000 dilution) in 5% (w/v) skim milk in TBST at RT for 1-2 hrs. After several washes with TBST, protein bands were visualized using an enhanced chemiluminescence detection kit. Band densities were quantified using Scion Image software (Version 1.6, National Institutes of Health, Bethesda, MD, USA). Equal protein loading was confirmed by immunoblotting for β-actin of same membrane.

Statistics

All values are presented as mean ± standard error of the mean assuming normal distribution (Sigmaplot 11 for Windows). Differences were assessed by Student's t-test or, for comparison of more than two groups, by two-way analysis of variance followed by Holm-Sidak comparison test. Significance was inferred where $p<0.05$.

RESULTS

BAL analysis

A 4-fold increase in total ceramide and dihydroceramide levels was found at day 2 after elastase instillation when compared to saline-treated controls (Figure 1 and Table 1). Ceramide levels were 20-fold greater than dihydroceramide levels. Specifically, long chain and very long chain ceramides (Cer16:0, Cer22:0, Cer24:0 and Cer24:1) were increased. All ceramides and dihydroceramides returned to baseline levels within 5 days after elastase treatment. No difference in ceramide levels were noted in remaining lung tissue samples (not shown), therefore only BAL was analyzed in subsequent experiments. Neither desipramine, zoledronic acid or sphingolactone treatment altered ceramide levels (Table 2), but myriocin treatment ameliorated elastase-induced increases in multiple ceramides (Cer22:0, Cer24:0, Cer24:1), and dihydroceramides (18:0 and 24:0) (Figure 2, Table 3). Protein and IgM content (Figure 3A, C) and cell counts (Figure 3B) in BAL were increased at day 1, 2 and 3 after elastase injection. Cytospins from the same BAL fluid showed an increase in normal and activated "foamy" macrophages, and neutrophils, which normalized by day 5 after elastase injection (Figure 3D). Neither desipramine, zoledronic acid nor sphingolactone treatment had any effect on the above mentioned parameters. Myriocin treatment decreased BAL protein levels, shifted the neutrophil/macrophage balance towards neutrophils (Figure 4), but had no significant effect on IgM.

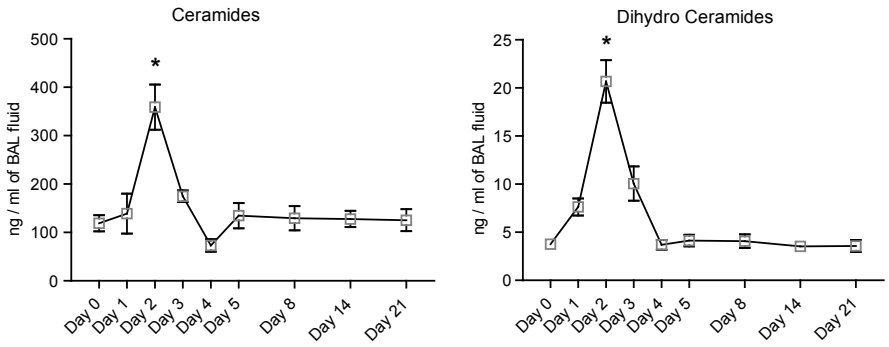

Figure 1. *Ceramide and dihydroceramide levels in BAL fluid during the first 21 days after elastase injection. Results represent a total of 4 mice per group for days 1, 3 and 4, 8 mice per group for days 8, 14, 21 and 12 mice per group for days 0, 2 and 5. * = p<0.05*

Table 1. *Ceramides after elastase injection.*

Ceramide	Day 0	Day 1	Day 2	Day 3	Day 4	Day 5	Day 8	Day 14	Day 21
Ceramide 16:0	45.63 ± 33.52	32.04 ± 14.16	110.54 ± 57.84 *	48.52 ± 3.87	21.91 ± 6.73	52.84 ± 1.86	40.97 ± 21.74	46.66 ± 27.52	38.04 ± 20.54
Ceramide 18:0	2.47 ± 0.68	3.55 ± 1.71	5.50 ± 1.55*	2.97 ± 0.48	1.38 ± 0.23	1.86 ± 0.61	2.20 ± 1.18	2.11 ± 0.72	2.46 ± 1.58
Ceramide 20:0	1.39 ± 0.40	1.92 ± 0.77	4.25 ± 1.98*	1.86 ± 0.36	0.79 ± 0.16	1.14 ± 0.40	1.41 ± 0.79	1.30 ± 0.41	1.32 ± 0.83
Ceramide 22:0	9.60 ± 2.47	14.12 ± 7.82	29.75 ± 11.28 *	16.31 ± 2.80	6.66 ± 2.30	9.00 ± 2.85	10.89 ± 5.74	10.13 ± 2.12	10.40 ± 5.40
Ceramide 24:0	34.83 ± 12.23	34.97 ± 20.00	112.76 ± 47.82 *	44.75 ± 6.09	19.09 ± 6.43	36.70 ± 16.82	40.97 ± 20.87	37.58 ± 9.04	41.64 ± 19.19
Ceramide 24:1	24.89 ± 8.47	52.02 ± 37.77	95.90 ± 41.08 *	60.25 ± 9.65 *	23.04 ± 9.75	33.03 ± 12.09	32.90 ± 20.18	30.01 ± 8.14	31.41 ± 16.8
Dihydro Ceramide 18:0	0.53 ± 0.24	2.01 ± 0.40 *	1.49 ± 0.53	1.51 ± 0.44	0.75 ± 0.34	0.36 ± 0.10	0.48 ± 0.31	0.40 ± 0.16	0.33 ± 0.15
Dihydro Ceramide 24:0	2.17 ± 0.68	4.64 ± 1.14	10.74 ± 4.32 *	3.77 ± 1.95	1.72 ± 0.34	1.83 ± 0.85	2.21 ± 0.99	1.85 ± 0.49	1.83 ± 0.85

*BAL fluid from 12 mice per group was collected and processed using LC-MS/MS. Data are expressed as mean + SEM in ng/ml BAL fluid. * = p<0.05, ** = p<0.001 when compared to control animals at the same time-point.*

Table 2. *Ceramides after Desipramine, Zoledronic Acid or Sphingolactone treatment.*

Sphingolipid	Control (n=5)	Control + Sph (n=9)	Control + ZA (n=9)	Control + Des (n=10)	Elastase (n=5)	Elastase + Sph (n=9)	Elastase + ZA (n=9)	Elastase + Des (n=10)
Ceramide 16:0	23.39 ± 2.92	25.55 ± 1.23	26.07 ± 2.85	32.70 ± 3.12 *	48.38 ± 4.46 *	53.07 ± 12.34 * $	44.47 ± 11.93 * $	63.15 ± 13.15 * # $
Ceramide 18:0	2.61 ± 0.54	2.74 ± 0.30	2.83 ± 0.20	4.01 ± 0.70	4.88 ± 0.60 *	5.66 ± 1.62 * $	4.43 ± 0.97 * $	7.45 ± 1.32 * # $
Ceramide 20:0	1.30 ± 0.34	1.24 ± 0.12	1.32 ± 0.14	1.97 ± 0.27	2.56 ± 0.37 *	2.86 ± 0.78 * $	2.44 ± 0.37 * $	4.07 ± 0.82 * # $
Ceramide 22:0	7.95 ± 2.41	7.37 ± 0.70	9.75 ± 1.29	14.17 ± 1.89 *	20.01 ± 4.39 *	20.43 ± 5.74 * $	19.80 ± 4.73 * $	33.90 ± 7.71 * # $
Ceramide 24:0	33.63 ± 13.22	25.92 ± 2.66	42.31 ± 6.19	56.01 ± 6.39 *	86.39 ± 22.72 *	71.40 ± 16.60 * $	84.40 ± 16.74 * $	145.10 ± 41.79 * # $
Ceramide 24:1	19.09 ± 6.27	17.97 ± 0.90	22.81 ± 4.10	33.25 ± 4.01 *	68.45 ± 19.42 *	64.66 ± 16.75 * $	70.20 ± 16.85 * $	113.70 ± 26.87 * # $
Dihydro Ceramide 18:0	0.32 ± 0.07	0.38 ± 0.23	0.39 ± 0.30	0.42 ± 0.08	0.88 ± 0.21 *	1.02 ± 0.35 * $	0.86 ± 0.20 * $	1.76 ± 0.24 * # $
Dihydro Ceramide 24:0	1.57 ± 0.67	1.67 ± 0.75	2.02 ± 1.11	2.32 ± 1.78	6.54 ± 1.78 *	6.28 ± 2.49 * $	6.29 ± 1.52 * $	13.11 ± 5.03 * # $

*BAL fluid was collected and processed using LCMS. Data are expressed as mean + SEM in ng/ml BAL fluid. Des = Desipramine, ZA = Zoledronic Acid, Sph = Sphingolactone. * = p<0.05 when compared to Control. # = p<0.05 when compared to Elastase. $ = p<0.05 when compared to control group with the same inhibitor (Elastase + Sph vs. Control + Sph, Elastase + ZA vs. Control + ZA, Elastase + Des vs. Control + Des).*

Table 3. *Ceramides after Myriocin treatment.*

Sphingolipid	Control (n=5)	Control + Myriocin (n=9)	Elastase (n=9)	Elastase + Myriocin (n=10)
Ceramide 16:0	30.01 ± 6.65	22.23 ± 7.95	41.04 ± 18.77	21.69 ± 4.91 ▯
Ceramide 18:0	3.13 ± 0.58	2.86 ± 0.75	4.00 ± 1.89	2.61 ± 0.60 ▯
Ceramide 20:0	1.94 ± 0.47	1.93 ± 0.43	2.73 ± 1.18	2.02 ± 0.43
Ceramide 22:0	7.97 ± 1.67	7.99 ± 3.42	15.13 ± 7.96 *	9.11 ± 3.02 ▯
Ceramide 24:0	37.34 ± 9.00	33.24 ± 13.50	77.75 ± 44.65 *	39.72 ± 13.00 ▯
Ceramide 24:1	24.66 ± 7.60	17.33 ± 8.02	41.48 ± 20.83 *	19.44 ± 6.27 ▯
Dihydro Ceramide 18:0	0.38 ± 0.21	0.37 ± 0.20	0.70 ± 0.27 *	0.44 ± 0.17 ▯
Dihydro Ceramide 24:0	1.97 ± 1.18	1.83 ± 0.65	6.12 ± 3.94 *	3.42 ± 2.21 ▯

*BAL fluid was collected and processed using LCMS. Data are expressed as mean + SEM in ng/ml BAL fluid. * = p<0.05 when compared to Control. # = p<0.05 when compared to Control + Myriocin. ▯ = p<0.05 when compared to Elastase + Myriocin.*

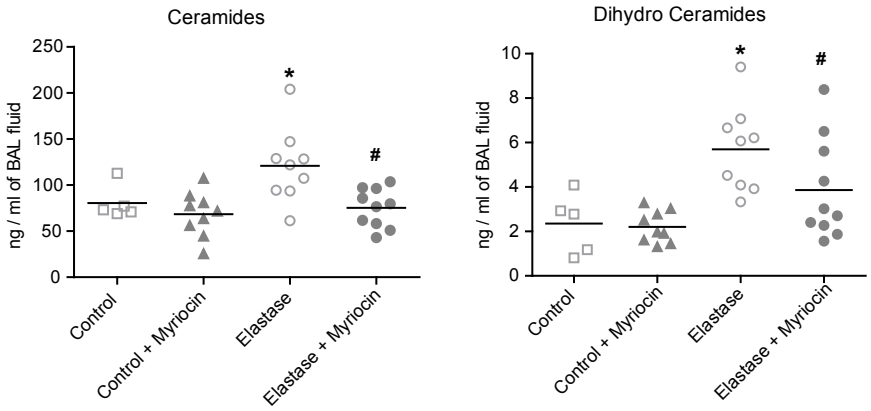

Figure 2. *Ceramide and dihydroceramide levels in BAL fluid at day 2 after elastase injection and myriocin treatment. Results represent a total of 5 mice for control, 9 mice for control + myriocin, 9 mice for elastase and 10 mice for elastase + myriocin group. * = p<0.05 when compared to Control. # = p<0.05 when compared to elastase.*

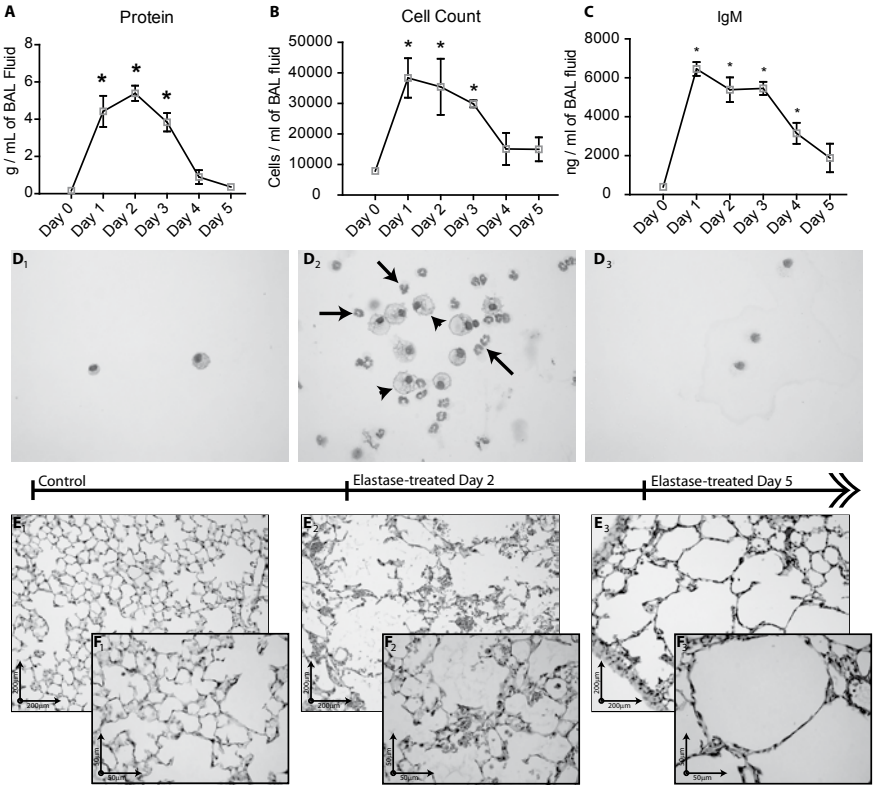

Figure 3. *Biochemical measurements in BAL fluid: protein levels (A) and cell count (B) at day 1, 2 and 3 after elastase injection. IgM levels (C) measured by ELISA. Cytospin slides (D) and haemotoxilin-eosin stained histological slides from control mice (E1 at 200x magnification, F1 at 400x magnification) and elastase-treated mice at 2 days after elastase injection (E2 at 200x magnification, F2 at 400x magnification) and 5 days after elastase injection (E3 at 200x magnification, F3 at 400x magnification). Arrows indicate neutrophils, arrowheads indicate macrophages. Graphs represent an n=4 for each group. * = p<0.05. (See colour section, page 192).*

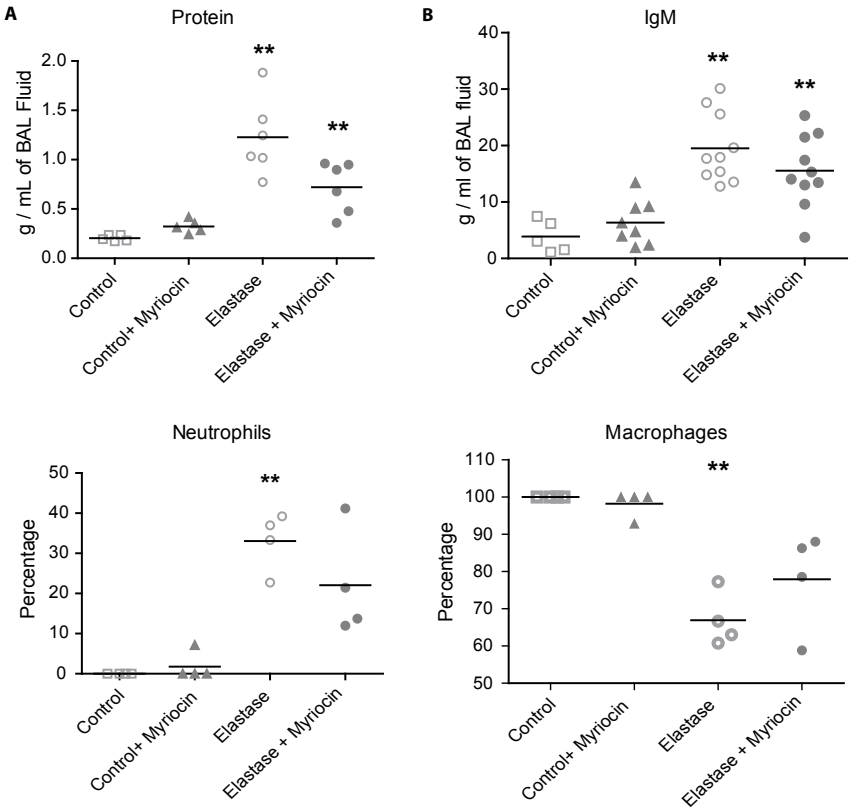

Figure 4. *Protein levels, IgM content, neutrophil and macrophage percentages in BAL fluid at day 2 after elastase instillation and myriocin treatment. ** = p<0.05 compared to controls. # = p<0.05 compared to elastase-treated mice.*

Enzyme expression

Western blot analysis of enzymes partaking in ceramide metabolism showed decreased acid ceramidase levels during the first 5 days after elastase treatment, reaching significance at day 3 and 5. Neutral ceramidase levels were only significantly downregulated at day 1 after elastase injection. Acid sphingomyelinase levels were only significantly upregulated at day 3 after elastase instillation (Figure 5).

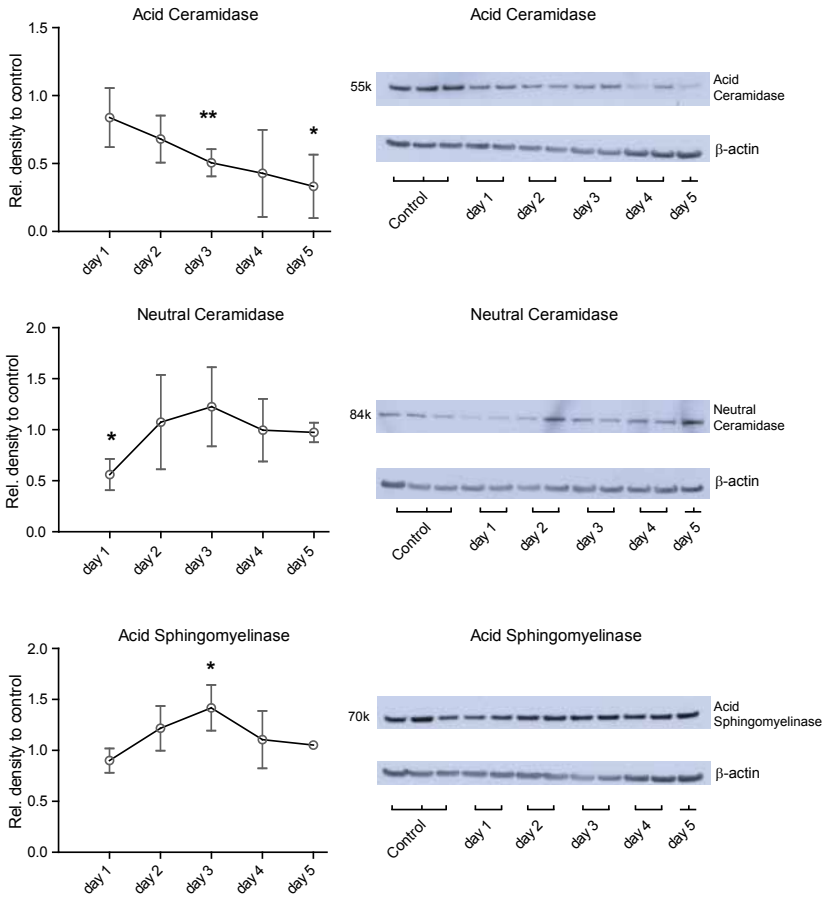

Figure 5. *Densitometric expression analysis of acid sphingomyelinase, acid- and neutral ceramidase proteins accompanied by representative western blots. Data are expressed as mean ± SEM. n=4 for day 1, 2 and 3, n=3 for day 4 and 5. * = p<0.05 and ** = p<0.001 compared to control levels (which were set at 1).*

Lung function

Lung function measurements of elastase-treated mice showed a significant reduction in resistance and tissue-specific elastance and an increase in dynamic compliance compared to controls (Figure 6, Table 4). Neither desipramine, zoledronic acid nor sphingolactone had any effect on lung function in elastase-treated animals compared to vehicle-treated elastase-exposed mice (Table 4). Elastase-treated mice receiving myriocin showed a significant decrease in compliance and increase in tissue elasticity compared to control elastase-exposed mice (even with a limited number of mice). Myriocin also prevented the decrease in resistance, normally seen in elastase-treated mice, compared to vehicle-treated elastase-exposed mice (Figure 6, Table 5).

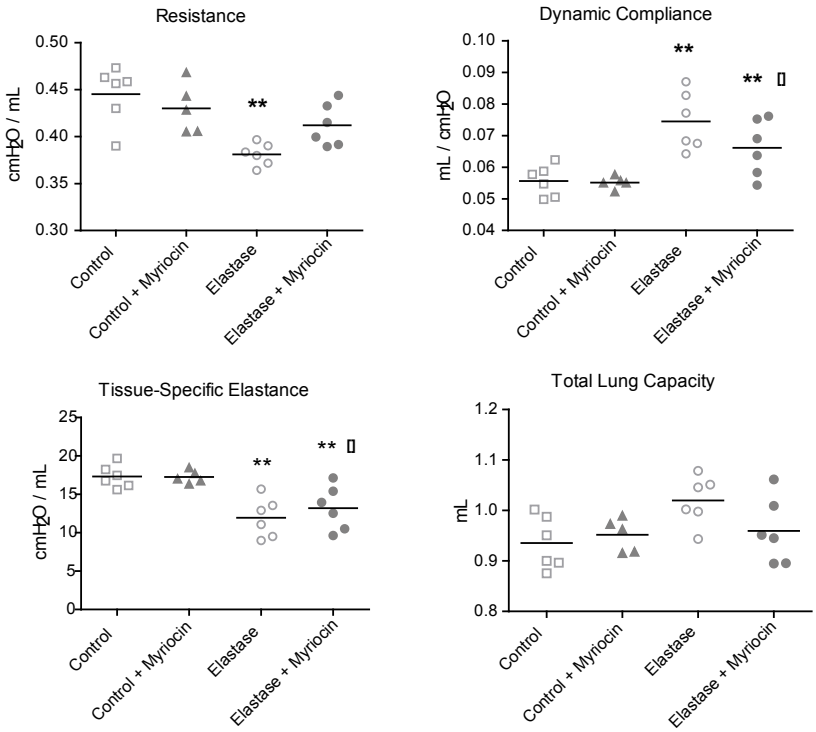

Figure 6. *Lung function 2 weeks after elastase injection in myriocin-treated mice. Results represent 6 mice for the control group, 5 mice for the control + myriocin treated groups, 6 mice for the elastase-treated and elastase-treated + myriocin group. Data are expressed as mean ± SEM. ** = p<0.05 when compared to the control and control + myriocin group. [] = p<0.05 when compared to the elastase-treated group.*

Table 4. *Invasive lung function measurements after Desipramine, zoledronic acid and sphingolactone treatment.*

Parameter	Unit	Control (n=9)	Elastase (n=10)	Elastase + Desipramine (n=5)	Elastase + zoledronic acid (n=4)	Elastase + sphingolactone (n=4)
Resistance (R)	cmH_2O/mL	0.67 ± 0.07	0.52 ± 0.03 *	0.47 ± 0.02 *	0.49 ± 0.01 *	0.54 ± 0.05 *
Compliance (C)	mL/cmH_2O	0.032 ± 0.004	0.052 ± 0.004 *	0.066 ± 0.007 *	0.067 ± 0.011 *	0.054 ± 0.007 *
Airway Resistance (Rn)	cmH_2O/mL	0.32 ± 0.03	0.23 ± 0.03 *	0.22 ± 0.02 *	0.25 ± 0.01 *	0.21 ± 0.02 *
Tissue Elasticity (H)	cmH_2O/mL	32.4 ± 4.2	16.9 ± 2.3 *	13.2 ± 1.3 *	13.9 ± 2.8 *	15.5 ± 2.7 *
Total lung capacity (A)	mL	0.70 ± 0.05	0.78 ± 0.04	0.88 ± 0.02	0.89 ± 0.07	0.77 ± 0.03
Inspiratory Capacity (B) from zero pressure	mL	1.14 ± 0.09	1.30 ± 0.11 *	1.47 ± 0.028 *	1.57 ± 0.19 *	1.29 ± 0.09 *
Static Compliance (Cst)	mL/cmH_2O	0.078 ± 0.008	0.094 ± 0.009 *	0.108 ± 0.002 *	0.115 ± 0.014 *	0.094 ± 0.008 *

*During invasive lung function measurements, an average for each individual mouse was calculated from 4 accepted (coefficient of determination: COD>0.95) measurements for each parameter. * = p<0.05 when compared to Control. # = p<0.05 when compared to Elastase.*

Table 5. *Invasive lung function measurements after Myriocin treatment.*

Parameter	Unit	Control (n=6)	Control + Myriocin (n=5)	Elastase (n=3)	Elastase + Myriocin (n=3)
Resistance	cmH_2O/mL	0.44 ± 0.03	0.43 ± 0.03	0.37 ± 0.01 *	0.41 ± 0.03
Compliance	mL/cmH_2O	0.056 ± 0.005	0.055 ± 0.002	0.082 ± 0.005 *	0.063 ± 0.005 # ▯
Airway Resistance	cmH_2O/mL	0.22 ± 0.01	0.22 ± 0.02	0.16 ± 0.03 *	0.18 ± 0.01 #
Tissue Elasticity	cmH_2O/mL	17.3 ± 1.5	17.3 ± 0.8	9.9 ± 1.1 *	14.0 ± 1.4 # ▯
Total lung capacity	mL	0.93 ± 0.05	0.95 ± 0.03	0.99 ± 0.05	0.93 ± 0.03
Inspiratory Capacity from zero pressure	mL	1.47 ± 0.08	1.49 ± 0.07	1.42 ± 0.06	1.36 ± 0.11
Static Compliance	mL/cmH_2O	0.105 ± 0.006	0.106 ± 0.005	0.104 ± 0.004	0.097 ± 0.009

*During invasive lung function measurements, an average for each individual mouse was calculated from 4 accepted (coefficient of determination: COD>0.95) measurements for each parameter. * = p<0.05 when compared to Control. # = p<0.05 when compared to Control + Myriocin. ▯ = p<0.05 when compared to Elastase.*

5

Histology and morphometry

Histological analysis of the lung at day 2 following elastase injection revealed the presence of erythrocytes in the alveolar spaces and massive influx of neutrophils and macrophages (Figure 3E). Alveolar enlargement was present from day 2 onwards. Erythrocytes and most of the inflammatory cells were cleared by day 5 after elastase injection. Immunofluorescent staining for ceramide showed increased positive reactivity in the epithelial lining and inflammatory cells in elastase-treated mice 2 days after elastase injection compared to controls (Figure 7). Three weeks after elastase installation we observed a patchy pattern of alveolar destruction leading to enlarged airspaces. This was reflected in a significant increase in mean linear intercept and decrease in alveolar number. Mice treated with SMase

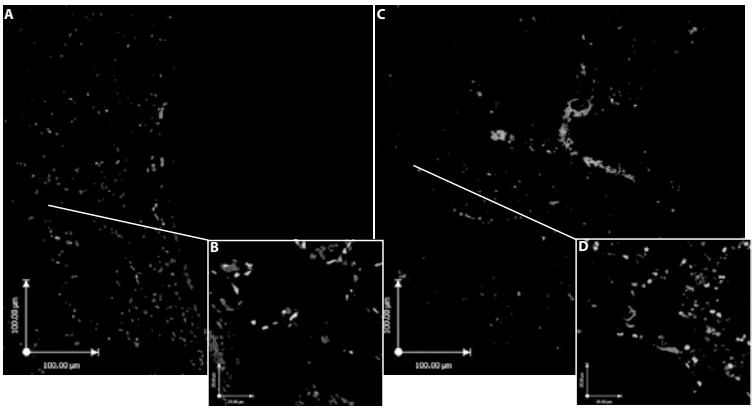

Figure 7. *Immunofluorescent images of ceramide expression. Control (A at 100x magnification, B at 400x magnification), elastase-treated mice 2 days after elastase injection (C at 100x magnification, D at 400x magnification). Ceramide (red), cell nuclei (DAPI blue) and autofluorescence (green). (See colour section, page 193).*

inhibitors or STP inhibitor showed no significant signs of histological recovery compared to elastase-treated controls (Table 6).

DISCUSSION

In this study we showed that intratracheal elastase caused a transient inflammatory response with influx of erythrocytes and inflammatory cells in the alveolar spaces, combined with an increase in multiple ceramide and dihydroceramide species in BAL fluid which peaked at day 1 and 2 and returned to control levels 3 days after elastase instillation. Ceramide expression was primarily localized to the epithelium and to inflammatory cells. Sphingomyelinase inhibitors did not prevent or reduce the effects of intratracheal elastase. In contrast, SPT inhibition reduced sphingolipid and protein levels and ameliorated lung function changes after elastase instillation.

Apoptosis of alveolar cells has been shown to play a crucial role in the development of emphysema[30–32]. Petrache *et al*. showed that direct intratracheal instillation of a synthetic short chain ceramide caused emphysema-like defects[33] and observed increased ceramide levels in the lungs of individuals with cigarette smoke-induced emphysema[33]. Our study shows for the first time that ceramide levels are increased in the first few days following the intratracheal instillation of elastase in mice. Earlier studies have described an increase in apoptosis in the elastase-induced emphysema model[34–37]. Long chain ceramides (Cer16:0, Cer18:0) have been shown in cancer cells to exhibit anti-proliferative and pro-apoptotic effects[38]. Our study shows that long chain ceramides are increased a few days after elastase instillation and we speculate that they were responsible for triggering apoptosis. Long chain ceramides have also been shown to increase the permeability of the lung endothelium after cigarette-smoke[39] and thereby enhance endothelial leakage leading to edema formation[40]. In our model we found evidence of significant edema formation at day 2 and 3 after elastase instillation, as measured by increased IgM and protein levels in the BAL fluid. Our observation of long chain ceramides being increased at those time-points is suggestive of a causal role of ceramides in this model. The elastase-induced emphysema model does not mimic the low-grade, long-term inflammatory pathophysiology of smoke-induced pulmonary emphysema in patients[41]. However, it is an excellent model to accurately reproduce the histological damage seen in emphysematous lungs and to evaluate the effect of interventions. The short developmental time of the model when compared to genetic or cigarette smoke models makes it easier to perform multiple experiments in a relatively short time period.

Staining of lung sections from patients with cystic fibrosis or lung emphysema for ceramides showed that ceramide formation is increased in the airway epithelium[20]. By immunofluorescent staining we indeed found increased ceramides in the airway epithelium, in agreement with the increased ceramide levels in BAL which mainly contains products from epithelial cells. We also found positive immunofluorescence signals for ceramide in

Table 6. *Morphometry after elastase instillation and inhibitor treatment.*

Parameter	Unit	Control (n=10)	Elastase (n=10)	Elastase + Desipramine (n=4)	Elastase + zoledronic acid (n=4)	Elastase + sphingolactone (n=4)	Elastase + Myriocin (n=6)
Mean Linear Intercept	µm	42.2 (40.8-43.2)	141.8 (133.3-152.0) *	119.8 (105.8-147.4) *	137.0 (108.1-170.8) *	129.5 (114.8-158.3) *	126.5 (85.6-164.4) *
Tissue-vs-Air ratio	count	19.9 ± 2.0	15.3 ± 2.8 *	13.7 ± 1.3 *	15.7 ± 2.4 *	15.9 ± 2.1 *	18.5 ± 3.1

*During morphometry, an average for each individual mouse was calculated from 15 counted images. * = p<0.05 when compared to Control.*

alveolar macrophages, which could be due to uptake of apoptotic alveolar epithelial cells, or internal ceramide production[42], triggered by the inflammatory response after elastase. Sphingomyelinase inhibition has been examined in a variety of animal models. In a model of cystic fibrosis, acid sphingomyelinase inhibitors (desipramine and amitriptyline) andand a glycosphingolipid inhibitor (Miglustat) decreased pulmonary inflammation[14,43]. In spinal cord injury, an inhibitor of acid sphingomyelinase (NB6) and an inhibitor of *de novo* ceramide synthesis (Fumonisin B1) reduced spinal cell apoptosis and inflammation after injury, and improved motor function[44]. Zoledronic acid has been shown to specifically inhibit acid sphingomyelinase[45]. Sphingolactone has previously been shown to ameliorate LPS-induced acute lung injury in mice by inhibiting neutral sphingomyelinase, thereby decreasing ceramide levels in the present study. Treatment with myriocin (SPT inhibitor) produced a marked reduction in overall sphingolipid levels, which suggests that *de-novo* ceramide synthesis was responsible for this increase. The *de novo* pathway was also implicated in VEGF-inhibition-induced emphysema, demonstrating the importance of *de novo* ceramide generation in the process of alveolar destruction[33]. This is further corroborated by the observation that neither acid- nor neutral sphingomyelinase inhibitors were able to block the increase in ceramides. Inadequate dosing of these inhibitors seems unlikely since similar doses have been used successfully in other animal models[46–48]. Since inhibition of synthesis of very long acyl chain (C22-C24) ceramides in Cer synthase 2 knockout mice has been shown to elevate C16-ceramide and sphinganine levels[49], it is possible that inhibition of one specific step in the complex ceramide pathway leads to unintended alterations in individual ceramide metabolites. In the present study, desipramine exhibited an unexpected effect, namely upregulation of very long chain ceramides in both vehicle and elastase-treated mice. However, zoledronic acid, another inhibitor of acid sphingomyelinase, did not have this effect. Desipramine has previously been described to not only inhibit ASMase, but also acid ceramidase and other lysosomal enzymes[45,50]. This non-specific inhibitory effect could account for the different effects on sphingolipid levels compared to zoledronic acid. Acid sphingomyelinase protein levels were transiently upregulated after elastase instillation, suggesting that it may have contributed to the transient increase in ceramides. However, the contribution must have been minimal as we found no effect of acid sphingomyelinase inhibitors. The increased ceramide levels after elastase instillation could also be due to reduced degradation by ceramidases. However, a major role in the transient rise in ceramides is unlikely since ceramide levels returned to normal 5 days after elastase instillation while acid ceramidase levels were still decreasing. The initial decrease of neutral ceramidase after elastase instillation may have contributed to the early increase in ceramide levels but neutral ceramidase levels were already increased and normalized at the time (day 2) ceramide levels peaked. Thus, contribution of neutral ceramidase to the elevation in ceramides after elastase treatment is most likely minimal.

Blocking the *de-novo* pathway of ceramide synthesis by myriocin had a positive effect on lung function but no effect on histology. A possible explanation for this structure-function discrepancy is that ceramides reduce surfactant synthesis, due to downregulation of Thyroid Transcription Factor-1 (TTF-1), and this may affect lung function without a

measurable morphological alteration[24,51]. However, our observed absence of a change in saturated phosphatidylcholine content in BAL of elastase-treated and control mice (not shown) makes this explanation less likely. Clinical studies in humans also show that structural abnormalities of the lungs and airways are at best weakly correlated with changes in lung function, and this is especially true for localized or inhomogeneous structural abnormalities, as seen in our model[52,53]. Alternatively, the morphometric methodology may be insufficiently sensitive to demonstrate relatively small changes that might underlie significant functional improvement. More sensitive approaches to the analysis of lung structure might be needed. Such approaches may include, but are not limited to, micro CT and advanced functional MRI imaging techniques.

It could be argued that desipramine, being a tricyclic antidepressant, and zoledronic acid, a bisphosphonate, have limited specificity to influence ceramide metabolism. Desipramine is known to inhibit the re-uptake of norepinephrine and to a lesser extent serotonin[54], however, both catecholamines are unlikely to affect ceramide levels in BAL. Zoledronic acid binds and blocks farnesyl diphosphate synthase in the HMG-CoA reductase pathway, preventing the formation of metabolites essential for sub-cellular protein trafficking. As a bisphosphonate it may bind to calcium in bone, thereby preventing the functioning of osteoclasts, the only bone-resorbing cells in the body[56]. Again, it is very unlikely that these additional actions of zoledronic acid interfered with our ceramide outcomes. Importantly, we showed that neither desipramine nor zoledronic acid influenced BAL ceramide levels, which argues against a significant contribution of SMases in the production of ceramides in our elastase model[57].

In conclusion, we demonstrated the involvement of ceramides and dihydroceramides in elastase-induced emphysema. Our findings suggest an important role for ceramides in the acute phase of elastase-induced emphysema. Further experiments should be undertaken to better evaluate the preventive and therapeutic potential of ceramide inhibition in this emphysema model, and ultimately in humans with COPD and emphysema.

FUNDING

This work was supported by an operating grant (MOP-86472) from the Canadian Institute of Health Research and infrastructure grants (CCURE, CSCCD) from the Canadian Foundation for Innovation.

REFERENCES

1. Mannino DM. Chronic obstructive pulmonary disease: definition and epidemiology. *Respiratory care*. 2003;48(12):1185–91; discussion 1191–3.
2. Mannino DM, Braman S. The epidemiology and economics of chronic obstructive pulmonary disease. *Proceedings of the American Thoracic Society*. 2007;4(7):502–6.
3. Finkelstein R, Fraser RS, Ghezzo H, Cosio MG. Alveolar inflammation and its relation to emphysema in smokers. *American journal of respiratory and critical care medicine*. 1995;152(5 Pt 1):1666–72.
4. Majo J, Ghezzo H, Cosio MG. Lymphocyte population and apoptosis in the lungs of smokers and their relation to emphysema. *European Respiratory Journal*. 2001;17(5):946–53.
5. Retamales I, Elliott WM, Meshi B, et al. Amplification of inflammation in emphysema and its association with latent adenoviral infection. *American journal of respiratory and critical care medicine*. 2001;164(3):469–73.
6. Olivera A, Rivera J. Sphingolipids and the Balancing of Immune Cell Function : Lessons from the Mast Cell. *The journal of immunology*. 2005;175:1153–1158.
7. Spiegel S, Milstien S. Sphingosine-1-phosphate: an enigmatic signalling lipid. *Nature reviews. Molecular cell biology*. 2003;4(5):397–407.
8. Waeber C, Blondeau N, Salomone S. Vascular sphingosine-1-phosphate S1P1 and S1P3 receptors. *Drug news & perspectives*. 2004;17(6):365–82.
9. Rosen H, Goetzl EJ. Sphingosine 1-phosphate and its receptors: an autocrine and paracrine network. *Nature reviews. Immunology*. 2005;5(7):560–70.
10. Gulbins E, Li PL. Physiological and pathophysiological aspects of ceramide. *American journal of physiology-Regulatory, integrative and comparative physiology*. 2006;290(1):R11–26.
11. Thon L, Möhlig H, Mathieu S, et al. Ceramide mediates caspase-independent programmed cell death. *The FASEB journal*. 2005;19(14):1945–56.
12. Taha TA, Mullen TD, Obeid LM. A house divided: ceramide, sphingosine, and sphingosine-1-phosphate in programmed cell death. *Biochimica et biophysica acta*. 2006;1758(12):2027–36.
13. McVerry BJ, Garcia JGN. Endothelial cell barrier regulation by sphingosine 1-phosphate. *Journal of cellular biochemistry*. 2004;92(6):1075–85.
14. Becker KA, Riethmuller J, Luth A, Doring G, Kleuser B, Gulbins E. Acid sphingomyelinase inhibitors normalize pulmonary ceramide and inflammation in cystic fibrosis. *American journal of respiratory cell and molecular biology*. 2010;42(6):716–724.
15. Futerman AH, Hannun Y a. The complex life of simple sphingolipids. *EMBO reports*. 2004;5(8):777–82.
16. Kolesnick RN, Krönke M. Regulation of ceramide production and apoptosis. *Annual review of physiology*. 1998;60:643–65.
17. Morita Y, Tilly JL. Sphingolipid regulation of female gonadal cell apoptosis. *Annals of the New York Academy of Sciences*. 2000;905:209–20.
18. Payne SG, Milstien S, Spiegel S. Sphingosine-1-phosphate: dual messenger functions. *FEBS letters*. 2002;531(1):54–7.
19. Becker KA, Tummler B, Gulbins E, Grassmé H. Accumulation of ceramide in the trachea and intestine of cystic fibrosis mice causes inflammation and cell death. *Biochemical and biophysical research communications*. 2010;403(3-4):368–374.

20. Brodlie M, McKean MC, Johnson GE, et al. Ceramide is increased in the lower airway epithelium of people with advanced cystic fibrosis lung disease. *American journal of respiratory and critical care medicine*. 2010;182(3):369–75.
21. Ammit AJ, Hastie AT, Edsall LC, et al. Sphingosine 1-phosphate modulates human airway smooth muscle cell functions that promote inflammation and airway remodeling in asthma. *The FASEB journal*. 2001;15(7):1212–4.
22. Petrache I, Natarajan V, Zhen L, et al. Ceramide causes pulmonary cell apoptosis and emphysema: a role for sphingolipid homeostasis in the maintenance of alveolar cells. *Proceedings of the American Thoracic Society*. 2006;3(6):510.
23. Calabrese F, Giacometti C, Beghe B, et al. Marked alveolar apoptosis/proliferation imbalance in end-stage emphysema. *Respiratory research*. 2005;6:14.
24. Sparkman L, Chandru H, Boggaram V. Ceramide decreases surfactant protein B gene expression via down-regulation of TTF-1 DNA binding activity. *American Journal of Physiology-Lung Cellular and Molecular Physiology*. 2006;290(2):L351–8.
25. Rauvala H, Hallman M. Glycolipid accumulation in bronchoalveolar space in adult respiratory distress syndrome. *Journal of lipid research*. 1984;25(11):1257–62.
26. Tibboel J, Joza S, Reiss I, Jongste JC De, Post M. Amelioration of hyperoxia-induced lung injury using a sphingolipid-based intervention. *European Respiratory Journal*. 2013;42(3):776-84.
27. Tsuchida S, Engelberts D, Roth M, McKerlie C, Post M, Kavanagh BP. Continuous positive airway pressure causes lung injury in a model of sepsis. *American Journal of Physiology-Lung Cellular and Molecular Physiology*. 2005;289(4):L554–64.
28. Ridsdale R, Roth-Kleiner M, D'Ovidio F, et al. Surfactant palmitoylmyristoylphosphatidylcholine is a marker for alveolar size during disease. *American journal of respiratory and critical care medicine*. 2005;172(2):225–32.
29. Manwani N, Gagnon S, Post M. Reduced viability of mice with lung epithelial-specific knockout of glucocorticoid receptor. *American journal of respiratory cell and molecular biology*. 2010;43:599–606.
30. Demedts IK, Demoor T, Bracke KR, Joos GF, Brusselle GG. Role of apoptosis in the pathogenesis of COPD and pulmonary emphysema. *Respiratory Research*. 2006;10:1–10.
31. Tuder RM, Zhen L, Cho CY, et al. Oxidative stress and apoptosis interact and cause emphysema due to vascular endothelial growth factor receptor blockade. *American journal of respiratory cell and molecular biology*. 2003;29(1):88–97.
32. Tuder RM, Petrache I, Elias J a, Voelkel NF, Henson PM. Apoptosis and emphysema: the missing link. *American journal of respiratory cell and molecular biology*. 2003;28(5):551–4.
33. Petrache I, Natarajan V, Zhen L, et al. Ceramide upregulation causes pulmonary cell apoptosis and emphysema-like disease in mice. *Nature medicine*. 2005;11(5):491–498.
34. Plantier L, Marchand-Adam S, Antico VG, et al. Keratinocyte growth factor protects against elastase-induced pulmonary emphysema in mice. *American Journal of Physiology-Lung Cellular and Molecular Physiology*. 2007;293(5):L1230–9.
35. Sawada M, Ohno Y, La BLB, et al. The Fas/Fas-ligand pathway does not mediate the apoptosis in elastase-induced emphysema in mice. *Experimental lung research*. 2007;33(6):277–88.
36. Lucey EC, Keane J, Kuang P-P, Snider GL, Goldstein RH. Severity of elastase-induced emphysema is decreased in tumor necrosis factor-alpha and interleukin-1beta receptor-deficient mice. *Laboratory investigation*. 2002;82(1):79–85.
37. Shigemura N, Sawa Y, Mizuno S, et al. Amelioration of pulmonary emphysema by in vivo gene transfection with hepatocyte growth factor in rats. *Circulation*. 2005;111(11):1407–14.

38. Hartmann D, Lucks J, Fuchs S, et al. Long chain ceramides and very long chain ceramides have opposite effects on human breast and colon cancer cell growth. *The international journal of biochemistry & cell biology*. 2012;44(4):620–8.
39. Schweitzer KS, Hatoum H, Brown MB, et al. Mechanisms of lung endothelial barrier disruption induced by cigarette smoke: role of oxidative stress and ceramides. *American Journal of Physiology-Lung Cellular and Molecular Physiology*. 2011;301(6):L836–46.
40. Göggel R, Winoto-Morbach S, Vielhaber G, et al. PAF-mediated pulmonary edema: a new role for acid sphingomyelinase and ceramide. *Nature medicine*. 2004;10(2):155–60.
41. Wright JL, Cosio M, Churg A. Animal models of chronic obstructive pulmonary disease. *American Journal of Physiology-Lung Cellular and Molecular Physiology*. 2008;295(1):L1–15.
42. Schilling JD, Machkovech HM, He L, et al. Palmitate and LPS trigger synergistic ceramide production in primary macrophages. *The Journal of biological chemistry*. 2012;288:2923–32.
43. Dechecchi MC, Nicolis E, Mazzi P, et al. Modulators of sphingolipid metabolism reduce lung inflammation. *American journal of respiratory cell and molecular biology*. 2011;45(4):825–33.
44. Cuzzocrea S, Deigner HP, Genovese T, et al. Inhibition of ceramide biosynthesis ameliorates pathological consequences of spinal cord injury. *Shock*. 2009;31(6):635–644.
45. Roth A, Drescher D, Yang Y, Redmer S, Uhlig S, Arenz C. Potent and selective inhibition of acid sphingomyelinase by bisphosphonates. *Angewandte Chemie International Edition*. 2009;48(41):7560–7563.
46. Nakatsuji T, Tang D-CC, Zhang L, Gallo RL, Huang C-M. Propionibacterium acnes CAMP Factor and Host Acid Sphingomyelinase Contribute to Bacterial Virulence: Potential Targets for Inflammatory Acne Treatment. *PloS one*. 2011;6(4):e14797.
47. Lin W-C, Lin C-F, Chen C-L, Chen C-W, Lin Y-S. Inhibition of Neutrophil Apoptosis via Sphingolipid Signaling in Acute Lung Injury. *The Journal of pharmacology and experimental therapeutics*. 2011;339:45–53.
48. Bäckman U, Svensson A, Christofferson RH, Azarbayjani F. The bisphosphonate, zoledronic acid reduces experimental neuroblastoma growth by interfering with tumor angiogenesis. *Anticancer research*. 2008;28(3A):1551–7.
49. Pewzner-Jung Y, Park H, Laviad EL, et al. A critical role for ceramide synthase 2 in liver homeostasis: I. alterations in lipid metabolic pathways. *The Journal of biological chemistry*. 2010;285(14):10902–10.
50. Canals D, Perry DM, Jenkins RW, Hannun Y a. Drug targeting of sphingolipid metabolism: sphingomyelinases and ceramidases. *British journal of pharmacology*. 2011;163(4):694–712.
51. Boggaram V. Thyroid transcription factor-1 (TTF-1/Nkx2.1/TITF1) gene regulation in the lung. *Clinical science*. 2009;116(1):27–35.
52. De Jong P A, Lindblad A, Rubin L, et al. Progression of lung disease on computed tomography and pulmonary function tests in children and adults with cystic fibrosis. *Thorax*. 2006;61(1):80–5.
53. Sly PD, Brennan S, Gangell C, et al. Lung disease at diagnosis in infants with cystic fibrosis detected by newborn screening. *American journal of respiratory and critical care medicine*. 2009;180(2):146–52.
54. Zhao Z, Zhang H-T, Bootzin E, Millan MJ, O'Donnell JM. Association of changes in norepinephrine and serotonin transporter expression with the long-term behavioral effects of antidepressant drugs. *Neuropsychopharmacology*. 2009;34(6):1467–81.
55. Van beek E, Löwik C, van der Pluijm G, Papapoulos S. The role of geranylgeranylation in bone resorption and its suppression by bisphosphonates in fetal bone explants in vitro: A clue to the mechanism of action of nitrogen-containing bisphosphonates. *Journal of bone and mineral research*. 1999;14(5):722–9.

56. Dunford JE, Thompson K, Coxon FP, et al. Structure-activity relationships for inhibition of farnesyl diphosphate synthase in vitro and inhibition of bone resorption in vivo by nitrogen-containing bisphosphonates. *The Journal of pharmacology and experimental therapeutics*. 2001;296(2):235–42.
57. Kornhuber J, Tripal P, Reichel M, et al. Functional Inhibitors of Acid Sphingomyelinase (FIASMAs): a novel pharmacological group of drugs with broad clinical applications. *Cellular Physiology and Biochemistry*. 2010;26(1):9–20.

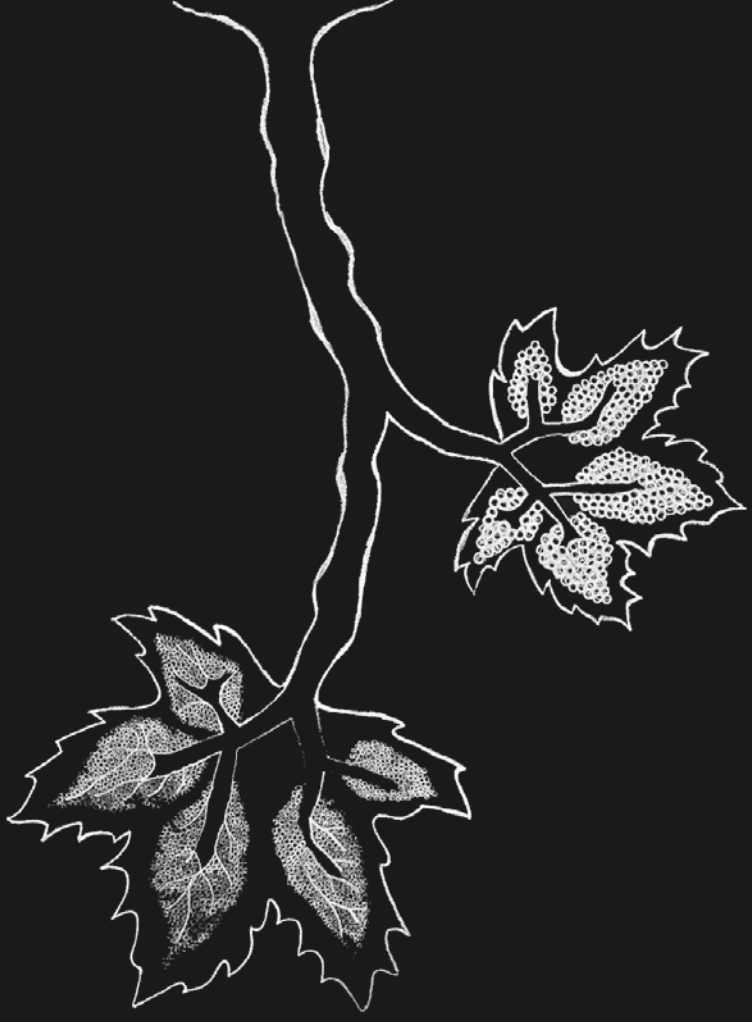

Chapter 6

Intravenous and Intratracheal Mesenchymal Stromal Cell Injection in a Mouse Model of Pulmonary Emphysema

Jeroen Tibboel[1,3]
Richard Keijzer[4]
Irwin Reiss[3]
Johan C. de Jongste[3]
Martin Post[1,2]

[1] Dept. of Physiology and Experimental Medicine, Hospital for Sick Children, Toronto, Canada.
[2] Dept. of Laboratory Medicine and Pathobiology, University Of Toronto, Toronto, Canada.
[3] Dept. of Pediatrics, Erasmus University Medical Center – Sophia Children's Hospital, Rotterdam, the Netherlands.
[4] Dept. of Pediatric General Surgery, Manitoba Institute of Child Health, Winnipeg, Canada.

Provisionally accepted Journal of Chronic Obstructive Pulmonary Disease

ABSTRACT

Aim: to characterize the evolution of lung function and -structure in elastase-induced emphysema in adult mice and the effect of mesenchymal stromal cell (MSC) administration on these parameters.
Methods: adult mice were treated with intratracheal (4.8 units / 100 gr bodyweight) elastase to induce emphysema. MSCs were administered intratracheally or intravenously, before or after elastase injection. Lung function measurements, histological and morphometric analysis of lung tissue were performed at 3 weeks, 5 and 10 months after elastase and at 19, 20 and 21 days following MSC administration.
Results: elastase-treated mice showed increased dynamic compliance and total lung capacity, and reduced tissue-specific elastance and forced expiratory flows at 3 weeks after elastase, which persisted during 10 months follow-up. Histology showed heterogeneous alveolar destruction which also persisted during long-term follow-up. Jugular vein injection of MSCs before elastase inhibited deterioration of lung function but had no effects on histology. Intratracheal MSC treatment did not modify lung function or histology.
Conclusion: elastase-treated mice displayed persistent characteristics of pulmonary emphysema. Jugular vein injection of MSCs prior to elastase reduced deterioration of lung function. Intratracheal MSC treatment had no effect on lung function or histology.

INTRODUCTION

Chronic Obstructive Pulmonary Disease (COPD) is the most common chronic lung disease in adults, characterized by an incompletely reversible airflow limitation, and is associated with high mortality[1] and health-care costs[2]. Pulmonary emphysema is an important component of COPD, and is characterized by alveolar destruction, resulting in a reduced alveolar surface area and increased alveolar size[3]. Not all patients with pulmonary emphysema exhibit airflow limitation, respectively COPD[4], showing that there is a discrepancy between lung function and histological abnormalities. Oxidative stress, sustained inflammation and protease-antiprotease imbalance[5] are believed to be major contributors to the pathogenesis of COPD. To date no curative therapy is available, and smoking cessation and domiciliary oxygen supplementation only prolong survival in a small subset of patients with resting PaO_2 < 60 mmHg[6].

Mesenchymal stromal cells have recently emerged as a successful, cell-based therapy in a variety of models of lung disease, such as hyperoxia[7], bleomycin[8] and endotoxin-induced lung injury[9]. MSCs are multipotent stromal cells that have the ability to self-renew. The hypothesis for the mechanism underlying the beneficial effects of MSC treatment has shifted from engraftment and differentiation of MSCs in the target organ towards the effects of paracrine factors produced by these MSCs[10]. Levels of engraftment below 1% were found in several studies[11–14]. Thus, it is highly unlikely that engraftment is responsible for the favourable effects of MSCs in various models of lung injury[11,15–17]. MSC have been shown to inhibit apoptosis[18] and secrete anti-inflammatory mediators[19] and growth factors, such as epidermal growth factor[20] and hepatocyte growth factor[21]. It has been shown that the intravenous infusion of conditioned medium, derived from MSCs, prevents LPS-induced lung injury, supporting that MSCs exert their effect via paracrine signalling[22]. Katsha *et al.* have shown that treatment with MSCs improves histological and morphometrical outcome in a low dose elastase-induced emphysema model (1 Unit/100 gram bodyweight) and decreases inflammatory cytokine levels[23]. Also Cruz *et al.* have shown that injection of bone marrow mononuclear cells (BMNCs) improves histological and morphometrical outcome in a low dose (4 times 0.4 Units/100 gram bodyweight) elastase model[24]. Based on the results of MSC treatment in different animal models, a phase II-trial of intravenous mesenchymal stem cell infusion in COPD patients was started in 2008. The interim report of this study stated that, although this treatment was safe and reduced C-reactive protein levels, lung function in these patients did not improve[25]. The absence of an improvement in lung function suggests that MSCs did not repair the structural defect[26]. Since these human trial findings were not in line with the aforementioned animal studies[23,24], the question arises whether the animal models may not mimic human COPD, and whether a better response to MSC is seen because of a lower level of lung damage. One possibility is that the elastase dose had been too low to cause the desired level of alveolar damage. We therefore examined the effects of MSC treatment in a mouse model of emphysema, using a relatively high dose of elastase (4.8 Units / 100 gram bodyweight). Since some previous studies[24,25] used an intravenous route of MSC administration while others[23] used intratracheal delivery, we

tested both methods of administration of MSCs, aiming at either prevention or repair of lung injury.

METHODS

Animals

All animals were obtained from Charles River (St. Constant, Quebec, Canada). Animal studies were conducted according to the criteria established by the Canadian Council for Animal Care and approved by the Animal Care and Use Committee of the Hospital for Sick Children, Toronto, ON, Canada. Adult C57BL/6 mice were used for all experiments described below, except for the extraction of MSCs from bone marrow, for which 4 week old C57BL/6 mice were used.

Elastase-induced lung injury

Porcine pancreatic elastase (Type I, aqueous suspension, ≥4.0 units/mg protein, Calbiochem, EMD biosciences USA) was dissolved in sterile saline to create a total volume for injection of 100 µl per mouse, with a concentration of 4.8 Units / 100 gram bodyweight, a dosage used previously[27–29]. Animals were anesthetized with 3% isoflurane and *ip* administration of Ketamine (75 mg/kg) and Xylazine (5 mg/kg). Following induction of anesthesia, a 25G intubation tube was inserted past the vocal cords and 100 µl of elastase was injected into the trachea. Control animals were treated similarly, but received sterile saline instead of elastase.

Mesenchymal stromal cell extraction and characterization

Bone marrow was collected from 4-week old C57BL/6 mice. Mice were sacrificed by cervical dislocation, and the tibia and femur removed, from which the bone marrow was extracted by flushing with Dulbecco's Modified Eagle Medium (DMEM). The suspension was filtered using a 70µm sterile filter before being cultured using StemXVivo Mesenchymal Stem Cell expansion medium (R&D systems, Minneapolis, USA) according to a modified protocol[30]. Mesenchymal stromal cells were isolated by plastic adherence, and prior to injection, passage 8 adherent MSCs were characterized using flow cytometry. MSCs characterized according to the International Society of Cellular Therapy consensus in 2006 must fulfill the following three criteria: (1) MSC must be adherent to plastic under standard tissue culture conditions; (2) MSC must express the cellular markers CD73, CD90 and CD105, and must not express CD34, CD45, CD14 or CD11b; and (3) MSC must have the capacity to differentiate into mesenchymal lineages under *in vitro* conditions[31]. Adherent cells were collected from their culture flasks by trypsin digestion and a subset of cells were stained with primary conjugated antibodies for CD34, CD45, CD73, CD105 and Sca-1 (Miltenyi Biotec, Bergisch Gladbach, Germany) according to manufacturer's protocol. Expression of the above mentioned markers was characterized using a Gallios flow cytometer (Beckman Coultier, Mississauga, Canada). A differentiation assay was performed on passage 8 MSCs to test their multi-lineage differentiation capacity. According

to a protocol by Lama *et al.*[32], MSCs were cultured in different media to obtain adipogenic, chondrogenic, and osteogenic differentiation. Adipogenic: DMEM + 1μM dexamethasone + 10μM insulin + 200μM indomethacin + 0.5mM isobutyl-methyl xanthine. Chondrogenic: DMEM + 10ng/mL TFG-β1. Osteogenic: DMEM + 100nM dexamethasone + 10mM beta-glycerophosphate + 0.05mM ascorbic acid-2-phosphate. Histological staining for adipocytes (Oil-red stain), osteoblasts (Von Kossa stain) and chondrocytes (Alcian Blue stain) were performed according to a previously published protocol[32].

Mesenchymal stromal cell administration

MSCs were dissolved in plasmalyte (Baxter, Mississauga, Canada) at a concentration of 500,000 cells per 200μl for intratracheal instillation and at a concentration of 100,000 cells per 100μl for jugular vein injection.

Intratracheal instillation of MSCs

Animals were anesthetized with 3% isoflurane and *ip* administration of Ketamine (75 mg/kg) and Xylazine (5 mg/kg). Following induction of anesthesia, a 25G intubation tube was inserted past the vocal cords and 500.000 MSCs suspended in 200μl of plasmalyte were injected into the trachea. Control animals were treated similarly, but received plasmalyte only. To test whether MSCs could prevent elastase-induced lung injury, intratracheal MSC installation was performed 24 hours before elastase injection in experimental group 1, and 24 hours after elastase injection in experimental group 2. To test whether MSC's could repair elastase-induced lung injury, intratracheal MSC installation was also performed 21 days after elastase treatment (Supplementary figure S1).

Infusion of MSCs via the jugular vein

Animals were anesthetized with 3% isoflurane, which was maintained during the entire procedure. The jugular vein was exposed and 100,000 MSCs suspended in 100μl plasmalyte were slowly infused. Pressure was applied on the jugular vein until bleeding ceased, the wound was sutured and the animals were allowed to recover. Jugular vein MSC infusion was performed 30 minutes before intratracheal elastase injection.

Lung function measurements

At multiple time points (Supplementary figure S1) following the instillation of elastase and/or MSC treatment, unrestrained whole body plethysmography (Buxco Research Systems, Wilmington, NC, USA) was used to measure breathing frequency, tidal volume and minute volume. Afterwards the Flexivent rodent ventilator (Scireq, Montreal, Canada) was used to invasively assess lung function (described in detail in the supplementary methods section) following a protocol previously published[33].

Bronchoalveolar lavage

A subset of mice was used to obtain BAL samples only. Immediately after sacrificing the animal, the lungs were lavaged at 6 hours, and 1-5, 8,14 and 21 days after elastase injection through a separate endotracheal tube with 3 x 600 μl sterile saline, followed by withdraw-

al[34,35]. The collected pooled aliquots were centrifuged at 1400 *g* for 8 min. The supernatant was collected for cytokine analysis.

Measuring cytokines
Cytokines were measured in BAL fluid using xMAP technology on a Luminex 200 (Luminex Corporation, Austin, Texas, USA) using a milliplex kit from EMD Millipore Corporation (Billerica, Massachusetts, USA) according to the manufacturers protocol. The following analytes were measured: IL-1β, IL-6, IL-10, IL-13, MCP-1, TNF-α, KC, GM-CSF.

Histology of the lungs
Following lung function measurements, histology was performed as described in the supplementary methods section.

Statistics
All values are presented as mean ± standard error of the mean when normally distributed (Sigmaplot version 11 for Windows). Differences were assessed by Student's t-test or, for comparison of more than two groups, by one-way analysis of variance, followed by Tukey HSD comparison test. $p < 0.05$ was considered significant.

RESULTS

Elastase-induced alveolar injury
Elastase-treated mice showed significant decreases in resistance and tissue-specific elastance, and significant increases in dynamic compliance, total lung capacity and static compliance when compared to saline-treated mice. Forced expiration measurements revealed a significant increase in forced vital capacity and a significant decrease in mean forced expiratory flow in elastase-treated mice (Figure 1, Table 1). At 5 months and 10 months after elastase instillation, the increase in dynamic compliance and FVC, as well as the decrease in tissue-specific elastance and forced expiratory flows seen at 3 weeks after elastase had persisted (Figure 2, Table 2). No significant changes in plethysmographic lung function parameters were found when compared to saline-treated controls (Table 2). Histology at 21 days after elastase showed a heterogeneous pattern of alveolar destruction with enlarged airspaces. This was reflected in a significant increase in mean linear intercept and a reduced alveolar number. No significant change in radial alveolar count was detected. Histological analysis of lungs at 5 and 10 months after elastase treatment revealed a persistent, heterogeneous pattern of enlarged airspaces and an increased mean linear intercept (Figure 3). Elastin staining at 21 days after elastase administration showed a disorganized pattern of elastin distribution in elastase-treated mice compared to controls. No significant difference in elastin content per total tissue area was observed (Figure 4). Histological slides of elastase-treated mice showed influx of inflammatory cells, and cytokine levels in BAL fluid showed a transient increase in IL-6, keratinocyte-derived-chemokine (KC) and MCP-1 levels at day 2 after elastase injection. Cytokine levels returned to

Table 1. *Invasive (Flexivent) lung function measurements.*

Parameter	Unit	3 weeks		5 months		10 months	
		Control (n=25)	Elastase (n=33)	Control (n=5)	Elastase (n=5)	Control (n=5)	Elastase (n=5)
Resistance	cmH_2O/mL	0.57 ± 0.07	0.51 ± 0.06	0.48 ± 0.03	0.43 ± 0.03 *	0.41 ± 0.02	0.39 ± 0.03
Elastance	cmH_2O/mL	25.1 ± 3.2	19.3 ± 2.9 **	22.2 ± 2.0	16.9 ± 1.2 **	17.8 ± 0.7	14.6 ± 0.9 **
Compliance	mL/cmH_2O	0.04 ± 0.01	0.05 ± 0.01 **	0.04 ± 0.01	0.06 ± 0.01 **	0.06 ± 0.01	0.07 ± 0.01 **
Airway Resistance	cmH_2O/mL	0.29 ± 0.03	0.25 ± 0.03 **	0.26 ± 0.02	0.25 ± 0.01 *	0.24 ± 0.01	0.22 ± 0.02 **
Tissue-specific elastance	cmH_2O/mL	25.2 ± 3.4	17.5 ± 2.9 *	20.7 ± 1.4	16.0 ± 1.8	17.0 ± 0.9	13.5 ± 0.7
Total lung capacity	mL	0.76 ± 0.09	0.83 ± 0.08	0.91 ± 0.05	0.98 ± 0.05	1.12 ± 0.03	1.11 ± 0.06
Inspiratory Capacity from zero pressure	mL	1.30 ± 0.19	1.45 ± 0.22	1.39 ± 0.14	1.46 ± 0.12	1.60 ± 0.045	1.54 ± 0.13
Static Compliance	mL/cmH_2O	0.09 ± 0.01	0.10 ± 0.02	0.10 ± 0.01	0.10 ± 0.01	0.11 ± 0.01	0.11 ± 0.01
Static Elastance	cmH_2O/mL	10.9 ± 1.5	9.7 ± 1.5	10.4 ± 1.1	9.7 ± 0.9	9.0 ± 0.2	9.3 ± 1.0
Forced Vital Capacity	mL	0.99 ± 0.11	1.20 ± 0.14 **	1.10 ± 0.08	1.26 ± 0.04 *	1.19 ± 0.03	1.34 ± 0.08 *
Mean Forced Expiratory Flow	mL/sec	23.3 ± 2.5	17.4 ± 3.7 **	25.8 ± 1.5	13.6 ± 5.1 *	22.0 ± 3.0	15.6 ± 2.9 *
Peak Expiratory Flow	mL/sec	27.8 ± 4.3	28.4 ± 4.0	35.5 ± 0.7	36.1 ± 0.6	32.1 ± 1.5	31.6 ± 1.3
Forced Expiratory Flow 0.05 sec / FVC	%	85.2 ± 9.0	75.1 ± 9.8 *	89.5 ± 2.2	75.8 ± 5.4 **	84.6 ± 3.2	75.0 ± 3.8 *
Forced Expiratory Flow 0.1 sec / FVC	%	96.4 ± 7.0	90.6 ± 10.0*	98.0 ± 0.5	91.0 ± 2.9 *	96.3 ± 1.0	93.1 ± 1.4 *
Forced Expiratory Flow 0.2 sec / FVC	%	99.5 ± 0.8	96.4 ± 8.8 *	99.8 ± 0.2	97.5 ± 1.6 *	99.2 ± 0.7	98.7 ± 0.3

*During invasive lung function measurements, an average for each individual mouse was calculated from 4 accepted (coefficient of determination: COD>0.95) measurements for each parameter. * = p<0.05, ** = p<0.001 when compared to control animals at the same time point.*

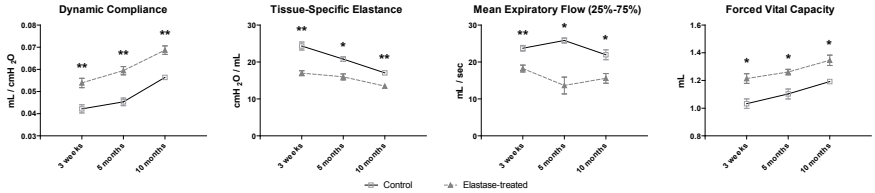

Figure 1. *Lung function measurements 21 days after elastase instillation (n=30) and in saline controls (n=25). Data are expressed as mean ± SEM. * = p<0.05.*

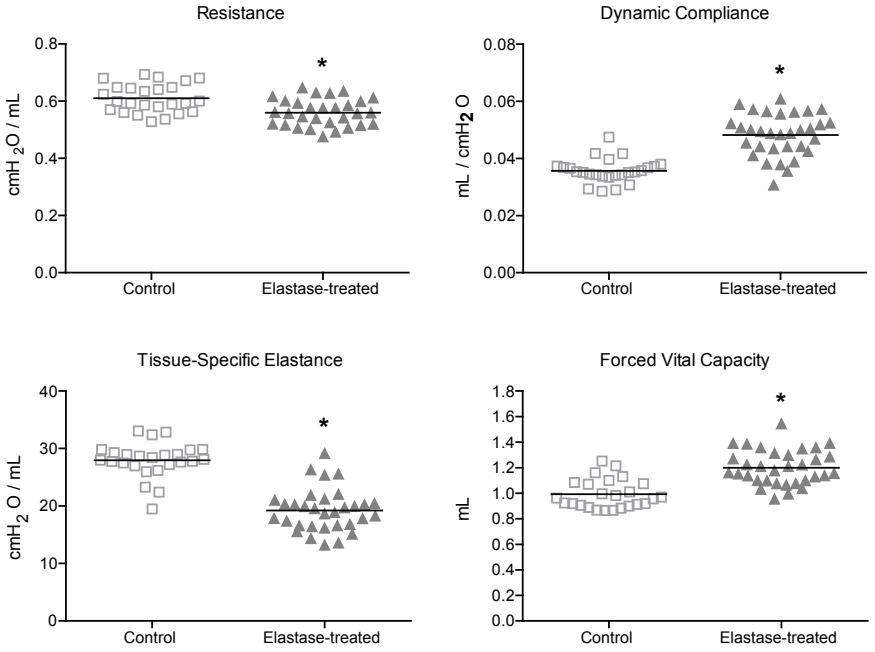

Figure 2. *Lung function measurements during long-term follow-up of elastase-treated mice (n=30 for 21 days. n=5 for 5 and 10 months) and saline controls (n=25 for 21 days. n=5 for 5 and 10 months). Data are expressed as mean ± SEM. * = p<0.05, ** = p<0.01.*

baseline at day 3 and remained stable for the follow-up period of 3 weeks. Levels of IL-1β, IL-10, IL-13 and GM-CSF were below the detectable range (Figure 5, Table 3).

Mesenchymal Stromal Cell characterization

Passage 8-adherent bone marrow stromal cells were characterized by differentiation assay and showed differentiation into adipocytes, chrondrocytes and osteoblasts. Flow cytometry revealed that a subset of bone marrow cells was positive for CD105 (28.2%), CD73 (28.8%), CD90 (69.2%) and Sca-1 (99.5%) and negative for CD34 (0%) and CD45 (0%) (Supplementary figure S2).

Table 2. *Non-invasive (WBP) lung function measurements.*

Parameter	Unit	Control (n=23)	Elastase-treated (n=27)
Breathing Frequency	Breaths/Min	315 (201-381)	334 (264-398)
Tidal Volume	mL	0.27 (0.23-0.30)	0.28 (0.24-0.32)
Minute Volume	mL/Minute	82 (53-119)	94 (66-140)
Inspiratory Time	sec	0.06 (0.06-0.11)	0.06 (0.06-0.08)
Expiratory Time	sec	0.18 (0.14-0.21)	0.15 (0.11-0.22)
Peak Inspiratory Flow	mL/sec	7.38 (4.22-8.49)	8.30 (5.85-9.53)
Peak Expiratory Flow	mL/sec	3.59 (2.28-5.73)	4.45 (3.04-6.44)
Relaxation Time	msec	0.11 (0.09-0.12)	0.09 (0.07-0.12)
End Inspiratory Pause	msec	4.94 (4.85-5.22)	5.01 (4.91-5.14)
End Expiratory Pause	msec	28.4 (19.4-41.1)	25.8 (15.1-55.0)
Enhanced Pause (PenH)		0.46 (0.38-0.55)	0.45 (0.35-0.57)

*During whole body plethysmography (WBP), mice were allowed to adjust to the measuring chambers for 30 minutes, afterwards measurements were taken continuously for 60 minutes, and an average was calculated for each mouse individually. * = p<0.05, ** = p<0.001 when compared to control animals.*

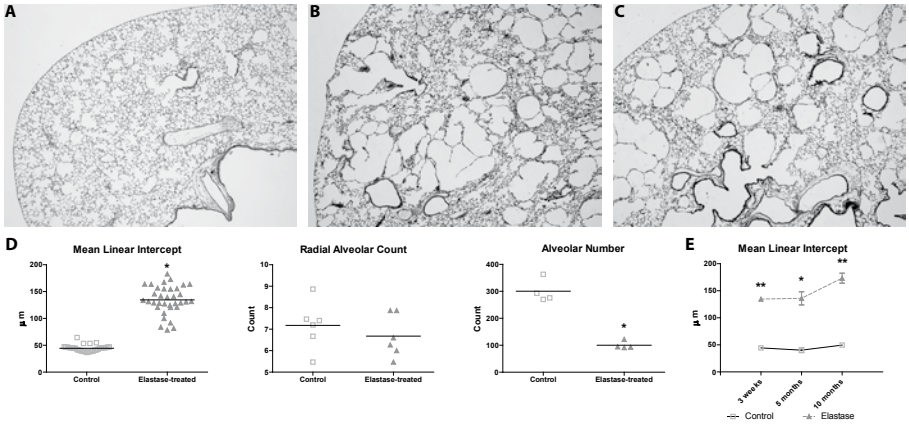

Figure 3. *Representative histological sections of saline-controls (A), elastase-treated mice 21 days after injection (B) and elastase-treated mice 10 months after elastase injection (C). Sections were stained with hematoxylin and eosin. Morphometry results (D) are expressed as mean ± SEM for both control and elastase-treated group for mean linear intercept (n=35), radial alveolar counts (n=6), and alveolar number (n=4). Morphometry results for 5 and 10 months of recovery in room-air (E) are expressed as mean ± SEM for mean linear intercept (n=5). * = p<0.05 ** = p<0.001.* *(See colour section, page 194).*

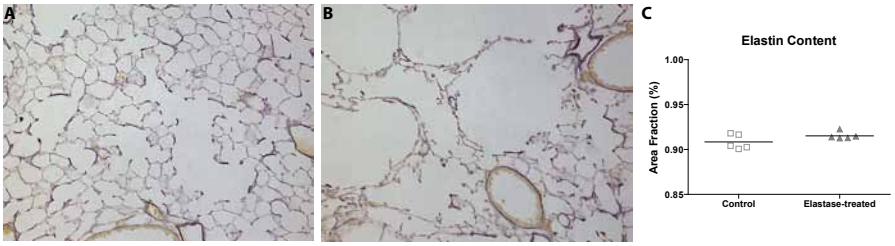

Figure 4. *Hart's Elastin stain of histological slides of the lungs of saline-treated (A) and elastase-treated mice (B) 21 days after injection. Morphometry shows the quantification of the elastin content when adjusted for total tissue area (C). All morphometrical data is expressed as mean ± SEM, n=5 for control and elastase-treated mice. # = p<0.05.*

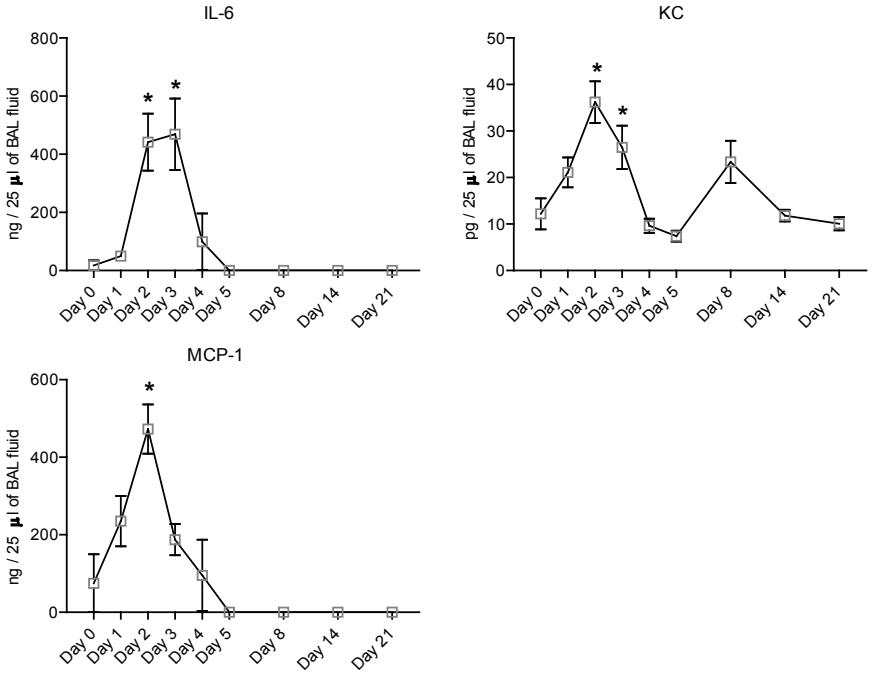

Figure 5. *Measurement of cytokine levels in BAL fluid after elastase injection show a significant increase in MCP-1 levels at day 2 after elastase injection and a significant increase in IL-6 and KC levels at day 2 and 3 after elastase injection. Results represent a total of 4 mice per group for all time-points. * = p<0.05.*

Intratracheal MSC instillation

Intratracheal instillation of $5x10^5$ of MSCs at 24 hours before, and at 24 hours or 21 days after elastase treatment had no effect on lung function or histology performed 21 days after MSC injection (Supplementary figure S3, Table 4).

Table 3. *Cytokines after elastase injection.*

Cytokine	Day 0	Day 1	Day 2	Day 3	Day 4	Day 5	Day 8	Day 14	Day 21
IL-6	0.29 (0.10-35.25)	42.93 (31.82-66.84)	509.42 (313.17-569.69) *	508.31 (298.56-639.20) *	2.14 (1.99-196.55)	0.00 (0.00-1.06)	0.00 (0.00-0.97)	0.25 (0.00-0.53)	0.19 (0.096-0.43)
KC	9.08 (8.6-12.6)	21.23 (15.97-26.36)	31.8 (31.6-36.4) *	23.7 (20.29-29.94) *	9.26 (7.44-11.44)	7.44 (5.74-9.09)	24.32 (18.02-29.66)	11.63 (10.93-12.50)	9.01 (8.27-10.80)
MCP-1	0.00 (0.00-149.50)	274.51 (138.07-332.05)	504.15 (376.47-569.18) *	176.26 (132.68-242.00)	4.79 (1.63-188.57)	0.00 (0.00-0.87)	0.00 (0.00-0.00)	0.00 (0.00-0.00)	0.00 (0.00-0.00)
TNF-α	2.34 (1.84-3.57)	7.16 (5.23-8.51)	2.22 (1.63-2.55)	1.98 (0.27-4.49)	1.84 ± 0.67	1.64 (1.14-2.06)	1.07 (0.92-1.74)	0.66 (0.58-1.54)	1.74 (0.73-2.28)

*BAL fluid from 6 mice per group was collected and processed using Luminex xMAP technology. Values for a subset of the measured cytokines (IL-1β, IL-10,IL-13,GM-CSF) were below the detectable range. *p<0.05, **p<0.001 when compared to control animals at the same time-point.*

Intravenous MSC infusion

Infusion of 10^5 MSCs 30 min before intratracheal instillation of elastase ameliorated the increase in dynamic compliance and tissue-specific elastance in elastase-treated animals compared to controls (Figure 6, Table 4). Intravenous MSC infusion had no effect on histology or morphometry (Supplementary figure S3).

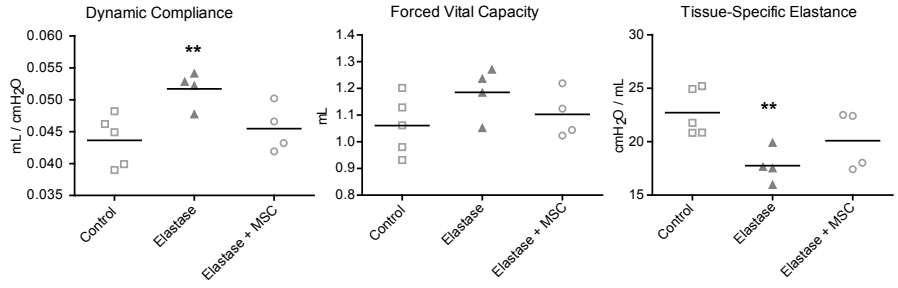

Figure 6. *Lung function measurements 21 days after elastase instillation (n=5), elastase instillation + jugular vein MSC injection (n=4) and saline controls (n=4). Data are expressed as mean ± SEM. ** = p<0.05.*

Table 4. *Invasive (Flexivent) lung function measurements 21 days after elastase + MSC treatment.*

Parameter	Unit	Intratracheal					Jugular Vein		
		Control (n=10)	Elastase (n=9)	Elastase + MSC 24h after (n=5)	Elastase + MSC 24h before (n=5)	Elastase + MSC 21 days after (n=5)	Control (n=5)	Elastase (n=4)	Elastase + MSC (n=4)
Resistance	cmH_2O/mL	0.53 ± 0.04	0.50 ± 0.03	0.49 ± 0.03	0.50 ± 0.02	0.53 ± 0.05	0.52 ± 0.04	0.50 ± 0.02	0.52 ± 0.01
Elastance	cmH_2O/mL	23.7 ± 2.2	19.6 ± 1.8 **	18.8 ± 2.9 **	20.0 ± 2.1 *	18.8 ± 1.7 **	23.1 ± 2.2	19.4 ± 1.1 *	22.1 ± 1.8 #
Compliance	mL/cmH_2O	0.043 ± 0.004	0.051 ± 0.005 **	0.054 ± 0.009 **	0.050 ± 0.006 **	0.053 ± 0.004 **	0.044 ± 0.004	0.052 ± 0.003 *	0.045 ± 0.004 #
Airway Resistance	cmH_2O/mL	0.28 ± 0.03	0.24 ± 0.02 **	0.22 ± 0.03 **	0.25 ± 0.01 *	0.25 ± 0.01 **	0.27 ± 0.02	0.24 ± 0.01 *	0.24 ± 0.02
Tissue-specific elastance	cmH_2O/mL	23.7 ± 2.5	17.6 ± 2.4 **	16.2 ± 3.3 **	19.1 ± 2.5 **	16.9 ± 2.17 **	22.7 ± 2.2	17.5 ± 1.6 *	20.1 ± 2.7
Total lung capacity	mL	0.78 ± 0.05	0.81 ± 0.05	0.80 ± 0.06	0.80 ± 0.04	0.80 ± 0.04	0.80 ± 0.05	0.83 ± 0.06	0.79 ± 0.02
Inspiratory Capacity from zero pressure	mL	1.33 ± 0.12	1.37 ± 0.19	1.31 ± 0.19	1.30 ± 0.18	1.33 ± 0.07	1.37 ± 0.12	1.46 ± 0.21	1.22 ± 0.06
Static Compliance	mL/cmH_2O	0.095 ± 0.009	0.100 ± 0.014	0.095 ± 0.015	0.094 ± 0.01	0.097 ± 0.006	0.098 ± 0.010	0.107 ± 0.015	0.087 ± 0.005 #
Static Elastance	cmH_2O/mL	10.61 ± 1.04	10.16 ± 1.34	10.72 ± 1.68	10.78 ± 1.39	10.34 ± 0.72	10.30 ± 1.05	9.48 ± 1.23	11.60 ± 0.54 #
Forced Vital Capacity	mL	1.03 ± 0.10	1.16 ± 0.10 *	1.23 ± 0.18 *	1.14 ± 0.13 *	1.22 ± 0.11 *	1.06 ± 0.11	1.18 ± 0.10	1.10 ± 0.09
Mean Forced Expiratory Flow	mL/sec	24.4 ± 3.6	19.5 ± 5.3	18.2 ± 6.0	16.6 ± 3.0 *	16.0 ± 3.3 *	23.1 ± 2.8	22.5 ± 4.0	23.0 ± 6.6
Peak Expiratory Flow	mL/sec	34.2 ± 1.3	33.7 ± 1.2	33.5 ± 0.8	34.5 ± 1.4	28.9 ± 5.8 *	34.8 ± 0.9	34.0 ± 1.3	34.0 ± 1.1
Forced Expiratory Flow 0.05 sec / FVC	%	84.7 ± 9.1	79.6 ± 13.6	78.4 ± 13.5	77.9 ± 20.5	74.5 ± 13.4	87.6 ± 2.0	83.1 ± 13.1	88.6 ± 4.8
Forced Expiratory Flow 0.1 sec / FVC	%	97.8 ± 9.5	97.1 ± 8.4	94.5 ± 9.24	86.4 ± 22.2	92.2 ± 5.9	96.3 ± 2.3	91.3 ± 12.8	97.6 ± 1.6
Forced Expiratory Flow 0.2 sec / FVC	%	99.6 ± 0.3	92.8 ± 12.6	97.6 ± 4.3	94.1 ± 11.5	98.6 ± 1.4	99.5 ± 0.3	93.6 ± 12.0	99.5 ± 0.3

*During invasive lung function measurements, an average for each individual mouse was calculated from 4 accepted (coefficient of determination: COD>0.95) measurements for each parameter. * = p<0.05, ** = p<0.001 when compared to control animals within the same experiment (intratracheal or jugular vein). # = p<0.05 when compared to elastase-treated mice within the same experiment (intratracheal or jugular vein).*

DISCUSSION

In this study, we induced pulmonary emphysema in adult mice by tracheal instillation of a relatively high dose of elastase. Three weeks after elastase administration we found evidence of histological abnormalities and obstructive lung function, characteristic of pulmonary emphysema. The structural and functional changes persisted up to 10 months and were not affected by intratracheal administration of MSC prior or after the injury. Jugular vein MSC treatment before elastase injection showed an improvement in lung function but no change in histology.

Intratracheal instillation of elastase resulted in increased dynamic compliance, total lung capacity, FVC and decreased tissue-specific elastance and forced expiratory flows 3 weeks after elastase injection. These results agree with earlier findings at 3 weeks after elastase injection[36–38] and are likely due to a loss of elastin and disruption of the integrity of the alveolar wall with loss of alveolar attachments. Indeed, we observed extensive alveolar damage. Hart's staining on lung tissue showed a disorganized elastin deposition after elastase treatment. Disorganisation of elastin fibers and loss of alveolar attachments reduces elastic recoil of the lung. This is likely to contribute to the decreases in forced expiratory flows, as well as to the static hyperinflation. Loss of structural integrity of the peripheral lung with disruption of the alveolar walls and loss of alveolar attachments could also be responsible for the increase in total lung capacity (TLC). A possible mechanism of increased TLC could be air trapping. However, we consider this unlikely, because the simultaneous increase in FVC argues against substantial air trapping. Note that the forced lung function manoeuvres performed in this study differ from those used in clinical setting because we used a negative pressure at the tracheal opening, whereas in human subjects the driving force is a positive pressure from the diaphragm and thoracic wall. This negative pressure could lead to earlier airway collapse and more pronounced airway obstruction than active forced exhalation.

In this study, we used both non-invasive and invasive lung function measurements. Non-invasive measurements are advantageous in longitudinal studies in which animals can be repeatedly measured, but the overall sensitivity for detecting lung function abnormalities appeared lower than that of invasive measurements[39]. The invasive measurements were more robust and sensitive, and accurately reflected alterations in lung mechanics. Thus, the Flexivent method was superior for detecting physiological differences in lung mechanics in mice with elastase-induced lung injury, in agreement with earlier findings in hyperoxia-induced lung injury[40]. The main advantage of whole body plethysmography is its repeatability. However, de Vleeschauwer *et al.* have recently shown that intubating mice for repeated invasive measurements yielded the same results as performing a tracheotomy[41] and therefore we consider Flexivent measurements the method of choice for future experiments.

To our knowledge, no long-term functional measurements have been performed in the elastase-induced mouse model of emphysema. During long term follow-up, we found no evidence of recovery of lung injury. This suggests that the elastase model is suitable for intervention studies aimed at tissue repair. The repeated use of lung function measurements in this model enables us to monitor disease progression and treatment efficacy in a manner that may be relevant to clinical practice. The findings with the forced expiration measurements do not agree with all other findings reflecting emphysema. We believe that this might well be due to the smaller number of animals used for the forced expiratory measurements, and the relatively large variation within the groups. Overall, these measurements suggest that forced expiration measurements are less sensitive, with a larger variation between animals in the same group, then the other lung function measurements obtained with the Flexivent system.

In our emphysema model, intratracheal MSC installation shortly after elastase injection, aiming to prevent lung injury, had no effect on lung function or histology. We chose the intratracheal route to ensure that the injected MSCs came into direct contact with the damaged alveolar epithelial layer. This intratracheal approach was successfully applied in the study by Katsha *et al.*[23]. As mentioned before, our elastase dose was significantly greater than that of Katsha *et al.* which might account for the difference in outcome of MSC treatment. We have repeated the intratracheal MSC experiments in a rat model of emphysema (elastase dose: 30 Units / 100 gram bodyweight) and $5x10^5$ rat bone marrow-derived MSCs (not shown). These experiments also showed no effect of intratracheal MSC treatment on lung function, histology and morphometry, indicating that our results are reproducible in different species.

We also administered MSCs intratracheally 21 days after elastase injection to induce repair of elastase-induced lung injury. MSC injection had no effect on lung function or histology. The discrepancy between our negative results of repair by MSCs and those of others, with long-lasting low grade inflammation in a low-dose elastase model and effects of intratracheal MSC injection shortly after elastase[7,8,20,42], may be due to the absence of a persisting inflammatory component in our emphysema model. Since MSCs have been shown to possess anti-inflammatory properties, administering them 21 days after elastase injection, when cytokine levels had normalized, might reduce their ability to exert positive effects on lung function and histology.

COPD has been shown to possess a large vascular disease component[43]. CT images of COPD patients show a decrease in small pulmonary vessels, even in smokers with mild emphysema[44]. Compared to non-smokers, COPD patients show increased invasion of inflammatory cells in the vascular adventitial layer[45]. The extent of pulmonary vascular remodelling directly correlates with the severity of the endothelial inflammation[46]. Intravenous injection of MSCs creates a systemic anti-inflammatory response on the endothelial surface of the pulmonary vasculature. Thus, the anti-inflammatory milieu on the endothelial side produced by MSCs injected via the jugular vein could decrease the vascular

inflammation shown to be present in the elastase-induced emphysema model[47]. There is a large body of work suggesting that MSC intervention using the endothelial route, either via the dorsal penile vein[48] or via the tail vein[8,19,49] could be successful in improving elastase-induced emphysema, thereby improving lung function. We used the jugular vein infusion method to infuse the cells closest to the pulmonary vasculature. Jugular vein infusion of 10^5 MSCs just prior to elastase installation to prevent elastase-induced lung injury significantly improved lung function in elastase-treated mice, while histology did not improve. Another possible explanation is that MSCs may have improved surfactant production or activity. It is well known that alveolar inflammation decreases surfactant production and activity[50–52] and as MSCs have an anti-inflammatory effect they may have improved surfactant production or activity and thereby improved lung function in the absence of histological improvement. This hypothesis is less likely, since intratracheal injection of MSCs showed no improvement in lung function. Delivery of MSCs directly into the alveolar spaces should generate a local anti-inflammatory effect, thereby improving surfactant function. This effect was not seen in the intratracheal injection groups. More work is needed to study the underlying mechanism responsible for the improvement in lung function after jugular vein injection of MSCs.

In contrast to our work, Cruz *et al.* showed that intravenous injection of bone marrow mononuclear cells 3 hours after elastase injection decreased inflammatory parameters, but also improved histology and morphometry[24]. Unfortunately, they did not measure lung function. The main difference in methodology between our study and the study of Cruz *et al.* is that they used a much lower dose of elastase, resulting in less alveolar enlargement, as measured by a MLI score of 68.5 compared to our MLI score of 128. The difference in alveolar destruction severity might account for the difference in treatment outcome, with our higher elastase dose surpassing the injury threshold for an effect of MSC treatment on histology and morphometry.

A major limitation of our study is the difference in timing of intravenous and intratracheal MSC injection, which invalidates comparison of the two interventions in the present study. Future studies are needed to examine whether the intravenous route might be beneficial after elastase. Another limitation is the different cell numbers used for intratracheal MSC injections when compared to jugular vein MSC injections. Unfortunately, we were limited in the number of cells for jugular vein injection because of 100% injection-induced mortality when using higher doses, such as those used for intratracheal MSC injections.

CONCLUSION

Our results demonstrate that MSC injection via the jugular vein just before elastase prevented lung function changes after elastase treatment. Intratracheal administration 24 hours before and 24 hours after elastase injection did not prevent lung function changes.

The severity of elastase-induced lung injury may be an important determinant of the effect of MSC treatment.

SUPPLEMENTARY METHODS

Non-invasive lung function measurements

Animals were each placed in an individual plethysmograph and a 30 min interval was used for the animal to adjust to their new environment before the measurements were started. Measurements were continuously recorded for 1 h after which animals were returned to their cages.

Invasive lung function measurements

Animals were anesthetized with an *ip* injection of Ketamine (150 mg/kg) and Xylazine (10 mg/kg) before tracheostomy. A 25G endotracheal tube was inserted and sutured to prevent leakage. Following intraperitoneal injection of Pancuronium (5 mg/kg), the animal was ventilated at 150 breaths/min with a tidal volume of 10 mL/kg, and lung function was measured using the Flexivent ventilator (SCIREQ, Montreal, QC, Canada). The flexivent measures flow-volume relationships of the respiratory system, and uses forced oscillations to discriminate between the airways and the alveolar compartment. The "Total Lung Capacity" (TLC), "Snapshot" (based on single-compartment model), and "Primewave-8" (based on constant phase model) perturbations were used to measure lung function. For the "TLC" maneuver, the lung is inflated to +30 cmH_2O and deflated afterwards. For the "Snapshot" maneuver, three sinusoidal waves of in- and expiration provide the resistance, elastance and compliance parameters. For the "prime-wave 8", multiple frequency forced oscillations were applied to measure tissue elasticity and airway resistance properties. Volume-driven pressure-volume loops were also obtained and provided TLC, inspiratory capacity from zero pressure and static and dynamic compliance. All measurements were repeated until 4 successful recordings, with a coefficient of determination of >0.95, were obtained. Animals also underwent forced expirations by inflating to TLC and then rapidly applying a negative pressure of -55 cmH_2O to the expiratory valve. In the current state of small animal ventilator technology, this technique is the closest to mimicking forced expiratory spirometry in humans. Parameters obtained from this maneuver were the forced vital capacity, mean forced expiratory flow, peak forced expiratory flow and forced expiratory flow at 0.05, 0.1 and 0.2 seconds.

Histology and morphometry

Following lung function measurements, the animals were exsanguinated by cutting the abdominal aorta while still under anesthesia. The thoracic cavity was opened and heparin dissolved in phosphate buffered saline (PBS) was injected into the right ventricle of the heart, and the lungs were flushed free of blood. A catheter was inserted into the trachea to allow 4% (w/v) paraformaldehyde (PFA) to inflate the tissue at a constant pressure of 20 cmH_2O. After 5 minutes, the catheter was removed and the trachea tied off. The lungs were removed from the thorax as a single block and fixed in 4% PFA overnight. Fixed lungs were embedded in paraffin at 60°C. Randomly orientated tissue blocks were cut into 7 µm sections, stained with hematoxylin-eosin and Hart's elastic stain, and morphometry was performed on digital images taken at x200. Images were captured from 5 non-overlapping

fields from each slide, with 4 slides per animal. Mean linear intercepts (Lm) was measured and calculated[53]. For alveolar number determination, 20 randomly selected non-overlapping fields from sections obtained from 4 animals per group were examined. Each field was viewed at x200 magnification and alveolar number was counted and expressed per mm^2 [54].

SUPPLEMENTARY FIGURES

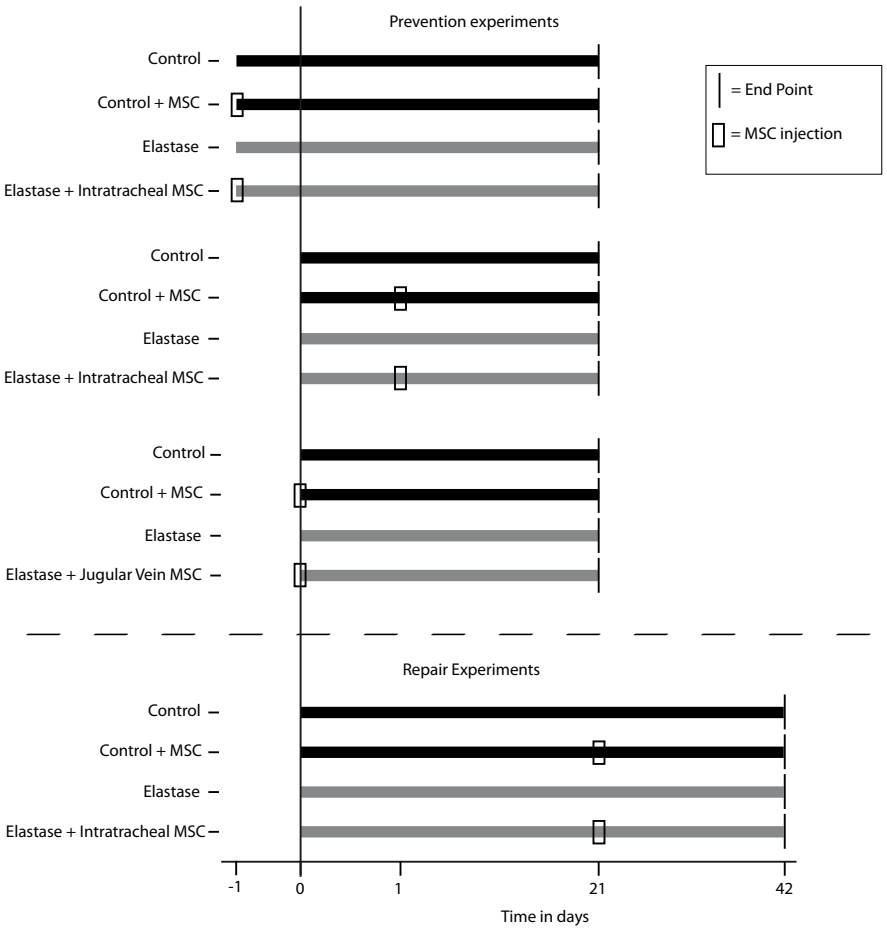

Supplementary figure S1. *Time-line of all MSC experiments performed.*

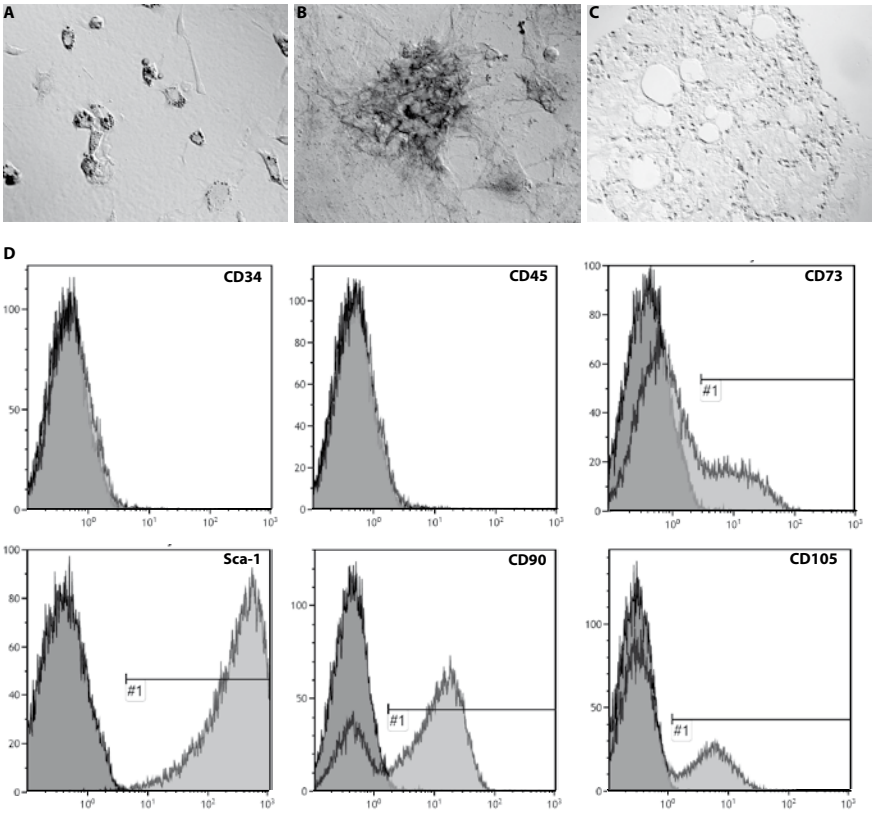

Supplementary figure S2. *Differentiated MSCs were directly stained on 6 well plates for adipocytes (A, Oil-red stain), osteoblasts (B, Von Kossa stain) and chondrocytes (C, Alcian Blue stain), and flow cytometry data (D) of passage 8 MSCs (red population) stained for CD34, CD45, CD73, CD90, Sca-1 and CD105 and passage 8 unstained MSCs as control (orange population). (See colour section, page 195).*

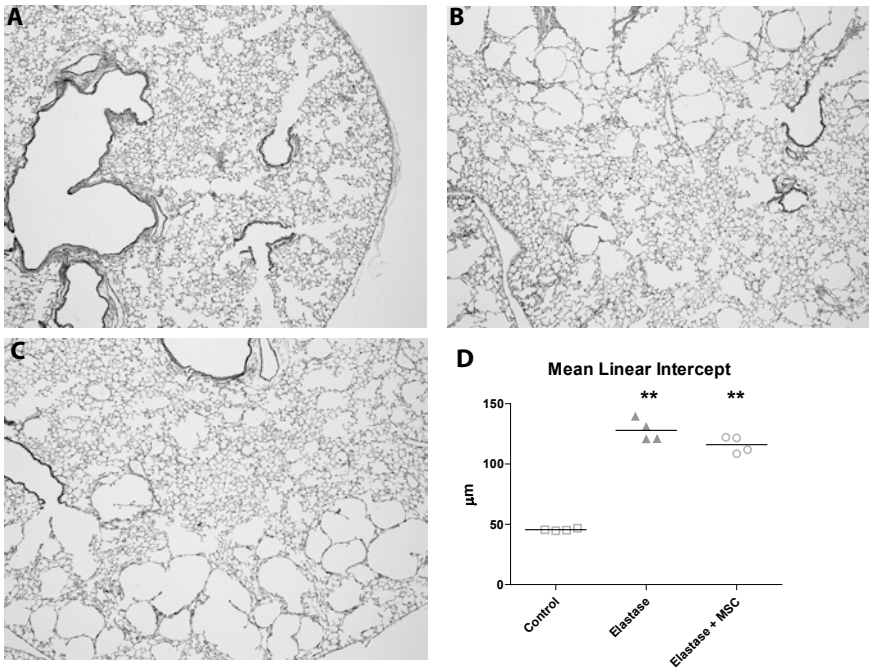

Supplementary figure S3. *Representative histological sections of saline-controls (A), elastase-treated mice 21 days after injection (B) and elastase-treated mice that received MSCs via the jugular vein route (C) and via the intratracheal route (D). Sections were stained with hematoxylin and eosin. Morphometry results (E) are expressed as mean ± SEM for all groups (n=4 per group) ** = p<0.001. (See colour section, page 196).*

REFERENCES

1. Mannino DM, Braman S. The epidemiology and economics of chronic obstructive pulmonary disease. *Proceedings of the American Thoracic Society*. 2007;4(7):502–6.
2. Faulkner M a, Hilleman DE. The economic impact of chronic obstructive pulmonary disease. *Expert opinion on pharmacotherapy*. 2002;3(3):219–28.
3. Baraldo S, Turato G, Saetta M. Pathophysiology of the small airways in chronic obstructive pulmonary disease. *Respiration*. 2012;84(2):89–97.
4. Galbán CJ, Han MK, Boes JL, et al. Computed tomography-based biomarker provides unique signature for diagnosis of COPD phenotypes and disease progression. *Nature medicine*. 2012;18(11):1711–5.
5. Bourbon JR, Boucherat O, Boczkowski J, Crestani B, Delacourt C. Bronchopulmonary dysplasia and emphysema: in search of common therapeutic targets. *Trends in molecular medicine*. 2009;15(4):169–79.
6. Sin DDD, McAlister FFA, Man SFP, Anthonisen NR. Contemporary management of chronic obstructive pulmonary disease: scientific review. *JAMA*. 2003;290(17):2301–2312.
7. Haaften T van, Byrne R, Bonnet S. Airway delivery of mesenchymal stem cells prevents arrested alveolar growth in neonatal lung injury in rats. *American journal of respiratory and critical care medicine*. 2009;(7):200902–0179OCv1.
8. Zhao F, Zhang Y, Liu Y, et al. Therapeutic effects of bone marrow-derived mesenchymal stem cells engraftment on bleomycin-induced lung injury in rats. *Transplantation proceedings*.Vol 40. Elsevier; 2008:1700–1705.
9. Gupta N, Su X, Popov B. Intrapulmonary delivery of bone marrow-derived mesenchymal stem cells improves survival and attenuates endotoxin-induced acute lung injury in mice. *The journal of immunology*. 2007;179(3):1855–63.
10. Loebinger MR, Janes SM. Stem cells for lung disease. *Chest*. 2007;132(1):279–85.
11. Ortiz L a, Gambelli F, McBride C, et al. Mesenchymal stem cell engraftment in lung is enhanced in response to bleomycin exposure and ameliorates its fibrotic effects. *Proceedings of the National Academy of Sciences of the United States of America*. 2003;100(14):8407–11.
12. Rojas M, Xu J, Woods CR, et al. Bone marrow-derived mesenchymal stem cells in repair of the injured lung. *American journal of respiratory cell and molecular biology*. 2005;33(2):145–52.
13. Kotton DN, Fabian AJ, Mulligan RC. Failure of bone marrow to reconstitute lung epithelium. *American journal of respiratory cell and molecular biology*. 2005;33(4):328–34.
14. Loi R, Beckett T, Goncz KK, Suratt BT, Weiss DJ. Limited restoration of cystic fibrosis lung epithelium in vivo with adult bone marrow-derived cells. *American journal of respiratory and critical care medicine*. 2006;173(2):171–9.
15. Yamada M, Kubo H, Kobayashi S, et al. Bone marrow-derived progenitor cells are important for lung repair after lipopolysaccharide-induced lung injury. *Journal of immunology*. 2004;172(2):1266–72.
16. Wong AP, Dutly AE, Sacher A, et al. Targeted cell replacement with bone marrow cells for airway epithelial regeneration. *American Journal of Physiology-Lung Cellular and Molecular Physiology*. 2007;293(3):L740–52.
17. Spees JL, Pociask D a, Sullivan DE, et al. Engraftment of bone marrow progenitor cells in a rat model of asbestos-induced pulmonary fibrosis. *American journal of respiratory and critical care medicine*. 2007;176(4):385–94.
18. Block G, Ohkouchi S, Fung F, et al. Multipotent stromal cells are activated to reduce apoptosis in part of upregulation and secretion of stanniocalcin-1. *Stem Cells*. 2009;27(3):670–81.
19. Lee RH, Pulin A a, Seo MJ, et al. Intravenous hMSCs improve myocardial infarction in mice because cells embolized in lung are activated to secrete the anti-inflammatory protein TSG-6. *Cell stem cell*. 2009;5(1):54–63.

20. Chen L, Tredget EE, Wu PYG, Wu Y. Paracrine factors of mesenchymal stem cells recruit macrophages and endothelial lineage cells and enhance wound healing. *PloS one*. 2008;3(4):e1886.
21. Crisostomo PR, Wang Y, Markel T a, Wang M, Lahm T, Meldrum DR. Human mesenchymal stem cells stimulated by TNF-alpha, LPS, or hypoxia produce growth factors by an NF kappa B- but not JNK-dependent mechanism. *American Journal of Physiology-Cell Physiology*. 2008;294(3):C675–82.
22. Ionescu L, Byrne RN, van Haaften T, et al. Stem Cell Conditioned Medium Improves Acute Lung Injury in Mice: In Vivo Evidence for Stem Cell Paracrine Action. *American Journal of Physiology-Lung Cellular and Molecular Physiology*. 2012;(September).
23. Katsha AM, Ohkouchi S, Xin H, et al. Paracrine factors of multipotent stromal cells ameliorate lung injury in an elastase-induced emphysema model. *Molecular therapy*. 2011;19(1):196–203.
24. Cruz FF, Antunes MA, Abreu SC, et al. Protective effects of bone marrow mononuclear cell therapy on lung and heart in an elastase-induced emphysema model. *Respiratory physiology & neurobiology*. 2012;182(1):26–36.
25. Osiris Osiris Therapeutics Reports interim data for COPD stem cell study. *Available from: http://investor.osiris.com/releases.cfm?Year=&ReleasesType=&DisplayPage=2*. 2009.
26. Bouloukaki I, Tsiligianni IG, Tsoumakidou M, et al. Sputum and nasal lavage lung-specific biomarkers before and after smoking cessation. *BMC pulmonary medicine*. 2011;11:35.
27. Foronjy RF, Mirochnitchenko O, Propokenko O, et al. Superoxide dismutase expression attenuates cigarette smoke- or elastase-generated emphysema in mice. *American journal of respiratory and critical care medicine*. 2006;173(6):623–31.
28. Ito S, Ingenito EP, Brewer KK, et al. Mechanics, nonlinearity, and failure strength of lung tissue in a mouse model of emphysema: possible role of collagen remodeling. *Journal of applied physiology*. 2005;98(2):503–11.
29. Ishii M, Emami K, Xin Y, et al. Regional Functional-Structure Relationships in Lungs of an Elastase Murine Model of Emphysema. *Journal of applied physiology*. 2011.
30. Sung JH, Yang H-M, Park JB, et al. Isolation and characterization of mouse mesenchymal stem cells. *Transplantation proceedings*. 2008;40(8):2649–54.
31. Dominici M, Le Blanc K, Mueller I, et al. Minimal criteria for defining multipotent mesenchymal stromal cells. The International Society for Cellular Therapy position statement. *Cytotherapy*. 2006;8(4):315–317.
32. Lama V, Smith L, Badri L. Evidence for tissue-resident mesenchymal stem cells in human adult lung from studies of transplanted allografts. *Journal of Clinical Investigation*. 2007;117(4):989–996.
33. Tibboel J, Joza S, Reiss I, Jongste JC De, Post M. Amelioration of hyperoxia-induced lung injury using a sphingolipid-based intervention. *European Respiratory Journal*. 2013;42(3):776-84.
34. Tsuchida S, Engelberts D, Roth M, McKerlie C, Post M, Kavanagh BP. Continuous positive airway pressure causes lung injury in a model of sepsis. *American Journal of Physiology-Lung Cellular and Molecular Physiology*. 2005;289(4):L554–64.
35. Ridsdale R, Roth-Kleiner M, D'Ovidio F, et al. Surfactant palmitoylmyristoylphosphatidylcholine is a marker for alveolar size during disease. *American journal of respiratory and critical care medicine*. 2005;172(2):225–32.
36. Emami K, Chia E, Kadlecek S, et al. Regional correlation of emphysematous changes in lung function and structure: a comparison between pulmonary function testing and hyperpolarized MRI metrics. *Journal of applied physiology (Bethesda, Md. : 1985)*. 2011;110(1):225–35.
37. Vanoirbeek J a J, Rinaldi M, De Vooght V, et al. Noninvasive and invasive pulmonary function in mouse models of obstructive and restrictive respiratory diseases. *American journal of respiratory cell and molecular biology*. 2010;42(1):96–104.

38. Hamakawa H, Bartolák-Suki E, Parameswaran H, Majumdar A, Lutchen KR, Suki B. Structure-function Relations in an Elastase-induced Mouse Model of Emphysema. *American journal of respiratory cell and molecular biology*. 2010;(C):1–38.
39. Glaab T, Taube C, Braun A, Mitzner W. Invasive and noninvasive methods for studying pulmonary function in mice. *Respiratory research*. 2007;8:63.
40. Peták F, Habre W, Donati Y. Hyperoxia-induced changes in mouse lung mechanics: forced oscillations vs. barometric plethysmography. *Journal of Applied Physiology*. 2001;(90):2221–2230.
41. De Vleeschauwer SI, Rinaldi M, De Vooght V, et al. Repeated invasive lung function measurements in intubated mice: an approach for longitudinal lung research. *Laboratory animals*. 2011;45(2):81–9.
42. Zhen G, Xue Z, Zhao J, et al. Mesenchymal stem cell transplantation increases expression of vascular endothelial growth factor in papain-induced emphysematous lungs and inhibits apoptosis of lung cells. *Cytotherapy*. 2010;12(5):605–614.
43. Peinado VI, Pizarro S, Barberà JA. Pulmonary vascular involvement in COPD. *Chest*. 2008;134(4):808–14.
44. Matsuura Y, Kawata N, Yanagawa N, et al. Quantitative assessment of cross-sectional area of small pulmonary vessels in patients with COPD using inspiratory and expiratory MDCT. *European journal of radiology*. 2013.
45. Barberà JA, Riverola A, Roca J, et al. Pulmonary vascular abnormalities and ventilation-perfusion relationships in mild chronic obstructive pulmonary disease. *American journal of respiratory and critical care medicine*. 1994;149(2 Pt 1):423–9.
46. Peinado VI, Barberà JA, Abate P, et al. Inflammatory Reaction in Pulmonary Muscular Arteries of Patients with Mild Chronic. *American journal of respiratory and critical care medicine*. 1999;159:1605–1611.
47. Artaechevarria X, Blanco D, de Biurrun G, et al. Evaluation of micro-CT for emphysema assessment in mice: comparison with non-radiological techniques. *European radiology*. 2011;21(5):954–62.
48. Shigemura N, Okumura M, Mizuno S, Imanishi Y, Nakamura T, Sawa Y. Autologous Transplantation of Adipose Tissue-Derived Stromal Cells Ameliorates Pulmonary Emphysema. *American journal of transplantation*. 2006;6(11):2592–2600.
49. Bauer J, Liebisch G, Hofmann C, et al. Lipid alterations in experimental murine colitis: role of ceramide and imipramine for matrix metalloproteinase-1 expression. *PloS one*. 2009;4(9):e7197.
50. Wright T, Notter R, Wang Z, Harmsen A, Gigliotti F. Pulmonary inflammation disrupts surfactant function during Pneumocystis carinii pneumonia. *Infection and Immunity*. 2001;69(2):758–764.
51. Enhorning G, Hohlfeld J, Krug N, Lema G, Welliver RC. Surfactant function affected by airway inflammation and cooling: possible impact on exercise-induced asthma. *European Respiratory Journal*. 2000;15(3):532–8.
52. Liu M, Wang L, Enhorning G. Surfactant dysfunction develops when the immunized guinea-pig is challenged with ovalbumin aerosol. *Clinical and experimental allergy*. 1995;25(11):1053–60.
53. Dunnill MS. Quantitative Methods in the Study of Pulmonary Pathology. *Thorax*. 1962;17(4):320–328.
54. Karadag A, Sakurai R, Wang Y, et al. Effect of maternal food restriction on fetal rat lung lipid differentiation program. *Pediatric pulmonology*. 2009;44(7):635–44.

Chapter 7

General Discussion

INTRODUCTION

In this thesis we focused on lung injury and repair in two rodent models of human disease; hyperoxia-induced Bronchopulmonary Dysplasia and elastase-induced pulmonary emphysema. In **chapter 2** we evaluated the available literature and provided an overview of the role of sphingolipids during lung growth and development. In **chapter 3** we characterized lung function and sphingolipid profile during hyperoxia exposure and recovery in room air in our hyperoxia-induced Bronchopulmonary Dysplasia model, and examined the effect of D-sphingosine, a pro-proliferative sphingolipid, during recovery in room air. We examined the effect of constitutive hypoxia-inducible factor 1-alpha expression on postnatal alveolarization and lung vascularisation, as well as its effect on preventing hyperoxia-induced lung injury in **chapter 4**. In the elastase-induced emphysema model we characterized ceramide levels, a pro-apoptotic sphingolipid, and examined the effects of blocking the *de novo* pathway of ceramide production on lung function and histology in **chapter 5**. Finally, we attempted to prevent elastase-induced lung injury by injecting mesenchymal stem cells in **chapter 6**.

CHRONIC LUNG DISEASE

The overall human life expectancy is gradually increasing, but there also is an increase in the number of patients living with and dying of chronic diseases. Of the 58 million deaths per year from all causes, 35 million are attributed to chronic disease[1]. Chronic lung diseases, including asthma, Chronic Obstructive Pulmonary Disease (COPD), pulmonary hypertension and Bronchopulmonary Dysplasia (BPD)[1], account for 4 millions of these deaths. Chronic lung diseases represent a major health problem, with respiratory symptoms being one of the major causes for visiting primary health care centres, ranging from 8 to 37%[2]. Chronic lung diseases are associated with a substantial loss of disability-adjusted life years, and a high mortality[3]. BPD and COPD, both diseases with a decreased number of alveoli, occur in different stages of life, but share common ground in pathogenesis, biological processes and etiological factors[4].

BRONCHOPULMONARY DYSPLASIA

In the Netherlands, prematurity is the number 3 cause of death in children under 5 years of age, directly accounting for 35 percent of neonatal mortality[5,6], and every week of preterm birth doubles the morbidity risk, up to 43% in preterms born between 23-27 weeks gestational age[7]. The percentage of preterm births increases with 1 percent each year, and worldwide projections show an expected 2.250.000 preterm births in the year 2025[8]. A lower birth weight is associated with an increased risk of developing BPD[9], and the rates of BPD in very preterm neonates (23-31 weeks gestational age) in Europe presently range from 10 to 25 percent[10]. Under the influence of advances in care of preterm infants the

survival of very preterm infants has improved. The increase in preterm births will cause a rise in overall prevalence of BPD. With the increased survival of very preterm infants and improvements in treatment of respiratory insufficiency, the 'old' BPD, characterized by parenchymal fibrosis, edema, vascular changes and inflammation, has evolved into the 'new' BPD, with fewer and larger alveoli as a result of interrupted septation and abnormal vascular organization[11]. The change in histological character of the disease has sparked new research towards the possible altered pathogenesis of this 'new' BPD.

Even though progress has been made in the management of infants with BPD, current treatment remains symptomatic. Antenatal steroids have reduced the incidence of neonatal death and respiratory distress, but have failed to reduce the incidence of BPD. Exogenous surfactant minimized the use of mechanical ventilation, but nasal continuous positive pressure and oxygen treatment with saturation targets between 88-95% did not prevent BPD, although it reduced BPD-associated mortality[12,13]. Vitamin A supplementation reduced oxygen dependence at 36 weeks postmenstrual age and improved BPD-associated mortality in one study[14], but due to the physical limitations of administering daily intramuscular injections in neonates this strategy has not been implemented as clinical standard of care.

CHRONIC OBSTRUCTIVE PULMONARY DISEASE

COPD is the most common chronic lung disease in adults and is associated with high mortality[15] and health-care costs[16]. COPD severity is commonly based on the GOLD criteria. GOLD staging requires an FEV1/FVC ratio below 0.70, and stages are based on FEV1, stage I >80% predicted, stage II between 50-80%, stage III between 30-60% and stage IV <30% predicted[17]. The prevalence of COPD (GOLD stage II and higher) was estimated at 11.8% for men and 8.5% for women aged 40 and above[18]. The incidence of COPD is rising, especially among women. Currently the number 4 cause of death in the Unites States, COPD is predicted to surpass stroke and become the number 1 cause of death in the coming decades[19].

There is no causal treatment for COPD. Smoking cessation is an important step in the treatment of COPD, and is currently the most effective measure to slow down the decline in lung function. Smoking cessation has been shown to be effective, also in heavy smokers and those with a poor baseline lung function. Smoking cessation improves lung function decline by 50%, when compared to patients who continue smoking[20]. Pharmacological treatment for COPD is primarily based on anti-inflammatory drugs and the use of bronchodilators, with oxygen supplementation as supporting measure. These treatments provide some symptom reduction and prevent exacerbations, but do not stop disease progression or decline in lung function that determines the high morbidity and mortality. For the Netherlands, the estimated prevalence of COPD will rise from 19 to 30 per 1000 inhabitants in 2025, of which 2.4 per 1000 inhabitants will die due to COPD[21]. This

increase in morbidity and mortality calls for better treatments to prevent the development of COPD, but also requires new therapeutic strategies aimed at repairing the damaged lung. Many government programs have attempted to discourage smoking by raising tobacco tax, through education, by putting warning labels on cigarette packaging, and banning smoking in public areas, sometimes with documented striking success. Multiple awareness programs have been set up in developing countries to prevent the development of COPD due to the burning of wood and other biomass fuels indoors for cooking or heating[3,22]. Not all smokers develop COPD, therefore these methods will not provide relief for all patients or for patients who have already developed COPD.

BPD AND COPD: SIMILARITIES AND DIFFERENCES

BPD and COPD share many pathophysiological pathways, such as increased apoptosis, vascular abnormalities, protease-antiprotease imbalance, oxidative stress and chronic inflammation[4]. Both diseases show permanently enlarged alveoli, but the mechanism behind this enlargement differs, with arrested development in BPD, and active destruction of already existing alveolar walls in COPD. A decreased number of pulmonary vessels is seen in both BPD and COPD[23]. Animal models have shown that neonatal hyperoxia contributes to an increased susceptibility for cigarette-smoke induced pulmonary emphysema later in life[24]. BPD patients show lung function abnormalities that persist into adulthood[25,26]. A high prevalence of airtrapping[27], parenchymal abnormalities[28] and emphysema-like structural defects have been reported in over 80% of adult survivors of 'old' BPD[29,30]. We propose that the lungs of BPD patients may well be more susceptible to injurious factors[31], making these patients more vulnerable for developing pulmonary emphysema earlier in life[32]. Figure 1, adapted from Bourbon *et al.*[4] shows the interplay of factors and biological processes suggested to play a role in the development of BPD and COPD.
We examined animal models of BPD and COPD to discover factors that contribute to the development/regulation of these diseases, to investigate repair mechanisms and evaluate potential therapeutic interventions, and to determine the differences and similarities between the two clinical entities.

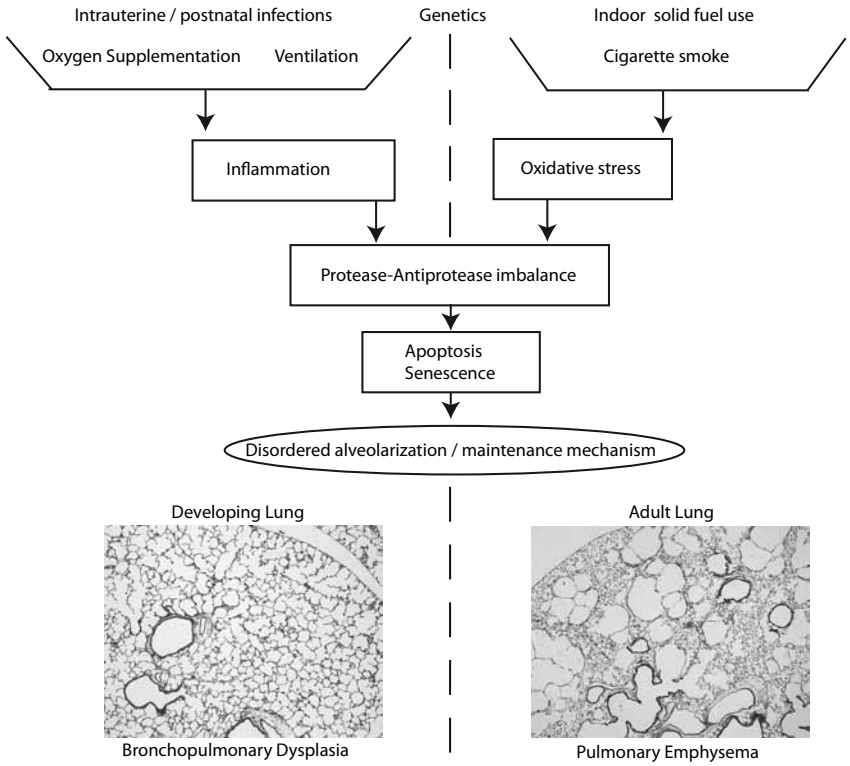

Figure 1. *The interplay of factors and biological processes suggested to play a role in the development of BPD and COPD. (See colour section, page 197).*

ANIMAL MODELS OF DISEASE

The mouse has been used in laboratories for decades to develop models of human lung disease, either by subjecting it to injury, administering toxic or damaging substances and/or through genetic manipulation. Mice and men exhibit similar physiological processes and share 99% of the genome. Genetic studies have been performed for more than 100 years[33], evolving from studying naturally occurring genetic variants and crossbreeding these to obtain specific traits, to directly altering the genetic code using transgenes which can be expressed at any time point during embryonic development or maturation, and expression can be localized to one specific organ system. Animal models for BPD and pulmonary emphysema have been used and reviewed extensively in the past[34–39]. In this thesis, we used two different animal models, namely hyperoxia-induced Bronchopulmonary Dysplasia (BPD) and elastase-induced pulmonary emphysema.

HYPEROXIA-INDUCED BRONCHOPULMONARY DYSPLASIA

Alveolarization in mice occurs from postnatal day 4-14 (36 weeks-2 years postnatal in humans)[40,41] and is followed by the microvascular maturation stage at postnatal day 14-21 (from birth-3 years in humans), completing the lung development. The preferred rodent model of BPD is by exposing mice or rats to hyperoxia during the postnatal period. This model accurately reproduces the arrest in alveolarization, vascular changes and lung function abnormalities of BPD patients, and is reproducible, with little variation between subjects as long as litter sizes are kept equal during the 14 days of hyperoxia exposure[42–44]. A minor consideration when using this model is that lung function measurements require mice to be 28 days old before accurate measurements can be taken. At this age mouse lungs are considered adult lungs[45], making it impossible to collect data on neonatal/adolescent lung function in mice.

ELASTASE-INDUCED EMPHYSEMA

Mouse models of COPD make use of various techniques to damage the lungs. These include inhalation of exogenous agents, such as porcine pancreatic or human neutrophil elastase, papain, coal dust, or cigarette smoke. Also, genetic knock-out models leading to alveolar enlargement have been developed[34]. A downside to these models is the limited severity of the emphysema. Patients that require intense treatment for COPD in combination with home oxygen supplementation have GOLD stage III/VI, while most of the above described animal models have lung abnormalities comparable to GOLD stage I/II[46]. We decided to study the commonly used elastase-induced emphysema model, since it provides consistent results in terms of alveolar destruction[37,47,48]. It also is a model that allows us to increase the elastase dose to obtain more severe histological and lung function abnormalities representing the characteristics seen in severe COPD (GOLD III/VI) patients. Recently the elastase model has been used to mimic COPD exacerbations by injecting LPS in the lungs of elastase-treated mice[49,50]. One of the major challenges in using this model is the small 'therapeutic' window for the elastase dose. Below this dose, mice show only minor histological abnormalities and no alterations in lung function, making *in vivo* follow-up impossible without having to sacrifice the animal. Above this dose, mice develop severe pulmonary haemorrhaging, resulting in a mortality rate of around 100 percent. To obtain adequate dosing, one should account for pulmonary dead space by injecting the elastase solution, followed by an additional air bolus equal to the measured dead space[51]. Proper intubation technique is important, since insertion of the endotracheal tube past the carina results in injection of the full dose of elastase into a single lung. This causes intense haemorrhaging and asphyxiation due to fluid overload in the lungs.

SPHINGOLIPIDS IN BPD AND COPD

Technological advancement in the field of metabolomics has provided insight into a new area of biological characterization of lung diseases. In the last decade, sphingolipid research has greatly benefited from this new approach. Sphingolipids are present in every cell membrane of the human body and form a stable outer leaflet of the plasma membrane lipid bilayer providing a central pathway for the regulation of many cellular processes, among which apoptosis, proliferation, necrosis, inflammation, autophagy and cellular senescence[52–55]. Sphingolipids have also been shown to regulate embryonic vascular organization[56].

Many reviews are available describing the different causal and contributing factors that are relevant for the pathogenesis of BPD[13,57,58]. One of these factors is apoptosis[57,59], a highly regulated form of cell death, influenced by many pathways[60]. Sphingolipids determine the balance between apoptosis and proliferation[52,61]. The most important pro-apoptotic sphingolipid is ceramide. Together with S1P, ceramide forms the so called sphingolipid rheostat, that regulates the balance between apoptosis and proliferation[54,62,63].

In our BPD model we found increased ceramide levels during hyperoxia, which returned to control levels during recovery in normoxia, and we discovered that adding an S1P precursor increased the rate of recovery. These results might indicate a role for ceramide-induced apoptosis in this model, and illustrate the possibility of pharmacological modification of the ceramide-S1P balance. We showed that we can improve recovery in our hyperoxia-induced BPD model, but we believe that prevention would be better than cure. Therefore, additional experiments should be undertaken to elucidate which ceramide-producing pathway is responsible for the increased ceramide levels, potentially to develop a preventative approach e.g. by pharmacological blockade of these pathways.

The main hypothesis underlying the pathophysiology of the development of pulmonary emphysema is that of cellular injury. Direct injury, leading to the destruction of alveoli, may be due to cigarette smoke, pollution or increased inflammation and apoptosis of alveolar type I, II and endothelial cells in the lung. Indeed, increased apoptosis has been found in lung samples of pulmonary emphysema patients[64–66]. New insights into the factors that determine the balance between apoptosis and proliferation have recently brought forth a new role for ceramides. We examined the contribution of ceramides to the development of pulmonary emphysema. We found that ceramide levels increased in BAL during the initial inflammatory phase, similar to what has been found in the BAL fluid of active smoking COPD patients[67]. Blocking the *de novo* pathway of ceramide generation diminished the rise in ceramides and ameliorated lung function changes suggesting a role for ceramide-driven apoptosis in our model of pulmonary emphysema. This hypothesis is strengthened by the fact that intratracheal instillation of long-chain ceramides produced pulmonary emphysema[68] and it is well-known that apoptosis plays a role in the development of emphysema[64,69,70]. Therefore the ceramide/S1P rheostat might play a pivotal role

in the regulation of this process and could therefore be considered as a new therapeutic target in the treatment of COPD patients.

BPD AND COPD AS 'PULMONARY VASCULAR DISEASES'

Angio- and vasculogenesis in lung development has been reviewed extensively[71–73]. Animal models and human autopsy specimens of BPD have shown abnormal distribution of vessels and a decrease in small arteries[58,74], suggesting that BPD is partly a vascular disease. COPD patients show a loss of alveolar capillary endothelial cells and small capillaries[75,76], combined with decreased VEGF levels[77]. VEGFR blockade causes apoptosis and pulmonary emphysema in mice[78], further delineating the important vascular disease component in COPD.

Lung development normally occurs under hypoxic conditions[79], and hypoxia-inducible factors (HIFs) are the main transcriptional regulators responsible for stimulating vascular development during this hypoxic period[71,80]. HIF is known as the master regulator of the hypoxic response and upregulation of HIF leads to the activation of genes[81] necessary for proper lung vascular, and thereby alveolar, development as well as surfactant production[82,83]. There are multiple isoforms of HIF, but a basic division can be made into an oxygen-sensitive subunit; HIF-1α, HIF-2α and HIF-3α, and a constitutively expressed subunit; HIF-1β/ARNT (Aryl Hydrocarbon Receptor Nuclear Translocator)[84]. HIF-1α expression increases after hypoxia exposure[85] and has been shown to influence vascular development through the regulation of VEGF mRNA levels[86]. HIF-1α is involved in many different types of human disease. In the lung decreased levels of HIF-1α have been found in BPD[87,88] whereas increased levels of HIF-1α have been found in pulmonary hypertension[89] and small and non-small cell lung cancers[90]. HIF-2α has been shown to be required for maturation of alveolar type II cells and proper surfactant production[91,92], and is associated with pulmonary hypertension and Congenital Diaphragmatic Hernia (CDH)[93] and is also increased in non-small cell lung cancer[90]. HIF-3α has been shown to play a role in epithelial cell differentiation and heart and lung development during the embryonic and neonatal phase[94].

We found that constitutive overexpression of HIF-1-alpha in alveolar epithelial cells led to enhanced alveolarization by stimulating postnatal vessel growth during normoxic conditions. This led us to hypothesize that constitutive overexpression of HIF-1-alpha in our hyperoxia-induced BPD model could be beneficial, since vessel formation is decreased during postnatal hyperoxia exposure[95]. In contrast to our functional and morphological findings during normoxia exposure, we found the reverse during hyperoxia exposure, as constitutive overexpression of HIF-1-alpha led to a deterioration of lung function during hyperoxia exposure without significant histological changes. We believe this is due to inhibition of HIF-1-alpha expression by factors inhibiting HIF-1 (FIH-1), whose activity is oxygen-dependent, and increases under hyperoxic circumstances. The deterioration

of lung function during hyperoxia was most likely caused by the measured changes in surfactant composition, since previous studies have shown a correlation between surfactant composition and lung function[96–99]. To this date, no human data on HIF-1-alpha levels in BPD patients has been collected, making it hard to correlate our data to the clinical setting. A drawback to data retrieved from autopsy specimens would be that most of these patients died under hypoxic circumstances, leading to increased HIF-1-alpha levels, which would not necessarily be causally involved in the disease process. Collection and correct determination of total lung HIF-1-alpha levels in tracheal aspirates is impossible due to the fact that we are looking at a transcriptional regulator only present in cells, thus tracheal aspirates will not represent the total HIF-1-alpha levels in lung tissue.

A NEW LINK BETWEEN THE DEVELOPMENT OF BPD AND COPD

In the above chapters we investigated two possible pathways influencing the development of BPD and COPD, figure 2 shows a summary of the pathways we believe to be involved in the development of BPD and COPD, as well as the hypothetical link between BPD and COPD: Lung injury in early life creates increased susceptibility for the development of pulmonary emphysema during adult life.

CELL BASED THERAPY USING MESENCHYMAL STEM CELLS

Mesenchymal stem cells, multipotent cells that possess the ability to self-renew[100], have successfully been used in numerous rodent models of disease as therapeutic agent[101–104], and recently their proposed mechanism of action has shifted from engraftment and differentiation into resident cells, to a paracrine effect, excreting a variety of anti-inflammatory mediators and endothelial and epithelial growth factors[105]. Cell-based therapy with MSCs has been applied with favourable effects in various models of lung injury[106–109]. MSC have been shown to inhibit apoptosis[110],secrete anti-inflammatory mediators[111], growth factors, such as epidermal growth factor[112] and hepatocyte growth factor[113]. It has been shown that the intravenous infusion of conditioned medium, derived from MSCs, prevents LPS-induced lung injury, supporting that MSCs exert their effect via paracrine signalling[114]. In the past 5 years, several research groups have examined cell-based therapies in the hyperoxia-induced BPD model, both in mice and rats, with different types of bone-marrow and umbilical cord-derived cells, and found attenuation and prevention of hyperoxia-induced lung injury[101,115–117]. The use of bone marrow-conditioned medium also showed amelioration of hyperoxia-induced lung injury by decreasing inflammation[117].

A driving factor in the development and progression of pulmonary emphysema is ongoing inflammation[118–121]. We showed that intravenous administration of mesenchymal stromal cells improved lung function when applied before elastase treatment, whereas intratracheal administration of mesenchymal stromal cells yielded no therapeutic effect. These

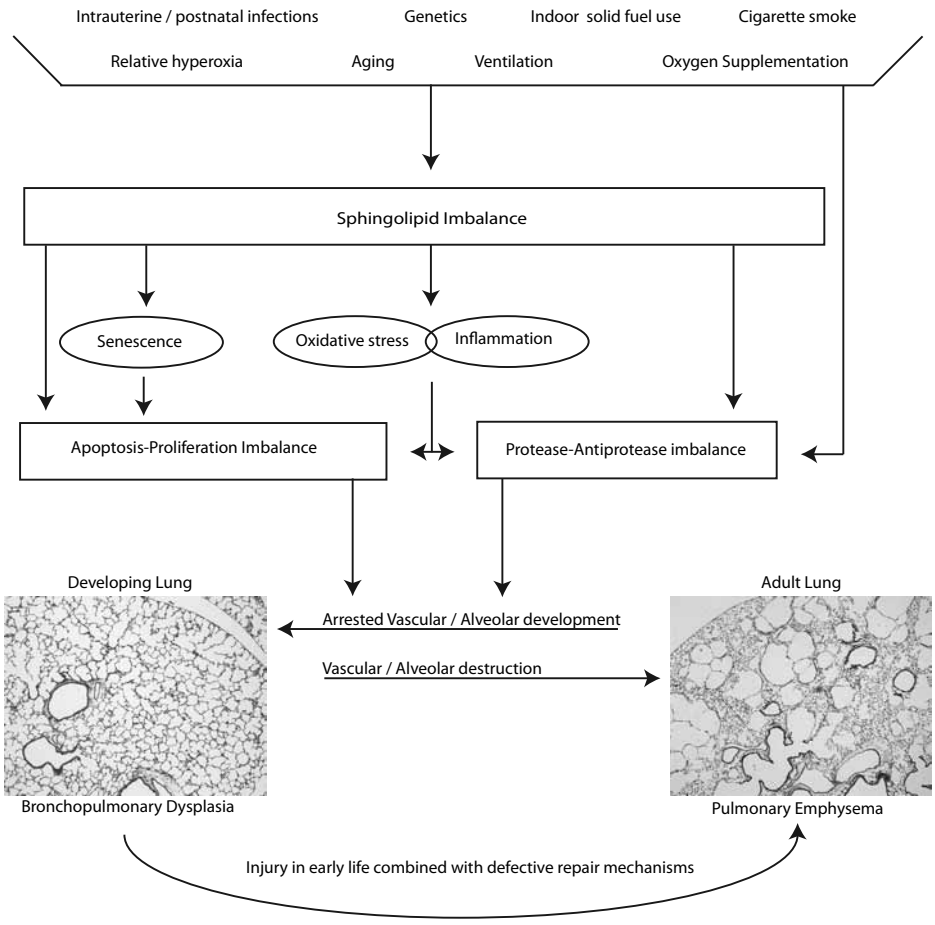

Figure 2. *Summary of the pathways believed to be involved in the development of BPD and COPD. (See colour section, page 198).*

results are in line with previous studies showing a positive effect of cell-based therapy via the intravenous route in the elastase-induced emphysema model[104,122,123]. Our experiments add to this data that even with severe pulmonary emphysema (using an elastase dose six times higher than that used in earlier studies looking at the effects of cell-based therapy), bone-marrow derived MSCs were still able to exhibit a therapeutic effect. Together with many other studies in different animal models[102,103,117,124–127], this data shows the potential of stem cell treatment in animal models of lung disease with an inflammatory component.

LUNG STRUCTURE – FUNCTION

In **chapter 3,** histology in our BPD model improved after D-sphingosine treatment, but no change in lung function was noted. In **chapter 4**, we noted a worsening of lung function in HIF-1αΔODD mice exposed to hyperoxia, whereas histology did not change. In **chapter 5**, in the elastase-induced emphysema model, we found improved lung function after Myriocin treatment, but no change in histology was noted. In **chapter 6** we also found an improvement in lung function after MSC treatment in the elastase-induced emphysema model, but no alterations in histology. These data from our experiments once again confirm the discrepancy between lung structure and function. Clinical studies have shown that structural lung and airway abnormalities correlate weakly or not at all with lung function, especially for localized or inhomogeneous structural abnormalities[128,129]. A possible explanation is that morphometrics may be insufficiently sensitive to demonstrate relatively small changes that might underlie significant functional improvement or worsening, therefore more sensitive approaches to the analysis of lung structure should be studied, such as micro CT and advanced functional MRI imaging techniques. Although advanced imaging could shed light on more subtle morphometrical changes, these techniques would not be able to capture differences in surfactant composition, or paracrine effects leading to altered lung function parameters. We therefore stress the importance of a combined approach of histological, biochemical and functional measurements when testing treatment effects in the lungs in animal models.

FUTURE RESEARCH PERSPECTIVES

- Proper long-term follow-up of BPD patients should take place in order to monitor the evolution of lung function during aging. This will gain new insights into the degree of premature aging of the lung in this patient group, leading to premature development of pulmonary emphysema-like defects.

- Biobanks should be created to obtain and store tissue and BAL/tracheal aspirates in these patients, together with prospective clinical data, in particular ventilator settings, O_2-supplementation, length of ventilation requirement, medication and many others

to provide a framework of samples and corresponding clinical parameters for future analysis.

- Equally important is a longitudinal follow-up of the incidence of pulmonary hypertension in survivors of BPD[130]. Given the detrimental effects of hyperoxia on postnatal pulmonary development, a delicate balance exists in these patients. Relative hypoxia might be beneficial for pulmonary vascular growth[71,80], but detrimental for cerebral development[131,132], while hyperoxia, commonly seen with supplementary O2 in home settings, induces oxygen radical production and may negatively affect pulmonary vascular growth.

- Research should focus on measuring sphingolipid levels in ethically and physically obtainable human samples, to discover if sphingolipid levels, specifically ceramides, are altered. This data could subsequently lead to the development of new pharmacological intervention strategies aimed at preventing BPD. Unfortunately, the frequent occurrence of low grade chorioamnionitis as etiological factor for increased susceptibility to BPD, as well as intra-uterine growth restriction and pre-eclampsia, will not be tackled by this approach, since this would require prenatal treatment[133–135].

- Not all infants that are born preterm develop BPD, and so far there is no way of predicting which preterm infant will develop BPD. Various potential biomarkers in tracheal aspirates have been studied to predict those at risk for BPD, but so far all results have been negative or irreproducible[136]. Genome-wide assays and targeted approaches have shown interesting results, but so far failed to identify those individuals susceptibility to developing BPD[137,138]. We propose that there could be a potential role for sphingolipids as a biomarker to make a distinction between which preterm infants are at risk for developing BPD: increased ceramide levels indicate an increased activation of the apoptotic pathway and inflammatory pathway, leading to increased alveolar defects and inflammation. These characteristics could influence morbidity and mortality in BPD patients, and using sphingolipid profiles we might be able to predict which preterms are at risk of developing BPD, similarly to what has been shown looking at the relation between ceramide and S1P levels, and lung cancer risk[139].

- Sphingolipid levels could be used to measure the effect of pharmacological treatment or other interventions. As has been shown in other diseases, sphingolipid levels, more specifically the ceramide/S1P balance could also function as a prognostic tool[140] predicting outcomes. The substrate in which these sphingolipid could be measured is diverse, ranging from tracheal aspirates to BAL and lung tissue. A direct comparison between the levels in these different sample types is not always possible, although for BAL and tracheal aspirates a reasonable correlation has been shown with respect to cytokine measurements and inflammatory cell percentages[141].

- As shown in our experiments in **Chapter 5**, there is no good correlation between sphingolipid levels in tissue and BAL, therefore future experiments should collect both tracheal aspirates/BAL and tissue samples, if this is clinically feasible. Extra caution should be taken when extrapolating results based on a single sample type or data representing 1 time point in a process of ongoing evolution of the disease.

- Further research in the area of sphingolipids and BPD should focus on discovering which enzymes in the sphingolipid pathway are responsible for the increased ceramide levels found and attempting to prevent hyperoxia-induced lung injury by treating mice with the appropriate enzyme inhibitors, based on the results from the above mentioned objective, from the start of hyperoxia-exposure.

- Attempts to repair hyperoxia-induced lung injury should also be made. Stimulating proliferation of lung endothelial cells and alveolar type I and II cells, by adding sphingosine-1-phosphate analogs at multiple time-points and increased doses after the injury has developed should be tested.

- In our pulmonary emphysema model, we concluded that *de novo* production of ceramides plays a role in the development of elastase-induced emphysema and this correlates well with the increased levels of ceramides found in the lungs of human COPD patients[67]. Studies have started looking at the interaction between ceramides and different signaling molecules, for instance RTP801, a hypoxic and oxidative stress sensor, has been shown to mutually upregulate ceramide levels after cigarette-smoke exposure[142]. This type of research should be continued to unravel the network of possible factors influencing the sphingolipid pathway during hypoxic and hyperoxic injury.

- In general, the route of administration of pharmacological inhibitors of sphingolipid metabolism should be evaluated in detail, specifically to answer the question as to which route of administration; intravenous (systemic) vs inhalation (local), yields the best results, allowing for the lowest dose to be used with minimal side effects. The fact that inhalation creates an effect on the epithelial side, whereas intravenous administration has its effect on the endothelial side, should also be taken into consideration for the proposed therapeutic effect.

- The acquired knowledge from sphingolipid inhibitor experiments could be used to attempt or optimize treatment in other animal models and human diseases where sphingolipids have been shown to play a role, such as cystic fibrosis, acute lung injury, asthma and viral infections of the respiratory tract[55,61].

- We examined the effect of HIF-1-alpha on alveolarization and during hyperoxia exposure. The effects of HIf-2-alpha and HIF-3-alpha on lung development have been studied, and indicate that these isotypes play an important role in the formation of alveoli, distal epithelial differentiation and surfactant formation. Overexpression of HIF-2-

alpha was found to be lethal and lungs from these mice revealed dilated alveoli, diminished alveolar type I cells and aberrant type II cells[92]. HIF-3-alpha overexpression led to aberrant branching morphogenesis and decreased number of alveoli, although these mice survived[94]. Further research in this area should focus on the effect of these factors and the interplay between epithelial and endothelial cell lining in co-culture and single cell conditions given the expression of the different HIF isoforms in both cell types.

- In the area of mesenchymal stem cell research, we should focus our attention on the culture protocols and flowcytometric characterization of MSC. The flowcytometry markers used for the characterization of MSCs are diverse, although guidelines have been established[143]. Many research groups use a random subset of markers, making a comparison between papers impossible. Another area of characterization that requires our attention is the comparison of MSCs from different locations. For instance, there are differences in differentiation capabilities and paracrine factor excretion between MSC derived from adipose tissue and those derived from bone-marrow[144,145].

- The different niche MSCs should be further characterized via flow cytometry and differentiation tests. In future experiments, we should look for specific stem cell populations that best fit our therapeutic needs. We should also continue to unravel the paracrine factors excreted by MSCs in order to better understand their mechanism of action and be able to make conscience decisions about when and how to administer these cells. The question remains whether direct injection of these factors creates the same results, since systemic administration could lead to severe side-effects. Mesenchymal stromal cells have the ability to home to sites of injury in the body to produce a specific paracrine effect on a local scale[146].

- Currently research labs are taking advantage of the homing ability of MSCs to use them as drug delivering vehicles, for instance in cancer therapy to deliver anti-proliferative, pro-apoptotic and anti-angiogenic agents[147]. Timing of administration, amount of administrations and dosing should be evaluated in each model where MSCs are used, since these factors greatly influence treatment outcome[148,149].

CONCLUSION

The evolution of chronic lung disease is the product of the underlying insult and a highly regulated, multifactorial cascade based on a balance between lung injury and repair over time. Sphingolipid metabolism plays an important part in maintaining this balance in well-established animal models of BPD and COPD. Within this context regulation of angiogenesis and vasculogenesis by hypoxia-inducible-factors determines proper alveolarization and incorrect expression either in time or dose is detrimental for postnatal lung development. Amongst the different therapeutic modalities, intravenous

mesenchymal stem cells, injected before or during the inflammatory peak, were shown to be effective in treating inflammation-based animal models of chronic lung disease, that mimic BPD and COPD. We propose that early lung injury may predispose for later development of emphysema.

Future therapeutic interventions should take into account the increasing knowledge at the molecular level of vascular and epithelial differentiation and the response to inflammatory mediators.

REFERENCES

1. World Health Organization. Preventing Chronic Diseases: a vital investment. *http://www.who.int/entity/chp/chronic_disease_report/contents/part1.pdf*. 2005.
2. World Health Organization. Respiratory Care in Primary Care Services: a survey in 9 countries. *http://whqlibdoc.who.int/hq/2004/WHO_HTM_TB_2004.333.pdf*. 2004.
3. World Health Organization. Global surveillance, prevention and control of Chronic Respiratory Diseases: a comprehensive approach. *http://whqlibdoc.who.int/publications/2007/9789241563468_eng.pdf*. 2007.
4. Bourbon JR, Boucherat O, Boczkowski J, Crestani B, Delacourt C. Bronchopulmonary dysplasia and emphysema: in search of common therapeutic targets. *Trends in molecular medicine*. 2009;15(4):169–79.
5. World Health Organization. Born too soon. *http://www.who.int/pmnch/media/news/2012/201204_borntoosoon-report.pdf*. 2012.
6. Liu L, Johnson HL, Cousens S, et al. Global, regional, and national causes of child mortality: an updated systematic analysis for 2010 with time trends since 2000. *Lancet*. 2012;379(9832):2151–61.
7. Shapiro-Mendoza CK, Tomashek KM, Kotelchuck M, et al. Effect of late-preterm birth and maternal medical conditions on newborn morbidity risk. *Pediatrics*. 2008;121(2):e223–32.
8. Blencowe H, Cousens S, Oestergaard MZ, et al. National, regional, and worldwide estimates of preterm birth rates in the year 2010 with time trends since 1990 for selected countries: a systematic analysis and implications. *Lancet*. 2012;379(9832):2162–72.
9. Reiss I, Landmann E, Heckmann M, Misselwitz B, Gortner L. Increased risk of bronchopulmonary dysplasia and increased mortality in very preterm infants being small for gestational age. *Archives of gynecology and obstetrics*. 2003;269(1):40–4.
10. Gortner L, Misselwitz B, Milligan D, et al. Rates of bronchopulmonary dysplasia in very preterm neonates in Europe: results from the MOSAIC cohort. *Neonatology*. 2011;99(2):112–7.
11. Jobe AJ. The new BPD: an arrest of lung development. *Pediatric research*. 1999;46(6):641.
12. Carlo W, Finer N, Walsh M. Target ranges of oxygen saturation in extremely preterm infants. *The New England Journal of Medicine*. 2010;362(21):1959–1969.
13. Gien J, Kinsella JP. Pathogenesis and treatment of bronchopulmonary dysplasia. *Current opinion in pediatrics*. 2011;23(3):305–13.
14. Darlow BA, Graham PJ. Vitamin A supplementation to prevent mortality and short and long-term morbidity in very low birthweight infants. *Cochrane database of systematic reviews (Online)*. 2007;(4):CD000501.
15. Mannino DM, Braman S. The epidemiology and economics of chronic obstructive pulmonary disease. *Proceedings of the American Thoracic Society*. 2007;4(7):502–6.
16. Faulkner M a, Hilleman DE. The economic impact of chronic obstructive pulmonary disease. *Expert opinion on pharmacotherapy*. 2002;3(3):219–28.
17. Rabe KF, Hurd S, Anzueto A, et al. Global strategy for the diagnosis, management, and prevention of chronic obstructive pulmonary disease: GOLD executive summary. *American journal of respiratory and critical care medicine*. 2007;176(6):532–55.
18. Buist AS, Vollmer WM, McBurnie MA. Worldwide burden of COPD in high- and low-income countries. Part I. The burden of obstructive lung disease (BOLD) initiative. *The international journal of tuberculosis and lung disease*. 2008;12(7):703–8.
19. Jemal A, Ward E, Hao Y, Thun M. Trends in the leading causes of death in the United States, 1970-2002. *JAMA*. 2005;294(10):1255–9.

20. Scanlon P, Connett J. Smoking Cessation and Lung Function in Mild-to-Moderate Chronic Obstructive Pulmonary Disease. The Lung Health Study. *American journal of respiratory and critical care medicine*. 2000;161:381–390.
21. Hoogendoorn M, Rutten-van Mölken MPMH, Hoogenveen RT, et al. A dynamic population model of disease progression in COPD. *European respiratory journal*. 2005;26(2):223–33.
22. Ezzati M, Lopez AD, Rodgers A, Vander Hoorn S, Murray CJL. Selected major risk factors and global and regional burden of disease. *Lancet*. 2002;360(9343):1347–60.
23. Peinado VI, Pizarro S, Barberà JA. Pulmonary vascular involvement in COPD. *Chest*. 2008;134(4):808–14.
24. McGrath-Morrow S a, Lauer T, Collaco JM, et al. Neonatal hyperoxia contributes additively to cigarette smoke-induced chronic obstructive pulmonary disease changes in adult mice. *American journal of respiratory cell and molecular biology*. 2011;45(3):610–6.
25. Filippone M, Bonetto G. Childhood course of lung function in survivors of bronchopulmonary dysplasia. *JAMA*. 2009:1–3.
26. Fawke J, Lum S, Kirkby J, et al. Lung function and respiratory symptoms at 11 years in children born extremely preterm: the EPICure study. *American journal of respiratory and critical care medicine*. 2010;182(2):237–45.
27. Aquino S, Schechter M, Chiles C, Ablin D, Chipps B, Webb W. High-resolution inspiratory and expiratory CT in older children and adults with bronchopulmonary dysplasia. *American Journal of Roentgenology*. 1999;173(4):963.
28. Aukland SM, Rosendahl K, Owens CM, Fosse KR, Eide GE, Halvorsen T. Neonatal bronchopulmonary dysplasia predicts abnormal pulmonary HRCT scans in long-term survivors of extreme preterm birth. *Thorax*. 2009;64(5):405–10.
29. Wong PM, Lees AN, Louw J, et al. Emphysema in young adult survivors of moderate-to-severe bronchopulmonary dysplasia. *European Respiratory Journal*. 2008;32(2):321.
30. Wong P, Murray C, Louw J, French N, Chambers D. Adult bronchopulmonary dysplasia: Computed tomography pulmonary findings. *Journal of medical imaging and radiation oncology*. 2011;55(4):373–8.
31. Bush A. COPD: a pediatric disease. *Copd*. 2008;5(1):53–67.
32. Ito K, Barnes PJ. COPD as a disease of accelerated lung aging. *Chest*. 2009;135(1):173–80.
33. Paigen K. One Hundred Years of Mouse Genetics: An Intellectual History. I. The Classical Period (1902–1980). *Genetics*. 2004;168(3):1097–104.
34. Mahadeva R, Shapiro SD. Chronic obstructive pulmonary disease * 3: Experimental animal models of pulmonary emphysema. *Thorax*. 2002;57(10):908–14.
35. Wright JL, Churg A. Animal Models of Cigarette Smoke-Induced COPD•. *Chest*. 2002;122(6 suppl):301S.
36. Meller S, Bhandari V. VEGF levels in humans and animal models with RDS and BPD: temporal relationships. *Experimental lung research*. 2012;38(4):192–203.
37. Fehrenbach H. Animal models of pulmonary emphysema: a stereologist's perspective. *European Respiratory Review*. 2006;15(101):136.
38. Ueda K, Cho K, Matsuda T, et al. A rat model for arrest of alveolarization induced by antenatal endotoxin administration. *Pediatric research*. 2006;59(3):396–400.
39. Coalson JJ. Experimental models of bronchopulmonary dysplasia. *Biology of the neonate*. 1997;71 Suppl 1:35–8.
40. Roth-Kleiner M, Post M. Genetic Control of Lung Development. *Biology of the Neonate*. 2003;84(1):83–88.
41. Rutter M, Post M. *Molecular basis for normal and abnormal lung development*. (Bancalari E, ed.). Philadelphia, PA: Saunders Elsevier; 2008:3–42.
42. Warner BB, Stuart LA, Papes RA, Wispé JR. Functional and pathological effects of prolonged hyperoxia in neonatal mice. *American Journal of Physiology-Lung Cellular and Molecular Physiology*. 1998;275(1):L110.

43. Yi M, Jankov RP, Belcastro R, et al. Opposing effects of 60% oxygen and neutrophil influx on alveologenesis in the neonatal rat. *American journal of respiratory and critical care medicine*. 2004;170(11):1188–96.
44. Yee M, White RJ, Awad H a, Bates W a, McGrath-Morrow S a, O'Reilly M a. Neonatal hyperoxia causes pulmonary vascular disease and shortens life span in aging mice. *The American journal of pathology*. 2011;178(6):2601–10.
45. Roth-kleiner M, Post M. Similarities and Dissimilarities of Branching and Septation During Lung Development. *Pediatric pulmonology*. 2005;40(February):113–34.
46. Churg A, Sin DD, Wright JL. Everything prevents emphysema: are animal models of cigarette smoke-induced chronic obstructive pulmonary disease any use? *American journal of respiratory cell and molecular biology*. 2011;45(6):1111–5.
47. Hamakawa H, Bartolák-Suki E, Parameswaran H, Majumdar A, Lutchen KR, Suki B. Structure-function Relations in an Elastase-induced Mouse Model of Emphysema. *American journal of respiratory cell and molecular biology*. 2010;(C):1–38.
48. Tasaka S, Inoue K-I, Miyamoto K, et al. Role of interleukin-6 in elastase-induced lung inflammatory changes in mice. *Experimental lung research*. 2010;36(6):362–72.
49. Kobayashi S, Fujinawa R, Ota F, et al. A Single Dose of LPS into Mice with Emphysema Mimics Human COPD Exacerbation as Assessed by Micro-CT. *American journal of respiratory cell and molecular biology*. 2013.
50. Anzueto A, Sethi S, Martinez FJ. Exacerbations of chronic obstructive pulmonary disease. *Proceedings of the American Thoracic Society*. 2007;4(7):554–64.
51. Schulz H, Johner C, Eder G, et al. Respiratory mechanics in mice: strain and sex specific differences. *Acta physiologica Scandinavica*. 2002;174(4):367–75.
52. Young MM, Kester M, Wang H-G. Sphingolipids: regulators of crosstalk between apoptosis and autophagy. *Journal of lipid research*. 2013;54(1):5–19.
53. Lahiri S, Futerman a H. The metabolism and function of sphingolipids and glycosphingolipids. *Cellular and molecular life sciences : CMLS*. 2007;64(17):2270–84.
54. Tirodkar TS, Voelkel-Johnson C. Sphingolipids in apoptosis. *Experimental oncology*. 2012;34(3):231–42.
55. Yang Y, Uhlig S. The role of sphingolipids in respiratory disease. *Therapeutic advances in respiratory disease*. 2011;5(5):325–44.
56. Mendelson K, Zygmunt T, Torres-Vázquez J, Evans T, Hla T. Sphingosine 1-phosphate receptor signaling regulates proper embryonic vascular patterning. *The Journal of biological chemistry*. 2013;288(4):2143–56.
57. Chess PR, D'Angio CT, Pryhuber GS, Maniscalco WM. Pathogenesis of bronchopulmonary dysplasia. *Seminars in perinatology*. 2006;30(4):171–8.
58. Thébaud B, Abman SH. Bronchopulmonary dysplasia: where have all the vessels gone? Roles of angiogenic growth factors in chronic lung disease. *American journal of respiratory and critical care medicine*. 2007;175(10):978–85.
59. Del Riccio V, van Tuyl M, Post M. Apoptosis in lung development and neonatal lung injury. *Pediatric research*. 2004;55(2):183–9.
60. Ola MS, Nawaz M, Ahsan H. Role of Bcl-2 family proteins and caspases in the regulation of apoptosis. *Molecular and cellular biochemistry*. 2011;351(1-2):41–58.
61. Uhlig S, Gulbins E. Sphingolipids in the lungs. *American journal of respiratory and critical care medicine*. 2008;178(11):1100.
62. Taha TA, Mullen TD, Obeid LM. A house divided: ceramide, sphingosine, and sphingosine-1-phosphate in programmed cell death. *Biochimica et biophysica acta*. 2006;1758(12):2027–36.

63. Yasuo M, Mizuno S, Allegood J, et al. Fenretinide causes emphysema, which is prevented by sphingosine 1-phoshate. *PloS one*. 2013;8(1):e53927.
64. Calabrese F, Giacometti C, Beghe B, et al. Marked alveolar apoptosis/proliferation imbalance in end-stage emphysema. *Respiratory research*. 2005;6:14.
65. Majo J, Ghezzo H, Cosio MG. Lymphocyte population and apoptosis in the lungs of smokers and their relation to emphysema. *European respiratory journal*. 2001;17(5):946–53.
66. Morissette MC, Vachon-Beaudoin G, Parent J, Chakir J, Milot J. Increased p53 Level, Bax/Bcl-xL Ratio, and TRAIL Receptor Expression in Human Emphysema. *American journal of respiratory and critical care medicine*. 2008;178(3):240.
67. Petrache I, Natarajan V, Zhen L, et al. Ceramide upregulation causes pulmonary cell apoptosis and emphysema-like disease in mice. *Nature medicine*. 2005;11(5):491–498.
68. Petrache I, Natarajan V, Zhen L, et al. Ceramide causes pulmonary cell apoptosis and emphysema: a role for sphingolipid homeostasis in the maintenance of alveolar cells. *Proceedings of the American Thoracic Society*. 2006;3(6):510.
69. Tuder RM, Zhen L, Cho CY, et al. Oxidative stress and apoptosis interact and cause emphysema due to vascular endothelial growth factor receptor blockade. *American journal of respiratory cell and molecular biology*. 2003;29(1):88–97.
70. Tuder RM, Petrache I, Elias J a, Voelkel NF, Henson PM. Apoptosis and emphysema: the missing link. *American journal of respiratory cell and molecular biology*. 2003;28(5):551–4.
71. Van Tuyl M, Liu J, Wang J, Kuliszewski M, Tibboel D, Post M. Role of oxygen and vascular development in epithelial branching morphogenesis of the developing mouse lung. *American Journal of Physiology-Lung Cellular and Molecular Physiology*. 2005;288(1):L167–78.
72. Yamamoto Y, Shiraishi I, Dai P, Hamaoka K, Takamatsu T. Regulation of embryonic lung vascular development by vascular endothelial growth factor receptors, Flk-1 and Flt-1. *Anatomical record (Hoboken, N.J. : 2007)*. 2007;290(8):958–73.
73. Ng YS, Rohan R, Sunday ME, Demello DE, D'Amore PA. Differential expression of VEGF isoforms in mouse during development and in the adult. *Developmental dynamics*. 2001;220(2):112–21.
74. Bhatt AJ, Pryhuber GS, Huyck H, Watkins RH, Metlay LA, Maniscalco WM. Disrupted pulmonary vasculature and decreased vascular endothelial growth factor, Flt-1, and TIE-2 in human infants dying with bronchopulmonary dysplasia. *American journal of respiratory and critical care medicine*. 2001;164(10 Pt 1):1971–80.
75. LIEBOW AA. Pulmonary emphysema with special reference to vascular changes. *The American review of respiratory disease*. 1959;80(1, Part 2):67–93.
76. San José Estépar R, Kinney GL, Black-Shinn JL, et al. Computed Tomographic Measures of Pulmonary Vascular Morphology in Smokers and their Clinical Implications. *American journal of respiratory and critical care medicine*. 2013;188(2):231–9.
77. Kasahara Y, Tuder RM, Cool CD, Lynch DA, Flores SC, Voelkel NF. Endothelial cell death and decreased expression of vascular endothelial growth factor and vascular endothelial growth factor receptor 2 in emphysema. *American journal of respiratory and critical care medicine*. 2001;163(3 Pt 1):737–44.
78. Kasahara Y, Tuder RM, Taraseviciene-Stewart L, et al. Inhibition of VEGF receptors causes lung cell apoptosis and emphysema. *The Journal of clinical investigation*. 2000;106(11):1311–9.
79. Lee YM, Jeong CH, Koo SY, et al. Determination of hypoxic region by hypoxia marker in developing mouse embryos in vivo: a possible signal for vessel development. *Developmental dynamics*. 2001;220(2):175–86.

80. Groenman FA, Rutter M, Wang J, Caniggia I, Tibboel D, Post M. Effect of chemical stabilizers of hypoxia-inducible factors on early lung development. *American Journal of Physiology-Lung Cellular and Molecular Physiology*. 2007;293(3):L557–67.
81. Semenza GL, Wang GL. A nuclear factor induced by hypoxia via de novo protein synthesis binds to the human erythropoietin gene enhancer at a site required for transcriptional activation. *Molecular and cellular biology*. 1992;12(12):5447–54.
82. Ito Y, Ahmad A, Kewley E, Mason RJ. Hypoxia-inducible factor regulates expression of surfactant protein in alveolar type II cells in vitro. *American journal of respiratory cell and molecular biology*. 2011;45(5):938–45.
83. Hosford GE, Olson DM. Effects of hyperoxia on VEGF, its receptors, and HIF-2alpha in the newborn rat lung. *American Journal of Physiology-Lung Cellular and Molecular Physiology*. 2003;285(1):L161–8.
84. Kenneth NS, Rocha S. Regulation of gene expression by hypoxia. *The Biochemical journal*. 2008;414(1):19–29.
85. Stroka D, Burkhardt T, Desbaillets I, et al. HIF-1 is expressed in normoxic tissue and displays an organ-specific regulation under systemic hypoxia. *FASEB journal*. 2002;16(12):1584–94.
86. Saini Y, Harkema JR, LaPres JJ. HIF1alpha is essential for normal intrauterine differentiation of alveolar epithelium and surfactant production in the newborn lung of mice. *The Journal of biological chemistry*. 2008;283(48):33650–7.
87. Asikainen TM, Waleh NS, Schneider BK, Clyman RI, White CW. Enhancement of angiogenic effectors through hypoxia-inducible factor in preterm primate lung in vivo. *American Journal of Physiology-Lung Cellular and Molecular Physiology*. 2006;291(4):L588–95.
88. Asikainen TM, Ahmad A, Schneider BK, White CW. Effect of preterm birth on hypoxia-inducible factors and vascular endothelial growth factor in primate lungs. *Pediatric pulmonology*. 2005;40(6):538–46.
89. Bonnet S, Michelakis ED, Porter CJ, et al. An abnormal mitochondrial-hypoxia inducible factor-1alpha-Kv channel pathway disrupts oxygen sensing and triggers pulmonary arterial hypertension in fawn hooded rats: similarities to human pulmonary arterial hypertension. *Circulation*. 2006;113(22):2630–41.
90. Giatromanolaki A, Koukourakis MI, Sivridis E, et al. Relation of hypoxia inducible factor 1 alpha and 2 alpha in operable non-small cell lung cancer to angiogenic/molecular profile of tumours and survival. *British journal of cancer*. 2001;85(6):881–90.
91. Compernolle V, Brusselmans K, Acker T, et al. Loss of HIF-2alpha and inhibition of VEGF impair fetal lung maturation, whereas treatment with VEGF prevents fatal respiratory distress in premature mice. *Nature medicine*. 2002;8(7):702–10.
92. Huang Y, Kempen MB, Munck AB, et al. Hypoxia-inducible factor 2α plays a critical role in the formation of alveoli and surfactant. *American journal of respiratory cell and molecular biology*. 2012;46(2):224–32.
93. Mohseni-Bod H, Bohn D. Pulmonary hypertension in congenital diaphragmatic hernia. *Seminars in pediatric surgery*. 2007;16(2):126–33.
94. Huang Y, Kapere Ochieng J, Kempen MB, et al. Hypoxia inducible factor 3α plays a critical role in alveolarization and distal epithelial cell differentiation during mouse lung development. *PloS one*. 2013;8(2):e57695.
95. Thébaud B, Ladha F, Michelakis ED, et al. Vascular endothelial growth factor gene therapy increases survival, promotes lung angiogenesis, and prevents alveolar damage in hyperoxia-induced lung injury: evidence that angiogenesis participates in alveolarization. *Circulation*. 2005;112(16):2477–86.
96. Schmidt R, Ruppert C, Markart P, et al. Changes in pulmonary surfactant function and composition in bleomycin-induced pneumonitis and fibrosis. *Toxicology and applied pharmacology*. 2004;195(2):218–31.
97. Schmidt R, Markart P, Ruppert C, et al. Time-dependent changes in pulmonary surfactant function and composition in acute respiratory distress syndrome due to pneumonia or aspiration. *Respiratory research*. 2007;8:55.

98. Schmidt R, Meier U, Markart P, et al. Altered fatty acid composition of lung surfactant phospholipids in interstitial lung disease. *American Journal of Physiology-Lung Cellular and Molecular Physiology*. 2002;283(5):L1079–85.
99. Mander A, Langton-Hewer S, Bernhard W, Warner JO, Postle AD. Altered phospholipid composition and aggregate structure of lung surfactant is associated with impaired lung function in young children with respiratory infections. *American journal of respiratory cell and molecular biology*. 2002;27(6):714–21.
100. Sung JH, Yang H-M, Park JB, et al. Isolation and characterization of mouse mesenchymal stem cells. *Transplantation proceedings*. 2008;40(8):2649–54.
101. Chang YS, Choi SJ, Sung DK, et al. Intratracheal transplantation of human umbilical cord blood derived mesenchymal stem cells dose-dependently attenuates hyperoxia-induced lung injury in neonatal rats. *Cell transplantation*. 2011:1–32.
102. Kim ES, Chang YS, Choi SJ, et al. Intratracheal Transplantation of Human Umbilical Cord Blood-Derived Mesenchymal Stem Cells Attenuates Escherichia coli-Induced Acute Lung Injury in Mice. *Respiratory research*. 2011;12(1):108.
103. Gupta N, Su X, Popov B. Intrapulmonary delivery of bone marrow-derived mesenchymal stem cells improves survival and attenuates endotoxin-induced acute lung injury in mice. *The journal of immunology*. 2007;179(3):1855–63.
104. Hoffman AM, Paxson J a, Mazan MR, et al. Lung-derived mesenchymal stromal cell post-transplantation survival, persistence, paracrine expression, and repair of elastase-injured lung. *Stem cells and development*. 2011;20(10):1779–92.
105. Lee JW, Fang X, Krasnodembskaya A, Howard JP, Matthay MA. Mesenchymal Stem Cells for Acute Lung Injury: Role of Paracrine Soluble Factors. *Stem Cells*. 2011;093026(415).
106. Yamada M, Kubo H, Kobayashi S, et al. Bone marrow-derived progenitor cells are important for lung repair after lipopolysaccharide-induced lung injury. *Journal of immunology*. 2004;172(2):1266–72.
107. Ortiz L a, Gambelli F, McBride C, et al. Mesenchymal stem cell engraftment in lung is enhanced in response to bleomycin exposure and ameliorates its fibrotic effects. *Proceedings of the National Academy of Sciences of the United States of America*. 2003;100(14):8407–11.
108. Wong AP, Dutly AE, Sacher A, et al. Targeted cell replacement with bone marrow cells for airway epithelial regeneration. *American Journal of Physiology-Lung Cellular and Molecular Physiology*. 2007;293(3):L740–52.
109. Spees JL, Pociask D a, Sullivan DE, et al. Engraftment of bone marrow progenitor cells in a rat model of asbestos-induced pulmonary fibrosis. *American journal of respiratory and critical care medicine*. 2007;176(4):385–94.
110. Block G, Ohkouchi S, Fung F, et al. Multipotent stromal cells are activated to reduce apoptosis in part of upregulation and secretion of stanniocalcin-1. *Stem Cells*. 2009;27(3):670–81.
111. Lee RH, Pulin A a, Seo MJ, et al. Intravenous hMSCs improve myocardial infarction in mice because cells embolized in lung are activated to secrete the anti-inflammatory protein TSG-6. *Cell stem cell*. 2009;5(1):54–63.
112. Chen L, Tredget EE, Wu PYG, Wu Y. Paracrine factors of mesenchymal stem cells recruit macrophages and endothelial lineage cells and enhance wound healing. *PloS one*. 2008;3(4):e1886.
113. Crisostomo PR, Wang Y, Markel T a, Wang M, Lahm T, Meldrum DR. Human mesenchymal stem cells stimulated by TNF-alpha, LPS, or hypoxia produce growth factors by an NF kappa B- but not JNK-dependent mechanism. *American Journal of Physiology-Cell Physiology*. 2008;294(3):C675–82.
114. Ionescu L, Byrne RN, van Haaften T, et al. Stem Cell Conditioned Medium Improves Acute Lung Injury in Mice: In Vivo Evidence for Stem Cell Paracrine Action. *American Journal of Physiology-Lung Cellular and Molecular Physiology*. 2012;(September).

115. Haaften T van, Byrne R, Bonnet S. Airway delivery of mesenchymal stem cells prevents arrested alveolar growth in neonatal lung injury in rats. *American journal of respiratory cell and molecular biology*. 2009;(7):200902–0179OCv1.
116. Balasubramaniam V, Ryan SSL, Seedorf GJ, et al. Bone marrow-derived angiogenic cells restore lung alveolar and vascular structure after neonatal hyperoxia in infant mice. *of Physiology-Lung*. 2010;298(December 2009):L315–23.
117. Aslam M, Baveja R, Liang OD, et al. Bone marrow stromal cells attenuate lung injury in a murine model of neonatal chronic lung disease. *American journal of respiratory and critical care medicine*. 2009;180(11):1122–30.
118. Izquierdo JL, Almonacid C, Parra T, Pérez J. Systemic and lung inflammation in 2 phenotypes of chronic obstructive pulmonary disease. *Archivos de bronconeumología*. 2006;42(7):332–7.
119. Retamales I, Elliott WM, Meshi B, et al. Amplification of inflammation in emphysema and its association with latent adenoviral infection. *American journal of respiratory and critical care medicine*. 2001;164(3):469–73.
120. Finkelstein R, Fraser RS, Ghezzo H, Cosio MG. Alveolar inflammation and its relation to emphysema in smokers. *American journal of respiratory and critical care medicine*. 1995;152(5 Pt 1):1666–72.
121. Peinado VI, Barberà JA, Abate P, et al. Inflammatory Reaction in Pulmonary Muscular Arteries of Patients with Mild Chronic. *American journal of respiratory and critical care medicine*. 1999;159:1605–1611.
122. Katsha AM, Ohkouchi S, Xin H, et al. Paracrine factors of multipotent stromal cells ameliorate lung injury in an elastase-induced emphysema model. *Molecular therapy*. 2011;19(1):196–203.
123. Cruz FF, Antunes MA, Abreu SC, et al. Protective effects of bone marrow mononuclear cell therapy on lung and heart in an elastase-induced emphysema model. *Respiratory physiology & neurobiology*. 2012;182(1):26–36.
124. Zhao F, Zhang Y, Liu Y, et al. Therapeutic effects of bone marrow-derived mesenchymal stem cells engraftment on bleomycin-induced lung injury in rats. *Transplantation proceedings*.Vol 40. Elsevier; 2008:1700–1705.
125. Maggini J, Mirkin G, Bognanni I, et al. Mouse bone marrow-derived mesenchymal stromal cells turn activated macrophages into a regulatory-like profile. *PloS one*. 2010;5(2):e9252.
126. Gonzalez-Rey E, Anderson P, González M a, Rico L, Büscher D, Delgado M. Human adult stem cells derived from adipose tissue protect against experimental colitis and sepsis. *Gut*. 2009;58(7):929–39.
127. Weiss DJ, Bertoncello I, Borok Z, et al. Stem cells and cell therapies in lung biology and lung diseases. *Proceedings of the American Thoracic Society*. 2011;8(3):223–72.
128. De Jong P a, Lindblad a, Rubin L, et al. Progression of lung disease on computed tomography and pulmonary function tests in children and adults with cystic fibrosis. *Thorax*. 2006;61(1):80–5.
129. Sly PD, Brennan S, Gangell C, et al. Lung disease at diagnosis in infants with cystic fibrosis detected by newborn screening. *American journal of respiratory and critical care medicine*. 2009;180(2):146–52.
130. Mourani PM, Abman SH. Pulmonary vascular disease in bronchopulmonary dysplasia: pulmonary hypertension and beyond. *Current opinion in pediatrics*. 2013;25(3):329–37.
131. Baburamani AA, Ek CJ, Walker DW, Castillo-Melendez M. Vulnerability of the developing brain to hypoxic-ischemic damage: contribution of the cerebral vasculature to injury and repair? *Frontiers in physiology*. 2012;3:424.
132. Zhao J, Chen Y, Xu Y, Pi G. Effect of intrauterine infection on brain development and injury. *International journal of developmental neuroscience*. 2013.
133. Romero R, Espinoza J. The role of inflammation and infection in preterm birth. *Seminars in reproduction medicine*. 2007.
134. Maritz GS, Morley CJ, Harding R. Early developmental origins of impaired lung structure and function. *Early human development*. 2005;81(9):763–71.

135. Prendergast M, May C, Broughton S, et al. Chorioamnionitis, lung function and bronchopulmonary dysplasia in prematurely born infants. *Archives of disease in childhood*. 2011;96(4):F270–4.
136. Bhandari A, Bhandari V. Biomarkers in Bronchopulmonary Dysplasia. *Paediatric respiratory reviews*. 2013.
137. Bhattacharya S, Go D, Krenitsky DL, et al. Genome-wide transcriptional profiling reveals connective tissue mast cell accumulation in bronchopulmonary dysplasia. *American journal of respiratory and critical care medicine*. 2012;186(4):349–58.
138. Davidson D, Zaytseva A, Miskolci V, Castro-Alcaraz S, Vancurova I, Patel H. Gene expression profile of endotoxin-stimulated leukocytes of the term new born: control of cytokine gene expression by interleukin-10. *PloS one*. 2013;8(1):e53641.
139. Alberg AJ, Armeson KE, Pierce JS, et al. Plasma sphingolipids as markers of future lung cancer risk: A population-based, nested case-control study. *Cancer epidemiology, biomarkers & prevention*. 2013.
140. Jenkins RW, Clarke CJ, Lucas JT, et al. Evaluation of the role of secretory sphingomyelinase and bioactive sphingolipids as biomarkers in hemophagocytic lymphohistiocytosis. *American journal of hematology*. 2013.
141. D'Angio CT, Basavegowda K, Avissar NE, Finkelstein JN, Sinkin RA. Comparison of tracheal aspirate and bronchoalveolar lavage specimens from premature infants. *Biology of the neonate*. 2002;82(3):145–9.
142. Kamocki K, Van Demark M, Fisher A, et al. RTP801 Is Required for Ceramide-Induced Cell-Specific Death in the Murine Lung. *American journal of respiratory cell and molecular biology*. 2013;48(1):87–93.
143. Dominici M, Le Blanc K, Mueller I, et al. Minimal criteria for defining multipotent mesenchymal stromal cells. The International Society for Cellular Therapy position statement. *Cytotherapy*. 2006;8(4):315–317.
144. Vidal MA, Robinson SO, Lopez MJ, et al. Comparison of chondrogenic potential in equine mesenchymal stromal cells derived from adipose tissue and bone marrow. *Veterinary surgery* ;37(8):713–24.
145. Monaco E, Bionaz M, Rodriguez-Zas S, Hurley WL, Wheeler MB. Transcriptomics comparison between porcine adipose and bone marrow mesenchymal stem cells during in vitro osteogenic and adipogenic differentiation. *PloS one*. 2012;7(3):e32481.
146. Fong ELS, Chan CK, Goodman SB. Stem cell homing in musculoskeletal injury. *Biomaterials*. 2010;32(2):395–409.
147. Shah K. Mesenchymal stem cells engineered for cancer therapy. *Advanced drug delivery reviews*. 2012;64(8):739–748.
148. Wei X, Yang X, Han Z-P, Qu F-F, Shao L, Shi Y-F. Mesenchymal stem cells: a new trend for cell therapy. *Acta pharmacologica Sinica*. 2013;34(6):747–54.
149. Richardson JD, Bertaso AG, Psaltis PJ, et al. Impact of timing and dose of mesenchymal stromal cell therapy in a preclinical model of acute myocardial infarction. *Journal of cardiac failure*. 2013;19(5):342–53.

Chapter 8

Summary

SUMMARY

The lung contains the largest surface of our body that is in direct contact with the environment and hence is exposed to many injurious components on a daily basis. The lung has a host of defense mechanisms to combat this constant invasion, but even with all these barriers, exogenous factors can still lead to lung injury. Worldwide, 15 million babies are born prematurely each year, and this incidence is on the rise. Preterm birth is an important risk factor for the development of BronchoPulmonary Dysplasia (BPD), a disease characterized by interrupted septation and abnormal vascularization, leading to fewer and enlarged alveoli. BPD is believed to have a multifactorial pathogenesis, with many pre- and postnatal factors playing a role, and even though progress has been made in the management of infants with BPD, current treatment remains symptomatic and limited. Pulmonary emphysema and chronic bronchitis, together chronic obstructive pulmonary disease (COPD), are the most common chronic lung diseases in adults in the developed world, and are associated with a high mortality risk. COPD poses a large economic burden due to exacerbations leading to hospitalization and home oxygen use. Pulmonary emphysema is characterized by progressive destruction of alveolar walls, leading to loss of elastic recoil, airflow obstruction and hyperinflation. Oxidative stress, sustained inflammation and protease-antiprotease imbalance are believed to be major contributors to the pathogenesis of COPD. These factors also play a role in the development of BPD, and long-term follow-up indicates that preterm infants with BPD develop reduced lung function and abnormal lung structure through childhood and into adolescence. Structural lung abnormalities resembling pulmonary emphysema have been reported in young adults with BPD (**Chapter 1**).

Sphingolipids play an important role in many biological processes, including apoptosis and proliferation, inflammation, vascular barrier integrity and smooth muscle cell contraction. The actions of sphingose-1-phosphate (S1P) promote proliferation and increased vascular barrier integrity, whereas ceramide enhances apoptosis and decreases vascular barrier integrity. These effects have been shown in a number of human and animal disease models, in relation to severe and prevalent diseases such as COPD, BPD, asthma and ARDS. Interventions in the sphingolipid pathway aimed at restoring the balance between ceramide and S1P levels have produced promising results in animal models. Pharmacological strategies to restore the balance of S1P and ceramide should now be tested in humans. Performing the required studies in newborns to test the effect on BPD development and progression will be a challenge. There is good reason to pursue the clinical use of sphingolipid inhibitors, as they may well offer protection and benefit for patients with a variety of diseases that are associated with lung damage and repair, for which limited alternative treatments are available (**Chapter 2**).

In **Chapter 3** we demonstrated that hyperoxia in the newborn mouse lung caused a transient increase of sphingolipids, including ceramides, which returned to normal during recovery in room air, while histology remained abnormal. The decrease in sphingolipid levels during recovery matched the normalization of airway resistance and compliance.

Importantly, D-sphingosine supplementation during recovery accelerated the normalization of ceramides, and significantly improved hyperoxia-induced lung damage. We propose that D-sphingosine and other inhibitors of bioactive sphingolipids should be studied further for their potential to reduce lung damage in human preterm infants who require neonatal oxygen treatment. The ultimate goal would be to develop a new strategy to prevent or correct bronchopulmonary dysplasia.

In **Chapter 4** we showed that stable hypoxia inducible-factor 1 alpha (HIF-1α) overexpression in room air is associated with increased postnatal vascularization and alveolarization through upregulation of angiogenic factors. However, stable HIF-1α overexpression did not prevent hyperoxia-induced BPD in neonatal mice, but led to a worsening of lung function, due to an altered surfactant composition, specifically decreased palmitoyloleic phosphatidylcholine and increased palmitoylmyristoyl phosphatidylcholine levels.

In **Chapter 5** we showed that intratracheal elastase instillation caused a transient inflammatory response with influx of erythrocytes and inflammatory cells in the alveolar spaces, combined with an increase in multiple ceramide and dihydroceramide species in bronchoalveolar lavage (BAL) fluid which peaked at day 1 and 2 and returned to control levels at day 3 after elastase instillation. Ceramide expression was primarily localized to the epithelium and to inflammatory cells. Sphingomyelinase inhibitors did not prevent or reduce the effects of intratracheal elastase. In contrast, serine palmitoyl transferase (SPT) inhibition reduced sphingolipid and protein levels and ameliorated lung function changes after elastase instillation, demonstrating the involvement of ceramides and dihydroceramides in elastase-induced emphysema. Further experiments should evaluate the preventive and therapeutic potencies of ceramide inhibition in this emphysema model, and ultimately in humans with COPD.

In **Chapter 6** we induced pulmonary emphysema in adult mice by tracheal instillation of a relatively high dose of elastase. Three weeks after elastase administration we found evidence of histological abnormalities and obstructive lung function, characteristic of pulmonary emphysema. The structural and functional changes persisted up to 10 months and were not affected by intratracheal administration of mesenchymal stem cells (MSC) prior or after the injury. Jugular vein MSC treatment before elastase injection did show an improvement in lung function but no change in histology. The severity of elastase-induced lung injury depended on the elastase dose used, and may be an important determinant of the effect of MSC treatment.

The general discussion in **Chapter 7** discusses the studies presented in this thesis and relates our findings to those of other studies performed on this subject and provides future research perspectives in the area of lung injury and repair. Sphingolipid metabolism plays an important part in maintaining the balance between lung injury and repair in well-established animal models of BPD and COPD. Within this context regulation of angiogenesis and vasculogenesis by hypoxia-inducible-factors determines proper alveolarization and

incorrect expression either in time or dose is detrimental for postnatal lung development. Amongst the different therapeutic modalities, intravenous mesenchymal stem cell treatment was shown to be effective in treating inflammation-based animal models of chronic lung disease.

Overall we conclude that evolution of chronic lung disease is the product of the underlying insult and a highly regulated, multifactorial cascade based on a balance between lung injury and repair over time, and propose that early lung injury may predispose for later development of emphysema.

SAMENVATTING

De long bevat het grootste lichaamsoppervlak dat in direct contact staat met de buitenwereld en wordt dagelijks blootgesteld aan potentieel schadelijke stoffen. Om deze continue invasie te weerstaan is de long uitgerust met een groot aantal verdedigingsmechanismen, maar desondanks kunnen exogene factoren nog steeds aanzienlijke longschade veroorzaken.

Wereldwijd worden jaarlijks 15 miljoen baby's prematuur geboren, en de incidentie neemt toe. Prematuriteit is een belangrijke risicofactor voor het ontstaan van zogenaamde BronchoPulmonale Dysplasie (BPD), een ziekte gekarakteriseerd door gestagneerde ontwikkeling van alveoli en bloedvaten in de long met als gevolg een verminderd aantal en een groter formaat van alveoli op latere leeftijd. De pathogenese van BPD is multifactorieel, en zowel pre- als postnatale factoren spelen een rol. Ondanks alle verbeteringen rondom de zorg en behandeling van kinderen met BPD is genezing niet altijd mogelijk en is symptoombestrijding maar in beperkte mate te realiseren.

Chronische obstructieve longziekten (COPD), bestaande uit longemfyseem en chronische bronchitis, vormen in de westerse wereld de meest voorkomende chronische longziekte op de volwassen leeftijd en leiden tot een verhoogde kans op overlijden. Het gebruik van zuurstof in de thuissituatie en ziekenhuisopnames als gevolg van exacerbaties zorgen voor grote druk op de gezondheidszorg. Longemfyseem wordt gekarakteriseerd door progressieve destructie van alveolaire wanden resulterend in verlies van elasticiteit, luchtstroombeperking en hyperinflatie van de long. In de pathogenese van COPD spelen oxidatieve stress, voortgaande ontsteking en een verstoorde protease-antiprotease balans een rol. Deze factoren zijn ook van belang voor het ontstaan van BPD. Lange termijn follow-up van prematuren met BPD laat een verminderde longfunctie en abnormale longstructuur zien gedurende de kinderleeftijd tot aan de adolescentie. Structurele longafwijkingen, lijkend op longemfyseem zijn aangetoond bij volwassen BPD patiënten (**Hoofdstuk 1**).

Sphingolipiden spelen een belangrijke rol bij multipele biologische processen, onder andere apoptose en proliferatie, ontsteking, doorlaatbaarheid van de vaatwand en contractie van gladde spiercellen. Sphingosine-1-fosfaat (S1P) stimuleert proliferatie en vermindert de doorlaatbaarheid van de vaatwand, terwijl ceramide apoptose stimuleert en voor een verhoogde doorlaatbaarheid van de vaatwand zorgt. Deze effecten zijn aangetoond in verschillende humane en proefdierstudies betreffende COPD, BPD, astma en acuut respiratoir distress syndroom (ARDS). Interventies in de sphingolipiden pathway, gericht op het herstellen van de balans tussen ceramide en S1P, laten veelbelovende resultaten zien in proefdierstudies. Farmacologische strategieën om de balans te herstellen zullen nu getest moeten worden in humane studies. De uitdaging zal zijn om de studies, die noodzakelijk zijn om het effect op het beloop van BPD te testen, uit te voeren bij pasgeborenen. Er zijn goede redenen om onderzoek te doen naar het klinische nut van sphingolipideremmers, omdat deze voordelen kunnen bieden voor patiënten met verschillende ziekten die geasso-

cieerd zijn met longschade en herstel, waarbij weinig alternatieve behandelmogelijkheden bestaan (**Hoofdstuk 2**).

In **hoofdstuk 3** laten we zien dat hyperoxie bij pasgeboren muizen histologische schade en een voorbijgaande verhoging in sphingolipiden, waaronder ceramiden, veroorzaakt. Na herstel in 21% zuurstof dalen deze waarden naar normaal maar de histologie blijft afwijkend. De normalisatie van de sphingolipiden gedurende herstel in 21% zuurstof verliep parallel aan de normalisatie van de longfunctie. De toediening van D-sphingosine gedurende de herstelperiode leidde tot een versnelde normalisatie van de ceramide waarden en tot verbetering van de door hyperoxie veroorzaakte longschade. Wij stellen voor het effect van sphingolipiden op longschade bij premature baby's nader te onderzoeken. Met als uiteindelijk doel om door interventie in het sphingolipiden metabolisme BPD te voorkomen dan wel te genezen.

In **hoofdstuk 4** beschrijven we dat stabiele overexpressie van hypoxia-inducible-factor 1 alpha (HIF-1α) geassocieerd is met toegenomen postnatale vascularisatie en alveolarisatie op basis van toename van angiogene factoren. Preventie van BPD bij neonatale muizen door stabiele HIF-1α overexpressie resulteerde juist in een verslechterde longfunctie ten gevolge van een veranderde surfactant samenstelling.

In **hoofdstuk 5** laten we zien dat intratracheale injectie van elastase een voorbijgaande ontstekingsreactie veroorzaakt met influx van erythrocyten en granulocyten in de alveolaire ruimte. Dit ging gepaard met verhoogde ceramiden in broncho-alveolaire lavage (BAL) vloeistof, met een piek op dag 1 en 2 en normalisatie op dag 3 na elastase injectie. Ceramide expressie werd primair gelokaliseerd in het alveolaire epitheel en in ontstekingscellen. Het effect van intratracheale elastase injectie werd niet voorkomen of verminderd door de toevoeging van sphingomyelinaseremmers. Serine palmitoyl transferase (SPT) remmers verminderden sphingolipiden wel en verbeterden de longfunctie na elastase injectie. Dit suggereert een rol voor ceramiden bij door elastase geïnduceerd longemfyseem. Toekomstige experimenten moeten zich richten op het evalueren van de preventieve en therapeutische mogelijkheden van ceramideremmers in dit longemfyseem model en uiteindelijk bij patiënten met COPD.

In **hoofdstuk 6** beschrijven we een longemfyseem model waarbij we een relatief hogere dosis elastase toedienden. Drie weken na elastasetoediening vonden we histologische afwijkingen en een obstructieve longfunctie, karakteristiek voor longemfyseem. The structurele en functionele afwijkingen bleven aanwezig tot 10 maanden na elastase toediening. Intratracheale behandeling met mesenchymale stamcellen (MSC) voor of na elastase toediening had geen effect op histologie en longfunctie. MSC behandeling via de vena jugularis voorafgaand aan elastase toediening liet een verbetering van de longfunctie zien, maar geen verandering in histologie. De ernst van het emfyseem was afhankelijk van de gebruikte elastase dosis, en een belangrijke bepalende factor van het effect van MSC.

In **hoofstuk 7** bediscussiëren we de studies beschreven in dit proefschrift en relateren we onze bevindingen aan die van andere onderzoeksgroepen. Ook geven we aanbevelingen voor toekomstig onderzoek op het gebied van longschade en -herstel. Het sphingolipide-metabolisme speelt een belangrijke rol in de balans tussen longschade en herstel in veel gebruikte diermodellen van BPD en COPD. Binnen dit concept is het van belang dat de regulatie van angiogenese door hypoxia-inducible-factor bijdraagt aan normale alveolarisatie en dat afwijkende expressie van deze factoren, zowel in de tijd als in dosering, leidt tot verstoring van de postnatale longontwikkeling. Van de verschillende therapeutische opties is intraveneuze mesenchymale stamcel injectie effectief bij de behandeling van chronische longziekten in diermodellen gebaseerd op schade door ontstekingsprocessen.

We concluderen dat het beloop van chronische longziekten bepaald wordt door de onderliggende ziekteactiviteit en het succes van de hierop reagerende herstelmechanismen. In deze cascade draait het om de balans tussen longschade en herstel. Hierbij kan longschade vroeg in het leven predisponeren voor longemfyseem op latere leeftijd.

Appendices

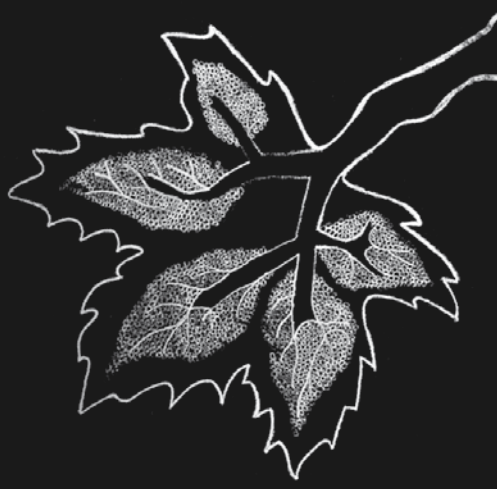

ABOUT THE AUTHOR

Jeroen Tibboel was born in Rotterdam, the Netherlands on the 5th of June 1984. After graduating from secondary school (Emmaus College, Rotterdam) in June 2003, he was at first excluded from studying medicine due to the numerus fixus. On the verge of starting biomedical sciences in Utrecht, four days before the first semester began in September 2003, he was accepted to study medicine at the Erasmus MC – University Medical Center in Rotterdam.

In September 2007, as part of a research elective, he moved to Toronto, Canada for a year, setting up and characterizing an elastase-induced animal model of pulmonary emphysema at the Hospital for Sick Children under the guidance of Prof. Martin Post and Prof. Johan C. de Jongste from the department of Pediatrics at the Erasmus MC – Sophia Children's Hospital.

In September 2008 he passed his *doctoraal examen* (Master's Degree) and was invited by Prof. Post to start a PhD project at the department of Physiology and Experimental Medicine at the Hospital for Sick Children in Toronto, Canada.

From October 2008, he spent 3 years researching 'lung injury and repair' under supervision of Prof. Martin Post together with Prof. Johan C. de Jongste and Prof. Irwin Reiss before returning to the Netherlands in September 2011 to finish writing his PhD thesis. Per February 2013 Jeroen has started his clinical rotations at the Erasmus MC – University Medical Center in Rotterdam.

PHD PORTFOLIO

Name PhD Student:	J. Tibboel
Erasmus MC Department:	Pediatrics
PhD Period:	2008-2013
Promotor(s):	Prof.dr. M. Post, Prof.dr. J.C. de Jongste
Supervisor:	Prof.dr. I.K.M. Reiss

1. PhD Training

General courses	**Year**	**Workload (ECTS)**
Biological, Chemical and Radiation Safety Seminars	2007/2011	2.0
Lab Animal Services General Orientation	2007	0.5
Lab Animal Services Animal Handling	2007	0.5
Lab Animal Services Injectable Anesthesia	2007	0.5
Lab Animal Services Gaseous Anesthesia	2007	0.5
Lab Animal Services Survival Surgery	2007	0.5
Lab Animal Services Rodent Intubation Training	2007/2008	1.0
Lab Animal Services Jugular Vein Injection Training	2009	1.0
Seminars & Workshops		
Research meetings dept. of Physiology and Experimental Medicine	2007/2011	8.0
Seminar of the "P.E.M. Program"	2007/2011	3.5
Research meetings dept. of Pediatrics, division of Respiratory Medicine	2012/2013	1.0
PhD day	2012	0.3
Grant & Article Writing Course	2012	1.5
Presentations		
Research Institute Scientific Retreat, Hospital for Sick Children [Poster]	2009	0.3
American Thoracic Society (ATS) conference [Poster]	2010	0.3
Research Institute Scientific Retreat, Hospital for Sick Children [Poster]	2010	0.3
Respirology Day, Hospital for Sick Children [Posters]	2011	0.3
European Respiratory Society annual conference [Poster]	2012	0.3
Longdagen [Poster]	2012	0.3
Sophia Onderzoekersdag [Poster]	2013	0.3
International Conferences		
American Thoracic Society conference, Toronto, Canada	2008	0.9
American Thoracic Society conference, New Orleans, USA	2009	0.9
European Respiratory Society annual conference, Vienna, Austria	2012	0.9

2. Teaching

Rodent Intubation training to laboratory technicians	2011	0.5
Flexivent Rodent Ventilator training to laboratory technicians	2011	0.5

DANKWOORD / ACKNOWLEDGEMENTS

Het is zover: het 'boekje' is klaar. Ik zie dit niet zozeer als afsluiting van de afgelopen 5 jaar, maar meer als het vastleggen ervan: het 'omtoveren' tot iets tastbaars en vooral als een begin van mijn toekomst als clinician-scientist. Alleen was me dit nooit gelukt en daarom wil ik de volgende mensen bedanken.

Mijn eerste promotor, Prof. Dr. J.C. de Jongste. Beste Johan, bedankt voor je begeleiding in dit hele traject, voor je kritische blik, zowel op de grote lijnen van het onderzoek, als op alle details in de artikelen. Ik sta nog steeds versteld van de snelheid waarmee ik revisies terugkreeg, die ik soms diezelfde ochtend pas gestuurd had. Ik wil je bedanken voor het bieden van de mogelijkheid om ook 'nieuwe' patiënten te zien op de polikliniek kinderlongziekten. Dit heb ik als zeer interessant en leerzaam ervaren en als een goede voorbereiding op mijn coschappen.

Mijn tweede promotor, Prof. Dr. M. Post. Beste Martin, bedankt voor de onderzoeksmogelijkheden die je mij hebt geboden in je laboratorium in Toronto. Beginnend bij het jaar keuze-onderzoek, dat werd omgezet in 4 jaar promotieonderzoek in jouw lab naar 'lung injury & repair'. In de afgelopen 5 jaar heb ik veel verschillende projecten uitgevoerd en me daarbij een breed scala aan laboratorium technieken eigen gemaakt. Dit zou niet zijn gelukt zonder jouw stimulerende houding en vertrouwen in mij. Geen idee was onuitvoerbaar zolang ik het zelf aandroeg! Bedankt voor je continue hulp bij het oplossen van problemen, zowel in de opzet van mijn experimenten, als bij de interpretatie van mijn resultaten en het opschrijven hiervan. Door alle nieuwe vragen die mijn resultaten opleverden, zag ik soms door de bomen het bos niet meer, maar gelukkig wees je mij dan weer de juiste richting. Met plezier denk ik terug aan het gedeelde enthousiasme voor het Nederlands elftal, totdat Robben het verpestte in die laatste minuten tegen Spanje. Tenslotte wil ik je bedanken voor de persoonlijke steun en je begrip bij de onverwachte gebeurtenissen, die het leven nu eenmaal met zich mee brengen, waarvoor ik enkele malen naar Nederland ben gevlogen.

Prof. Dr. I.K.M. Reiss. Beste Irwin, bedankt voor je onuitputtelijke positiviteit en je continue stroom aan innovatieve ideeën omtrent het onderzoek. Ook onze brainstorm sessies bij Café Ari of bij de gehaktballen en bloemkool bereid door Janine zullen mij bij blijven. Met jouw idee over de sphingolipiden is je motto: "Alles kommt gut" weer van toepassing geweest.

Prof. Dr. W.A. Helbing, Prof. Dr. R.W. Hendriks en Prof. Dr. L.J.I. Zimmermann wil ik graag bedanken voor het plaatsnemen in de kleine commissie en het beoordelen van mijn proefschrift. Prof. Dr. T. Kuiken en Dr. P.J.F.M. Merkus, bedankt voor het plaatsnemen in de grote commissie. Prof. Dr. F.W.J. Hazebroek, beste Frans, je hebt alle Tibboel-telgen zien opgroeien en het doet me genoegen dat je op wilt treden als 'rector' tijdens mijn promotieplechtigheid.

The Post lab and the rest of the second floor of the McMaster building has been my home away from home for 5 years. You guys made me feel welcome, for which I am grateful. Stephen, thanks for your jokes, magic tricks and providing the answer to almost every science question I could think of. Emily, thanks for all your help in the cell culture world of stem cells, and for all the nice coffee breaks, even though I always bought tea! Martin Rutter, thanks for all your help with my experiments and your continuing support with the MACS and FACS after you started working for that 'brightly coloured' company. Sherry, thank you for making a day's work more enjoyable. We are still on for that soccer match! Michael (and Efrat & Tal), thanks for showing me the 'Canadian life': Maple Syrup, ice-hockey and last but not least: Steak at Barbarians. Rhiannon, bedankt voor de 'Nederlandse' samenwerking. Het zal je goed doen om te weten dat ik nog steeds geen Mac bezit! André, bedankt voor het delen van je kennis omtrent BPD en de koelkast en vriezer waar we elke dag met plezier gebruik van maken.

Dennis and Michael, thanks for all the work you put into measuring sphingolipids for me and the good talks we had. Irene, Jinxia, Zhen, Maciek, Doa-chun and Jing-chun: thank you for teaching me all the different techniques necessary to complete my experiments and your constant support in helping me optimize my protocols and trouble-shoot any problems I encountered. Sanita and Palma, thank you for all the warmth and kindness you showed me, all your help with arranging my visa to stay in Canada and I will keep on supporting Lazio!

David, thanks for all the craziness we shared and the late night talks during experiments. Hayley (and Rory of course), thanks for all the lunches, coffee breaks, dinners and small talk we shared. You always made me feel very welcome! Pascal, I will not forget our soccer game, I still want a re-match! Neil, thanks for all the good advice and the time spent in those OR's on the first floor! Leonardo, thanks for all the photography and movie theater trips. I hope we meet up again at some point. Doreen, Thomas, Marie-Chantal, Omar, Monica and Stephane, thanks for the good times spent together. Richard, Els, Teun en Cato, bedankt voor het logeerweekje, de gezelligheid en de gehaktballen! Geert, Inge en Noor, bedankt voor de stedentrips en de gezellige uitjes.

Dear members of Lab Animal Services: Debby, Ursula, Marvin and many others, thank you for helping me with my experiments when animals were involved.

Joshua, Niels and the rest of CNB United, thanks for accepting me in your team and allowing me to clear my head from research frustrations while chasing a soccer ball.

Violette, ik kijk terug op een mooie tijd met jou in Canada. Het was een groot avontuur waar we samen ingestapt zijn. Ik ben je daar dankbaar voor.

Het kinderlongziekten team van het Erasmus MC Sophia, beste Harm, Mariëlle, Hettie, Els, Saskia en Liesbeth, bedankt voor alle input tijdens de research besprekingen op de

vrijdagmiddag. Collega's en vrienden van de kinderlongziekten: Leonie, Pierluigi, Karla, Elizabeth, Aukje, Ralf, Marjolein, Sandra, Daan, David en Agnes, bedankt voor het geduld om mijn translationeel-biologische papers door te lezen en van commentaar te voorzien. Maar vooral voor de gezelligheid tussen het schrijven door. Dear Alexandra Quitner, thank you for reading my papers as part of the Grant & Paper Writing Course, and providing valuable comments to help improve them. Beste Karin, Irma en Annemarie, bedankt voor alle hulp met de formulieren en regeltjes rondom het promoveren. Bewoners van het Z-gebouw, bedankt voor de gezellige lunches. Beste Charlotte, bedankt voor het delen van de frustraties van het afronden van een promotietraject en het gezamenlijk doorstaan van de herrie tijdens het heien voor de nieuwbouw. Bram, bedankt dat ik af en toe gebruik mocht maken van je brein rondom het promoveerproces. Mijn Co-groepje wil ik bedanken voor het bieden van een luisterend oor tijdens de laatste loodjes van mijn promotie. Esther, bedankt dat je mijn project een vervolg hebt gegeven en het verder draagt dan ik ooit had durven dromen. Ik ben benieuwd naar de resultaten!

Laurens, al 29 jaar lang vrienden, bedankt voor je gekke dag/nacht ritme, waardoor je altijd de enige Nederlander was die 's avonds in Toronto online was. Aan de game sessies die voor jou midden in de nacht plaatsvonden heb ik veel plezier beleefd. Ik hoop dat er na Kick & Fennick nog veel mooie ideeën van Vincent en jou mogen volgen.

Martijn, bedankt voor het rennen in de Belgische bossen. Nathal, bedankt voor je psychologische visie en de film avondjes.

Sjoerd en Marije, ik ben er trots op dat jullie mijn paranimfen willen zijn. Sjoerd, bedankt dat je op deze belangrijke dag naast me staat. Maar vooral bedankt voor alle jaren dat we al vrienden zijn, alle gesprekken over de dingen waar het leven echt om draait, alle steun in de soms moeilijke tijden en vooral voor het delen van plezier in de vele mooie tijden. Marije, bedankt dat ook jij op deze dag naast me staat, als grote zus en als iemand waarbij ik altijd terecht kan. Ik geniet van onze kopjes thee en het feit dat ik nu gewoon even kan komen buurten in plaats van dat ik daarvoor een oceaan over moet steken. Gezelligheid is altijd te vinden bij jullie thuis, al vanaf het moment waarop ik jullie bovenverdieping grasgroen verfde (om over de vloerbedekking maar niet te spreken), tot op heden, zeker nu er ook nog eens een klein 'mandarijntje' rondloopt.

Mark Moonen, bedankt voor die overheerlijke koffie waar ik maar geen genoeg van kan krijgen! Ook voor de puntentelling van Mahjong die ik me nog steeds niet eigen heb gemaakt! Kleine Vafaartje, bedankt voor je aanstekelijke schaterlach en je knuffeltjes.

Sander, als grote broer ben je er altijd als het nodig is: voor goede gesprekken en het delen van levenservaringen, tot aan de 9 uur 's ochtends sessies voor het werken. Samen met Cathy hebben jullie voor heerlijke etentjes gezorgd en mij in ieder geval dingen leren eten die "..de boer niet kent". Wanneer is het tijd voor de volgende horrorfilm?

Mark, ondanks dat er vroeger tijden zijn geweest waarin we elkaar het leven zuur maakten (jij vooral met woorden, ik vooral met daden), ben ik erg blij jou als broertje te hebben. Van CS1.2 tot BF3 (en misschien 4 binnenkort) en samen met Ellen van Rozenoorlog tot Boonanza hebben we altijd dezelfde passies gedeeld. Bedankt voor het vele contact via Skype tijdens onze sessies om de wereld weer eens te redden. Ellen, veel succes met jouw PhD stress. Werkontwijkend gedrag is maar een telefoontje van je verwijderd.

Lieve opa, hoewel ik heb leren voetballen van de beste (en daarmee bedoel ik niet die man die meer praatte met de tegenstander dan voetbalde), is mijn profcarrière bij HFC Haarlem niet echt van de grond gekomen. Vandaar dat ik een andere weg heb bewandeld. Ik wil u bedanken voor de steun en interesse die u altijd heeft getoond.

Pap, bedankt voor je onuitputtelijke inspiratie en het stimuleren van mijn onderzoeksgeest. De Airport Express strippenkaart heb je goed gebruikt met al je bezoekjes aan Toronto op doorreis naar een congres of voordracht op uitnodiging. Deze bezoekjes hebben mij altijd goed gedaan ongeacht welk steak house we uitprobeerden. Bedankt dat je als coach binnen je vakje bent gebleven en ik je toch soms als wisselspeler mocht inzetten. Je ervaring met en tips rondom het promoveren zijn erg waardevol geweest. De lasagne zal altijd klaarstaan.

Lieve mama, bedankt dat je altijd voor me klaar staat. Met een luisterend oor of goede adviezen, zowel over onderzoek als over alle andere dingen des levens. En niet te vergeten de speklapjes als ik weer in Nederland op vakantie was. Ik heb enorm veel van je kalmte en acceptatie van het leven geleerd. Dit zijn vaardigheden die elke keer van pas komen, zowel in het dagelijkse leven, als tijdens het doen van onderzoek. Je reactie toen ik onverwachts bij het huisje op Texel aan kwam rijden, een paar dagen eerder dan je had verwacht, zal me altijd bij blijven.

Allerliefste Lara, bedankt dat je er altijd voor me bent, zowel om het plezier van een geaccepteerd artikel te vieren, als om de frustraties waar ik tegenaan liep tijdens het afronden van het proefschrift te doen vergeten. Bedankt voor het bewaken van mijn innerlijke rust en het duwtje in mijn rug als ik het nodig had! De steun die ik van jou voel is enorm en daar ben ik je erg dankbaar voor.

Colour Section

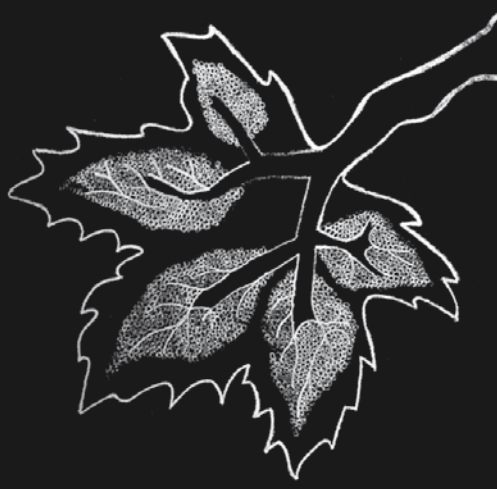

CHAPTER 3

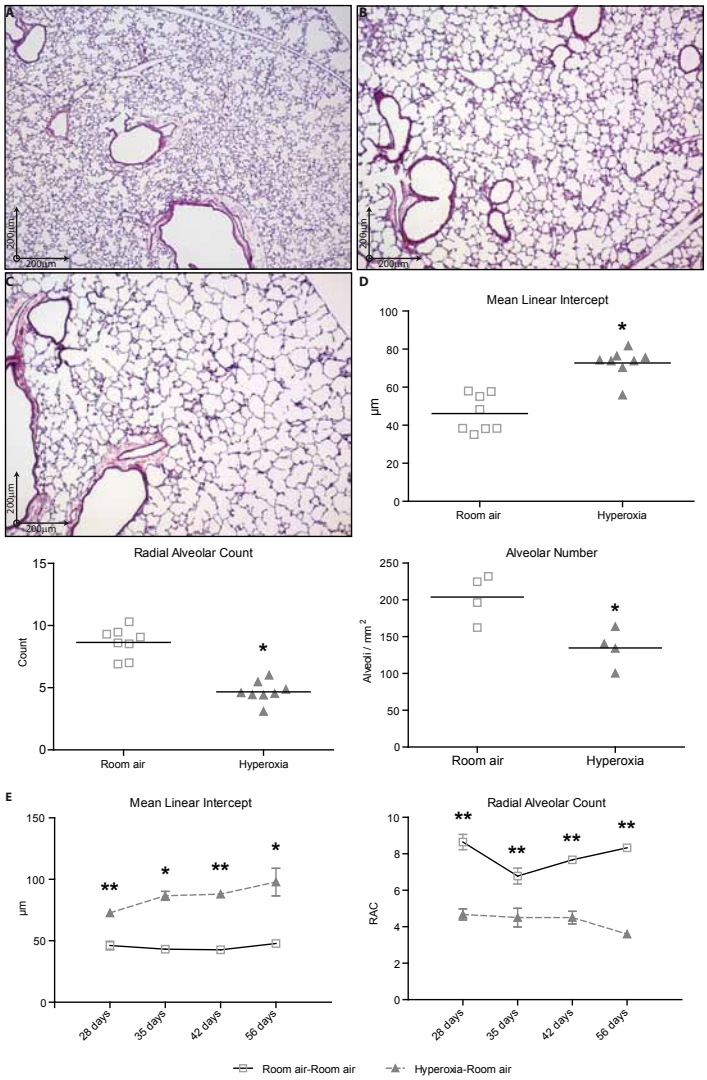

Figure 4. *Effect of hyperoxia and subsequent room air recovery on lung histology. Representative histological sections of room air-exposed newborn mice (A), hyperoxia-treated newborn mice after 4 weeks of exposure (B) and hyperoxia-treated newborn mice that were allowed to recover for another 4 weeks in room-air (C) are shown. Sections were stained with hematoxylin and eosin. Morphometry results (D) are expressed as mean ± SEM for both room air and hyperoxia groups for mean linear intercept (n=8), radial alveolar counts (n=8), and alveolar number (n=4). Morphometry results for 4 weeks of recovery in room-air (E) are expressed as mean ± SEM for mean linear intercept (n=4) and radial alveolar count (n=3). * = p<0.05 ** = p<0.001.*

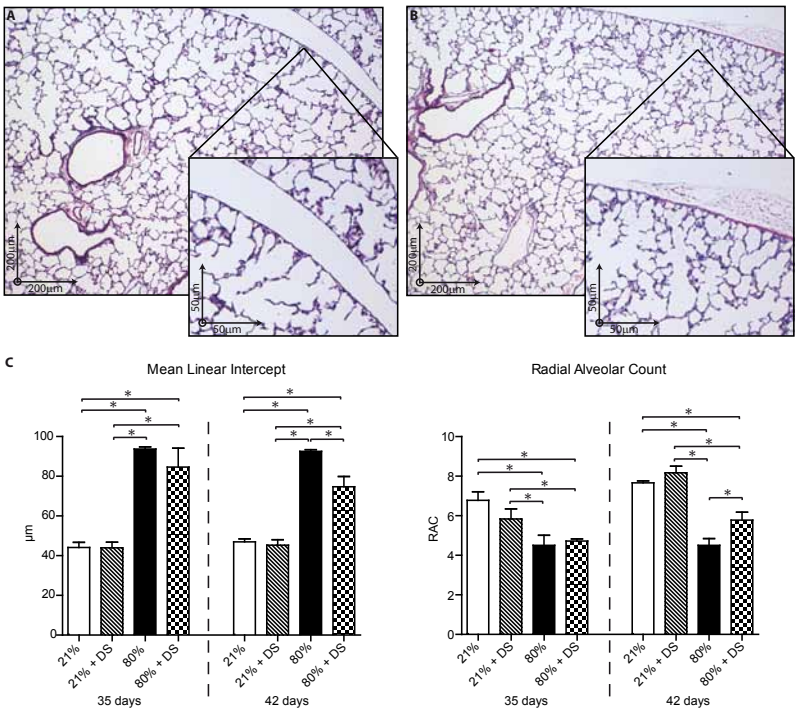

Figure 5. *Effect of D-sphingosine supplementation on lung histology. Representative histological lung sections are shown after 4 weeks of hyperoxia exposure followed by 2 weeks of room air recovery (A), and 4 weeks of hyperoxia exposure followed by 2 weeks of room air recovery with D-sphingosine supplementation (B). Sections were stained with hematoxylin and eosin. High power inserts were taken at 200x magnification. Morphometry results (C) represent a total of 3 mice per group and are expressed as mean ± SEM for all groups. * = p<0.05.*

CHAPTER 4

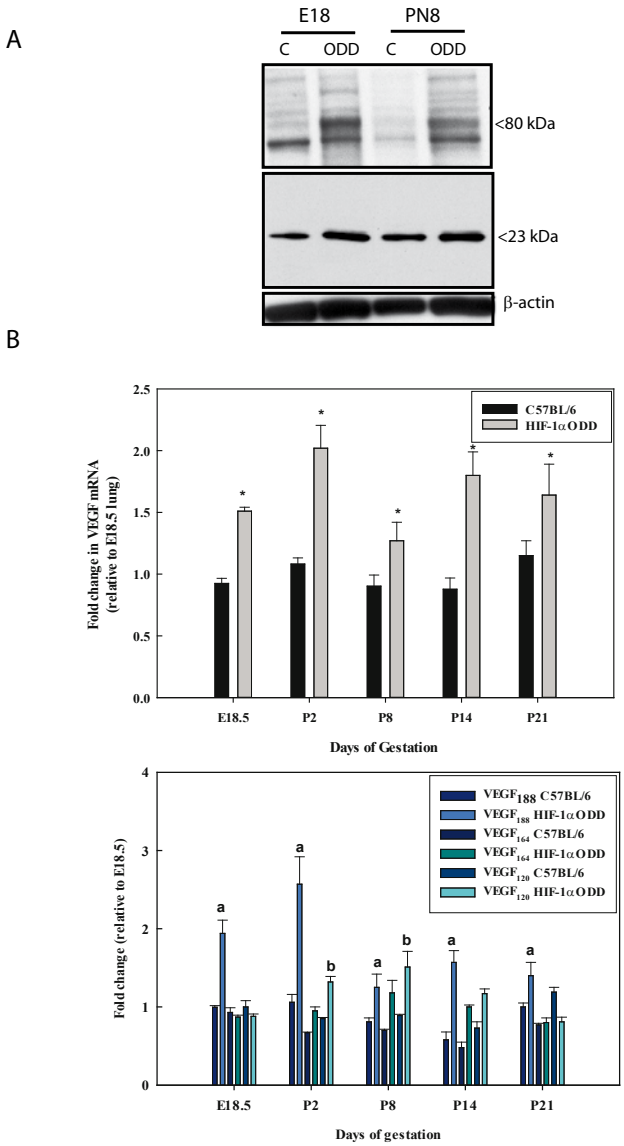

Figure 2. *Immunoblot analysis of HIF-1α and VEGF gene expression in C57 control lungs and HIF-1αΔODD lungs. (A) Western blot of HIF-1α and VEGF on E18.5 and PN8 lungs. Equal loading and transfer was probed with β-actin. (B) Expression of total VEGF mRNA and expression of $VEGF_{188}$, $VEGF_{164}$ and $VEGF_{120}$ mRNA in murine lung, as assessed by real-time qPCR. Data are expressed as relative fold changes in expression when compared to E18.5 lungs. Data are expressed as mean ± SEM for 4 lungs in each group. * = p<0.05.*

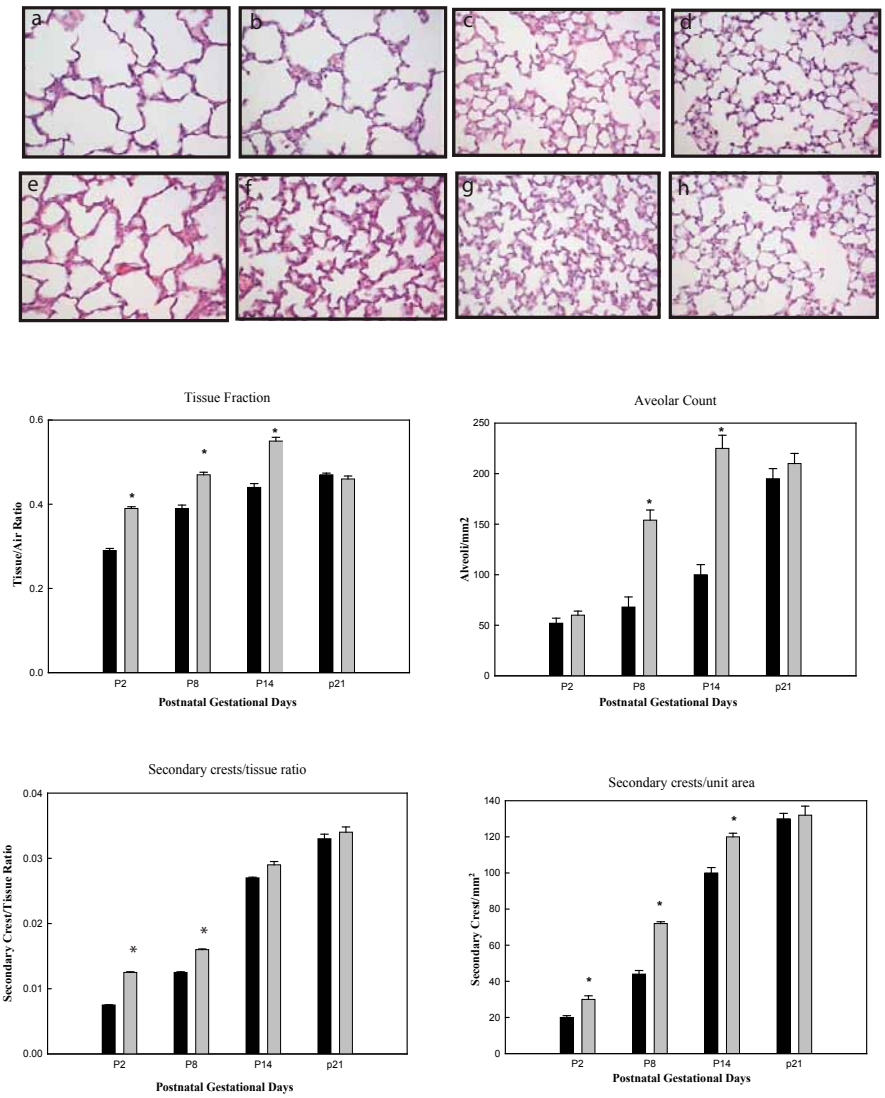

Figure 4. *Histology and morphometry of neonatal C57BL/6 control lungs and HIF-1αΔODD lungs. Hematoxylin and eosin staining of HIF-1αΔODD lungs (e-h) showed increased parenchymal tissue per unit area of lung and smaller distal airspaces compared to C57BL/6 lungs (a-d) consistent with enhanced alveologenesis (Bar = 200 μm). Tissue fraction and number of alveoli per unit area were significantly increased in HIF-1αΔODD lungs at postnatal day 2, 8 and 14. The secondary crest/tissue ratio was increased in HIF-1αΔODD pups at postnatal days 2 and 8. Secondary crest number per unit area was significantly increased in HIF-1αΔODD lungs at postnatal days 2, 8 and 14. Data are expressed as mean ± SEM for five pups in each group. * = p<0.05.*

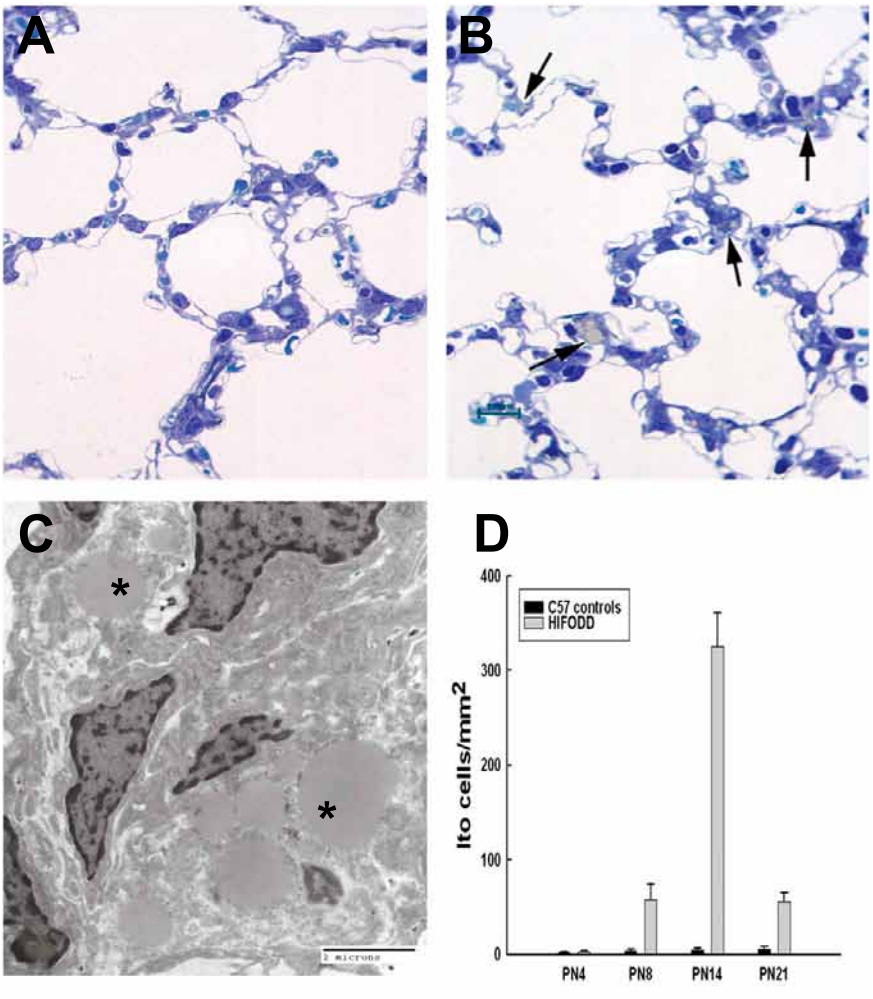

Figure 6. *Stable HIF-1α-expression increases number of lipid-laden interstitial (Ito) cells during postnatal development. Toluidine blue staining of ultrathin section shows an increase in lipid-laden cells (arrows) in HIF-1αΔODD lungs (A) vs. C57 control lungs (B) at PN14. (C) Electron micrograph of lipid droplet-laden interstitial (Ito) cells (* denotes lipid droplets). (D) Number of lipid droplet-laden interstitial cells was significantly increased at PN 8, 14 and 21. * = p<0.05.*

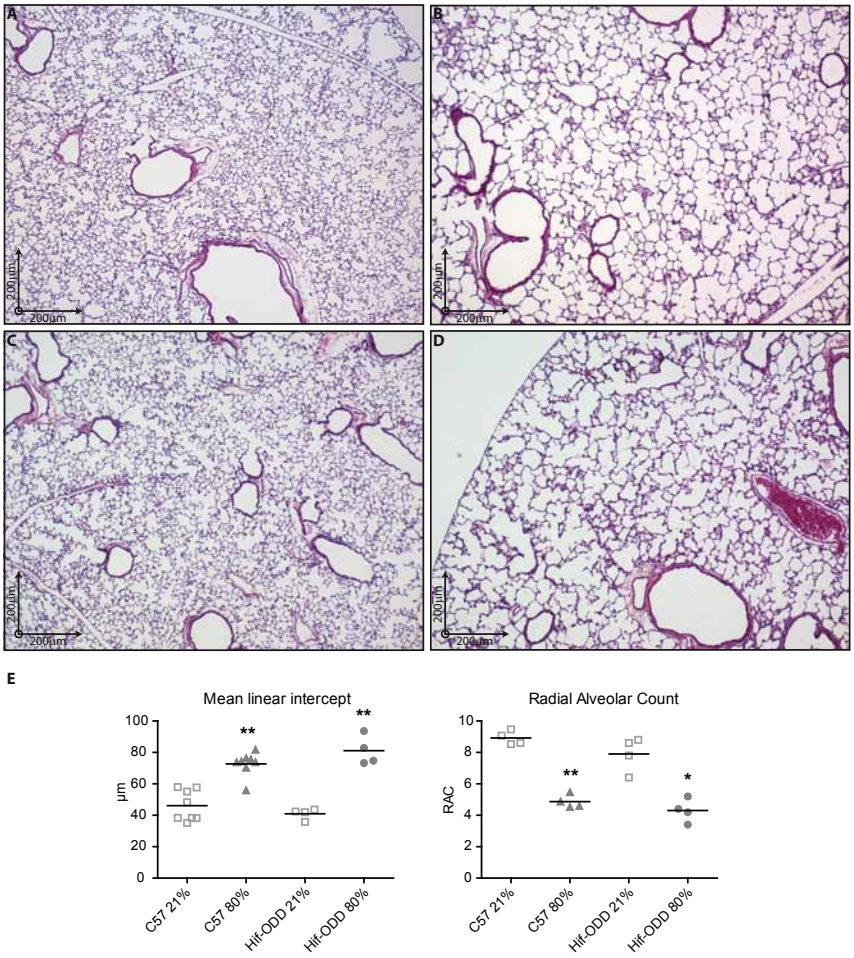

Figure 8. *Representative histological sections of normoxia-exposed C57BL/6 mice (A), hyperoxia-exposed C57BL/6 mice (B), normoxia-exposed HIF-1αΔODD mice (C) and hyperoxia-exposed HIF-1αΔODD mice (D) are shown. Sections were stained with hematoxylin and eosin. Morphometry results (E) are expressed as mean ± SEM for mean linear intercept and radial alveolar counts. * = p<0.05, ** = p<0.001.*

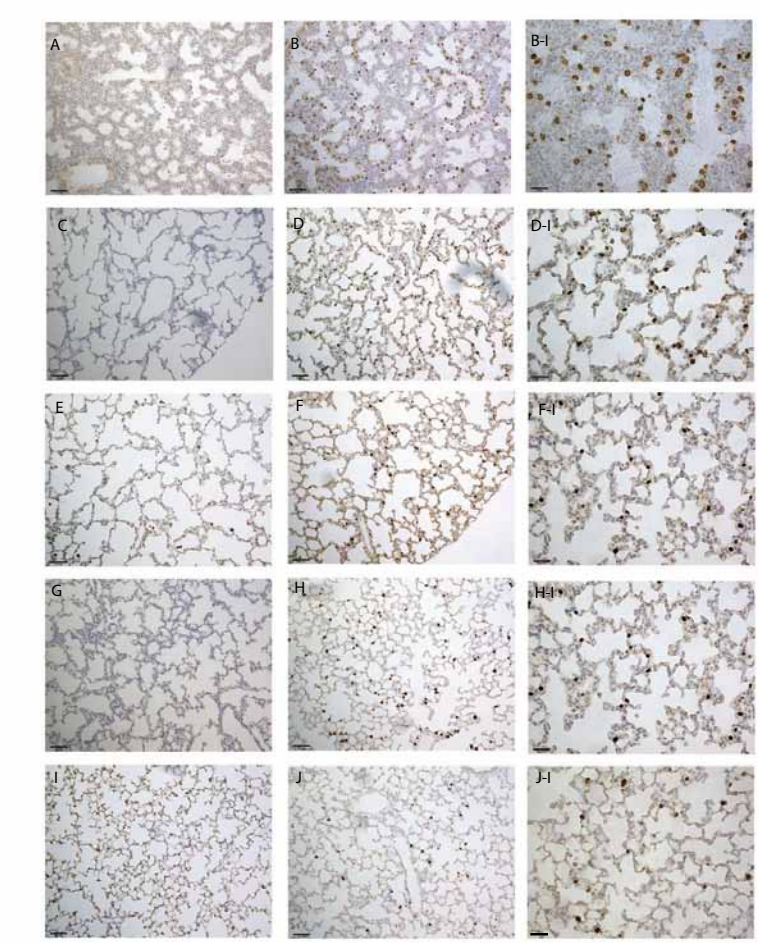

Supplementary figure S2. *Immunohistochemical analysis of HIF-1α in C57BL/6 control lungs and HIF-1αΔODD lungs. Strong positive brownish staining for HIF-1α is noted in the nuclei of distal airway epithelial type II cells of HIF-1αΔODD mice (B, B-I, D, D-I, F, F-I, H, H-I, J, J-I), but not C57BL/6 control mice (A,C,E,G,I) during all postnatal ages (E18.5: A,B,B-I; P2: C, D, D-I; P8: E, F, F-I; P14: G, H, H-I; P21: I, J, J-I. Bar = 200 μm (A-J); 50 μm (B-I, D-I, F-I, H-I, J-I).*

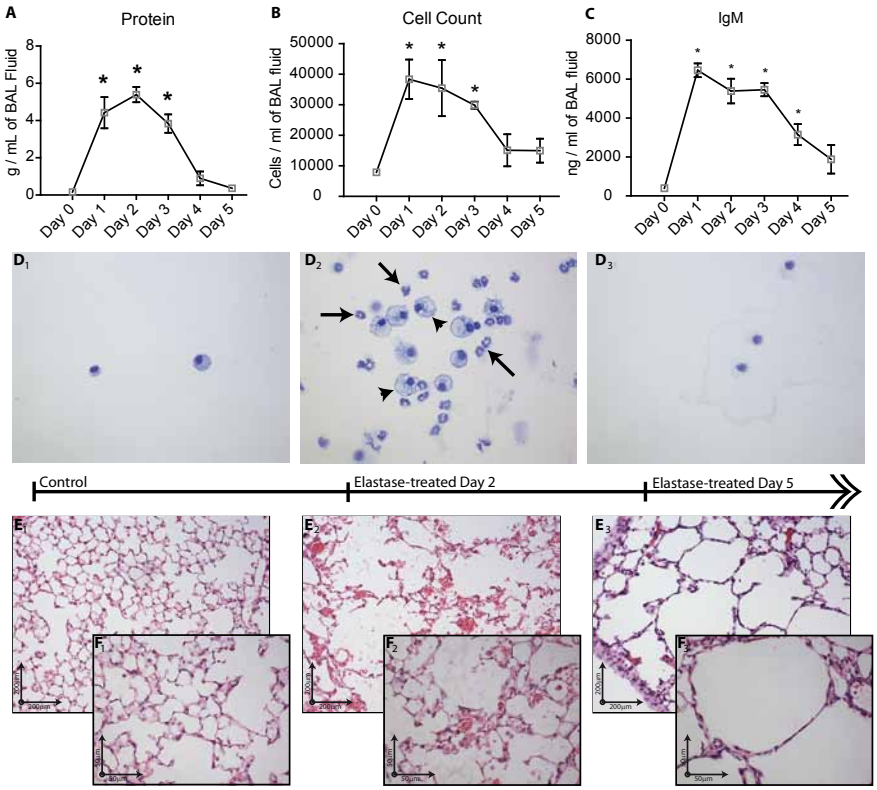

Figure 3. *Biochemical measurements in BAL fluid: protein levels (A) and cell count (B) at day 1, 2 and 3 after elastase injection. IgM levels (C) measured by ELISA. Cytospin slides (D) and haemotoxilin-eosin stained histological slides from control mice (E1 at 200x magnification, F1 at 400x magnification) and elastase-treated mice at 2 days after elastase injection (E2 at 200x magnification, F2 at 400x magnification) and 5 days after elastase injection (E3 at 200x magnification, F3 at 400x magnification). Arrows indicate neutrophils, arrowheads indicate macrophages. Graphs represent an n=4 for each group. * = p<0.05.*

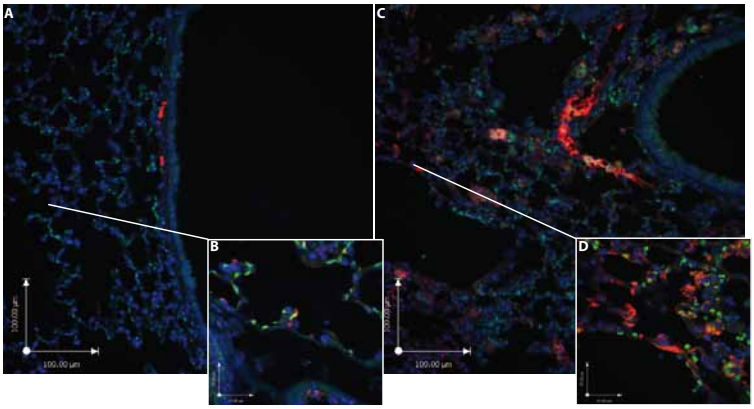

Figure 7. *Immunofluorescent images of ceramide expression. Control (A at 100x magnification, B at 400x magnification), elastase-treated mice 2 days after elastase injection (C at 100x magnification, D at 400x magnification). Ceramide (red), cell nuclei (DAPI blue) and autofluorescence (green).*

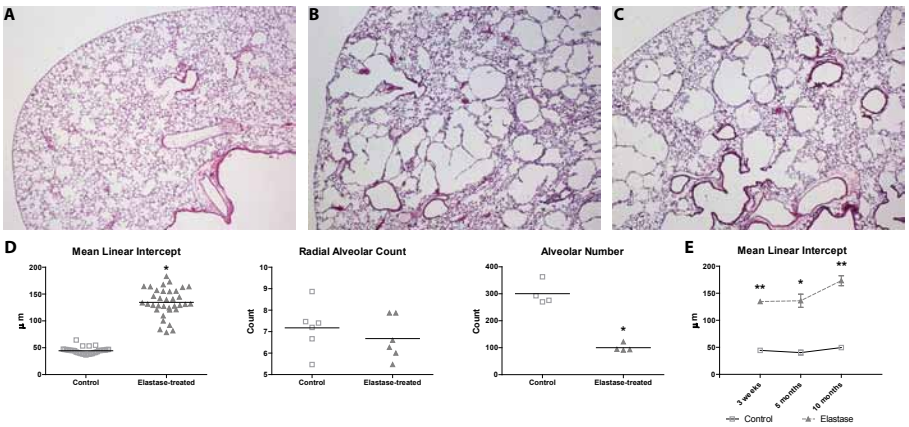

Figure 3. *Representative histological sections of saline-controls (A), elastase-treated mice 21 days after injection (B) and elastase-treated mice 10 months after elastase injection (C). Sections were stained with hematoxylin and eosin. Morphometry results (D) are expressed as mean ± SEM for both control and elastase-treated group for mean linear intercept (n=35), radial alveolar counts (n=6), and alveolar number (n=4). Morphometry results for 5 and 10 months of recovery in room-air (E) are expressed as mean ± SEM for mean linear intercept (n=5). * = p<0.05 ** = p<0.001.*

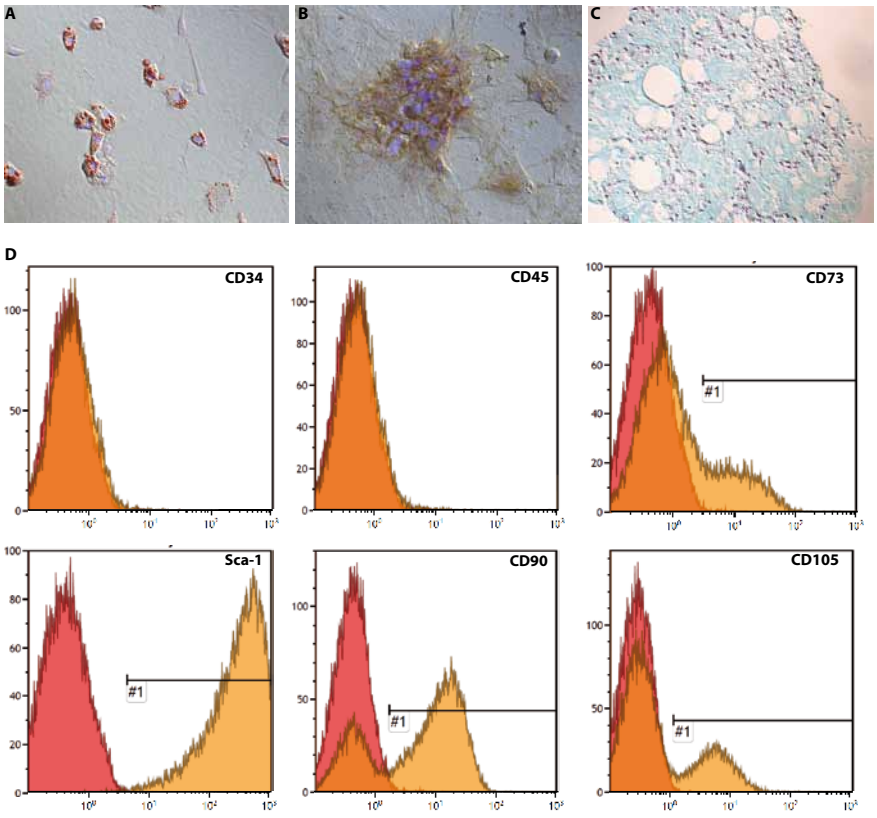

Supplementary figure S2. *Differentiated MSCs were directly stained on 6 well plates for adipocytes (A, Oil-red stain), osteoblasts (B, Von Kossa stain) and chondrocytes (C, Alcian Blue stain), and flow cytometry data (D) of passage 8 MSCs (red population) stained for CD34, CD45, CD73, CD90, Sca-1 and CD105 and passage 8 unstained MSCs as control (orange population).*

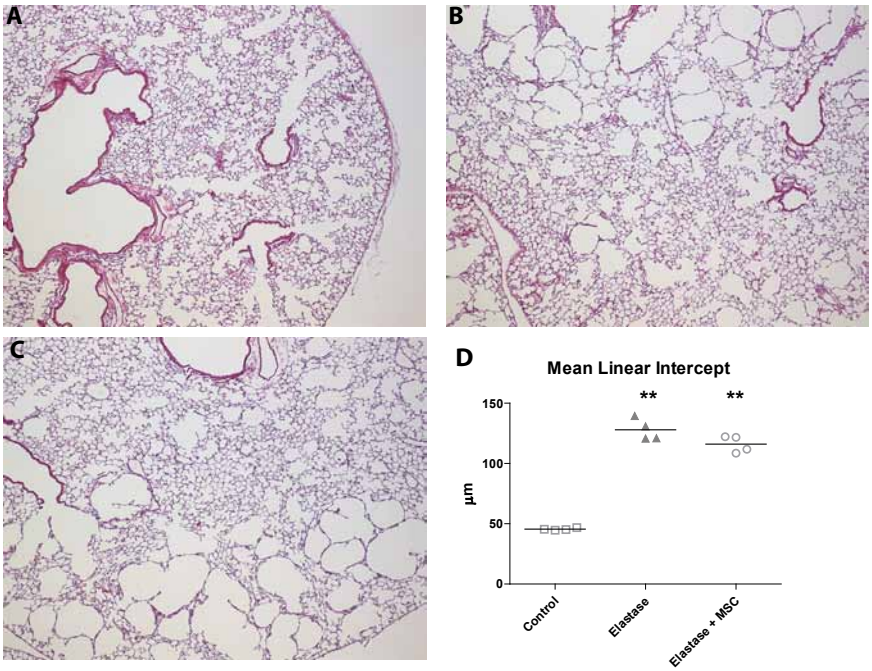

Supplementary figure S3. *Representative histological sections of saline-controls (A), elastase-treated mice 21 days after injection (B) and elastase-treated mice that received MSCs via the jugular vein route (C) and via the intratracheal route (D). Sections were stained with hematoxylin and eosin. Morphometry results (E) are expressed as mean ± SEM for all groups (n=4 per group) ** = p<0.001.*

CHAPTER 7

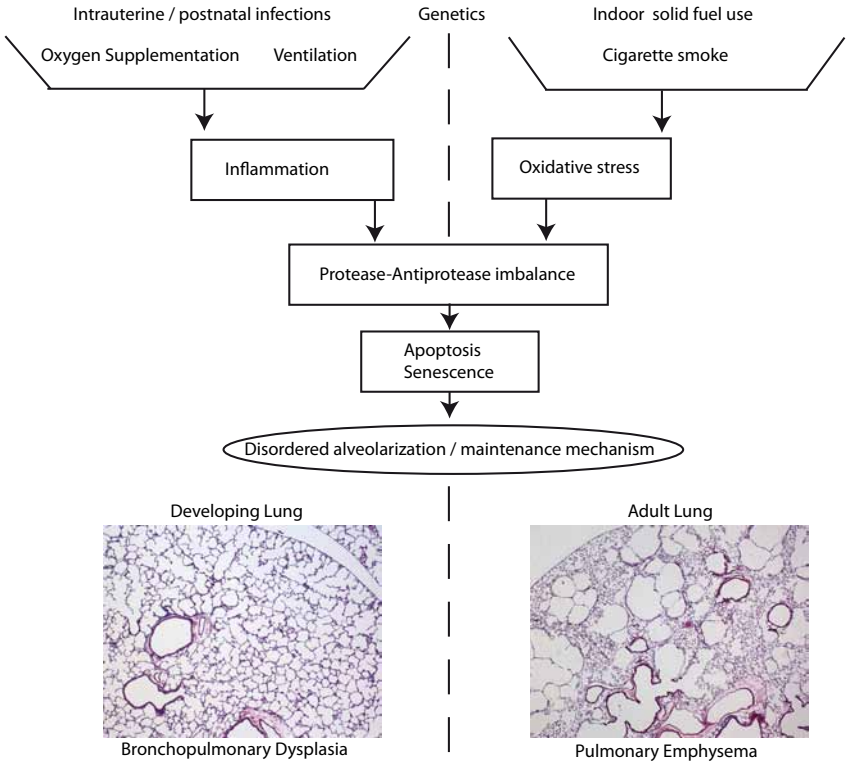

Figure 1. *The interplay of factors and biological processes suggested to play a role in the development of BPD and COPD.*

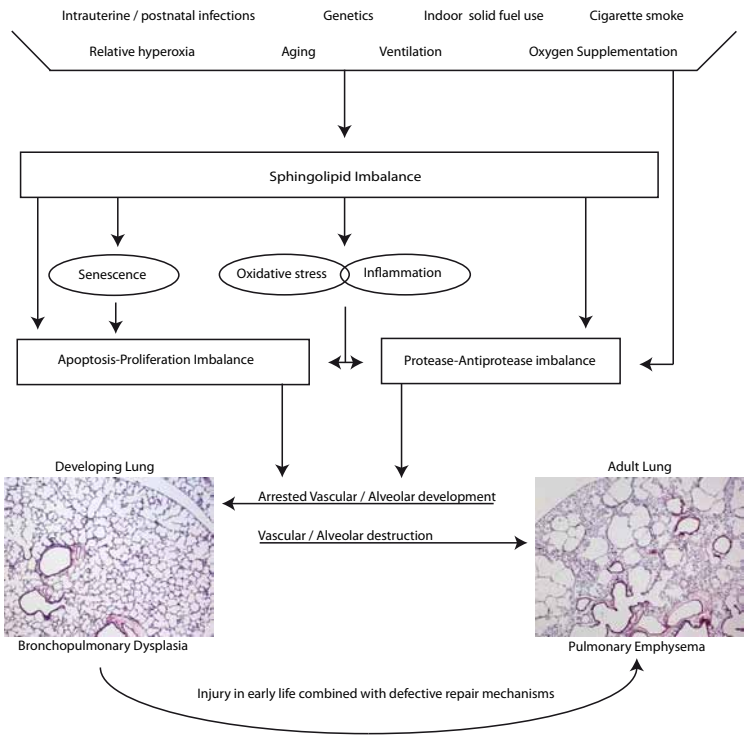

Figure 2. *Summary of the pathways believed to be involved in the development of BPD and COPD.*